UNIVERSIDADE D
COIMBRA

Kaushik Hebbar Kannur

Optimization of Nitrogen-Alloyed MoSx Coatings for Low Friction Applications

Doctoral Thesis in Mechanical Engineering, Surface Engineering Branch, supervised by Professor Albano Augusto Cavaleiro Rodrigues de Carvalho and Doctor Christophe Héau, submitted to the Department of Mechanical Engineering, Faculty of Science and Technology of the University of Coimbra.

December 2020

• U C •

FCTUC FACULDADE DE CIÊNCIAS
E TECNOLOGIA
UNIVERSIDADE DE COIMBRA

DEPARTAMENTO DE
ENGENHARIA MECÂNICA

OPTIMIZATION OF NITROGEN-ALLOYED MoSx COATINGS FOR LOW FRICTION APPLICATIONS

Submitted in Partial Fulfilment of the Requirements for the Degree of Doctor of Philosophy in Mechanical Engineering

Author **Kaushik Hebbar Kannur**

Supervisor **Doctor Albano Augusto Cavaleiro Rodrigues de Carvalho**
Full Professor in University of Coimbra

Co-supervisor **Doctor Christophe Héau**
Research & Development Manager in HEF's Institute for Research in Surface Engineering (IREIS)

In the framework of PhD in Mechanical Engineering

Coimbra,
December 2020

Dedication

"No one who does good work will ever come to a bad end, either here or in the world to come."

(The Bhagavad Gita)

To my father, Venkatesh Rao Kannur and my mother, Shailaja Venkatesh Rao who always picked me up on time and encouraged me to go every adventure, especially this one. For believing in me throughout my life and making me what I am today.

To all my teachers who guided me all along.

To my siblings and my better half for their encouragement and endless support.

And

"To my inner desire and motivation, that pushed me to where I am."

Acknowledgements

First and foremost, praise and thanks to God, the Almighty, for His showers of blessings throughout my research work to complete the research successfully.

I want to express my deep and sincere gratitude to my research supervisor, Prof. Dr. Albano Augusto Cavaleiro Rodrigues de Carvalho, Full professor, Centre for Mechanical Engineering, Materials and Processes (CEMMPRE), Department of Mechanical Engineering, University of Coimbra, for giving me the opportunity to do research and providing invaluable guidance throughout this research. His dynamism and motivation have deeply inspired me. He has taught me the methodology to carry out the research and present the research works as clearly as possible. It was a great privilege and honour to work and study under his guidance. I am incredibly grateful for what he has offered me. I would also like to thank him for his friendship, empathy, and a great sense of humour.

I would also like to express my sincere gratitude to my research co-supervisor, Dr. Christophe Héau, R&D Manager, IREIS, HEF Group, for giving me the required training on physical vapour deposition, its equipment, and guidance. I am grateful for his dedication and time to nurture me during research activities. I am grateful for his guidance and for sharing his industrial experiences and knowledge in detail during our meetings. It was a great privilege and honour to work under his guidance. I would also like to thank Dr. Christophe Pupier, President, IREIS, HEF Group, for giving me the necessary support and motivation during my research work. He made sure my stay in France easy and convenient. Under his guidance, I acquired knowledge and interests on the management of project and team building.

I am extremely grateful to my parents for their love, prayers, caring, and sacrifices to educate and prepare me for my future. I am very much thankful to my wife, Arpita, for her love, understanding, prayers and continuing support. Also, I express my thanks to my in-laws, brothers, sister-in-law, for their support and valuable prayers. My Special thanks goes to my mentor and friend Prof. Dr. Seshan Sivam, Emeritus Professor, Department of Mechanical Engineering, Indian Institute of Science, Bangalore for the keen interest and faith shown on me to grow professionally.

I would also like to express my gratitude to institutions such as Institute Pedro Nunes, Coimbra and Czech Technical University, Prague, which was involved in my research project to carry out testing.

I would also like to extend my gratitude to consortium coordinator, Prof. Dr. Tomas Polcar, Full professor, University of Southampton, Southampton and Czech Technical University, Prague, who identified my research motivation and providing me the platform to pursue my dreams.

I also extend my special thanks to my colleague researchers and management at the University of Coimbra and Institut de Recherches en Ingénierie des Surfaces (IREIS), HEF group for their kindness and support. I express my special thanks to friends and colleagues Dr. Teodor Huminiuc and Dr. Talha Bin Yaqub, for their genuine support throughout this research work as collaborators.

And, I am grateful to IREIS, HEF group and University of Coimbra for hosting me and providing me to use the facilities for my research work. I acknowledge the Marie Sklodowska-Curie Actions selection committee for honouring me with the Early Stage Researcher fellowship to undertake my research. I thank SOLUTION-ITN (grant number: – 721642). I am also grateful for other research and funding bodies such as South of England Analytical Electron Microscope (EP/K040375/1) Within the David Cockayne Centre for Electron Microscopy, Department of Materials, University of Oxford, the Henry Royce Institute (EP/R010145/1), CEITEC Nano Research Infrastructure (ID LM2015041, MEYS CR, 2016-2019), CEITEC Brno University of Technology, CEMMPRE – UID/EMS/00285/2019 [co-financed via FEDER and FCT (COMPETE)] University of Coimbra.

Finally, my thanks go to all the people who have supported me to complete this research journey directly or indirectly.

Abstract

Transition-metal-dichalcogenide coatings (such as MoS_2) provide low friction due to its characteristic low shear strength along the basal plane of the lamellar structure; however, the material can easily degrade through exfoliation and poor adhesion to the metallic substrates. Furthermore, its low load-bearing capacity leads to high wear and high coefficient of friction (COF). All these issues prevent these coatings for a wide range of applications meant for dry or solid lubrication. Physical vapour deposition (PVD) has provided new insights into the field of tribology and lubrication with the possibility to deposit tailored thin coatings based on the application requirements. The present work is aimed towards the development and optimization of direct current (DC) magnetron sputtered Mo-S-N coatings for low friction applications, particularly for space components. Then coatings with high adhesion to the substrate, high hardness and a stable tribological performance in vacuum environment are deposited.

Initially, in this work, an innovative approach was employed to improve the coating's adhesion. A secondary plasma source was used during deposition to generate an additional charged particle flux which was directed to the growing coating independently of the magnetron cathode. Therefore, Mo-S-N solid lubricant coating were deposited by DC magnetron sputtering from a single molybdenum disulphide (MoS_2) target in a reactive atmosphere. Nitrogen was introduced during the deposition with increasing partial pressures, resulting in a high N content in the alloyed coatings (37 at. %). The variation in the incident ion energy and flux of the energetic species bombarding the growing coating allows for the control of the S/Mo ratio through the selective re-sputtering of sulphur from the coating. The S/Mo ratio was progressively increased, with a gradient-like effect, up to the range of 1.2 - 1.8, i.e., from an almost metallic Mo(N) layer up-to-the lubricious sulphide. The coatings were nanocrystalline from 0 to 28 at. % N and, further addition, led to the amorphous structure. Combining the ion bombardment with nitrogen incorporation, the cohesive critical load (Lc1) reached 38 N, one order of magnitude higher than MoS_2 coating. The adhesion at coating-substrate was above 80 N. A maximum hardness of 8.9 GPa was measured for the 37 at. % N-alloyed coating. For high N content coatings, high-resolution transmission electron microscopy (HR-TEM) revealed an amorphous structure as well as a perfect bonding with the substrate, with zones with epitaxial growing.

Afterwards, the tribological performance of Mo-S-N coatings were analysed in vacuum (10^{-4} Pa) and room (20 - 25 °C, 20 - 30 % RH) conditions. The tribological tests were performed at relatively low contact stresses to replicate real industrial needs using a cylinder-on-flat reciprocating tribometer. The interaction between different mating surfaces (coating versus steel, coating versus coating) was carried out. Additionally, the effects of loads on the sliding properties were also studied for coating versus coating interactions, and endurance testing for one of the Mo-S-N coatings with coating versus steel interaction. In all mating conditions, the pure MoS_2 coating had COF in the range of 0.1 – 0.25 and the least specific wear rates were found to be 3.0×10^{-6} mm^3/N.m for flat and 2.5×10^{-6} mm^3/N.m for the cylinder. As compared to MoS_2 coating, the COF and specific wear rates decreased with N additions. The COF lied in the range of 0.05 – 0.1 for Mo-S-N coatings, while coating versus coating displayed the lowest specific wear rates (8.6×10^{-8} mm^3/N.m for flat and 4.4×10^{-8} mm^3/N.m for cylinder). The increase in the load resulted in lower COF but higher wear rate. The Mo-S-N coatings performed for longer duration at low COF without any failures compared to pure MoS_2. Finally, one of the Mo-S-N coatings tested for different mating conditions in ambient air resulted in an increasing trend of COF, reaching the maximum value of 0.3. The detailed mechanism behind the COF behaviour for the different mating conditions was also presented and discussed. This work brings some important issues when testing transition metal dichalcogenides based coatings under low contact stress conditions more appropriated for simulating real service applications.

In the final part of this thesis, the aim was to investigate the tribological behaviour of an amorphous Mo-S-N coatings, especially, (i) the role of nitrogen incorporation, (ii) the formation mechanism of MoS_2 tribo-film at the sliding interface and, (iii) the changes in the friction behaviour under different environments. One of the Mo-S-N coatings (30 at. % N) was tested using standard ball-on-disc rotating tribometer with high contact stresses. The coating was predicted to have either a Mo-S-N phase with N filling some of the S sites or a $MoS_2(N_2)$ structure where the gas molecules prevent the formation of a crystalline lamellar structure. The tribological studies performed in vacuum and ambient air resulted in steady-state COF values of 0.03 and 0.15, respectively. HR-TEM analysis performed on the wear-tracks revealed that the low coefficient of friction (COF) in vacuum was attributed to the formation of a thick and continuous lamellar tribo-film with a low amount of

nitrogen. Contrarily, in ambient air, the surface oxidation disturbed the formation of a continuous MoS_2 tribo-film from the amorphous coatings, leading to an increase in the COF and wear rate. This study shows through indirect measurements of the chemical composition of the as-deposited coating and wear debris that nitrogen is stored in gaseous form (N_2) within the amorphous matrix and is released from the contact during sliding.

Keywords: Molybdenum disulphide, Physical vapour deposition, Magnetron sputtering, Mo-S-N coatings, cylinder-on-flat contact, low contact stresses.

Resumo

Os revestimentos de dicalcogenetos de metais de transição (como p.ex. o MoS_2) mostram baixo atrito devido à resistência reduzida ao corte característica dos planos basais da estrutura lamelar; no entanto, o material pode degradar-se facilmente devido à sua esfoliação e má adesão aos substratos metálicos. Além disso, devido à baixa resistência a cargas de contato, estes revestimentos podem apresentar coeficientes de atrito (COF) e desgaste muito elevados. Estes problemas têm tido um impacto negativo que os tem impedido de serem utilizados numa gama mais alargada de aplicações onde é requerida lubrificação sólida. Com o advento das técnicas de deposição física em fase de vapor (PVD), abriram-se novas possibilidades para as áreas de tribologia e lubrificação, já que é possível ajustar as propriedades dos revestimentos finos aos requisitos impostos pela aplicação. O presente trabalho visa o desenvolvimento e otimização de revestimentos Mo-S-N depositados por pulverização catódica magnetrão em corrente contínua (CC) para aplicações de baixo atrito destinadas a componentes espaciais. O objetivo é depositar revestimentos com elevada adesão ao substrato, maior dureza e desempenho tribológico estável em condições ambientais e de vácuo.

Inicialmente, neste trabalho, foi utilizada uma abordagem inovadora para melhorar a adesão do revestimento. Foi usada uma fonte secundária de plasma durante a deposição para gerar um fluxo adicional de partículas carregadas eletricamente que foi direcionado para o filme em crescimento independentemente do cátodo magnetrão. Assim, o revestimento de lubrificante Mo-S-N foi depositado por pulverização catódica CC magnetrão a partir de um único alvo de bissulfureto de molibdénio (MoS_2) em atmosfera reativa. O azoto foi introduzido durante a deposição com pressões parciais crescentes, resultando num teor elevado de N nos revestimentos (37 at. %). A variação na energia e no fluxo dos iões que bombardeiam o revestimento em crescimento permite o controlo da relação S / Mo por meio de uma repulverização seletiva do enxofre do filme. A razão S / Mo foi aumentada progressivamente, dando origem a um gradiente de composição, até um valor na faixa de 1,2 - 1,8, desde um camada quase metálica até ao bissulfureto lubrificante. Combinando o bombardeamento iónico com a incorporação de azoto, a carga crítica coesiva (Lc_1) atingiu 38N, uma ordem de grandeza maior do que o revestimento MoS_2. A adesão ao substrato de revestimento atingiu valores acima de 80 N. A dureza máxima atingida foi de 8,9 GPa e foi medida para o revestimento com 37 at. % N. A microscopia

eletrónica de transmissão de alta resolução (HR-TEM) dos revestimentos com elevado teor de N revelou uma estrutura amorfa e uma ligação perfeita com o substrato, com zonas onde pode ser detetado um crescimento epitaxial.

Numa fase posterior, foi analisado o desempenho tribológico dos revestimentos Mo-S-N em vácuo (10^{-4} Pa) e ao ar ambiente (20 - 25 ° C, 20 - 30% UR) . Os testes tribológicos foram realizados com tensões de contato relativamente baixas, para replicar as necessidades industriais reais, num tribómetro alternativo usando uma geometria de cilindro / plano. Foi variada a interação entre diferentes superfícies de contato (revestimento versus aço, revestimento versus revestimento). Além disso, também foram estudados o efeitos da carga aplicada nas propriedades tribológicas para a interação revestimento vs. revestimento assim como testes de resistência para um dos revestimentos Mo-S-N para a interação de revestimento versus aço. Em todas as condições de pares de deslizamento, o revestimento de MoS_2 puro mostrou COF na faixa de 0,1 - 0,25 e taxas de desgaste específicas de $3,0 \times 10^{-6}$ mm^3 / Nm, para o plano, e $2,5 \times 10^{-6}$ mm^3 / Nm, para o cilindro. Em comparação com o revestimento MoS_2, os COF e as taxas de desgaste específicas diminuíram com a adição de N. O COF ficou na faixa de 0,05 - 0,1 para revestimentos Mo-S-N, enquanto que na configuração revestimento vs. revestimento foram exibidas as menores taxas de desgaste específico ($8,6 \times 10^{-8}$ mm^3 / Nm, para o plano, e $4,4 \times 10^{-8}$ mm^3 / Nm, para o cilindro). O aumento da carga resultou numa diminuição do COF, mas foi observado um aumento na taxa de desgaste. Os revestimentos Mo-S-N mostraram uma vida mais longa com COF reduzido, e sem qualquer falha, em comparação com o MoS_2 puro. Finalmente, um dos revestimentos Mo-S-N testados para diferentes configurações de contato em ar ambiente mostrou uma tendência crescente do COF atingindo um valor final de 0,3. O mecanismo que está por trás deste comportamento do COF nas diferentes configurações, foi apresentado e discutido. Este trabalho traz algumas questões importantes ao testar revestimentos à base de dicalcogenetos de metais de transição sob condições de baixa tensão de contato mais adequadas para simular aplicações reais em serviços.

Na parte final desta tese, o objetivo foi investigar o comportamento tribológico de revestimentos amorfos de Mo-S-N, especialmente, (i) o papel da incorporação de nitrogênio, (ii) o mecanismo de formação da tribo-camada MoS_2 na interface de contato e, (iii) as variações do comportamento de atrito em diferentes ambientes de ensaio. Para tal,

foi testado um dos revestimentos Mo-S-N com 30 at. % N num tribómetro tradicional tipo pino-disco, sob tensões de contato elevadas. O revestimento poderia ser constituído por uma fase Mo-S-N, onde o N preenchia alguns dos sítios S, ou por uma estrutura MoS_2 onde as moléculas de N_2 estavam incorporadas evitando a formação de uma estrutura lamelar cristalina. Os estudos tribológicos realizados em vácuo e atmosfera ambiente resultaram em valores de COF em estado estacionário de 0,03 e 0,15, respetivamente. A análise HR-TEM realizada nas pistas de desgaste revelou que o baixo coeficiente de atrito em vácuo era atribuído à formação de um tribo-filme lamelar espesso e contínuo com uma baixa quantidade de azoto. Pelo contrário, em atmosfera ambiente, a oxidação da superfície perturbava a formação do tribo-filme de MoS_2 contínuo, a partir dos revestimentos amorfos, levando a um aumento no COF e na taxa de desgaste. Este estudo mostrou por meio de medições indiretas da composição química do revestimento como depositado e dos detritos de desgaste que uma parte do azoto é armazenado na forma gasosa (N_2) dentro da matriz amorfa e é liberado do contato durante o deslizamento.

Palavras-chave: Bissulfureto de molibdénio, Deposição física fase vapor, Pulverização catódica, revestimentos Mo-S-N, Contacto cilindro/plano, Tensões de contato baixas

Table of contents

List of figures

List of tables

Nomenclature

Acronyms

AFM – atomic force microscopy

COF – coefficient of friction, friction coefficient

CVD – chemical vapour deposition

DC – direct current

DCMS – direct current magnetron sputtering

DLC – diamond-like-carbon

EDS – energy dispersive spectroscopy

FESEM – field emission scanning electron microscope

HiPIMS – high power impulse magnetron sputtering

HR-TEM – high-resolution transmission electron microscope

IBED – ion beam enhanced deposition

PVD – physical vapour deposition

RF – radio frequency

RFMS – radio frequency magnetron sputtering

RH – relative humidity

RPM – revolutions per minute

SEM – scanning electron microscope

TMD – transition metal dichalcogenide

ToF-SIMS – time of flight-secondary ion mass spectrometry

WDS – wavelength dispersive spectroscopy

XPS – x-ray photoelectron microscope

Units and symbol

A – ampere

a.u. – arbitrary units

at. % – atomic percent

GPa – gigapascal

keV – kiloelectron-volts

kgf – kilogram-force

kHz – kilohertz

MPa – mega pascal

mm – millimetre

nm – nanometer

N – Newton

ns – nanosecond

N.m – Newton meter

Pa – pascal

s – second

sccm – standard cubic centimetres per minute

V – voltage

W – watt

Ø – diameter

θ – theta

Elements and compounds

Ar – argon

Ag – silver

Al – aluminium

Au – gold

a-C – amorphous carbon

AlN – aluminium nitride

BaF_2 – barium fluoride

C – carbon

c-BN – cubic boron nitride

Co – cobalt

Cr – chromium

Cu – copper

C_2H_2 – acetylene

CH_4 – methane

CrN – chromium nitride

CrAlN – chromium aluminium nitride

CrC – chromium carbide

CrBN – chromium boron nitride

CaF_2 – calcium fluoride

CeF_3 – caesium fluoride

Fe – iron

H_2O – water

Mo – molybdenum

MoN – molybdenum nitride

MoO_3 – molybdenum trioxide

MoS_2 – molybdenum disulphide

$MoSe_2$ – molybdenum diselenide

N_2 – nitrogen

Ni – nickel

O – oxygen

Pb – lead

Pb – lead oxide

Pt – platinum

PTFE – polytetrafluoroethylene

S – sulphur

Se – selenium

Si – silicon

SiC – silicon carbide

Ta – tantalum

Ti – titanium

TiC – titanium carbide

TiCN – titanium carbonitride

TiN – titanium nitride

TiAlN – titanium aluminium nitride

TiBN – titanium boron nitride

W – tungsten

WN – tungsten nitride

WS_2 – tungsten disulphide

WSe_2 – tungsten diselenide

W_2C – tungsten carbide

WO_3 – tungsten oxide

WC – tungsten carbide

ZnO – zinc oxide

Zr – zirconium

Chapter I

1. INTRODUCTION

The study of the interactions between contacting bodies in relative motion is known as tribology. The study of tribology is relatively new in the field of science, having strongly benefited with the development of advanced instrumentation in the 20th century, which opened many possibilities for investigation of its fundamentals. The study of tribology itself is much older: we can consider that, for instance, in the 15th century, the fundamental laws of friction were formulated by Leonardo da Vinci [1]. In any case, the term tribology was only introduced as a new field of science in 1967, having its root in the Greek tribos, for rubbing or sliding [1]. In one way or another, tribology covers almost all the interactions happening around us from writing to walking, driving a bicycle to a space shuttle, cutting tools to welding and joining operations, large mechanical components to micro and nanodevices, etc… Tribology can also be related with human bodies, most of the joints working under lubrication. In a recent study, it was proposed that the skin on the tips of our fingers develop wrinkles when wet due to an evolutionary mechanism, to improve the grip on wet surfaces [2] and so as, to avoid low friction. Certainly, there is a very wide range of applications associated to tribology.

The study of interacting surfaces is a way of expanding the lifetime of most devices created by the humanity or nature, by finding ways to reduce friction and wear. Amid these interactions, forces are transmitted, mechanical energy is converted, and the physical and the chemical nature, including surface topography of the interacting materials, are changed. Understanding the nature of these interactions and, thus, solving the technological problems associated with the interfacial phenomena constitutes the essence of tribology. To make a tribological system highly efficient the sliding forces and the friction must be optimized according to the required limits. This optimization helps in the sustainability of the tribological system by overcoming the degradation due to wear. Wear is the major cause of the waste of material and the degradation of the mechanical performance, and friction is directly related to significant worldwide energy misfortunes. About 30 % of the energy assets in the world are spent in friction [3]. Studies conducted since the second half of the

twentieth century estimated that the effort to overcome friction would cause losses of about 1 – 5 % of the Gross National Product of an industrialized country [1,4,5]. The most widely used means to reduce the friction is the use of liquid lubricants which are under use since the beginning of the industrial revolution. Still, there are environmental issues associated with the disposal of lubricants.

To overcome such losses and damages caused by friction as well as to avoid the liquid lubricants, various other means are being researched by scientists around the globe. The domain of this new mean is known as solid lubricants, which made an entry in the beginning of 1940s. Other aims of these solid lubricants were to reduce the weight and cost of the large machines or industrial setups. A solid lubricant can be applied on sliding components by many processes, such as burnishing [6], a film prepared by electrochemical process [7] or a thin film or coating deposited by physical vapour deposition (PVD) [8] etc... Out of these, the best method is by depositing solid lubricant coatings using PVD sputtering.

One of the most important and critical application of these solid lubricants is the aerospace industry. The space conquest, motivated in its beginnings by political and military ambitions, has transformed over the past 20 years, to give birth to a veritable industry. Today, space techniques are necessary for our society, for telecommunications, earth observation (meteorology) or satellite location. Simultaneously, the numerous scientific space missions have enabled us to increase the knowledge of our planet, solar system and universe as a whole significantly. Given the exorbitant costs of spacecraft and their launching into orbit, their lifetimes are regularly revised upwards. The current target for the new generation of satellites is at least 15 years of operation in orbit. Many critical devices in vacuum technology, like spacecraft, involve relative motion of contacting surfaces. Hence, the tribological stability of the components is a crucial concern in the efficiency and stability of these devices [9,10]. In this regard, these applications demand low friction (COF in range of 0.1 or even less) and low wear (specific wear rates below 10^{-6} $mm^3/N.m$), in order to achieve low power consumption, extreme reliability, high stability and highly precise sliding processes [11]. High reliability and great precision are must for space equipment such as satellites with no possibility for maintenance after launching [12,13]. Therefore, in the quest to achieve a mechanically ideal space machine, many

difficulties must be overcome, especially those related to tribology. Indeed, in high vacuum, it is very difficult to use liquid lubricant in an efficient way. Thus, in some parts, the interactions between surfaces only involve solids, which lead to a fairly radical behaviour. In general, contacts between metals lead to galling. On a spacecraft, if these kinds of problems arise, it is impossible to intervene, and the mission is usually compromised. On a satellite, many devices are operating under various mechanical and environmental conditions. Of course, until now, a number of solutions are already tried based on solid lubrication. However, designers and manufacturers of spacecraft industries are always looking for new and sustainable solid lubricants to widen the operating range of spatial mechanisms by obtaining more efficient solutions.

Despite the fact that space mechanisms are required to operate in vacuum conditions, they remain under ambient atmosphere during their assembly stage, testing phase, and storage [14]. Assembling is done in clean rooms with controlled humidity rate (55 ± 10%) and temperature (22 ± 3 °C) [15]. Once assembled, every single component has to be tested to certify that they will handle launch stresses and, then, properly function once in space [16,17]. Mechanisms are, therefore, tested either in vacuum, air, or dry N_2 environments. Specific equipment, such as those operating under cryogenic conditions, is tested under both standard laboratory conditions (clean rooms) and realistic working conditions. So, it can be said that the optimization of tribological needs in the space environment is challenging due to: First, the vacuum environment demands the use of materials with low vapour pressure. Solid lubricants become suitable here as they exhibit negligible vapour pressure. Secondly, is the inaccessibility of the application: since once launched, there is no opportunity to replace the lubricant or provide service to device. Some applications where solid lubricant coatings can be applied in spacecraft are actuators, space journal bearings and gearbox [18]. An actuator consists of a motor and a gearbox. The support bearings and gears operate at relatively low speeds, so solid lubrication is suitable [19].

Another important point is that the tribological requirements can vary between various parts of the gearbox. For example, the input phase (i.e., driven by the motor) operates at a higher speed and lower torque. In contrast, the output phase (i.e., that drives the mechanism) operates at lower speed and higher torque. As such, dissimilar materials

may be required to meet cycle life and load-bearing prerequisites for the gears utilized in the different phases. The interface of these devices is often a sphere-on-a-sphere or cup / cone arrangement. But, it is very rare to have area contacts, they are often line contacts (around the cup, cone, or sphere circumference) and so, generally, exhibit low Hertzian contact stress values, i.e., in the tens of megapascal (MPa) range [18].

Continuous research is going on for the development of a solid lubricant system capable of providing all the needs as mentioned above. As mentioned previously, the introduction of the PVD process for the deposition of coatings revolutionized the field of solid lubrication. Still, there are relatively few types of solid lubricant used on spacecraft. MoS_2 is the most commonly used [20]. Others include, PTFE and low shear strength metals (such as lead (Pb)), are used in niche applications, like ball bearings [21,22]. PTFE, although considered an excellent solid lubricant with low COF, its low shear strength limits its use to low loads only. Also, there is a limited use of hard coatings tailored to exhibit reduced wear and friction, such as TiCN [18].

Generally, an ideal solid lubricant has low shear strength and low surface reactivity, which is the basis for their low friction, but this condition may induce high wear rate, affecting their life span. So, an ideal requirement for a tribological spacecraft material is a low friction solid with high hardness; this means they should achieve the low friction of materials, such as MoS_2 or PTFE, but also exhibit a much lower wear rate. Diamond-Like-Carbon (DLC) and other hard carbon-containing coatings are very promising for specific niches, but they also present some drawbacks. In fact, the coatings are typically used in terrestrial applications. Still, they do not show interesting frictional properties in the vacuum of the space, since graphite requires some ambient humidity to provide the low friction and wear as they contain little or no hydrogen [23]. Contrarily, highly hydrogenated DLC (HH-DLC; 40 % H) coatings have shown different behaviour, in particular very low friction and wear in the absence of water vapour. In these coatings, H bonded to carbon atoms, effectively passivating their unoccupied sites [23]. HH-DLC was applied to races, cages and balls of thrust bearings and tested in a vacuum; they survived up to 1.7 million cycles compared to an uncoated one (less than 10000 cycles) [24]. Recently, it was proven they show an interesting performance when used with liquid lubricants [25]. Bearing failures are usually caused by lubricant loss or degradation. Cubic boron nitride (c-BN) is

another hard coating used for spacecraft [26] applications, showing low friction and wear values against CVD-diamond. However, when sliding against uncoated metals in vacuum, the COF became very high (0.8) against steel and 0.4 against aluminium. Thus, it is very important to understand the sliding behaviour with different mating conditions.

Nanocomposite solid lubricant coatings based on Transition metal Dichalcogenides (TMDs) are potential candidates for low friction and wear applications in dry and vacuum environments. The research on TMDs for aerospace applications started in the early '60s [27] and is now a subject of research for the past few decades [28]. Pure TMDs display remarkably low friction values of 0.1 down to 0.001 in dry and ultra-high vacuum conditions [29–32]. Their low friction behaviour is attributed to the crystal structure, which plays a vital role in the sliding process. A strong covalent bonding exists between the metal and the chalcogen atoms, while weak Van der Waals bonding prevails between adjacent layers, allowing the easy shear of the planes [28]. Despite the ideal conditions from the friction perspective, the low packing density (or porosity) and the presence of dangling bonds in sputtered TMDs not only decrease their load-bearing capability but also make them vulnerable to oxidation, moisture, and other environmental attacks. Additionally, pure TMDs fail to provide long-term durability and consistent tribological performances due to the exfoliation of the lamellar layers. These drawbacks, coupled with a low adhesion to the substrates, resulting in high wear of the TMD coatings. Ultimately, the coatings become unsuitable for efficient mechano-tribological applications.

Sputter deposited pure MoS_2 coatings are more vulnerable to humidity-induced degradation than burnished or bonded MoS_2 coatings since they usually display greater crystal defect levels and crystallite sizes. For example, surface chemical studies were conducted for the storage robustness of pure sputter-deposited MoS_2 coatings in ambient air atmospheres [33]. For samples stored in 100 % RH air for two weeks, the surfaces showed virtually the complete oxidation of the surface. Also, the samples stored in 100 % RH air for two weeks revealed a decrease in cycle life down to 240 cycles, compared to 10,000 cycles for unstored coatings. Newer coating growth techniques involving co-deposition of MoS_2 with additives, including metals and inorganic compounds, are producing coatings with nanocomposite structure [34]. These nanocomposite coatings show improved tribological performance and better humid storage reliability, due to either

a lower porosity (or higher density) or the passivation of the surfaces of the MoS_2 crystallites by the additives [35]. Besides, the coatings are harder, more fracture tough, and better resisting to wear [36,37].

To overcome the issues of pure TMDs, they were alloyed with different metals [38–47] and non-metals (e.g., C and N) [28,48–51]. Metal doping has shown beneficial results [41], but drawbacks, such as i) the detrimental effects of hard metal particles (e.g., Ti), ii) the abrasion of the tribo-films [52], iii) the rapid oxidation of the tribo-films into metal oxides [53], iv) the delamination of the TMD / metal multilayer interfaces due to thermal–cycling in space environments [54] and, v) the high COF and wear with the increase in the metal layer thickness [55], have limited their use. Additionally, the reactive sputtering of metals (in gaseous form) is not possible, and the use of multiple sputtering targets further adds complexity in the repeatability of the process due to the need for synchronization between the two cathodes. In the case of non-metals, carbon alloying has attracted both industry and researchers due to its impressive properties, but again, reactive sputtering is an issue. The carbon incorporation in reactive sputtering was tried by using precursor gases such as CH_4 or C_2H_2. In such cases, hydrogen can react with the chalcogen, not only changing the stoichiometry of MoS_2 but also becoming a contamination source [56].

Nitrogen alloying has been less explored but seems a more suitable option to improve the properties of TMDs. Pure nitrogen can be used for reactive sputtering, avoiding the contamination (by other elements) along with low operational costs [57]. Furthermore, when compared to carbon, a small amount of nitrogen can be sufficient to achieve a dense amorphous coating, further reducing the operating costs [58]. Moreover, the hardness improvement can be greater than with C doping, for similar C and N contents. In order to grow mechanically stable coatings, it is crucial either to prevent the easily sheared planes that are formed parallel to the sliding direction or to reduce the crystallinity of the soft TMD phase; this can easily be achieved by nitrogen alloying [59]. On the other hand, despite disturbing the crystalline structure of MoS_2 in the coating, N does not affect the crystalline tribo-film formation to provide the required low friction [52,60]. Mutafov et al. [61] reported that magnetron sputtered amorphous W-S-N coatings exhibited a low COF, high load-bearing capacity and good wear resistance. Isaeva et al.

[58], with a theoretical approach, reported that, during the sliding of W-S-N coatings, nitrogen was released from the contact region in the gaseous form (e.g., N_2, NO_2), without disturbing the formation of the tribo-films. Ju et al. [62] recently reported that Mo-S-N coatings showed higher oxidation resistance due to the formation of Mo-N bonds. Zhang et al. [53] reported that incorporating a small amount of nitrogen into MoS_2 sputtered coatings produced a nanocomposite structure, increasing the hardness and reducing the wear. Similar works were also reported by Nossa et al. [63].

To overcome the gap of a suitable solid lubricant coating for vacuum applications and identification of the promising results of TMD-N coatings, an effort is made in this thesis to deposit and optimize Mo-S-N coatings. This research is performed purely in industrial deposition environment by utilizing a deposition setup that reduces the operating cost by only using one sputtering target of MoS_2. There are still some problems in relation to adhesion, particularly if we do not want to use any additional metallic interlayer. The deposition is highly controlled to replicate and simulate a large-scale deposition. Many shortcomings, like the low adhesion of the coatings to the substrates, can be overcome with a suitable choice and development of new interlayer material without compromising the cost. The enhancement of the mechanical properties, as well as the stoichiometry of MoS_2 in Mo-S-N coatings, the optimization of their morphology and structure and, finally, their efficiency in vacuum environment sliding, are the focus of this research. The tribological analysis is carried out, for the first time, in a way to replicate the actual industrial needs by using very low contact pressures. The used Hertz contact pressures are in the range of those applied in space applications. Finally, a thorough investigation is carried out to differentiate the sliding tribological behaviour and tribo-film formation in vacuum and ambient air atmospheres.

1.1. Thesis Organization

Apart from the introduction section, the present thesis will be divided into seven chapters. **Chapter 2** describes the current state of the art on surface engineering, coatings and their deposition methods. The literature search includes the basics of TMDs and, their drawbacks, including their adhesion to the substrates. The last section covers a description of the current state of the art on alloyed TMD coatings, especially, Mo-S-N and W-S-N.

Chapter 3 deals with the methodology used in the current study. The substrate materials, the deposition procedure and the characterisation tools used during this research are specified. **Chapter 4** deals with the study of the adhesion of Mo-S-N based coatings. A detailed study of the interlayer optimization is presented. In **Chapter 5,** the basic characterisation of the deposited Mo-S-N coatings is discussed. A detailed analysis of the chemical composition, chemical bonding, structure, cross-section and surface morphologies, surface roughness, hardness and scratch resistance of the coatings are described. **Chapter 6** presents the tribological properties of the Mo-S-N coatings. It begins with the vacuum tribology study consisting of 3 different testing geometries: (i) steel cylinder versus coated flat, (ii) coated cylinder versus steel flat and, (iii) coated cylinder versus coated flat. Later, the study of the load variation for the coated cylinder versus coated flat geometry, during vacuum testing, is described. The best among Mo-S-N coatings is also tested for its endurance and behaviour in ambient air. **Chapter 7** presents the issues of Mo-S-N coatings in an ambient air atmosphere. This study is performed with high contact stresses, and the HR-TEM analysis of the wear tracks is discussed. **Chapter 8** deals with the general discussion, conclusion and future aspects of Mo-S-N coatings. It also presents the necessary care to be taken for the industrialisation of alloyed - TMD coatings.

1.2. List of Publications

A. Hebbar Kannur, K.; Yaqub, T. B.; Huminiuc, T.; Polcar, T.; Pupier, C.; Héau, C.; Cavaleiro, A. Synthesis and Structural Properties of Mo-S-N Sputtered Coatings. *Appl. Surf. Sci.* 527 (**2020**) 146790. https://doi.org/10.1016/j.apsusc.2020.146790.

B. Yaqub, T. B.; Hebbar Kannur, K.; Vuchkov, T.; Pupier, C.; Heau, C.; Cavaleiro, A. Molybdenum Diselenide Coatings as Universal Dry Lubricants for Terrestrial and Aerospace Applications. *Mater. Lett.* 275 **(2020)**, 128035. https://doi.org/10.1016/j.matlet.2020.128035.

C. Hebbar Kannur, K.; Yaqub, T. B; Pupier, C.; Héau, C.; Cavaleiro, A. Mechanical Properties and Vacuum Tribological Performance of Mo-S-N Sputtered Coatings. *ACS*

Appl. Mater. Interfaces 12 (**2020)** 43299–43310. https://doi.org/10.1021/acsami.0c12655.

D. Hebbar Kannur, K; Huminiuc, T.; Yaqub, T. B.; Polcar, T.; Pupier, C.; Héau, C.; Cavaleiro, A. An insight on the MoS_2 tribo-film formation to determine the friction performance of Mo-S-N sputtered coatings, *Surf. and Coat. Technol.* 408 (**2021)** 126791. https://doi.org/https://doi.org/10.1016/j.surfcoat.2020.126791.

Chapter II

2. STATE OF THE ART

This chapter deals a brief introduction on surface engineering and deposition methods. Afterwards, the current state of the art on solid lubricants will be presented which will include the basics of TMDs, the structural issues of TMD and the problems faced by the industry towards the successful large-scale deposition of TMD based coatings. Finally, the description of the current state of the art of alloyed TMD coatings will be shown with a major focus on the Mo-S-N and W-S-N systems.

2.1. Surface Engineering

Surface engineering is the study involving the modification of properties of a material / component surface over a depth of few microns (near-surface regions). This modification can be achieved by laser treatment, deposition of thick or thin coatings or by making composites. These engineered surfaces usually have properties different from those of bulk material. These modifications aim to obtain specific materials properties. The surface engineering can, for example, result in: (i) improved hardness and toughness, (ii) better corrosion resistance, (iii) improved tribological properties such as low COF and wear, and (iv) high-temperature resistance, etc...

In general, coatings are considered desirable, or sometimes necessary, for multiple reasons, such as, economic concerns, material conservation, unique properties, or the engineering and design flexibility that can be reached by having a different set of properties on the surface in relation to the bulk [64]. The coatings can be applied by various processes such as physical vapour deposition (PVD), chemical vapour deposition (CVD), electrodeposition, thermal spray, diffusion or chemical conversion, and ion implantation of a new material so that the surface layer is consistent between the parent and the newly added material. The extensive possibilities achieved with coatings made them as the most common approach towards surface engineering.

The coating / substrate together combines to form a composite material. This composite's behaviour will depend on the properties of these two components and the interaction between them. This interaction is mainly quantified in the form of the adhesion of the coatings to the substrate. For tribological applications, the coatings should be able to provide low COF and an improved wear resistance. Still, if the adhesion of the coatings to the substrate is weak, then, there are big chances that the entire system fails under the application of loads.

The selection of any deposition process will depend on several factors, such as: (i) the material to be deposited, (ii) the deposition rate, (iii) the substrate limitations (e.g., maximum supporting temperature), (iv) the adhesion of the coating to the substrate, (v) the purity of the target material, (vi) the cost and apparatus, (vii) the abundance of the deposition material in the world, and (viii) the ecological considerations etc… [64]. The coatings were initially used for decorative purpose, and, in recent times, their application was extended for many other fields such as optical, mechanical, electrical and tribological needs.

In the field of tribology, to reduce the friction and wear at the tribological contacts, solid lubrication has been in the study for decades. A mechanism to provide lubrication under relatively dry conditions, without liquid lubrication, where two surfaces are moving relatively to each other, can be defined as solid lubrication. Some important examples include graphite, soft metallic film (lead, gold, silver, zinc), non-metallic films (titanium dioxide, calcium fluoride, lead oxide, zinc oxide and tin oxide), PTFE, MoS_2, WS_2 etc. Solid lubricants were used, besides liquid lubricants (such as oils and greases), in the application where the later cannot be used as occurred in the inception of space program or space explorations. Solid lubricants are used as additives to oils or greases to improve the lubrication system. It has also been used in applications with large operating temperature variations, such as cryogenic sensors and turbopumps for liquid hydrogen / oxygen fuelled engines. They are also used in applications that possess material contamination issues such as optical components, where lubricants need to be kept in contact to prevent damage.

Other prominent applications such as slip ring assemblies, actuators, and journal bearings find solid lubricants [18].

There are many hindrances involved to implement an appropriate lubricant system in space equipment. It requires to have certain material properties which can tackle the challenges induced by vacuum. Therefore, one of the main properties is to have a material with low vapour pressure. Another challenge is the inaccessibility of the system when in application. The component, once in space, is difficult to repair or replace the lubricant [18]. This brings the requirement of having materials with long lifetime and less need of maintenance and, simultaneously, providing low COF and low wear rate. The material or lubricant system must also be efficient in various environments since, before launch; it should be kept on earth with a suitable resistance to environmental degradation [18]. A solid lubricant as powders or thin coatings are typically used for applications such as: (i) low to medium number of duty cycles, (ii) moderate to high contact pressures (approximately ~10 – 600 MPa), (iii) extreme environments, and (iv) low-speed contacts. The general properties that can make good solid lubricant are: (i) low shear strength, (ii) good adhesion to the corresponding substrates, (iii) low abrasion, (iv) thermodynamic stability in the environment where it is used, (v) low surface reactivity and, (vi) high hardness [65]. The usage of solid lubricants is not a remedy to be applied on any surface. A good selection of the substrate material to apply / deposit the solid lubricant is equally crucial while considering the application. Thus, it is important to evaluate and consider the use of solid lubricant in the design phase of the mechanism to prevent poor robustness and device failure. Other advantages of solid lubricant over liquid lubricant include electrical conductivity, stringent limits on the weights and wider operating temperatures [18].

A relatively small number of solid lubricants have been used for space applications, out of which, MoS_2 is the most commonly used [20]. Others options, such as PTFE and low shear strength metals (such as lead), are used in niche applications, like ball bearings [21,22]. PTFE, although considered an excellent solid lubricant with low COF, its low shear strength limits its use to only low applied loads. Also, there is a limited use of hard coatings tailored to exhibit reduced wear and friction, such as TiCN. PTFE is a crystalline

polymeric material consisting of arrays of long macromolecules held together by physical forces. The bonding within the chains is strong and covalent, while between chains the bonds are weaker, thus, providing one-dimensional low shear force. This structure is less likely to prone to chemical attacks by other atoms or molecules, resulting in a low-friction, low-energy surface. The formation of uniform transfer films of aligned molecular chains is appropriate under certain low energy dissipation conditions such as slow speed and low loads [18].

Diamond-like-carbon (DLC) is also considered as a lubricant that provides good mechanical and tribological results when used as coatings. This is the reason why its use has been very common in various industrial applications. The DLC, along with providing good mechanical strength to the coating, restricts its application depending on the type of environment tribological contacts because of its strong carbon bonding. The DLC has been well known to work properly in the presence of ambient air (humidity) and dry atmospheres but lack its usage in vacuum environment due to their very high COF values. The presence or addition of hydrogen can enhance their performance in dry atmospheres. Also, DLC are not very effective in high temperature (above 300 ^{0}C) since it will result in higher friction and wear [66–69]. Thus, there exists a major gap for a solid lubricant which can function in a vacuum and dry environment together.

When the synergy concept of surface engineering is considered concerning tribological properties, there are two different views: first, a hard substrate with a soft coating (with soft-on-hard feature), and a soft substrate with a hard coating (with hard-on-soft feature). In the first view, the concept is based on having a low shear strength material to provide easy sliding and relative motion between the surfaces in contact, then, low friction. The second, with the purpose of reducing the real area of contact to decrease the friction [70,71]. It is well known from Bowden and Tabor [72] that the frictional force is the product of the shear strength by the real area of contact; then, to achieve a lower friction, the shear strength should be reduced, or the interface should have smaller contact areas. Despite the quite high number of materials for solid lubrication, many limitations still exist, particularly when it is necessary to provide adequate lubricating performance under high

load and low-speed conditions [70,71]. Under such conditions, there are chances of formation of abrasive wear debris that accelerates the wear and degradation. So, a potential material that can provide efficient protection should provide enough hardness and good lubricating properties, preferentially using the wear debris to form tribo-films.

Among the solid lubricants currently in use, MoS_2 holds an extraordinary importance in modern technology in the last century [73]. MoS_2 being a lamellar material, possesses atomically planes that can easily slide against each other. MoS_2 has been used in release mechanisms, precision bearing applications, weather sensor bearings and gimbal bearings. Unlike liquid lubricants, MoS_2 is suitable for use in a vacuum because of its low outgassing pressure and lack of migration. Similar to graphite, MoS_2 is used as a dry lubricant as an additive in oils or greases. However, lubricant formulations containing MoS_2, with either epoxy binders or liquid dispersants, are unsuitable for use in vacuum, as outgassing can be a problem [41]. MoS_2 does not require ambient air atmosphere to perform well and, thus, it has shown to improve lubricating properties in the oxygen-deficient atmosphere [74]. MoS_2 was deposited using sputtering to provide successful lubrication for space journal bearings. However, due to its softness, poor adhesion to the substrates and non-reliability in terrestrial, ambient air atmosphere, it has not been considered for a wide range of applications [75]. The idea of depositing coatings with high hardness combined with low friction is still updated. If such coatings can be developed, combined with good adhesion, low wear rates should be expected, and very high load-bearing capacity will be achieved. Thus, the ideal direction to start into this hunt would be to improve the mechanical strength of transitional metal dichalcogenides (TMD) based material, known to be excellent from the frictional point of view but too soft due to their lamellar structure. The understanding of the deposition methods and the alternative of coating types can help in searching for the best solution. More details about the various methods to deposit a coating is given in next section.

2.2. Deposition Methods

With the initial success in the application of decorative coatings during the late 1950s, the use of deposition techniques has rapidly increased [76]. Moreover, the fast growth in micro-electronics during the last two decades, resulted in the development of many new deposition processes and procedures in the coatings sector [77]. The high number of new methods created the need to classify the coating processes based on their functions. For example, Kern et al. [78] have classified thin-film deposition technologies based on glow-discharge, evaporation, gas-phase chemical, and liquid chemical process. Chapman et al. [79] have suggested a classification based on the base procedure of the deposition process, such as conduction, diffusion, chemical, wetting and, finally, spraying. Holmberg et al. [76] and R.F. Bhunshah [64] divided the processes into four groups (gaseous, solution, molten or semi-molten) as shown in figure 2-1. Although there are many coatings deposition methods, not all are reliable and suitable for tribological applications. This is due to various reason such as poor bonding strength, thin achievable thickness, homogeneity, etc… Some of the deposition processes are mainly developed for decorative, optical or electronic applications. For the purpose of tribological coatings, electrochemical deposition, thermal spraying, CVD, and PVD are used. For the large scale and robustness, almost always the PVD method is considered.

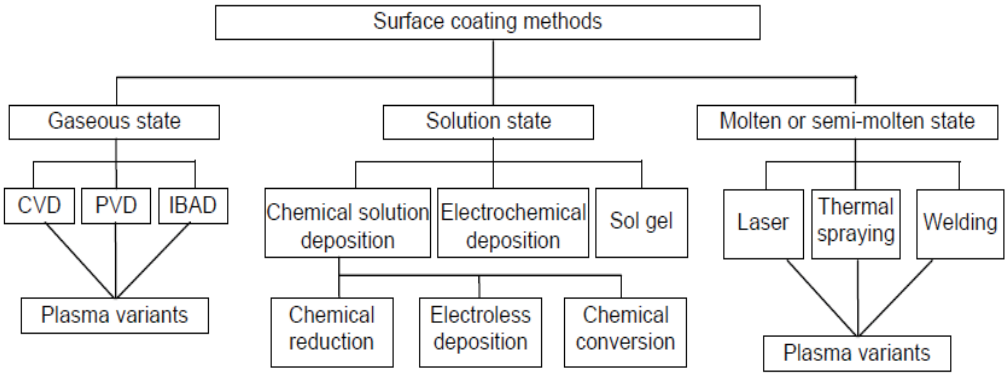

Figure 2-1: Various surface coatings methods (adapted from [77]).

2.2.1. Sputtering in Physical Vapour Deposition (PVD)

Sputtering is one of the PVD techniques for the deposition of atoms on a substrate, taking place in a vacuum. Three important components should be considered in sputtering, a cathode (target material that needs to be deposited), an anode (substrate materials on which deposition needs to be made) and a carrier gas (mainly argon). The target is connected to either direct current (DC) or radio-frequency (RF) power sources. The substrate can be either floating or connected to a DC, pulsed DC or RF power supplies. The anode and the cathode are placed inside a chamber with provision of gas inlets. The chamber is connected to primary and turbopumps to create the low pressure (secondary vacuum) needed to clean the chamber and to keep the appropriate pressure for the deposition runs.

Sputtering technique is mainly used to deposition thin coatings (thickness below 10 μm), based on a physical phenomenon to produce the atomic depositing species. When a fast ion strikes the surface of a material, the surface atoms can be ejected in consequence of a momentum transfer process. The ejected atoms or molecules can be condensed on a substrate to form a coating [64]. Several parameters are determinant to achieve a sputtering efficiency, i.e. the number of atoms ejected from a target per ion bombardment. For high efficiencies, not only the sputtering rate should be optimized but also an easy movement of the ejected material to the substrate should be achieved. Vacuum is therefore essential to meet these criteria. Low vacuum helps maintain high ion energies and avoid gas-atom collisions keeping high mean free paths [80].

In conclusion, the deposition rate of any material on a substrate surface will depend on the sputtering rate, the transport of sputtered species and the adsorption of the depositing species on the growing coating. Concerning the final characteristics and properties of the coatings, there many other parameters to be considered such as the discharge pressure, substrate temperature, substrate bias, rotation of substrate holder, voltage and current applied to the target and, finally, the cleanness of the chamber. There are various ways by which the target material can be powered for sputtering purpose such as DC, pulsed-DC,

RF and HiPIMS, etc... As this work is mainly focused on DC sputtering, further details will be given about this variant.

DC magnetron sputtering is one of the simplest and widely used technique for depositing metallic materials in industrial environments. The DC power supplies are cheap and simple to manufacture. In DC magnetron sputtering, the target is directly connected to an electric current requiring electrically conductive targets. The application of a DC to the target allows the ionization of the discharge gas simultaneously. Thus, many positive ions are produced within the chamber, which are, then, accelerated to the negatively biased surface of the target. For metallic materials, the deposition rates of several thousand nanometres per minute can be achieved. DC magnetron sputtering provides good adhesion to the substrate, minimal defect density, good uniformity and thickness control of the deposited films. Application areas include microelectronics, adhesive films, metallurgical coatings, decorative coatings or other metallic film deposition applications.

2.3. Plasmas in deposition processes

A glow discharge plasma utilized in a deposition process is a low-pressure gas that is partially ionized and will contain an equal number of positive and negative particles. The plasma occurrence is due to the mass difference between the electrons and the ions. When an electric field is applied to an ionized gas, the energy is transferred faster to the electrons than to the ions. Then, the kinetic energy from an electron can be transferred to a heavy particle in a collision having a high probability of excitation or ionization of the gas species. The production of these excited species and their interaction with the coating growth is one more parameter to control the final properties of the deposited coatings. Some examples of processes involving a plasma environment are: sputter deposition, activated reactive evaporation, ion plating, plasma-assisted chemical vapour deposition, plasma-assisted etching and plasma polymerization [64].

Among the many different ways to generate a plasma, such as, (a) DC diode discharge, (b) RF discharge, (c) electron emitter sustained discharge, (d) magnetron enhanced discharge, (e) microwave discharge, (f) vacuum arcs, and (g) plasma arcs, DC magnetron and microwave discharges will be discussed briefly since they will be the basis of the deposition process in this thesis.

DC magnetron configuration usually consist of an anode and a cathode in a low-pressure gas. The cathode (negative potential) attracts the positive ions from the edge of the plasma region, which are accelerated to impinge on the cathode. The energetic particles (ions and neutrals) impinging the cathode (target) cause the ejection of secondary electrons, which accelerate near the cathode, and collide with the gas species creating ions which sustain the discharge process. To sustain the DC discharge, the emitted secondary electrons must create enough ionization collisions to compensate their low emission rate (typically, for each bombarding ion only 0.1 secondary electrons are emitted). If the anode is brought too close to the cathode, the discharge is extinguished. Insulated surfaces cannot be utilized as a cathode in a DC diode as the charge build-up on the surface will prevent any ion bombardment. Any electrically insulated films deposited in a DC discharge will cause arcing through the films. In addition to causing the ejection of secondary electrons, the high energy ions and neutrals that impinge on the target surface will cause the physical ejection of surface atom (physical sputtering) by momentum transfer process. There are several advantages of DC diode configuration: (a) uniform plasma generated over large cathode area, (b) high power input, (c) simple and cheap yet, powerful power supplies, (d) repeatability of the process by controlling the geometry, gas pressure and target power. The disadvantages include, a) inability to bombard electrically insulated surface and, b) significant heating of the substrates by secondary electrons [64].

The other method to generate a plasma is by using microwaves. A typical example of microwave discharge is the electron cyclotron resonance (ECR) ion sources. Microwaves frequency uses 2.45 GHz. The microwaves are injected into a small volume at a certain frequency corresponding to the ECR that is defined by the magnetic field applied to a region inside the volume, where a low-pressure gas is present. The alternating

electric field of microwaves is synchronous with that of free electrons, thereby increasing the perpendicular kinetic energy. Later, these energized free electrons collide with the gas, causing its ionization if their kinetic energy is larger than the ionization energy of the gas atoms [64]. The ions produced can be accelerated by a bias potential and extracted from that volume to bombard, for example, a substrate with high ion energy. In the case of sputtering deposition processes, the ECR ion or plasma sources can be used to etch the substrates as well as to control the ion to neutral ratio of the species coming towards the substrates.

Overall, the use of a secondary plasma source along with a DC sputtering target could be beneficial to improve the coating thickness, densification and compactness of the coatings.

2.4. Classification of coatings

Ever since the effective application of titanium carbide (TiC) and titanium nitride (TiN) coatings on tools for cutting purposes, the availability of various types of coatings connected to tribological applications has significantly increased. In the tribological field, coatings are commonly classified as soft and hard based on their hardness [81]. If coatings are within 10 GPa hardness, they are considered soft, whereas those above are considered hard. Soft coatings, such as soft metals, polymers, some carbon-based compositions (like a-C: H DLC) and lamellar solids (including transition-metal dichalcogenides and graphite), are used for reducing friction, whereas hard coatings, such as oxides, carbides, nitrides, borides, and other carbon-based compositions (a-C: DLC), are accepted for improving the wear resistance, particularly the ultra-hard coatings which have an excellent abrasion resistance. Additionally, the coatings are also classified based on their thickness, as thick and thin. For thin coatings, the substrate is the load bearer, and the tribological response depends on the properties of the coating and the substrate. On the other hand, as for bulk materials, the whole load is supported by the coating in the case of thick ones [82]. Finally, the tribological coatings structure has changed with time from single layer to more complex

arrangements such as multilayer, gradient or adaptive concepts. Given the above considerations, basically, seven types of coatings groups can be considered as follows [83].

2.4.1. Single component coatings

Single component coatings are those comprising one single layer of only one material. Many commercial PVD and CVD coatings are of this type, such as TiC, TiN, CrN, CrC, TiAlN, TiCN, DLC, W_2C, MoS_2, soft metals or polymers. Sometimes, to enhance the bonding strength with the substrates, an adhesion interlayer is used. Except a few rare applications, when a combination of low friction and good wear resistance is needed, the usage of single component coatings is limited, and more complex structure is required [77].

2.4.2. Multicomponent coatings

Multicomponent coatings are made up of two or more components, in the form of grains, particles or fibres that offers additional possibilities to improve the tribological properties. With this approach, each component can provide one particular characteristic to the system allowing to achieve in the final a multifunctional performance. In the field of tribological coatings, these coatings have been extensively used for cutting applications, many times based on ceramic phases. Besides the improved friction and wear behaviour, these ceramic phases allow to improve the oxidation resistance, impact resistance and high-temperature hardness [70].

2.4.3. Multilayer coatings

The synergy concept of multicomponent coatings can be extended to the multilayer type where, in this case, the materials, each contributing with a particular functionality, are disposed in a stack of layers. The coatings can be of two types: (i) successive layers, starting from the substrate, of diverse composition to diminish the mismatch in chemical or mechanical properties between the final functional coating and the substrate, thus improving the adhesion between them; (ii) periodical repetition of layers of two or more

materials. From the perspective of tribological applications, besides the multifunctionality that can be achieved, the alternating layers / interfaces can act as crack-stoppers by providing either a tough medium through which the proliferation is dismissed or allowing the crack deflection at the boundaries between the layers [77].

2.4.4. Nanostructured coatings

Nanostructured coatings consist of coatings containing grains with size in the nanometer range. In this type, nanocomposite coatings are also included, showing the synergetic effect of different phases but now at a nanometric dimension; the combination of amorphous and crystalline phases are often used inside this approach. Generally, with decreasing the grain size, the yield strength, hardness and the toughness can be significantly improved [77].

2.4.5. Gradient coatings

The functionally gradient coatings are improved versions of the multilayer system to tailor the microstructure of the coatings. Any sudden change in the physical, chemical and mechanical properties between the layers and the substrate can induce significant residual stresses at the interfaces causing failure in the form of detachment or cracks. Thus, a gradient transition from the substrate to a different layer, and / or between the layers, is preferred. For example, to improve the load-bearing capacity of DLC coatings for low friction under high normal load, Voevodin et al. [84] had designed a metal-ceramic functional gradient stacking. Ti-TiN-TiCN-TiC-Ti-DLC gradient layer was designed over a steel substrate, which provided low COF with low wear rate.

2.4.6. Superlattice coatings

Periodically repeated multilayer coatings with a thickness of each individual layer in the range of 5-50 nm are known as superlattice coatings. The best examples of superlattice coatings are TiN/WN, TiN/CrN, TiN/TaN and TiN/MoN, which in comparison to single layers can improve the hardness, toughness and thermal stability [83].

2.4.7. Adaptive coatings

Adaptive or chameleon coatings are those which can alter their properties to adapt to the running conditions. A well-known example was a solid lubricant composite made of metal-oxides and TMD (PbO/MoS_2, ZnO/MoS_2) which was able to operate in a wide temperature range [85]. The oxides displayed a better lubricating performance under high temperature (500 – 800 °C) while TMD gave a suitable response below 500 °C [85,86]. Other examples are nanocomposite structures that combine carbides (TiC, WC) and TMDs (MoS_2, WS_2) embedded into amorphous carbon matrices [87,88]. The coatings had high hardness (27 – 32 GPa), that resisted to the wear, provided lubrication in dry nitrogen and vacuum, due to the presence of the WS_2 phase, and assured the lubrication in ambient air environment, with the DLC phase [89]. With the applied load and the change in the operating environment, the surface chemistry, structure and mechanical behaviour of the coatings are adapted to respond with a convenient tribological performance.

Based on the different coating types and structures, it would be useful to take the required characteristics from each subset and employ in one single coating system to make it an efficient solid lubricant. For example, superlattice effect can improve the hardness of coatings while gradient coatings help achieve an improved adhesion and low wear rates. Similarly, adaptive coatings can work in diverse sliding conditions. Combining all these useful characteristics in a single coating can tailor the needs for a highly efficient self-lubricating coating / solid lubricant coating. Pure TMDs, along with their main issues and later the alloyed TMDs, will be discussed in greater details in the upcoming sections. However, the main focus will be towards N-alloyed TMD coatings, as per the objective of this thesis.

2.5. Transition metal dichalcogenides (TMDs)

Transition metal dichalcogenides (TMDs): sulphides, selenides or tellurides of tungsten or molybdenum are well known for their lubricating properties [90]. MoS_2 and WS_2 are compounds with unique characteristics originating from an extreme degree of

crystalline anisotropy originated from their hexagonal structure. Therefore, TMDs have gained considerable attention in the research community for a variety of mechanical, electronic and optical applications [28,91–93]. TMDs have X-M-X lamellar structure in which M is a transition metal atom while Xs are the chalcogenide atoms. In a characteristic TMD structure, each metal atom is surrounded by 6 chalcogenide atoms and each chalcogenide is linked to 3 metal atoms. The bonding structure within the S-Mo-S sandwich plane is strong covalent type, while the planes are held together by very weak Van der Waal forces which result in interlamellar mechanical weakness [48,94], thus providing easy shear properties. The TMDs have also been used for their electrical properties. They have been considered for the replacement of silicon in electronic industries.

Despite the greater resistance to high-temperature oxidation of WS_2 [95], MoS_2 has been more widely studied due to its lower cost and lubricating performance in vacuum and dry atmospheres. Initially, MoS_2 coatings were deposited by burnishing [6], electrochemical process [7] and physical vapour deposition [6–8,29,96,97] techniques. Following the development of magnetron sputtering techniques, further research efforts have been carried out to deposit these coatings with crystalline and chemical properties, which have led to improvements on the tribological performance [8]. However, sputtered MoS_2 coatings exhibit porous morphology, which reduces their load-bearing capacity, oxidation resistance, adhesion to the substrates, and adversely affects the mechanical and easy shear properties [98,99]. TMDs like MoS_2 behave according to the Hertzian Contact Model [100], where the COF decreases as the normal load is increased. Specifically, the COF for MoS_2 is inversely proportional to the Hertzian contact stress, unlike solids that follow Amontons' Law, where the COF is independent of load [101]. This behaviour is caused by the low shear strength of TMD's, as opposed to harder materials where the COF is related to surface interactions.

The shear strength of a particular TMD is related to the ability of the crystallites to move relative to each other. The mechanical cohesion between crystallites would be expected to vary with differences in crystallinity. Bulk MoS_2 exhibits a shear strength of 38 MPa [100]. Pure sputter-deposited MoS_2 exhibits lower values for typical coatings (7

MPa) [101]. Pure MoS_2 coatings with high sulphur vacancy defect levels exhibit higher values (40 MPa) [102], and nanocomposite amorphous Au-MoS_2 coatings show yet higher values (83 MPa) [103]. The shear strength is also a system property and a material one as the values vary as a function of the applied loads / pressure and environments.

The mechanism of any TMDs to provide low friction is based on the formation of tribo-films with (002) basal planes aligned parallel to the substrate and the sliding direction. Usually, the as-deposited TMD would contain these hexagonal basal planes which can be random, (100) or (002) oriented depending on the deposition methods. E.g., it is possible to deposit very thin (002) oriented MoS_2 coating using PVD technique with a proper selection of the substrate and the deposition procedure [104]. If the coatings do not present this preferential orientation, to transform or reorient the basal planes parallel to the substrate, some energy and / or stress are required. These conditions are provided by the combined effects of the normal applied load and the sliding speed during testing of the TMDs coated sample. The formation of this tribo-films would require enough time for the transformation to occur from the as-deposited conditions, known as the running-in time. Many factors determine the length of the running-in time, such as the applied load, sliding speed, temperature, humidity, asperities or surface roughness, hardness of the coating, etc… The increase in the applied load would facilitate the formation of the tribo-film with the application of higher contact stresses. The presence of humidity would distract the formation of the tribo-film due to a process of oxidation [105]. Thus, most of the works on TMDs for low friction application focus on the easy formation of the tribo-films and reducing the moisture or the oxidation process. These procedures are easily met in a vacuum. Continuous efforts are underway towards finding solutions for TMDs to work in the ambient air environment.

Among various types of TMDs, MoS_2 and WS_2 were the most studied ones. The use of MoS_2 as lubricant for vacuum applications was considered in the first half of the twentieth-century [106]. MoS_2 has also been used as powder or additives in oil [107], as well as a paste in high-temperature operations [107]. Past studies showed that MoS_2 performed better in dry air compared to ambient air and even better in the inert gas

atmosphere [108]. It was only in 1986 that Robert et al. first utilized magnetron sputtering to deposit MoS_2 coatings with the main purpose to gain control over the coating properties [109].

The relative performance of various TMDs is basically related to the subtle differences in their electronic and crystal structures. For the case of WS_2, as a lubricant, it has virtually the same structure as MoS_2 with W belonging to the same group as Mo in the periodic table. $MoSe_2$, which is also a good lubricant, with Se is in the same group as S, but being a much more expensive option than MoS_2. A similar situation occurs with WS_2, in relation to which MoS_2 has demonstrated reliably superior at normal operating temperatures in vacuum [110]. Although selenides show somehow better frictional properties in ambient air environments than sulphides, their poor availability makes their penetration into the industry limited. There are several drawbacks which make TMDs into back foot in relation to other solid lubricants such as, environmental degradation, low hardness and adhesion problems. Next section explains more about drawbacks of TMDs solid lubricants.

2.5.1. Drawbacks of TMDs

Typically, the main problems that make difficult to use TMD coatings deposited by conventional magnetron sputtering, are:

- The deposition of TMDs by PVD leads to an inevitably disordered crystal structure, leading to the absence of the easy shear (002) planes, which play a very crucial role for the low friction. (002) cannot be achieved in sputtered coatings, except for very thin coatings not exceeding tens of nanometres [8,28].

-The sensitivity to environmental attacks, since TMDs are porous (partially due to their columnar morphology), oxygen, water vapour and other reactive species could easily penetrate the coatings and promote transformation [28].

-The hardness of TMDs is very low compared to other competitive coatings, such as DLCs. The hardness of TMD coatings is typically in the range of 0.3 to 2 GPa depending on the stoichiometry, morphology and deposition conditions [28].

-The adhesion to steel substrates is very low. The TMDs crystalline structure is prone to delaminate or cohesively detach parts from the coatings. Thin metallic interlayers, typically Ti or Cr, have been tried but the adhesion / cohesion is still limited. Consequently, the load-bearing capacity is very low, and frequently the TMD coatings peel off the substrate or the metallic layer under high contact pressure [28].

Most of the issues mentioned above have been extensively studied in literature aiming to tackle and improve the properties. Researchers have tried: (i) alloying TMDs with other elements (such as Cr, Ti, Au, C, N) [38–45,111–114], amorphized the TMDs structure, develop multilayer design and pattering, etc… [28,115]. However, these approaches are less reliable and still far from industrialization. Some of the major and vital adhesion important approaches reported in the literature are summarized in the next section.

2.5.2. Adhesion of TMDs

Adhesion of TMDs with steel was quite low from the macroscopic point of view. The load-bearing capacity is very low, and TMD coatings peel off the substrate under high contact pressure [28].

Lloyd et al. [116] studied the adhesion of single and few-layer MoS_2 fabricated by CVD process. The adhesion energy of monolayer MoS_2 was higher than the samples with few layers (two to five). A perfectly crystalline lamellar layer in (0002) orientation is formed, which is possible only in CVD process but unachievable with a PVD deposition. Due to gas desorption in a PVD system, the possibilities are low to obtain highly crystalline pure MoS_2 coatings. The deposition of TMDs by PVD leads, inevitably, to a disordered structure. The low-friction preferable orientation, (002), cannot be achieved except for a very thin coating not exceeding tens of nanometres [28]. The issue of low adhesion is also persistent due to the presence of water vapour or oxides between the substrate and the coatings [117]. Therefore, a high purity of substrate surface is required. . Those impurities will form active sites (H_2O or -OH groups on the surfaces) for reaction with the incoming sputtered species. Various methods have been developed to improve the adhesion of the

coatings to the substrates, either steel or silicon wafers. Bertrand in 1989 [118] described the need to heat the deposition chamber in a vacuum, before deposition, to remove all the active sites on the substrates. If the active sites can be removed, the TMD crystallites will form in order to achieve the lowest surface energy, i.e. with the basal planes parallel to the substrate in order to minimise the interfacial energy. The active sites are present normally at high energy locations such as ledges, kinks, and grain boundaries. Heating of the chamber along with the substrates is required to desorb all the water molecules present on the chamber walls and substrates. The heating should be performed while pumping to remove the moisture out of the chamber. The longer the heating, the higher purity of chamber will be. Another way to tackle this problem is by using titanium vapour. A titanium target was used initially to act as an oxygen getter. When Ti atoms are sputtered, they can react with O-containing species allowing to reduce the water vapour pressure in the chamber. Then, using to follow up of the coatings deposition, a titanium interlayer can be deposited which helps to improve the adhesion.

Inspired from the carbon coatings, some researchers also used chromium (Cr) as an adhesion layer for TMD coatings. The use of Cr with co-deposition increased the toughness and the load-bearing capacity.

The use of Ti or Cr as a metallic interlayer was considered a breakthrough in the deposition of TMDs to improve the adhesion of TMDs with steel. The use of Ti as a metallic layer to improve the adhesion was also extended to modify the properties of MoS_2, being the alloyed coatings known as MoST [41]. MoST coatings displayed an increase in the lifetime due to the improved mechanical properties of denser and harder structures while retaining a low COF. The scratch test results provided critical loads up to 81 N for the total failure and initial flaking from 52 N. Ti was specifically selected due to its mechanical strength, interfacial compatibility and high oxygen affinity [119]. Ti can also support the composite structure and absorbs oxygen when in contact. With Ti, the formation of fibrous surface morphology was eliminated, which resulted in a densified and compact microstructure. Furthermore, many reports suggest the improvement of the adhesion with the use of metal interlayer in the range of 300-700

nm between the substrate and coatings [120]. Some references in the literature refer that the improved hardness of the coatings, when deposited with a Ti interlayer, can be based on the better adhesion [121]. A Ti interlayer for MoS_2 deposition was first used by Wang et al. [119], who reported that the growth of MoS_2 columnar platelets could be effectively suppressed. Metallic interlayers were specifically used with a purpose of densifying TMD morphologies, increasing their mechanical resistance and improving the adhesion, ultimately converging towards higher wear lives [94].

Overall, the benefits of the use of Ti as interlayer can be expressed as follows:

1. With increasing alloying, stronger bonds arise because more grains are oriented with the basal planes non-parallel to the substrate.
2. The formation of transition layer of TiN or TiC between the Ti interlayer and the coating creating an interface zone of high cohesion [120].
3. The decrease of pore density promotes bonding between TMD-N and the Ti interlayer.

Nossa et al. [120] concluded that the adhesion improvement of W-S-C (N) coating through the deposition of a Ti interlayer is only effective if high contents of C or N are incorporated. This is due to the formation of a TiC or TiN phase between the coating and the Ti interlayer. Actually, they showed that spalling is the main reason behind the adhesion failure between the coatings and the Ti interlayer. Higher doping content was correlated with increasing critical loads. With increasing the doping element content (N or C), they suggested that inwards diffusion of these elements towards Ti interlayer led to a mixed interface between both layers, making it stronger and avoiding the spalling for low applied scratch loads [94].

Polcar et al. [121] reported the occurrence of detachment of TMD-C coatings due to poor hardness. The same authors [28] also suggested that the use of gradient layer from pure metal (e.g., Ti or Cr) to TMD-C, could improve the adhesion. In fact, the adhesion problems occurred at the interface between the metallic interlayer and the functional coating.

Even with the use of Ti or Cr as interlayer, the improvement in adhesion was not considerable. Simmond et al. [122] found values (~ 6 N) for Mo-S composite coatings co-deposited with Au, Ti, Cr and WSe_2 in spite of the use of a Cr interlayer. Such low values are similar to other doped TMDs without using any interlayers where the reason for adhesion failure is due to spalling [51]. The lack of adhesion is also considered the main reason for high wear of TMD coatings.

Along with all the issues of the metallic interlayers, in view of the industrialisation of TMD coatings with high adhesion cost is a very important remark. The use of metallic interlayer means using more than one target in the deposition chamber, which adds a significant operational cost as it requires an additional individual power supply (DC or RF) with independent control, eventually, with synchronization with the other power sources. If these drawbacks are taken into account, the advantage of using metallic interlayer can be seen as not so advantageous as expressed above. Thus, an innovative idea is required for the adhesion optimization of the coatings for industrial developments with the final aim of having high adhesion, low COF, and longer lifetime but at a much-reduced cost.

Other approaches could be found in the literature to improve the adhesion of TMD-based coatings. Liu et al. [123], in 1994, showed that without the use of any metallic interlayer, the adhesion of MoS_2 coatings could be improved based on the densification using N^+ ion implantation. The scratch critical load increased with increasing implantation energy as a result of the interfacial zones mixing. With the increase of N^+ implantation energy from 50 to 180 keV, the critical load (adhesion) increased from 22 N to 61 N. The film densification / compactness is due to the rearrangement of the deposited atoms and the vanishing of free space between the lamellae or grains [124,125]. An additional reason is the enhanced (100) edge plane orientation contributing for a strong adherence with the steel substrate. Daming et al. [126] showed that the critical loads could be significantly improved if TiN is used as interlayer instead of Ti. The authors used ion beam enhanced deposition (IBED) and magnetron sputtering (MS) to deposit MoSx coatings. IBED MoSx + IBED TiN showed higher COF, stronger

adhesion and longer wear life than MS MoSx + IBED TiN. The ion beam mixed interface between IBED MoSx film and the substrates led to an ideal line distribution of elements on both sides of the interfaces and, thus, resulted in stronger adhesion. The multilayered structure dispersed the accumulated stress by plastic deformation, and the stress evolution was interrupted at the layer boundaries, which positively affected the adhesion of the coating [127].

2.5.3. Alloying of TMDs

2.5.3.1. Metal alloying of TMDs

As it is well established, TMDs in their purest form possess low load-bearing capacity and low hardness which is due to their crystalline structure. The pure sputtered TMDs have a crystalline structure with a random orientation of the lattice planes. TMDs tend to exfoliate even at low applied loads causing delamination. This is primarily due to the weak Van der Waal bonding between the basal planes of the hexagonal structure. Therefore, the coatings wear faster and limit their lifetime.

The possible solution to overcome these issues is the addition of a third element to the coatings, which can disrupt the crystal structure and allow the growth of coatings more compact with the consequent improvement on the mechanical strength and the oxidation resistance. TMDs have been doped with different metals such as Ti [38–41,111,113,114], Ag [42], Al [40], Co [42], Au [43–45], Cr [42], Fe [37], Ni [29,42,45,128], Pb [30,45], Pt [42], Ta [42,129], W [42], Zr [130]. Regardless of the beneficial results [41], the industrial implementation of metal-doped MoS_2 coating is limited (e.g., MoST by Teer coatings [41]) due to either the rapid oxidation of the tribo-films into metal oxides [53] or the detrimental effects of hard metal particles (e.g. Ti) on the abrasion of tribo-films [52]. Moreover, economics do not favour the use of metal doping since this procedure requires a minimum of two targets for the PVD systems (i.e. one for the metal and one for the TMDs), consequently, increasing the costs for the processing and development.

2.5.3.2. Non-metal alloying

Non-metal doping (e.g. N and C) has attracted both researchers and industry [53,94,121,131] as a potential solution for making TMDs more used. Carbon introduction in TMDs was firstly reported by Voevodin et al. [132]. TMD-C coatings have been widely explored in the past few decades, owing to their attractive mechanical and tribological properties both in terrestrial and non-terrestrial environments. To deposit TMD-C coatings using only one cathode, the carbon incorporation was achieved by reactive sputtering, with precursor gases such as CH_4 or C_2H_2. In such cases, hydrogen can react with the chalcogen not only changing the stoichiometry of MoS_2 but also acting as a contamination source [56].

The other way to alloy TMD coatings is to use separate carbon and TMD targets in the PVD process. Additionally, some researchers have tried to use small C pellets inserted in the TMD target or vice-versa calling it a composite target. However, the efficiency and reliability of this solution rose several questions. Basically, the repeatability of the results, such as the chemical composition, structure and hardness of the coatings is very difficult to be achieved. The optimization process is also quite tricky, and the upscaling to industrial production is a cumbersome task. Thus, all these issues are not in favour of an efficient industrialization of TMD coatings alloyed with C. The nitrogen-alloying is thus an alternative and researchers have hardly studied it. The next section provides state of the art behind the nitrogen-alloying of TMDs coatings. Some of the tungsten disulfide (WS_2) alloyed with nitrogen alloying reported in literature is also presented as it behaves similar to MoS_2.

2.5.4. Nitrogen-alloying of TMD coatings

Nitrogen doping has been rarely explored but seems a promising strategy for changing the structure of TMD coatings. As a reactive process with nitrogen gas, the use of only one cathode (with the TMD target) is allowed, reducing the production complexity and costs, and avoiding the coating's contamination by other elements [57]. Moreover, when compared to carbon, a small amount of nitrogen can be sufficient to achieve a dense

amorphous coating, further reducing the operating costs [58]. In order to grow mechanically stable coatings, it is important to prevent the easily sheared planes from forming and to reduce the crystallinity of the softer phase, which can easily be achieved by nitrogen doping [59]. Mutafov et al. [61] reported that magnetron sputtered amorphous W-S-N films exhibit low COF, high load-bearing capacity and good wear resistance. The atomic-level structure and bonding arrangements in amorphous W-S-N have been described by Isaeva et al. [58]. They also reported that, during sliding, nitrogen is released from the contact zone in the gaseous form (e.g. N_2, NO_2) without disturbing the formation of tribofilms. Zhang et al. [53] reported that the incorporation of a small amount of nitrogen into MoS_2 sputtered coatings produced a nanocomposite structure, increasing the hardness and reducing the wear. Similar works were also reported by Nossa et al. [63].

Until now, most of the studies on the TMD-N (particularly Mo-S-N) systems were performed for a stationary substrate holder placed in front of the target; the effect of rotating the substrate holder for industrial purpose is still unexplored. Also, as per literature, the desired amorphous phase was achieved at the cost of a high nitrogen alloying and consequent sub-stoichiometry of the TMDs. Therefore, further studies are required to overcome chalcogen atom depletion with nitrogen additions. Another important shortcoming in TMD-N coatings is the lack of adhesion to the substrates, even after the use of metallic interlayers. All previous works related to TMD-N coatings report the use of Ti or Cr interlayers for adhesion improvement [51,126,133], with Ti being a more suitable option [41]. Nonetheless, Nossa et al. [94] showed that spalling occurred between the coatings and Ti interlayer during the scratch test, preventing the substrate exposure. Besides, TiN was also used as interlayer, which resulted in an improved adhesion over Ti, due to a good interface bonding between TiN and TMD coatings [126]. However, the drawback is the associated cost increments due to the use of an additional Ti target sputtering as well as the risk of Ti oxidation even with minor exposure of the gradient or interlayers. The next two tables summarize important results obtained for TMD-N coatings. The first table provides details about the deposition method (DC or RF), the target details with single or two targets (e.g., MoS_2 and Ti), biasing conditions, adhesion

improvement technique employed and the characterisation of the coatings. The second table is about the tribological testing results with COF obtained in relation to environment, counterbody used, sliding duration, etc...

Table 2-1: Main deposition parameters and characterization results of PVD magnetron sputtered TMD-N coatings reported in literature.

Deposition and Basic Characterization Details									
System	**Year**	**Deposition Method**	**Target Details**	**Bias Condition**	**Adhesion Improvement Technique**	**Coating-Substrate Adhesion (N)**	**N content (at. %)**	**S/Mo or S/W**	**Hardness (GPa)**
Mo-S-N-1 [123]	1994	RF	MoS_2	DC Bias 80 V	N^+ ion implantation source	22–62	–	1.2–1.6	–
Mo-S-N-2 [134]	2016	RF	MoS_2 + Reactive sputtering with N_2 gas	0 V	No interlayers	–	0–35	0.7–1.6	0.2–9.6
W-S-N-1 [51]	2001	RF	WS_2 + Reactive sputtering with N_2 gas	0 V	No interlayers	5–6	0–24.4	1.5–1.8	0.5–4.5
W-S-N-2 [135]	2003	RF	WS_2 + Reactive sputtering with N_2 gas, Ti	0 V	Ti interlayer	5.2–36.6	0–29	1.1–1.9	0.6–6.3
W-S-N-3 [136]	2004	RF	WS_2 + Reactive sputtering with N_2 gas, Ti	0 V	Ti interlayer	–	0–29	1.1–1.9	–
W-S-N-4 [120]	2005	RF	WS_2 + Reactive sputtering with N_2 gas, Ti	0 V	Ti interlayer	36.6	29	1.15	4.6
W-S-N-5 [60]	2013	RF	WS_2 + Reactive sputtering with N_2 gas, Ti	0 V	Ti interlayer	–	34	0.86	7.7
W-S-N-6 [137]	2014	DC	WS_2 + Reactive sputtering with N_2 gas, Ti	0 V	Ti interlayer	–	0–47	0.25–1.0	0.3–10
W-S-N-7 [138]	2015	DC	WS_2 + Reactive sputtering with N_2 gas, Ti	0 V	Ti interlayer	–	0–37	–	–
W-S-N-8 [61]	2015	DC	WS_2 + Reactive sputtering with N_2 gas	0 V	No interlayers	9–14	0-30	0.6–1.6	2.2–9

Table 2-2: Tribological testing parameters and COFs of PVD magnetron sputtered TMD-N coatings reported in Table 2-1.

Tribological Properties						
Ambient air Performance						
System	**Tribometer configuration**	**Applied load**	**Test duration**	**COF**	**Counter body**	**Humidity**
Mo-S-N-1	ball-on-disc tribometer-rotating	5.6 N	-	0.07 (pure MoS_2) 0.13 (for Mo-S-N)	100Cr6 steel	60% RH
W-S-N-1	Pin-on-disc tribometer-reciprocating	10 N	-	0.1-0.3	100Cr6 steel	60% RH
W-S-N-2	Pin-on-disc tribometer-reciprocating	5 and 10 N	-	0.08-0.20 (5 N) 0.11-0.22 (10 N)	100Cr6 steel	60% RH
W-S-N-3	Pin-on-disc tribometer-reciprocating	5 and 10 N	-	0.08-0.20 (5 N) 0.11-0.22 (10 N)	100Cr6 steel	60% RH
W-S-N-4	ball-on-disc tribometer-reciprocating	5 N	-	0.35	100Cr6 steel	60% RH
W-S-N-5	ball-on-disc tribometer-rotating	5 N	5000 cycles	0.008	100Cr6 steel	10% RH
W-S-N-5	ball-on-disc tribometer-rotating	55.8 N	5000 cycles	0.003	100Cr6 steel	10% RH
W-S-N-6	Pin-on-disc tribometer-reciprocating	5 N	10000 cycles	0.13-0.5	100Cr6 steel	50% RH
W-S-N-6	Pin-on-disc tribometer-reciprocating	5 N	10000 cycles	0.05-0.2	100Cr6 steel	1% RH
W-S-N-8	Pin-on-disc tribometer-rotating	1 N	3000 cycles	0.2-0.3	100Cr6 steel	45% RH
Vacuum Performance						
System	**Tribometer configuration**	**Applied load**	**Test duration**	**COF**	**Counter body**	**Vacuum pressure (Pa)**
Mo-S-N-1	ball-on-disc tribometer-rotating	5.6 N	-	0.04-0.06	100Cr6 steel	5×10^{-3}
Mo-S-N-2	Pin-on-disc tribometer-rotating	3 N	60000 cycles	0.05-0.1	100Cr6 steel	0.08

Dry Nitrogen Performance					
System	**Tribometer configuration**	**Applied load**	**Test duration**	**COF**	**Counter body**
W-S-N-4	ball-on-disc tribometer-reciprocating	5 N	-	0.05	100Cr6 steel
W-S-N-5	ball-on-disc tribometer-rotating	5 N	100000 cycles	0.03	100Cr6 steel
W-S-N-5	ball-on-disc tribometer-rotating	20 N	2100000 cycles	0.015	100Cr6 steel
W-S-N-6	ball-on-disc tribometer-reciprocating	5 N	10000 cycles	0.02-0.04	100Cr6 steel
W-S-N-6	ball-on-disc tribometer-reciprocating	5 N	10000 cycles	0.1-0.5 (humidity 50%)	100Cr6 steel
W-S-N-8	ball-on-disc tribometer-rotating	1 N	3000 cycles	0.08	100Cr6 steel

In summary, W-S-N were deposited initially using RFMS, and in later years, DCMS were also used. The use of Ti interlayer improved the coating-substrate adhesion critical load from 6 N to values as high as 36.6 N. The highest N content was about 47 at. % for W-S-N-6 [137] using DCMS, with a high hardness reaching up to 10 GPa, but it also resulted in the reduction of S/W ratio down to 0.25. All the tribological testing was performed using a ball-on-disc (flat) tribometer with applied Hertz contact stresses higher than 600 MPa. The COF values were lower when tested in dry nitrogen compared to the one in ambient air. There were only two reports on Mo-S-N coatings which will be explained in detail in the following.

Liu et al. [123] in 1994 studied the effect of N^+ implantation on MoS_2 coatings deposited by RFMS on bearing steel discs. A negative DC bias voltage of 80 V was applied to the substrates. The ion implantation was performed with ion energies of 50, 100, 150 and 180 keV; the ion influence was 1×10^{16} N^+ cm^{-2}. The tribological testing was performed in a rotating ball-on-disc tribometer with RH of 60 - 70 % and vacuum of 5×10^{-3} Pa. The uncoated steel ball (Ø = 8 mm) was loaded with 5.6 N, and the rotational speed was 1000 RPM). As-deposited MoS_2 coatings showed a loose columnar structure and, after N^+ implantation, an increase in the density was observed. 50%

reduction in the coating thickness was also observed. The high–energy N^+ has a compacting effect on the sputtered MoS_2 coatings; however, a decrease in the S/Mo ratio was also observed. This decrease is related to the different sputtering yields of Mo and S. In addition, the re-sputtering of surface atoms is also another reason for the decrease in the coating thickness. Regarding the structure, the as-deposited MoS_2 coatings presented a mixture of (002) and (100) XRD peaks, 47 % of (002) and 53 % of (100) peaks. With increasing N^+ implantation, the (002) peak intensity decreased in relation to (100) peak intensity. At 180 keV of N^+ implantation, that ratio was 18 % for (002) and 82 % for (100), showing that MoS_2 coatings have an enhanced (100) edge plane orientation character. Parallelly, the coating-substrate adherence increased from 22 N (as-deposited) to 61 N (180 keV). This enhancement is due to a better interface mixture between the coating and substrate. The tribological study in ambient air (RH = 60 – 70 %) gave a COF value of 0.07 for 0 keV (as-deposited) and 0.13 for all N^+ implanted MoS_2 coatings (50, 100, 150, 180 keV). In vacuum (5×10^{-3} Pa), all coatings gave COF from 0.04 to 0.06. The wear life improved with N^+ implantation of MoS_2 films by nearly 3-fold in both environments. The reason suggested for the increased COF was due to the dense structure and the decrease in the sulphur content caused by N^+ implantation. A lubrication model was also proposed. For the high energy N^+ implanted MoS_2 coatings, the friction led to a gradual reorientation of the crystal planes from (100) to (002) within the top layers, which led to a better wear life, higher adhesion and lower COF.

Zhang et al. [53] in 2016 performed a systematic study on the structure and tribological performance of Mo-S-N coatings. They used RFMS for the deposition of MoS_2 in N_2 / Ar mixture. The RF power on the target was 275 W, and the N_2 gas was varied from 0 to 50 sccm (0, 2, 3.5, 5, 20, 30 and 50), and Ar was fixed at 40 sccm. The N content in the films increased from 0 up to 30 at.% for increasing N_2 flow. The S/Mo ratio was reduced from 1.51 down to 0.70. The so low S/Mo ratio for pure MoS_2 coating was due to either the reaction of sulphur with the residual atmosphere (H_2O and O_2) or the preferential re-sputtering of S due to the argon neutral bombardment during the sputtering process [139]. The reduction of the sputtering yield of MoS_2 was also due to the poisoning of the MoS_2 target, forming a nitride compound layer on the target surface

by reaction with N_2. This effect is commonly observed in reactive sputtering, as for example, occurred for CrNx deposition [140]. The incorporation of N led to the decrease of both S/Mo and deposition rates, increase in the density, reduction of porosity and increase in hardness. S/Mo was below 0.7 for the highest N content in the coating. The microstructural analysis revealed that pure coatings showed long fibre-like platelets; with the N incorporation, a progressive densification was achieved until the morphology turned featureless. The incorporation of N suppressed the growth of the columnar structure resulting in more compact coatings. With the increase in N, XPS analysis revealed the presence of Mo-N bonding and the decrease in Mo-S peak. However, no nitride crystals were found by XRD analysis. The interruption of the MoS_2 crystalline growth with the N addition, causing a great structural disorder, was confirmed by XRD analysis. The hardness, elastic modulus and elastic recovery were improved with the increase in N content due to the increased density of the coating. Moreover, although MoNx crystal phases were not detected, the presence of an amorphous nitride phase, as revealed by XPS for the Mo-N bond, also contributed to the higher hardness. Thus, the mechanical properties and the load-bearing capacity of Mo-S-N coatings were reinforced with the addition of N. The tribological studies were performed in a rotating ball-on-disc tribometer against steel balls. The coatings below 20 at. % N showed a stable COF below 0.1 until 60000 cycles whereas, for the 28 at. % N coating, the COF drastically increased to 0.45 after 20000 cycles. The wear rates for pure MoS_2 coatings was very high, 40×10^{-4} mm^3/N.m, dropping progressively down to 5×10^{-4} mm^3/N.m for increasing N content. However, for the highest N content, the wear rate increased significantly, which can be associated with the increase in COF. The authors concluded that the strong reduction of the S/Mo ratio in this latter coating, with excessive incorporated nitrogen atoms, hindered the formation of the MoS_2 tribo-film at the contact surface, with the consequent increase in the COF and wear rate.

2.6. Research gaps

From the literature review presented above, the development of a coating system which can be utilized for space applications is still required. A coating having high adhesion, high hardness, low COF, low wear and long lifetime would be considered ideal. This coating would also perform reasonably well in ambient air since the space system can sometimes remain / tested in earth atmosphere before launching. This is a very important point when tested in ambient conditions; the coatings should not degrade or detach from the substrate, meaning that the coating system must possess sufficient adhesion. Most of the coating systems based on TMDs use metallic layers (e.g., Ti or Cr) to improve the adhesion, but industrially this solution brings additional costs.

From the literature analysis, N-alloyed TMDs such as Mo-S-N and W-S-N can be suitable candidates for coating systems for aerospace applications. Although there are some researches on TMD-N systems, an in-depth and organised study is still missing. Above, a detailed analysis of all the present Mo-S-N and W-S-N system has been already reported, and one of the main conclusions is that information on the improvement of the adhesion, even considering the use of metallic interlayers, is very scarce. Most of the literature (on TMD-N coatings) is for W-S-N system (as reported in table 2-1). Despite this focus, a uniform study towards the improvements in the adhesion and scratch-resistance of the N-alloyed TMDs is missing. Moreover, the literature reports only RFMS Mo-S-N system and no reference was done on DCMS deposition of the same type of coatings. The useful advantages of DCMS system are yet to be explored. For example, it is well known for TMD based coatings that a better chalcogen to metal ratio can be achieved with DCMS compared to RFMS. This would be an advantage when frictional behaviour is considered. The use of substrate bias favours the compactness of the coatings, thus improving the hardness. This has hardly been explored for any of N-alloyed TMDs. The literature also reports the possibility to improve the adhesion by nitrogen bombardment of MoS_2 coatings. Then, this is also a point to be further explored. The adhesion failures, by delamination at the coating-substrate interface during tribological testing or application, cause the loss of material or wear. This results in the complete failure of the coating system, no matter how

stoichiometric the TMD coating can be (chalcogen to metal ratio ~ 2), which is known to providing an efficient lubrication performance. Furthermore, the literature reports many incongruencies in relation to the composition, stoichiometry, compactness, hardness and COF. Additionally, the economic factors of using multiple targets were not discussed.

Therefore, considering all the issues mentioned above, a study is required where only one TMD target can be utilized that will be capable of depositing properly a coating tuned for high stoichiometry, compactness, adhesion and low COF. Having dense and adherent coatings will also be a focus to potentially reduce the effect of oxidation. An ideal situation would be to deposit a defect-free coating, with passive basal planes to prevent the reaction with the environmental species and, later, to provide a low shear strength interface. The coating must also show high hardness that can further reduce the wear rate.

Regarding the tribology, the space application would seek the requirement of having coatings tested in high or secondary vacuum environment ($<10^{-3}$ Pa). Hardly any study has been performed to test the coatings at high vacuum which can accurately simulate the space environment. TMDs are known to perform well in vacuum; thus, it is important to study them in this environment. From the application point of view, the space journal bearings operate with low speed and low to moderate contact pressure (10-150 MPa). Thus, the solid lubricants (here N-alloyed TMDs) need to be tested under low contact pressures. No studies with this focus have been carried out for any of TMDs. Although there is some literature reported on N-alloyed TMD (W-S-N) as referred to above, no detailed explanations are provided on the role / behaviour of nitrogen during tribo-testing. The tribological analysis in ambient air is performed for many W-S-N systems, but no convincing explanation was given to justify the high COF and wear. Among all the TMDs, MoS_2 is, for decades, one of the widely used additives due to its low cost, abundance in nature and ease of extraction from minerals. Thus, the study of this compound, especially as Mo-S-N system, should be a priority since it was one of the less explored TMDs, under the form of coatings. Finally, the process of tribo-film formation in vacuum and ambient air needs to be investigated and understood. This research will focus exclusively on the Mo-S-N system as it can effectively address all the research gap explained above. The

optimisation of Mo-S-N coatings will be studied, being the goal for the development of a reliable solid lubricant system for vacuum and ambient air.

2.7. Aims and objectives

PVD is a process to synthesize thin coatings with a great control of the chemical composition, structure, mechanical properties and tribological performance. The deposition and optimization of Mo-S-N coatings by PVD technique using DCMS will be the basis of this research. The optimization will be developed to make the coatings capable of reliable and efficient frictional performance for vacuum and ambient air environments. The literature suggests that the coatings for tribological needs should have high adhesion to the substrate, high hardness and ability to transform MoS_2, in the near-surface contact zone, in a crystalline oriented layer with the easy shear basal planes parallel to the substrates. The coatings should be dense and compact. DCMS will be utilized for the deposition of the Mo-S-N coatings since, (i) it has never been explored before for the deposition of this system and, (ii) it is a more appropriate technique for an easy upscaling for industrial dimensions. The depositions will be carried out entirely using a PVD equipment within an industrial environment complying all the future upscaling requirements and norms. The main objectives and tasks of this thesis are as follows:

- First, a systematic study will be carried out to identify the basic range of parameters for the deposition by DCMS such as cathode power, argon flow, etching parameters using plasma source, and pre-heating conditions, for depositing pure MoS_2 coatings. The etching of the substrates will be performed by bias etching with a different procedure as the one usually reported in the literature; an additional plasma source will be used. To optimize the adhesion, trials will be carried out to deposit a strong metal-metal layer with low sulphur content (low lubricious layer) using a single target MoS_2 deposition and strong bombardment with the additional plasma source. The substrate bias parameter will be the most important in this phase, and the adhesion will be preliminarily evaluated by Rockwell C indentation. Later on, a high flow of nitrogen will be introduced in the deposition chamber to avoid the formation of lamellar MoS_2 inducing the amorphisation and the reinforcing of the layers with

possible nitride formation. The substrate bias will be eventually reduced to a desired value slowly to increase and optimize the sulphur content in the coatings. The goal is to achieve a high adhesion of the coatings to the substrate, which will be analysed by Rockwell C indentation and confirmed by scratch testing. HR-TEM will be performed at the coating / substrate interface to understand the bonding characteristics.

- In a second step, the nitrogen content will be varied at the top layer of the coatings to optimize the tribological performance based on the thickness, chemical composition, chemical bonding, surface and cross-section morphologies, structure, roughness, hardness, reduced modulus and scratch resistance. The S/Mo ratio will be one of the most important information to understand the frictional performance. The substrate bias will be fixed after several trials to get a good compromise between the S/Mo ratio and the mechanical properties. HR-TEM analysis will be performed to better understand the structure of the coatings.
- In the next part, high vacuum (10^{-4} Pa) tribological studies will be performed using a cylinder-on-flat reciprocating tribometer. Commercial cylinders will be tribo-finished prior to the depositions and tribo-testing. Several mating pairs will be tested to identify the most interesting conditions to achieve low COF and wear rates. The variation of the load and an endurance test will be performed for the in-depth analysis of Mo-S-N coatings. The ambient air tribological study will also be performed on one of the nitrogen alloyed MoS_2 coatings.
- Finally, the coatings will be tribo-tested in vacuum (10^{-2} Pa) and ambient air using a ball-on-disc (flat) tribometer. This study will be carried out to compare low friction performance when high contact stresses are applied in comparison to the conditions in the cylinder-on-flat tribometer. The formation of the MoS_2 tribo-film, as well as the role of nitrogen within the Mo-S-N coatings, will be analysed using HR-TEM.

With the completion of all the tasks mentioned above, it is expected to have an optimized Mo-S-N coatings system that can be applied to industrial components.

Chapter III

3. MATERIALS AND METHODS

This chapter provides information on the substrate materials, the deposition equipment, and the characterization techniques used in the experimental work of this thesis.

3.1. Substrates

The following three types of substrates were used in this study:

(a) Si wafer (100)
(b) M2 steel flats (discs), and
(c) 100Cr6 steel cylinders.

Further details of each of these substrates are as follows:

3.1.1. Silicon wafer:

Silicon (Si) wafers with an orientation of (100) ± 0.5°, thickness of 500 ± 25 µm and diameter of 76.2 ± 0.3 mm (3 inches) were utilized for analysing the chemical composition, the surface and cross-section morphologies of the coatings. The wafers were cut to 15 mm × 15 mm size using a diamond pen cutter.

3.1.2. M2 steel flat (discs):

M2 steel flat discs having Ø 25 mm × 6 mm thickness were used to study the failure mechanisms of the deposited coatings using the calot-test, Rockwell C indentation and scratch test. In addition, the characterization of the coatings by ToF-SIMS, XRD, XPS, AFM, nano-indentation and tribometer testing was performed on the same substrates. Before deposition, the substrate surface was mirror-polished to achieve a roughness of 0.010 ± 0.005 µm. The composition and properties of the M2 steel are given in table 3-1.

Table 3-1: Properties of M2 steel [141].

M2 steel-Compositions and properties	
Element	***Content (at. %)***
Tungsten, W	*5.50 – 6.75*
Molybdenum, Mo	*4.50 – 5.50*
Chromium, Cr	*3.75 – 4.50*
Carbon, C	*0.78 – 0.88*
Vanadium, V	*1.75 – 2.20*
Silicon, Si	*0.20 – 0.45*
Manganese, Mn	*0.15 – 0.40*
Sulphur, S	*≤ 0.03*
Iron, Fe	*Balance*
Properties	
Hardness	*62 – 65 HRC*
Elastic modulus	*190 – 210 GPa*

3.1.3. 100Cr6 steel cylinder:

A commercially SKF's 100Cr6 steel cylindrical roller RC–10×10C, 10 mm diameter × 10 mm length was used as the counter body for tribological testing. These cylindrical substrates were tribo-finished prior to deposition down to a roughness of 0.011 ± 0.005 µm. Their composition and properties are shown in table 3-2.

Table 3-2: Properties of 100Cr6 steel [142].

100Cr6 steel-Compositions and properties	
Element	***Content (at. %)***
Chromium, Cr	*1.35 – 1.60*
Carbon, C	*0.93 – 1. 05*
Manganese, Mn	*0.25 – 0.45*
Silicon, Si	*0.15 – 0.35*
Copper, Cu	*≤ 0.30*
Molybdenum, Mo	*≤ 0.10*
Sulphur, S	*≤ 0.015*
Iron, Fe	*Balance*
Properties	
Hardness	*60 – 64 HRC*
Elastic modulus	*190 – 210 GPa*

3.2. Substrate cleaning techniques

The steel substrates were cleaned using *Umicore*® cleaner products. The first product contains fine alumina powder and ammonia for cleaning and partial removal of native oxide. The second product is based on an alcohol mixture to rinse the sample before drying. The Si wafer substrates were ultrasonically cleaned in acetone and ethanol for 10 minutes each before placement in the chamber. Once cleaned, the steel substrates were fixed to the substrate holder using tiny magnets while the Si wafers were first attached to a metallic clip and then fixed to the tiny magnets. Later, the substrate holder was then placed in the deposition chamber.

3.3. Deposition system

A direct current magnetron sputtering configuration, using a HEF-built TSD 400 small-sized industrial PVD machine was used in this study (figure 3-1). The chamber was equipped with a single cathode and an additional independent plasma source. A HEF patented electronic cyclotron resonance (ECR) plasma source is used as the additional plasma source [143]. The schematic top view of the deposition chamber is shown in figure 3-2.

Additional plasma source:

The additional secondary plasma source serves for the following:

(i) Etch the substrates to remove passive layers before coating.
(ii) To vary the ion to neutral ratio during the coating process.
(iii) To tune the plasma density or current density at the substrate by adjusting the plasma source power, independently of magnetron cathode parameters.

Figure 3-1: TSD-400 small size industrial deposition machine with one target and additional plasma source.

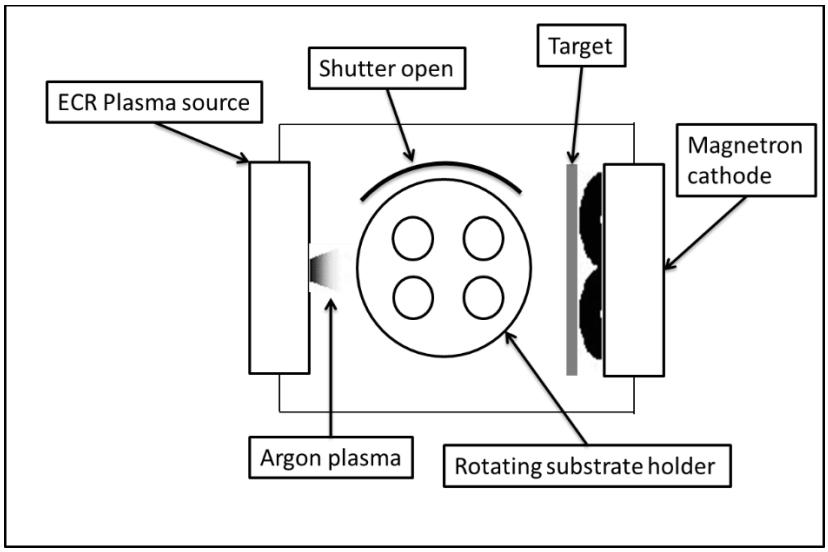

Figure 3-2: Schematic setup of the TSD 400 PVD chamber (top view).

3.3.1. Deposition process

Prior to the depositions, the chamber and substrates were heated to 150 °C for 5 hours with subsequent pumping to the base pressure of ~10^{-4} Pa, to remove any moisture and adsorbed contaminants. The secondary plasma source power was kept constant at 750 W for all the deposition steps. Sintered molybdenum disulphide MoS_2 target (450 mm × 150 mm × 5 mm, 99.5 % purity) was sputtered in N_2 and Ar (99.99 % purity) gas atmosphere. The MoS_2 target was brazed on a copper backing plate. The substrates were placed over a planetary (double rotation) substrate holder which was rotated at a speed of 5 RPM.

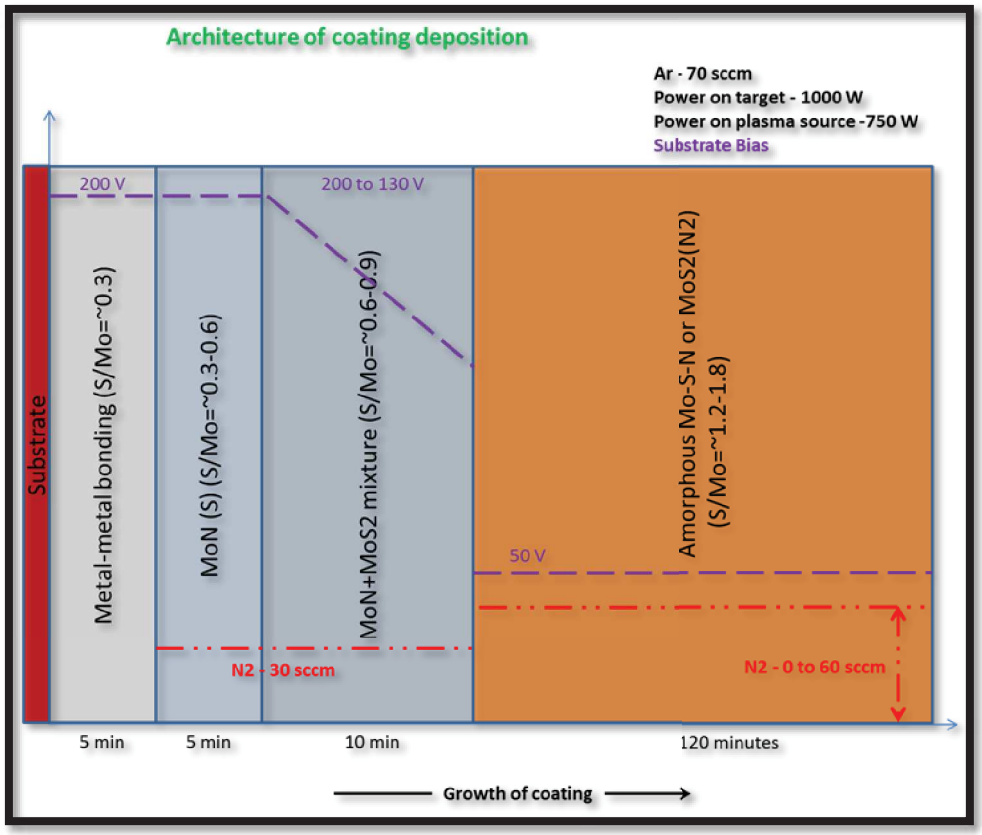

Figure 3-3: Architecture of the coatings growth.

After attaining the required vacuum, substrate etching was performed with Ar^+ ions bombardment by applying 150 V pulsed DC at 0.3 Pa for 60 minutes using the secondary plasma source (plasma etching). The target was sputtered cleaned for 7 minutes during the end of plasma etching, by applying 1000 W DC power (cathode power density = 1.48 W/cm^2). The first step in the coating recipe was the 20 minutes deposition of the '*novel*

gradient layers'. Initially, the Mo - rich layer was deposited under an energetic Ar^+ ions bombardment of the growing coating which resulted in the preferential re-sputtering of S atoms. The idea was to achieve a metal-metal bonding with the steel substrate. In the next steps, nitrides were deposited by introducing nitrogen keeping energetic ion bombardment in the gradient layer. Then, progressively, the ion energy (substrate bias) was decreased to incorporate more sulphur and produce a graded coating. After 20 minutes, the final coating was deposited in the presence of nitrogen. The substrates animated of double rotation motion underwent alternating exposure to the cathode (target) and the ion bombardment from the additional secondary plasma source. During the deposition of Mo-S-N coatings, the Ar gas flow was kept constant at 70 standards cubic centimetres per minutes (sccm), whereas N_2 gas flow was varied from 0 to 60 sccm to achieve different N content in the coatings (Table 5-1). The resulting process pressure ranged from 0.45 Pa to 0.70 Pa (Chapter 5). The detailed coating architecture was optimized after multiple preliminary depositions, to grow the coatings from sulphur deficient to lubricious coatings, as shown in figure 3-3. The preliminary depositions were made to fix the parameters of substrate bias, power on secondary plasma source on cathode (target). All the coatings were deposited with a negative pulsed DC substrate bias of 50 V to enhance the compactness. The pulse conditions were set at 250 kHz of frequency and 950 ns off-time duration (76.25 % duty cycle). The target to substrate distance was 100 mm at its closest position. The total deposition time was 2 hours in the N_2 reactive atmosphere. This deposition time was selected to yield a final coating thickness of 1.2 - 3.0 µm (figure 3-4).

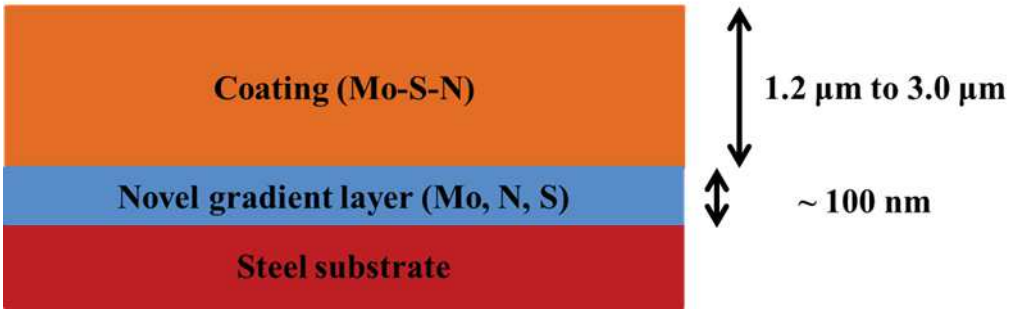

Figure 3-4: Schematic representation of the layer structure and thickness.

3.4. Basic characterisation methods

3.4.1. Calot-test

The Calot-test device (GENCOA Ltd, United Kingdom) consists of a steel ball (Ø 30 mm) which was rotated at 0.2 m/s over the coated steel substrate with dead-weight load of 1.0 N for 40 seconds. The coated substrate was firmly fixed so that it exposes only a point contact while testing. A drive shaft was used to rotate the steel ball. The grinding creates a crater through the coating and down to the substrate. Post-test analysis included optical microscopy imaging and calculation of the diameters of the two rings. The inner ring would correspond to the substrate, and the outer one corresponds to the coating. Any interlayers used can also be observed with its own ring corresponding to its location with respect to the steel. A simple formula was used to calculate the coating's thickness, as shown in figure 3-5 and equation (1).

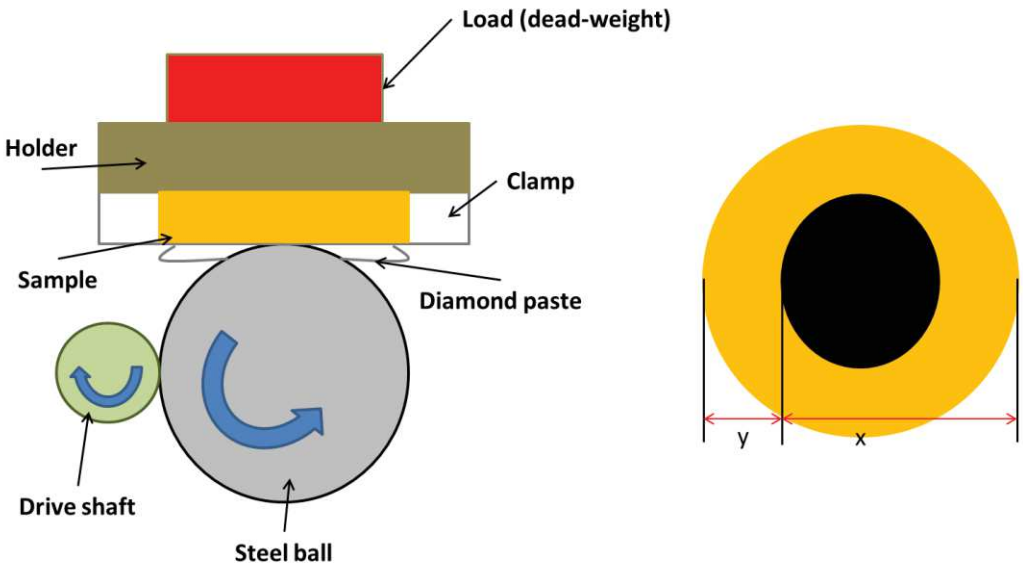

Figure 3-5: Representation of the Calot-test.

$$Coating\ thickness\ (t) = \frac{x.y}{Diameter\ of\ ball} \text{ ----------Equation (1)}$$

3.4.2. Rockwell test

Rockwell C test (Malicet & Blin, France) was performed to determine the adhesion and mechanical cohesion of the coatings. After the Rockwell C test, the flaking-off of the

coatings is a measure of the coatings adhesion or mechanical cohesion. A Rockwell C diamond indenter was applied on the coated surface at 1470 N (150 kgf) load for 20 seconds and pulled out. The size and type of the coating chipped off / cracked/damaged was observed using an optical microscope. Figure 3-6 shows different failure analysis criteria as observed on an optical microscope.

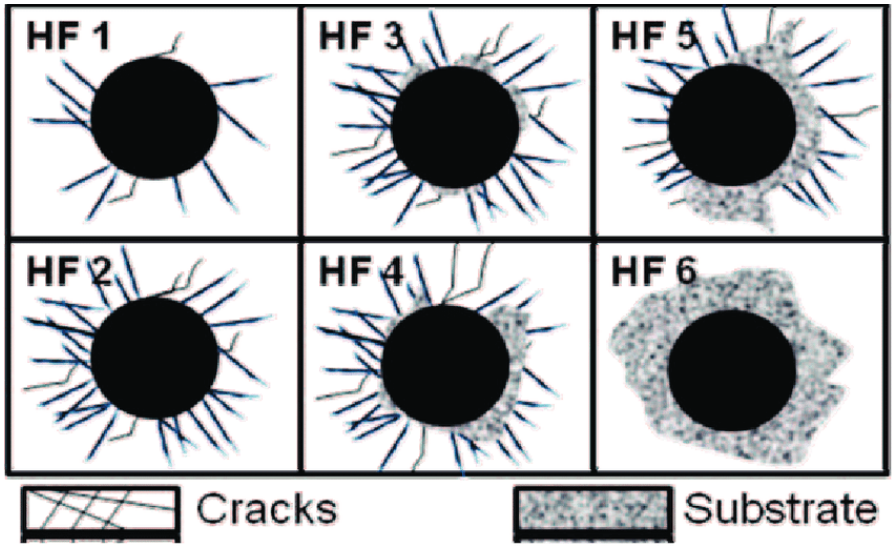

Figure 3-6: The Rockwell C adhesion test chart (adapted from reference [144]).

3.4.3. Scratch test

The integrity or the adhesion and mechanical cohesion of the coatings on the substrates was evaluated by scratch-testing (CSM Revetest). The coated flats were scratched as the normal force was gradually increased from 5 N to 80 N, utilizing a Rockwell indenter (tip radius: 0.2 mm, scratch speed: 10 mm/min and loading rate: 100 N/min). Later, the cohesion and adhesion critical loads were determined by analysing the scratches using optical and scanning electron microscopes.

3.4.4. Scanning electron microscopy (SEM)

The surface, cross-section morphologies and the thickness of the coatings were checked by field emission scanning electron microscopy (FESEM) (Zeiss Merlin). The coating thickness was also measured by SEM using the cross-sectional images.

(a) Wavelength dispersive spectroscopy (WDS):

The chemical composition of the coatings was determined by wavelength dispersive spectroscopy (WDS-Oxford Instruments) detector attached to FESEM. INCA software and 15 kV accelerating voltage were used. The calibration standards used in WDS were provided by Micro Analysis Consultants.

(b) Energy-dispersive X-ray spectroscopy (EDS):

A Jeol JSM-1100 SEM microscope with EDS facility operated by InTouchScope^{TM} software was used to determine the chemical composition. Some of the coated substrates after the Calot-test, Rockwell C indentation and scratch tests were also analysed by SEM / EDS for composition measurements and detection of any adhesion failure. The accelerating voltage used during the measurements was 5 kV.

3.4.5. Atomic force microscopy

Roughness measurements were performed using a contact mode atomic force microscopy (AFM) (Nanosurf AG, Liestal, Switzerland). To eliminate the external noise, the AFM was placed on an active vibration-isolation table (TS-150, S.I.S, Herzogenrath, Germany). The scans were performed at a rate of 1 line/s with the final image of 20 μm × 20 μm in size. The average roughness parameter (Sa) was considered as the roughness of the coatings. The tests were performed immediately after the deposition in order to prevent any possible oxidation damages or surface change.

3.4.6. Time of flight – secondary ion mass spectroscopy (ToF-SIMS)

A qualitative element analysis was performed using time of flight-secondary ion mass spectroscopy (ToF-SIMS) from ION-TOF. An analysis gun of Bi – 25 keV was used for sputtering of elements. One test was performed on each sample at an area of 50 × 50 μm^2 using a sputter gun with Cs^+. The depth profiling was performed in negative polarity, from the outermost surface to the substrate. The analysed surface was adapted to the area of interest. The size of the erosion crater was adapted to the analysis area to minimize the edge effects and the re-deposition. SurfaceLab software was used to treat the data. Each point of the profile was obtained from a mass spectrum, which allowed an elemental analysis throughout the probed depth. Thus, every element or contaminant present on either

the outermost surface or in the core of the layers or at the interfaces was automatically detected. According to the mass spectra analyses in negative polarity, the ionic species selected for the depth profiles were: H^-, C, O^-, NH^-, F^-, CN^-, P^-, Si^-, $^{34}S^-$, $^{34}SS^-$, Cr^-, Co^-, Fe^-, $^{92}Mo^-$, MoS_2^-, AlS^- and FeS^-.

3.4.7. Optical spectroscopy

Spectroscopic investigations of plasma and element-specific plasma analysis were performed to evidence the re-sputtering effects of sulphur from the growing coating. A quartz window (transmittance cut-off ~ 180 nm) was arranged with a view parallel to the substrate surface and perpendicular to the substrate–plasma source axis (i.e. magnetron and secondary plasma source), capturing light emitted from the plasma region between the plasma source and the substrate location. For spectral line recording, the fibre optic spectrometer (AVS-S2000) accepts light energy transmitted through the single-strand optical fibre and disperses it via a fixed grating across the linear CCD array detector. The obtained spectral intensities versus wavelengths were processed using SpectraWIN BASIC 5.0 software. The monochromator provides ~ 0.1 nm resolution of spectral bands collected over a 300–1000 nm range. The peak intensity corresponding to the wavelength of 550 nm was considered for sulphur and 811 nm for argon. These wavelengths correspond to the single ionized states of each element.

3.4.8. X-ray photoelectron spectroscopy (XPS)

X-ray photoelectron spectroscopy (XPS) was performed for the chemical bonding analysis. The samples were analysed in a KratosAxis Ultra HAS equipment with monochromatic Al Kα X-beams (hν = 1486.6 eV). The X-ray beam source's power was set to 90 W, and a charge neutralizer was utilized during the estimations. The survey spectra were captured by setting the pass energy at 80 eV with steps of 1 eV and a dwell time of 200 ms. The high-resolution spectra of the regions of interest were acquired utilizing a pass energy of 40 eV with steps of 0.1 eV and a dwell time of 600 ms. Sputter-etching was performed utilizing Ar^+ ion gun operated at 2.2 keV and current density of 2.2 $\mu A/cm^2$. Sputter-etching can lead to preferential removal of light elements and, thus, must be considered while analysing the results. The data collection and analysis were done at pressures lower than 10^{-6} Pa. The data was investigated utilizing the CasaXPS software.

The baselines of the spectra were obtained through the Shirley strategy, and peak fitting was completed using Gaussian-Lorentzian functions.

3.4.9. X-ray diffraction (XRD)

Grazing incidence (3°) X-ray diffraction (XRD) measurements were performed using an X-Pert Pro MPD diffractometer with copper $K_{\alpha 1}$ (λ = 1.5406 Å) radiation source. The scan was performed in a 2θ range of 10–90°. Step size used was 0.025°, with a time per step of 3 seconds. The structural analysis was performed to check the presence of MoS_2 in the coatings. The grazing incidence configuration is used to acquire depth-resolved structural information [145] and limit the X-ray beam's penetration depth. For thin coatings, there are possibilities of substrate influence the spectra as X-rays can penetrate some microns into the sample [146]. The data thus obtained provides the structural information of the material. Crystalline materials provide intense peaks resulting from the single crystals and preferentially oriented structures. The small grain sizes or randomly oriented grains causes broad peaks, and amorphous materials do not reflect any spectra peaks.

3.4.10. Nanoindentation

Nano-indentation (Micro Materials-Nano Test Platform) hardness measurements were performed using Berkovich diamond indenter under 3 mN load. Repeatability was checked by performing a total of 32 indentations at various locations. In order to avoid the influence of the substrate, all tests were performed with indentation depths lower than 1/10 of the thickness of the coatings. The load-displacement data obtained were analysed using the Oliver and Pharr method [147].

3.4.11. High resolution transmission electron microscopy (HR-TEM)

The microstructural and high-resolution (HR) TEM imaging was carried out using a probe corrected Jeol ARM 200F electron microscope operating in STEM mode at 200 kV acceleration voltage, and an image corrected FEI Titan^3 operating in TEM mode at 300 kV acceleration voltage. The lamellae were prepared by focused ion beam (FIB) using a FEI Helios Nanolab electron microscope.

3.4.12. Tribological testing in cylinder-on-flat reciprocating tribometer

Linear reciprocating sliding tests were carried out in secondary or high vacuum (at 10^{-4} Pa) and ambient air (20 - 25 °C, 20 - 30 % relative humidity) using a cylinder-on-flat tribometer (see figure 3-7 b).

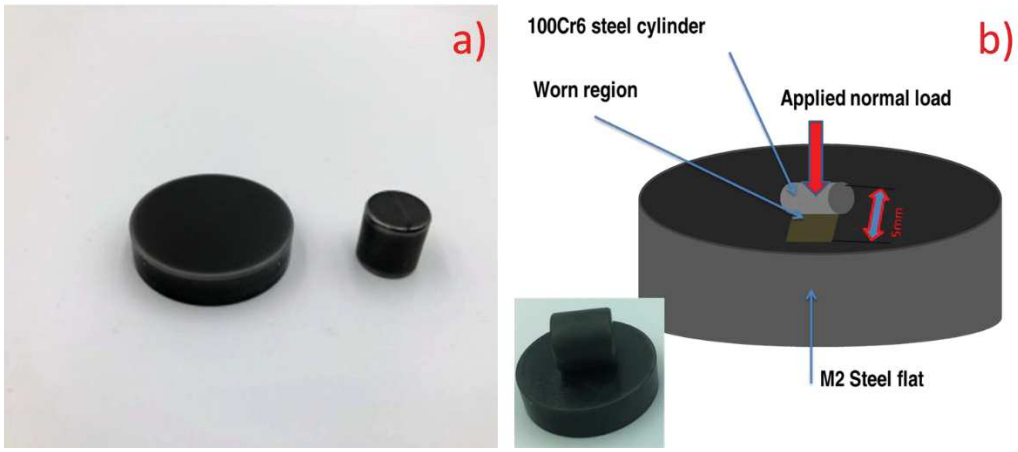

Figure 3-7: a) Image of the coated flat and coated cylinder post-deposition used in tribo-testing, b) Pictorial representation of the linear reciprocating cylinder on a flat tribometer.

The tribometer system has been designed for the cylinder to self-align on the flat surface. The cylinders were made of 100Cr6 steel, and they are used in manufacturing for roller bearings. Their geometry is very reproducible but not exactly a cylinder. It can be considered as a cylinder over the 4 mm centre in the middle of the length. There is a small bulge/curvature for 3 mm at each end of the length of the cylinder which impacts the initial contact stresses (see profile in figure 3-8 a)). This results in an initial effective line contact length of ~ 4 mm. The effective length can increase during testing because of wear, depending on the sliding parameters and mating surfaces (see figure 3-8 c)). Figure 3-8 c) and d) show the increase in the initial contact length after testing for a coated cylinder versus uncoated M2 steel flat. A stroke length of 5 mm and a linear speed of 2 mm/s were selected for all the tests. The tests were carried out at 5 N applied load, which resulted in a maximum initial Hertzian contact stress of ~ 95 MPa (typical of journal bearings). The tangential load was measured by a high precision sensor (FUTEK) connected to the data recorder (SEFRAM). **In Chapter 6,** The tests were carried out for 5000 cycles (equivalent

of 50 m distance) with each cycle comprising both to-and-fro motions (alternative linear tests). All the coatings slide sufficiently to achieve a steady-state regime.

Three different conditions of mating surfaces were tested during the tribological analysis: (i) Uncoated 100Cr6 steel cylinder versus Coated flat, (ii) Coated cylinder versus Uncoated M2 steel flat, and (iii) Coated cylinder versus Coated flat. In the last case, the coatings of the cylinder and flat were the same for each test. The sample displaying the best frictional properties in case (iii) was further tested at 2 N (contact stress ~ 60 MPa) and 10 N (contact stress ~ 135 MPa). Additionally, endurance testing in vacuum was also performed for one of the Mo-S-N coatings (Mo-S-N40) and was compared with pure MoS_2 coating. Later, one of the coatings (Mo-S-N40) was tested in ambient condition with all the three mating configurations similar to vacuum tests. The wear volume was calculated using MarSurf CM mobile 3D optical profilometer (MARS) and MountainMaps software (DigitalSurf). In the case of flats, the depth profile of the wear-scar was measured using 3D optical profilometry (BRUKER), and the specific wear rate of the coating was calculated as the worn material volume per sliding distance and normal load.

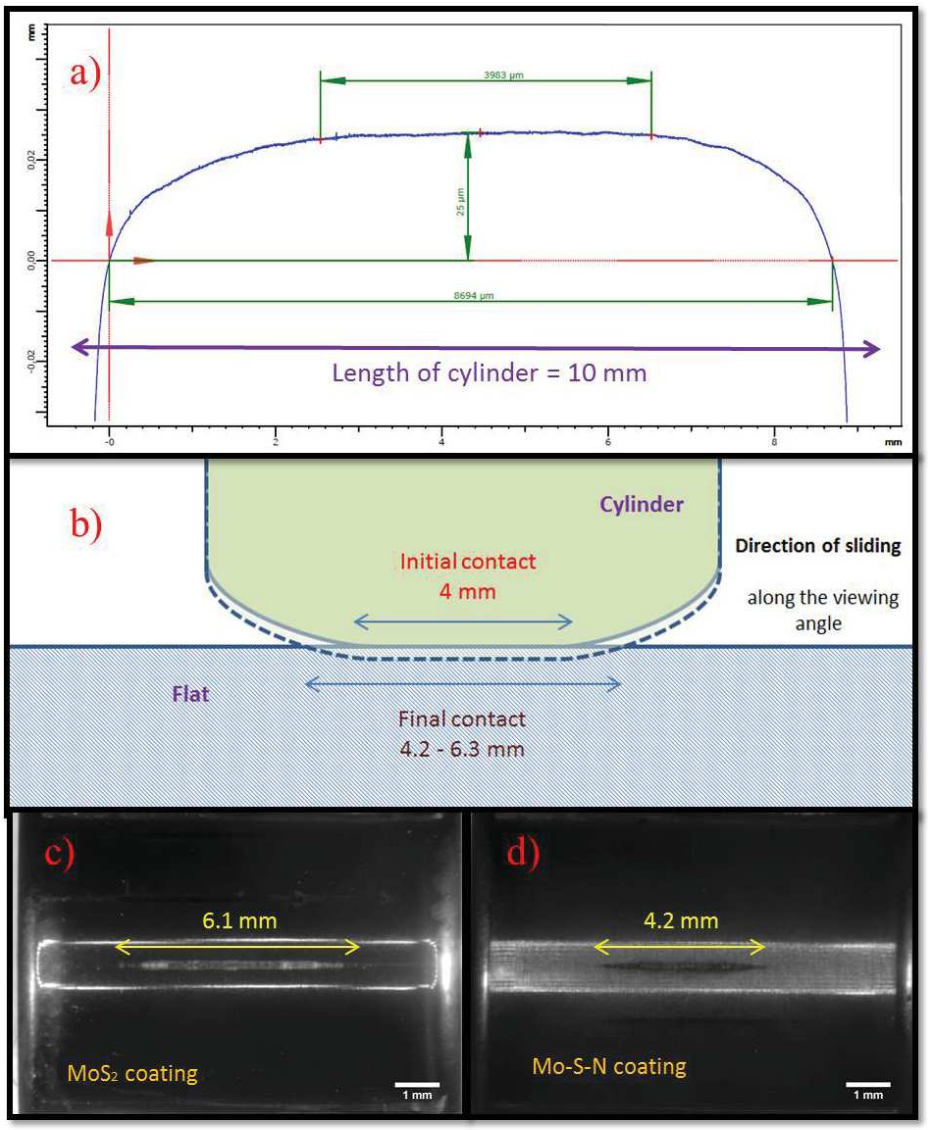

Figure 3-8: a) Profile along the length of the steel cylinder shows the bulge/curvature with ~ 4 mm of flat. b) Schematic view of an increase in the length of line contact with the evolution of wear. c) Worn length of line contact on MoS_2 coated cylinder, d) Worn length of line contact on Mo-S-N coated cylinder after sliding against M2 steel flat.

3.4.13. Tribological testing in ball-on-flat (disc) tribometer

The sliding tests were performed on a custom-built rotating ball-on-flat (disc) tribometer. The testing was carried out in vacuum (10^{-2} Pa) for 5000 cycles and in ambient air (24 °C and 20 – 30 % RH) for 10000 cycles. In all the tests, a 100Cr6 steel ball (Ø 10 mm) counter body, an applied load of 5 N (initial Hertzian contact stresses ~ 801 MPa) and a sliding speed of 50 mm/s were adopted. The wear track profile was plotted using 3D profilometer.

Chapter IV

4. COATING INTEGRITY – ADHESION AND COHESION

4.1. Introduction

This chapter deals with the enhancement of the integrity of the coating over the steel substrate. The characteristics of the *novel gradient layer (hereafter referred as gradient layer)* without the use of any third element developed in this work (as described in chapter 3), to improve the coating adhesion are covered in this chapter. The integrity, or the adhesion and mechanical cohesion, of MoS_2 and Mo-S-N with and without gradient layer, will be compared in relation to their scratch resistance. The basic deposition parameters of each of the layers, forming the gradient layer, are provided in table 4-1. As previously described in section 3.3.1 (deposition process), the top layer coating will be deposited above the gradient layer. The goal or the strategy behind this development was to start from a metal (here steel) to have a metal / metal bonding. Later, nitrogen is introduced before increasing the sulphur (by decreasing the re-sputtering effect). Therefore, if S becomes large enough, nitrogen prevents the lamellar structure from occurring. In this chapter, a Mo-S-N coating with 30 at. % N, later denoted as Mo-S-N40, is used for analysis of the gradient layer effects. The results narrated here are published as a scientific paper in a refereed journal, as shown in annex A.

Table 4-1: Basic deposition parameters of each layer.

	Substrate Bias (V)	Power on target (W)	Ar flow rate (sccm)	N_2 flow rate (sccm)
Layer 1	200	1000	70	0
Layer 2	200	1000	70	30
Layer 3	200 to 130 (gradient)	1000	70	30

4.2. Results

4.2.1. Rockwell C indentation evaluation

The preliminary test for the coating adhesion was made using Rockwell C indentation test. The test details are already explained in section 3.4.2. Figure 4-1 shows the differences observed with the use of a gradient layer as compared with the coating without its use. Figure 4-1 b shows a large delamination which is attributed to an adhesion failure. The single target deposition coupled with an additional secondary plasma source offered a remarkable improvement of the adhesive strength and integrity of the coating. This has been achieved without the use of any third metallic element interlayer (such as Ti or Cr) which is a widely followed approach. The proof and reasons behind such high adhesion to the steel substrates using this novel gradient layer are discussed in detail in this chapter.

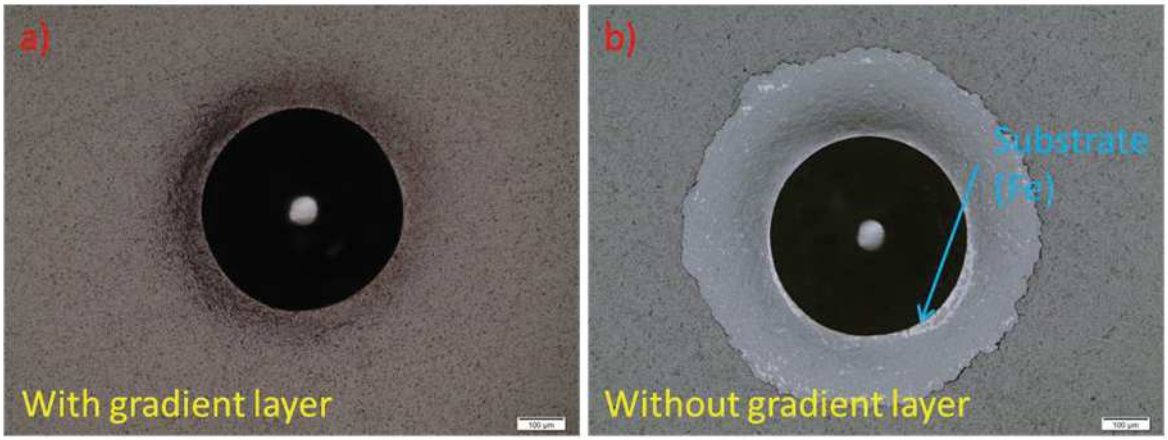

Figure 4-1: Mo-S-N coatings a) with and b) without novel gradient layer after testing for adhesion with a Rockwell C indenter. Based on ISO 26442:2008-06 coating adhesion classification guidelines, the coating with gradient layer follows HF1 and the coatings without gradient layer follows HF6 failure mode [148].

4.2.2. Scratch test

The effects of the coating architecture (*gradient layer*) on the scratch resistance behaviour of the pure MoS_2 and a selected Mo-S-N coating are shown in Table 4-2. The coatings deposited without the gradient layer had a substantially lower adhesive failure limit, while the introduction of the gradient layer in the coatings enhanced the adhesion

failure resistance beyond the maximum test range (80 N). No evidences of the delamination / penetration through the steel were observed. Therefore, it is clear that such an enhancement is solely related to the strong adherence achieved by metal-metal bonding (layer 1), induced by the deposition procedure.

Table 4-2: Table representing the cohesive failure limit and adhesive failure limit for pure MoS_2 and Mo-S-N coatings deposited with and without the novel gradient layer. The adhesive failure limit is beyond the tested load.

Sample	*Cohesive failure limit (Lc1)*	*Adhesive failure limit*
Pure MoS_2 coating without novel gradient layer	2.9 N	14.9 N
Pure MoS_2 coating with novel gradient layer	3.3 N	>80 N
Mo-S-N coating without novel gradient layer	1.6 N	22.8 N
Mo-S-N coating with novel gradient layer	35.1 N	>80 N

The tracks after scratch testing were analysed in SEM and are shown in figure 4-2. The testing procedure can be found in section 3.4.3. It was again observed that the gradient layer improved the scratch resistance (mechanical cohesion) of the coating. Large flakes were observed as a result of cohesive cracking in the coatings deposited without the gradient layer. Interestingly, the nitrogen-alloying further enhanced the adhesion and the scratch resistance.

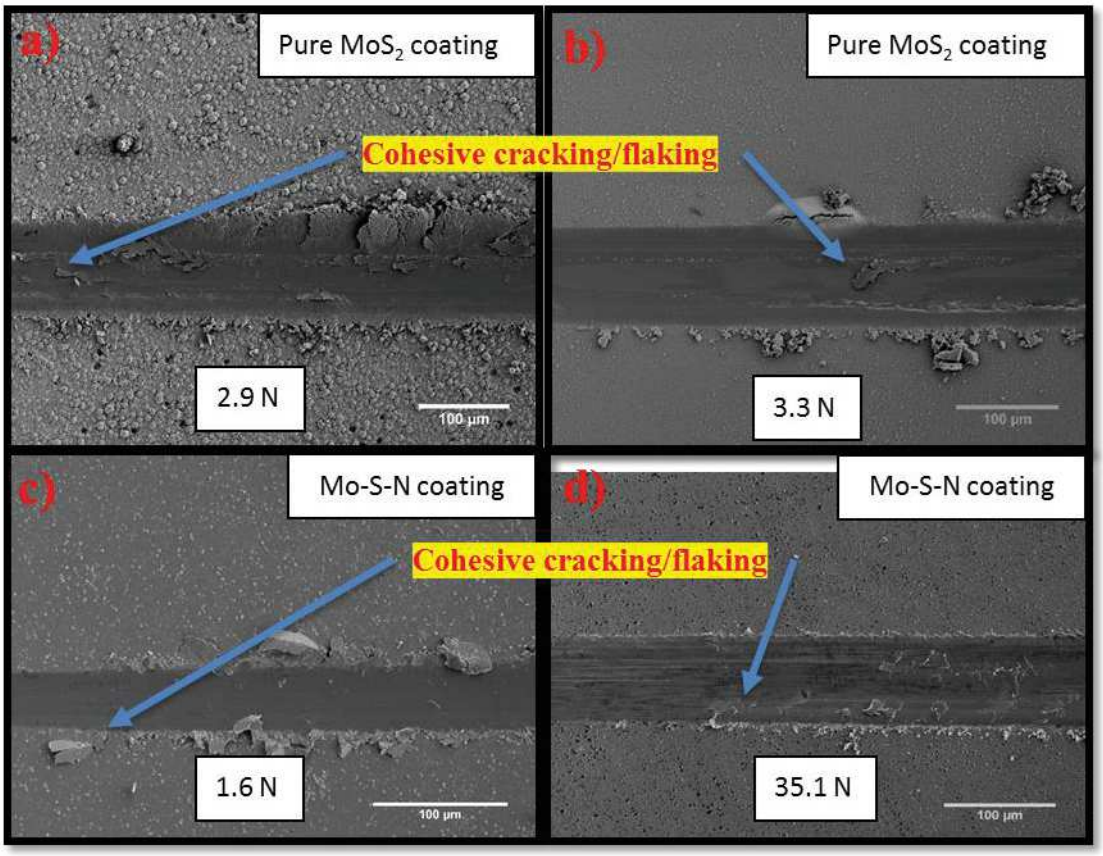

Figure 4-2: SEM images of cohesive failures of materials with MoS_2 and Mo-S-N with & without novel gradient layer. (a) MoS_2 coating without novel gradient layer, (b) MoS_2 with novel gradient layer, (c) Mo-S-N coating without novel gradient layer, (d) Mo-S-N coating with novel gradient layer.

Comparing figures 4-2 a and b, for the pure MoS_2 coatings without and with gradient layer, the cohesive cracking or flaking load is reduced for the former coating. This can be attributed to the lesser amount of columnar growth compared to MoS_2 coatings deposited directly on steel. In summary, lower flaking is achieved with the use of the gradient layer. Similar effects were observed when comparing Mo-S-N coatings (figure 4-2 c and d). Due to the more resistant layers in the bottom of the coatings, the deformation induced by the scratch indenter is less when the gradient layer is applied. Compared to the pure coatings, the improvement for the nitrogen-alloyed coatings is attributed to the formation of denser structures, disappearance of either the anisotropic behaviour or the easy shear structures, all preventing easy crack propagation. Thus, delamination or exfoliation of the lamella within the coatings is prevented, increasing the load-bearing capacity. The cohesive critical load with varying nitrogen content will be described in chapter 5.

4.2.3. High resolution transmission electron microscopy (HR-TEM)

In order to further investigate the mechanisms behind the high adhesion values (>80 N) and the scratch resistance, cross-sectional analysis was performed for the nitrogen-alloyed coating deposited with the gradient layer. Figure 4-3 shows HR-TEM images at the substrate-coating interface. At the substrate surface, a ~10 nm thick Mo - rich coating accompanied by an ultra-thin multilayer system with a periodicity of 5 nm was observed. The structural analysis showed that the first Mo layer forms the base for the growth of a nanocomposite MoN multilayer. The layer structure formation is caused by the planetary motion of the substrate holder and the alternating exposure to the magnetron cathode and the plasma source, providing the sputtered species and the nitrogen ions, respectively.

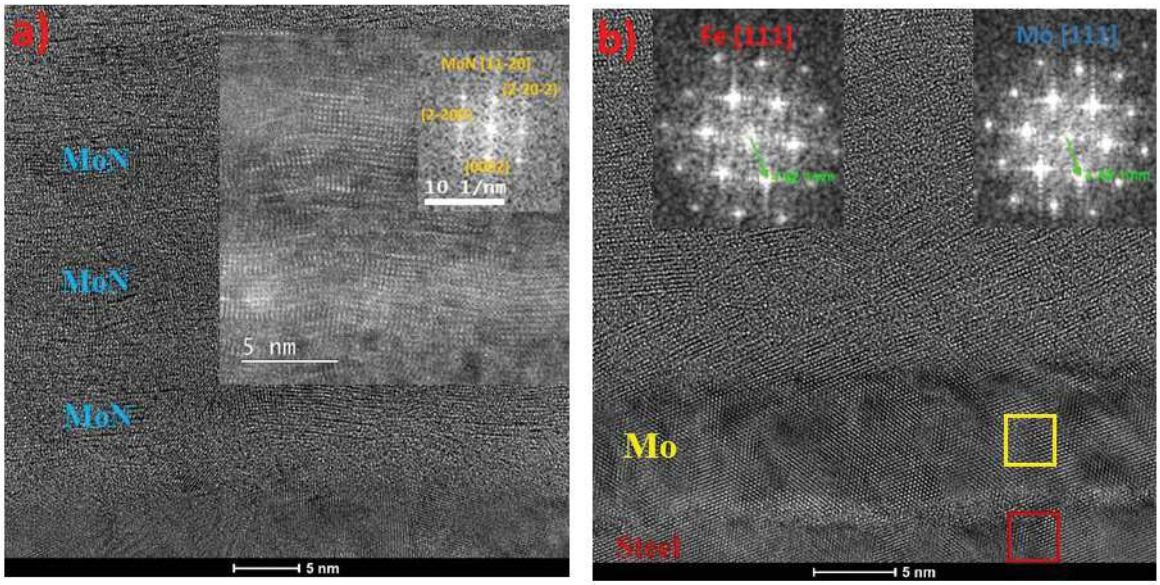

Figure 4-3: a) Microstructure of gradient layers - cross-section of as-deposited coating. b) The first layer Mo over steel, making metal-metal bonding with Fe, results in improved adhesion. Preferential re-sputtering of sulphur had caused this layer to be sub-stoichiometry (S/Mo = approx. 0.3).

Epitaxial stacking between Fe and Mo was observed along the substrate interface, as a result of a small lattice mismatch (7.3%) [149] between the two-unit cells, leading to a defect-free coherent crystal growth in large areas of the substrate. The first Mo layer becomes the seed for the formation of a laminar MoN composite. The hexagonal MoN provides an increased hardness and shear strength with the consequent superior mechanical strength of the coating. Nitrides are formed by selective removal of the sulphur through re-sputtering through the exposure of the growing to a high energy (substrate bias) nitrogen

ions bombardment (secondary plasma source). As shown in figure 4-4, the growth direction of Mo followed by the MoN-rich composition gradient layer (S deficient), is dependent on the orientation of the neighbouring substrate grains; therefore, the gradient layer changes the crystalline direction depending on the substrate interface orientation. For the Mo bonding layer to withstand the increased mechanical strain and to allow for plastic deformation without brittle failure under increased loads, coherent interfaces are required. Figure 4-4 shows examples of such atomic arrangements that occur due to the matching crystal structures of Fe, Mo and MoN.

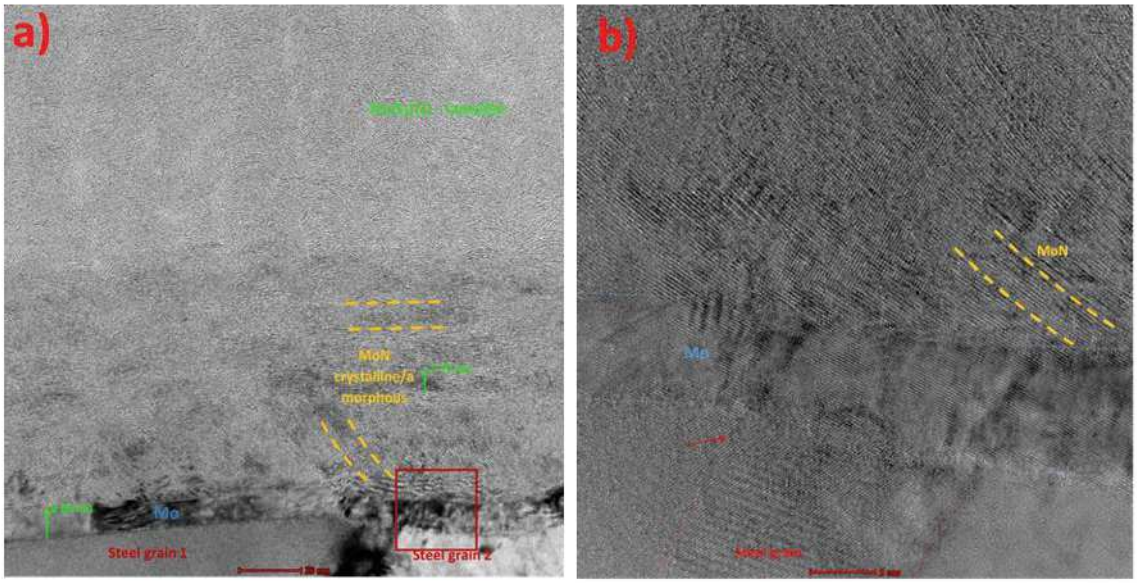

Figure 4-4: a) Morphology of the Mo/MoN(S) gradient layer. b) Epitaxial deposition of Mo and MoN on steel substrate; strong substrate interface.

4.2.4. Time of flight – secondary ion mass spectroscopy (ToF-SIMS)

To further characterise the *novel gradient layer*, especially the reduced S content and the layer contrast observed in HR-TEM, ToF-SIMS was carried out. This was an attempt made to measure the thickness of each layer and its periodicity as well as the qualitative composition of each layer. The results shown in figure 4-5 refers to a sample having the gradient layers (3 layers) plus a ~100 nm Mo-S-N layer (deposited with 30 at. % N) on the top. It should be noted that SIMS is based on the analysis of the sputtered material after ion bombardment. The sputtering process involves, usually, the preferential sputtering of some elements in relation to others. Therefore, many times [150,151] the

analysis of the interfaces can be blurred by this phenomenon. Also, during the SIMS analysis, a crater is formed. As the crater goes deeper, the shape of the crater becomes less flat, and the depth resolution is lost progressively. To prevent this drawback, the coating was made thin, especially for this analysis, i.e., the coatings was stopped at the point in the stack from where the analysis had to be performed.

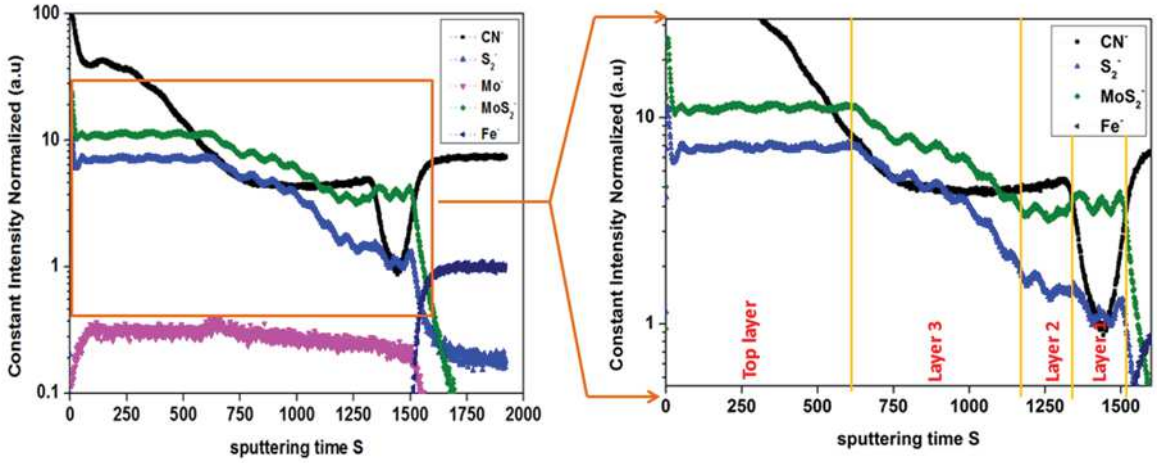

Figure 4-5: ToF-SIMS analysis of a sample with a gradient layer + Mo-S-N layer with respect to sputtering time. The normalised composition intensity means that the intensities of all signals were normalised with respect to the highest signal detected among all ions. The layer 1 is made with 200 V substrate bias without N, layer 2 is made with 200 V substrate bias with N, layer 3 is made with gradient substrate bias in presence of N and top layer is the Mo-S-N coating.

The values for the first 600 s of ion sputtering correspond to the Mo-S-N coating. The intensity of CN^- refer to the intensity of either C or N. For instance, in the coating, the intensity refers to N whereas, in the end of the sputtering, corresponds to the C from the steel. In the top surface, the increase in the CN^- can be due to contamination which contributes to a less clear evolution of the signal (a mixture of C and N contributions for the signal), in the first moments of the sputtering. Then S_2^- intensity drops as it gets closer to steel interface along with MoS_2^-, whereas the Mo^- intensity remains almost constant throughout the coating thickness. However, it is clear that the decreasing trend in the MoS_2^- is less steep than the one of S_2^- meaning that a progressive diminution of the S is occurring in this layer. This decreasing trend corresponds to the gradient of the substrate bias increasing from 130 V up to 200 V (layer 3 from the substrate). In this zone, N content is approximately constant in agreement with the constant value of the N_2 flow (30 sccm N_2 flow). This figure also shows a periodic fluctuation in the signal of the elements which can

be related to the position of the substrates in front of either the target or the plasma source. It should be remarked that, during the time the growing coating is in front of the plasma source, a preferential sputtering of the S should occur as well as an enrichment of N in the exposed surface. Although not perceptible in this figure, an experiment carried out without the top Mo-S-N layer, avoiding its initial removal as well as the intermixing always occurring during the erosion process, allows to show that the same fluctuation occurs for the CN^- signal (see figure 4-6). It is clearly observed that the peaks in the S_2^- signal correspond to valleys in the CN^- one and vice-versa. This trend is explained by either the preferential sputtering of the S when facing the plasma source or the higher incorporation of N during the ion bombardment from the plasma source. The figure 4-6 also confirms the higher decreasing slope of S_2^- in comparison to MoS_2^- signal.

Going deeper, a constant range in the elemental signals are visible in layer 2, as seen in figure 4-5. Finally, in layer 1, as expected, CN^- signal almost vanishes since no N exists in the chamber atmosphere. The S/Mo ratio reaches its minimum value in agreement with the suggested presence of an almost metallic layer in contact to the steel substrate.

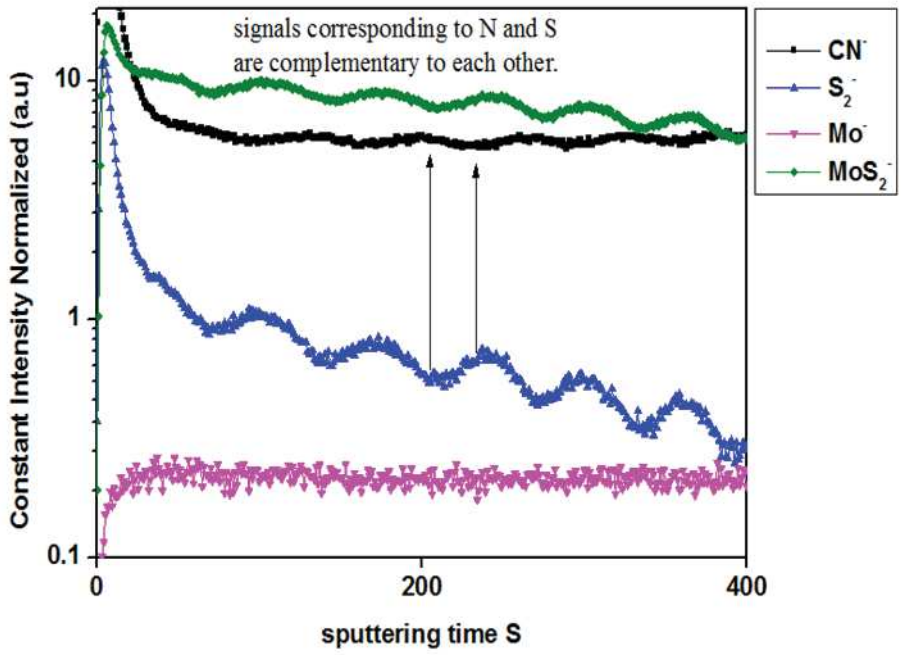

Figure 4-6: ToF-SIMS analysis for a sample deposited without the top Mo-S-N layer.

In conclusion, the *novel gradient layers* had alternate deposition of MoS_2 from target and preferential re-sputtering of S and deposition of N (by forming MoN(S)) from

the secondary plasma source. This was caused by the rotation of samples between the two processing sources.

4.3. Discussion

This chapter deals with the innovative approach made in this thesis to improve the mechanical strength and adhesion of MoS_2 and N-alloyed MoS_2 coatings with steel substrate (without any metallic interlayer, such as Ti or Cr, which is conventionally used as adhesion improving layer). The deposition process started (after heating along with pumping and bias etching) with creating a metal-metal bonding with steel using the only target of MoS_2. A thin Mo - rich layer was created with high ion energy and high ion bombardment, resulting in the preferential re-sputtering of sulphur from the growing coating, leaving only a Mo - rich layer. Later, nitrogen was introduced for forming a MoN (S deficient) layer. Due to the alternating between target and the secondary plasma source, a multilayer feature made up of varying nitrogen content layers was deposited, as observed in figure 4-3 and figure 4-6. The ion bombardment also contributed to a further incorporation of nitrogen in the coatings. Following this, the ion energy was reduced to increase the sulphur content in the layers, still with the presence of nitrogen in the plasma. This approach avoids the formation of highly crystalline MoS_2, thus, preventing exfoliation / delamination within the coatings. After 20 minutes of the *novel gradient layer*, the coatings were deposited at -50 V substrate bias for 2 hours. Therefore, the coatings are grown with metallic bonds in metal-alloyed S interface layer. The novel gradient layer began with only Mo(S), with only a few S, i.e. a metal-rich Mo in contact with steel. The second layer consists of a mixture of Mo(S) and MoN. During one rotation of the substrate holder, the growing film receives from the target the sputtered Mo and S species forming a Mo-S layer (with a high S/Mo ratio). This layer then goes in front of the plasma source where it will be submitted to a strong N ions bombardment. S will be preferentially re-sputtered, and N will be incorporated. However, the in-depth effect of the bombardment will not be homogeneous, i.e. in the original layer formed by the sputtered species from the target, there will be a fluctuation of the chemical composition from the surface (where the N content will be the highest and the S the lowest) down to the original composition. Although not possible to confirm the exact values of the chemical composition, the fluctuation is clearly confirmed by the SIMS analysis.

From the moment that the substrate bias is reduced (layer 3), i.e. the energy of the bombarding ions decreases, a decreasing re-sputtering of the S occurs with the consequent increase in the S/Mo ratio until the deposition in the final Mo-S-N layer. In this case, for the sample analysed by SIMS, the N_2 flow rate increased, which gave rise to an increase in the N incorporated in the coating. Therefore, this third layer was a gradient one which transforms from metallic (or metal nitride) to an amorphous lubricous sulphide. The multilayered structure dispersed the accumulated stress in its structure by plastic deformation, and it is believed that the stress evolution was interrupted at the layer boundaries, which positively affected the cohesion property of the coating [127]. This multilayer arrangement deposited previously to the main functional layer allows to improve the adhesion and the integrity of the coating significantly.

The coating integrity or mechanical resistance was assessed by scratch testing, which validates the strategy employed to improve the adhesion. The pure MoS_2 coatings without gradient layer provided very low cohesive (2.9 N) and adhesive (14.9 N) strengths. This is mainly due to the predominant presence of the lamellar structure which exfoliated or delaminated either in the interface film/substrate or within the coating. The Mo-S-N coating, without the novel gradient layer, showed a significant increase in the adhesion failure limit (22.8 N) compared to the pure MoS_2 coatings. Such a behaviour can be explained by the improved mechanical properties of the coatings containing N. Similar studies were performed by Mutafov et al. [61] for W-S-N coatings without any adhesion improving interlayer and found increment in adhesive failure limit compared to pure WS_2 coating. In fact, among the coatings with gradient layers, alloying with nitrogen showed a 10-fold increase in the cohesive failure limit compared to pure MoS_2 coatings (Table 4.2). These coatings are much harder which means that the penetration of the sliding indenter during scratch testing will be lower and lower will be the shear stresses at the interface [152] allowing the coating to support higher loads without spallation. Additionally, The N presences can amorphize the coating, thereby preventing it from delamination / exfoliation. Thus, the cohesive strength improvement was attributed to the prevention of any exfoliation due to the induced amorphousness of the Mo-S-N coatings. Thus, it can be concluded that the mechanical cohesive strength improvement is due to the combination of the gradient layer and enough nitrogen content in the coatings. The impact of the transition in the

growing of coatings is observed in its scratch resistance. The novel gradient layer approach used in this study is the primary reason for such a strong adhesion of the coatings.

4.4. Conclusions

This chapter describes the effect of the deposition of Mo-S-N based novel gradient layer on the integrity of the coatings, without the use of any third metallic interlayer (which are normally used and reported in the literature). Prior to the depositions, the chamber and substrates were heated to 150 °C for 5 hours with subsequent pumping to the base pressure of ~10^{-4} Pa, to remove any moisture and adsorbed contaminants. Later, the adequate bias etching in the presence of Ar^+ ion bombardment from additional plasma source removes any surface oxides on the substrate. The additional plasma source contributed towards important changes in the chemical composition and, therefore, to the type of contact between the coatings and the substrate. The deposition procedure adopted here achieved high adhesion critical load on steel substrate for Mo-S-N and pure MoS_2 coatings (> 80 N). The Mo-S-N coatings with the gradient layers also achieved high cohesive strength (35.1 N) is due to the combined effect of gradient layer and the mechanical strength provided by the alloying with nitrogen. Thus, this adhesion improvement approach, excluding additional targets, not only simplifies the depositions in the industrial environment but also solves major industrial issues related to the integrity of the coating system.

Chapter V

5. CHARACTERISATION OF Mo-S-N COATINGS

5.1. Introduction

After the deposition of gradient layers to improve the mechanical behaviour / adhesion of coatings, the next phase was the deposition and characterization of a set of MoS_2 coatings with different N-alloying. Different coatings were developed for the investigation of the role of N on the properties of the coatings, especially on the tribological performance. This chapter only deals with the basic characterisation of these coatings. The Mo-S-N coatings were analysed concerning to: (a) the chemical composition and the deposition rate (b) the chemical bonding (c) the surface and cross-section morphologies (d) the structure (e) the hardness and, finally, (f) the scratch resistance. The details regarding the deposition procedure and the characterization of the coatings were already presented in sections 3.3.1 and 3.4, respectively. These findings culminated as parts of 2 publications which are attached in annexes A and B.

5.2. Results

5.2.1. Chemical composition and deposition rate

The chemical compositions of the pure MoS_2 and all Mo-S-N coatings are shown in table 5-1. The nitrogen content ranged from 0 to 37 at. %. The S/Mo ratio is in the range from 1.25 to 1.79. Even for the pure MoS_2 coatings (0 at. % N), the S/Mo ratio was less than that of MoS_2 stoichiometric composition (S/Mo ~ 2). Several physical mechanisms such as re-sputtering by fast reflected neutrals [94,120], re-sputtering by ion bombardment [153], reduction in sticking coefficient [85] or even self-desorption of sulphur from the coating surface [154] can be involved in the sulphur depletion.

Table 5-1: Chemical composition, S/Mo ratio, thickness and deposition rates of the deposited coatings. The reported thickness and deposition rates correspond to the coating without considering the gradient layer. For ease, the volumetric flow rate is expressed in sccm (standard cubic centimetres per minute), which corresponds to the SI unit of Pa. m^3/s, (1 sccm = 1.69×10^{-3} Pa. m^3/s). The number-suffix of the code indicates the nitrogen flow used for a particular test sample.

Sample	N_2 flow (sccm)	Mo (at. %)	S (at. %)	N (at. %)	S/Mo	Thickness (μm)	Deposition rate (nm/min)
MoS_2(N0)	0	35.4 ± 0.4	63.4 ± 0.5	0	1.79	6.1	51.3
Mo-S-N10	10	30.8 ± 0.3	48.5 ± 0.3	18.4 ± 0.8	1.57	2.4	20.0
Mo-S-N20	20	30.5 ± 0.4	43.2 ± 0.4	24.2 ± 0.7	1.42	2.2	18.5
Mo-S-N30	30	30.2 ± 0.3	40.3 ± 0.3	28.4 ± 0.8	1.33	1.5	12.9
Mo-S-N40	40	29.0 ± 0.4	39.4 ± 0.6	30.2 ± 0.5	1.36	1.3	11.5
Mo-S-N50	50	27.9 ± 0.4	34.8 ± 0.4	35.4 ± 0.7	1.26	1.2	10.5
Mo-S-N60	60	27.3 ± 0.4	34.1 ± 0.4	37.0 ± 0.8	1.25	1.2	10.0

Optical spectroscopy studies performed by collecting the light emissions of the plasma at both the secondary plasma source and the target for pure MoS_2 sputtering allowed to plot the ratio of intensities between S and Ar as a function of the applied substrate bias, as shown in figure 5-1. Close to the target, the ratio between the two elements is fairly constant for all applied bias, suggesting that S is similarly sputtered independently of the substrate bias. However, the same is not observed in the plasma source zone. From 0 V to 50 V, no change in the ratio of intensities were observed. This could indicate that the re-sputtering effect, due to the ion bombardment induced by the substrate bias voltage, is minor or even absent, thus, not adding further S atoms to the nearby gas phase. On the other hand, beyond 50 V, an increase in that ratio occurs due to a higher number of S atoms in the discharge, showing that the re-sputtering of S from the coating becomes intense. Similar behaviour was also observed in an earlier work reported in ref. [133]. The re-sputtering effect increases with the substrate bias, which has a direct impact in the final chemical composition of the coatings. For 50 V, the value used for the deposition of the coatings, led to the such sub-stoichiometry of MoS_2(N0), as shown in table 5.1, with S/Mo = 1.79.

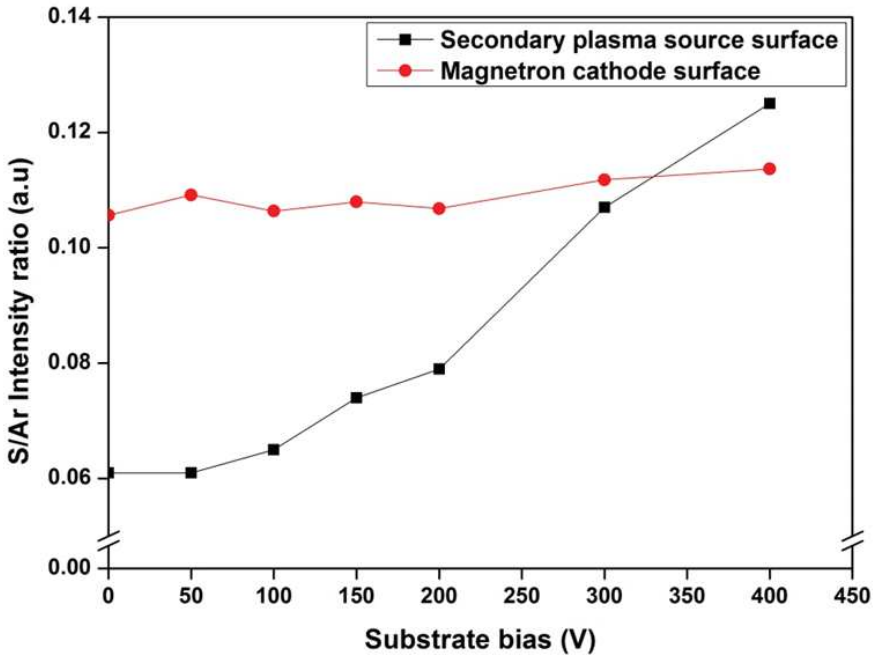

Figure 5-1: Optical emission of sulphur atom at 550 nm wavelength, normalised to the Ar intensity, as a function of substrate bias (V). The tests were performed with a cathode power of 1000 W.

The substrate bias is known to increase the compactness of the coatings through the re-deposition of atoms in the less dense areas. The acceleration voltage also increases ad-atom mobility [111,155]. The measured S/Mo ratio for pure coating was 1.79, which is a higher value when compared to some other reported results for pure MoS_2 coatings (S/Mo: 1.60) [53,156]. This observation is probably due to the highly degassed chamber due to a long heating and pumping prior to deposition. This process minimizes the presence of residual gases such as H_2O which could react with sulphur atoms and, subsequently, decrease the S content of this element in the coating. This was further evidenced by a comparative experiment performed with just 1 hour of degassing, during which an evidently strong smell was prevalent (H_2S or SO_x), indicating the reaction of sulphur with the residual gas (S/Mo = 1.51, O/Mo = 0.24). On the other hand, for the normal 5 hours of heating prior to deposition, no smell was detected when opening the chamber after the coating deposition, meaning that the chamber is almost free of contamination gases (mainly H_2O) (S/Mo = 1.79, O/Mo = 0.10). Further, the oxygen concentration in the N-doped and pure MoS_2 coatings was low at 0.5-1.5 at. % and up to 4 at. % respectively; a factor of ~ 2 lower when compared to values reported in the literature [156].

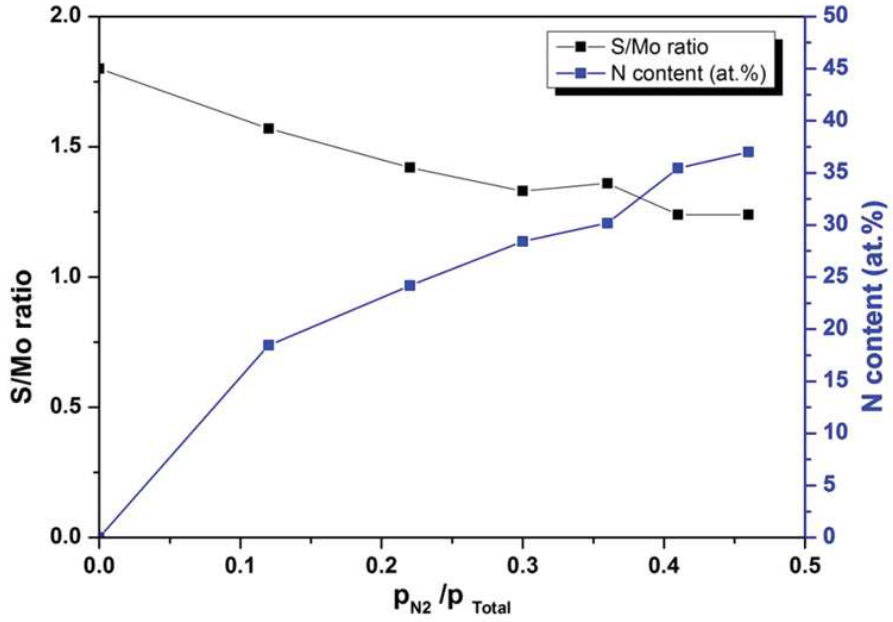

Figure 5-2: Evolution of S/Mo ratio and N content in the coatings as a function of the partial pressure of nitrogen gas.

The increase in the nitrogen flow rate during the deposition and the effect on the composition of the coating are shown in table 5-1 and figure 5-2. The Mo content remained nearly unchanged whereas the sulphur content gradually decreased, suggesting that nitrogen is replacing sulphur in the Mo-S compound. Overall, the minimum value for S/Mo was 1.25, and the (S+N)/Mo ratio was in the range of 2.17-2.50. These values higher than 2.00 could also indicate that nitrogen molecules can be trapped between the lamellas of MoS_2, similar to what was reported for W-S-N system by Isaeva et al. [58]. N could also be located at the interstitial positions in the $MoS(N)_2$ compound, which causes the formation of an amorphous material.

To understand the influence of the ion bombardment, one of the coatings (Mo-S-N with 30 sccm flow) was deposited without the use of additional secondary plasma source (keeping the other parameters constant), and the results are shown in Table 5-2. In the latter case, the coating had only 18.0 at. % of nitrogen content and S/Mo ratio of 1.57 against the 28.0 at. % and 1.33, respectively; the O content was also higher. This evolution is in agreement with the influence of the bombardment on the coating growth, promoting the re-sputtering of the lighter elements (or of the highest sputtering yield, i.e., S) from the growing coating and the consequent densification. The bombardment with nitrogen ions

can facilitate their sub-plantation in the coating and the replacement of the re-sputtered sulphur atoms.

Table 5-2: Chemical composition of deposited coatings with and without the use of secondary plasma source Mo-S-N coatings with 30 sccm nitrogen flow rate.

Sample	Mo (at. %)	S (at. %)	N (at. %)	O (at. %)	S/Mo	Deposition rate (nm/min)
With secondary plasma source	30.2 ± 0.3	40.3 ± 0.3	28.4 ± 0.8	1.1 ± 0.2	1.33	12.9
Without secondary plasma source	30.7 ± 0.3	48.4 ± 0.4	18.0 ± 0.4	2.9 ± 0.2	1.57	15.8

Table 5-1 also shows that MoS_2(N0) coating has a much higher deposition rate compared to Mo-S-N coatings. The reported deposition rates correspond to the coatings without considering the gradient layer. The following factors can contribute to this trend:

(i) With the introduction of nitrogen in the chamber, N_2 is mixed with Ar in the plasma thereby, the plasma contains lighter ions, decreasing the sputtering efficiency, thus leading to a reduction of Mo and S sputtering yields from target [140].

(ii) Nitrogen is being ionized by the secondary plasma source, with the consequent increasing bombardment of the growing coating. Therefore, densification of the coating occurs. The bombardment and incorporation of N affect the atomic arrangements and lead to removing pores and voids, as reported in the literature [156]. Compaction decreases the coating thickness for the same amount of deposited material with the consequent decrease in the deposition rate.

5.2.2. Chemical bonding

The XPS spectra have been fitted using Gaussian-Lorentzian curves. The relative contents of the various valence states are estimated from the integral area under the Gaussian curves. The Mo3d spectrum is fitted to the doublet peaks at 229.0 eV and 232.4 eV [153], corresponding to MoN bonds with approximately 3.4 eV spin-orbit splitting; the 228.3 eV and 231.5 eV peaks with 3.2 eV spin-orbit splitting are corresponding to the chemical bonds between Mo and S typical for MoS_2, and the doublet peaks at 230.0 eV and 233.3 eV belongs to Mo-O with 3.3 eV splitting. It can be seen that the MoS_2

contribution is still dominant in the Mo3d spectrum. The Mo-O bond has almost vanished, indicating that there was no oxidation in the coating bulk. The peak at 226.3 eV corresponds to S2s. The S2p spectrum at 162.0 eV becomes slightly broader with lower intensity from 18 at. % (10 sccm) to 35 at. % (50 sccm) due to the loss of S in the coating. The N1s spectrum partially overlaps with $Mo3p_{3/2}$ peaks, which is in good agreement with the reported results in the literature [53,156]. With the increase of N content, the intensity of the N1s signal increases. The binding energy of N1s displays a main contribution at 397.5 eV, corresponding to γ-Mo_2N [156] represents N-Mo bonds. N1s XPS peaks are important to understand the Mo-S-N coatings because the N-Mo bond peaks increase with the incorporation of nitrogen into the coatings; exactly, similar results were observed in other experiments [157,158]. From the measurements, we can conclude that with the increase of N content from 0 at. % (0 sccm) to 35 at. % (50 sccm), the relative amount of Mo-N increases. Still, there is much more Mo-S present as evident from the intensity of S2s peaks at 226.3 eV and the presence of Mo-S peaks. This is achieved through the periodic exposure to N-rich ion bombardment and MoS_2 target during the rotation of the substrate holder. The XPS probes 10 nm of top of the coating after the etch, thus able to probe sufficient thickness of coating.

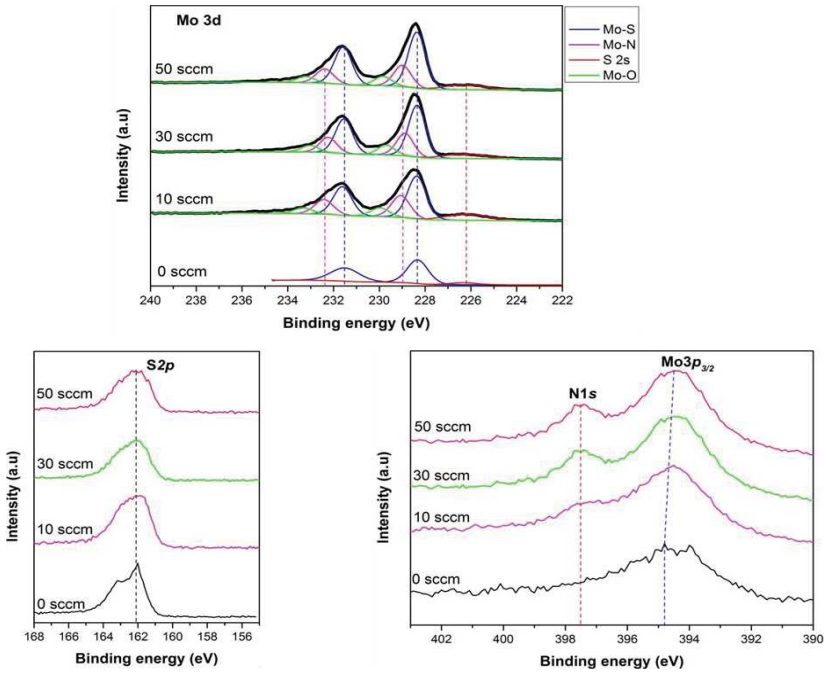

Figure 5-3: XPS spectra from Mo3d, S2p and N1s-$Mo3p_{3/2}$ from the Mo-S-N coatings deposited at 18 at. % N (10sccm), 28 at. % N (30 sccm) and 35 at. % N (50 sccm) respectively. 0 sccm refers to pure MoS_2 spectra.

5.2.3. Cross-section and surface morphologies

Figure 5-4 shows the fractured cross-section and surface morphologies of the deposited coatings. The sputtered pure MoS_2 coating displayed highly porous and low-density cross-section morphology with a large presence of dendritic growth throughout the coating (figure 5-4 *a*). The surface morphology of this coating was in accordance with the cross-sectional results, and the evidences of dendritic growth were clearly seen (figure 5-4 *b*). For Mo-S-N coatings, even with the introduction of the lowest amount of nitrogen (18 at. %), the coatings started to become compact although displaying columnar morphology (figure 5-4 *c*). The surface morphology micrograph for this coating also displayed less porous and sponge-like morphology aspect (figure 5-4 *d*). With further nitrogen incorporations, the compactness and density continued to increase, while the surface displayed cauliflower-like morphology due to surface limited diffusion conditions [28,159]. A significant increase in the compactness was observed after 28 at. % N addition.

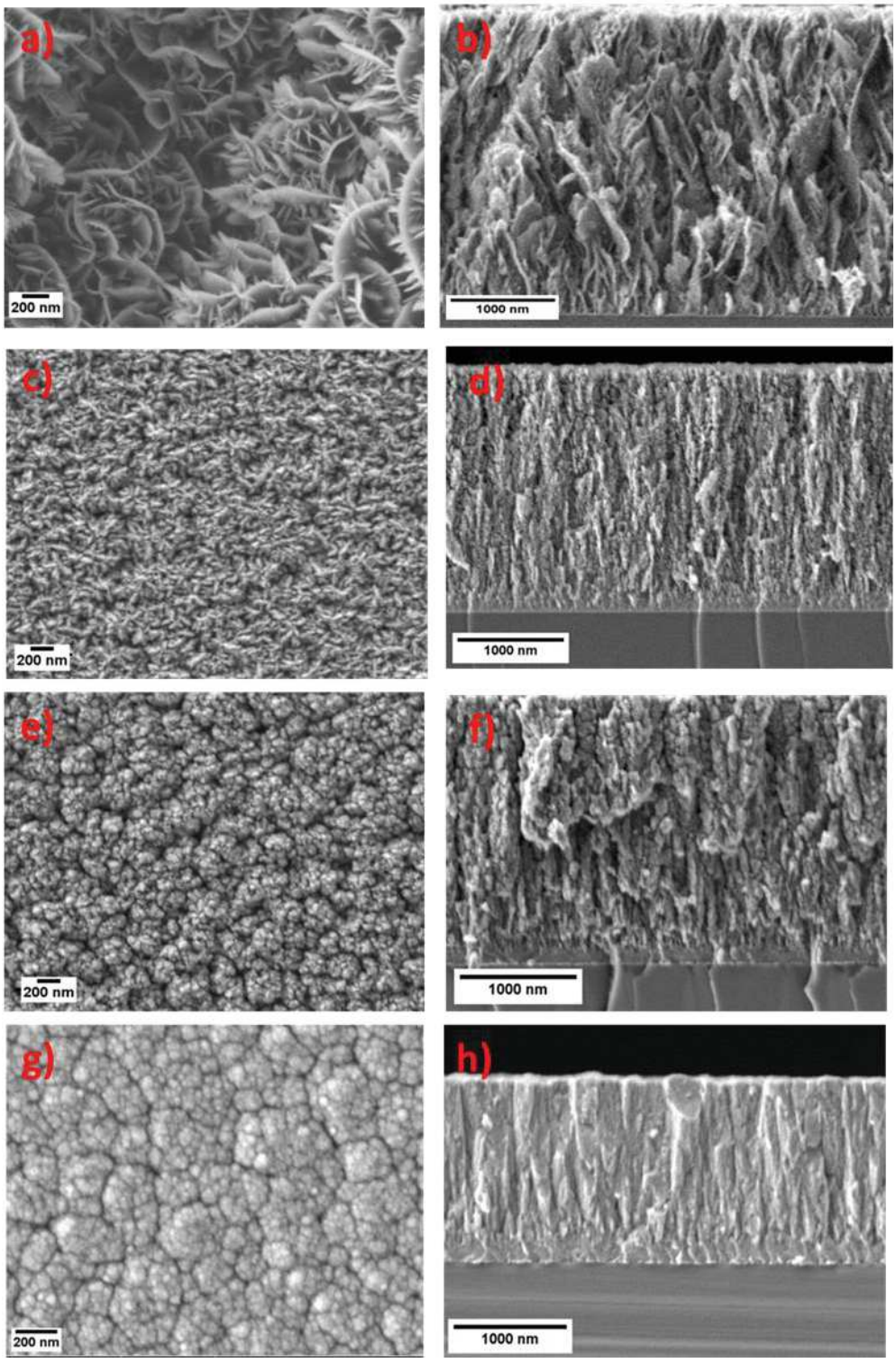
a)
200 nm
b)
1000 nm
c)
200 nm
d)
1000 nm
e)
200 nm
f)
1000 nm
g)
200 nm
h)
1000 nm

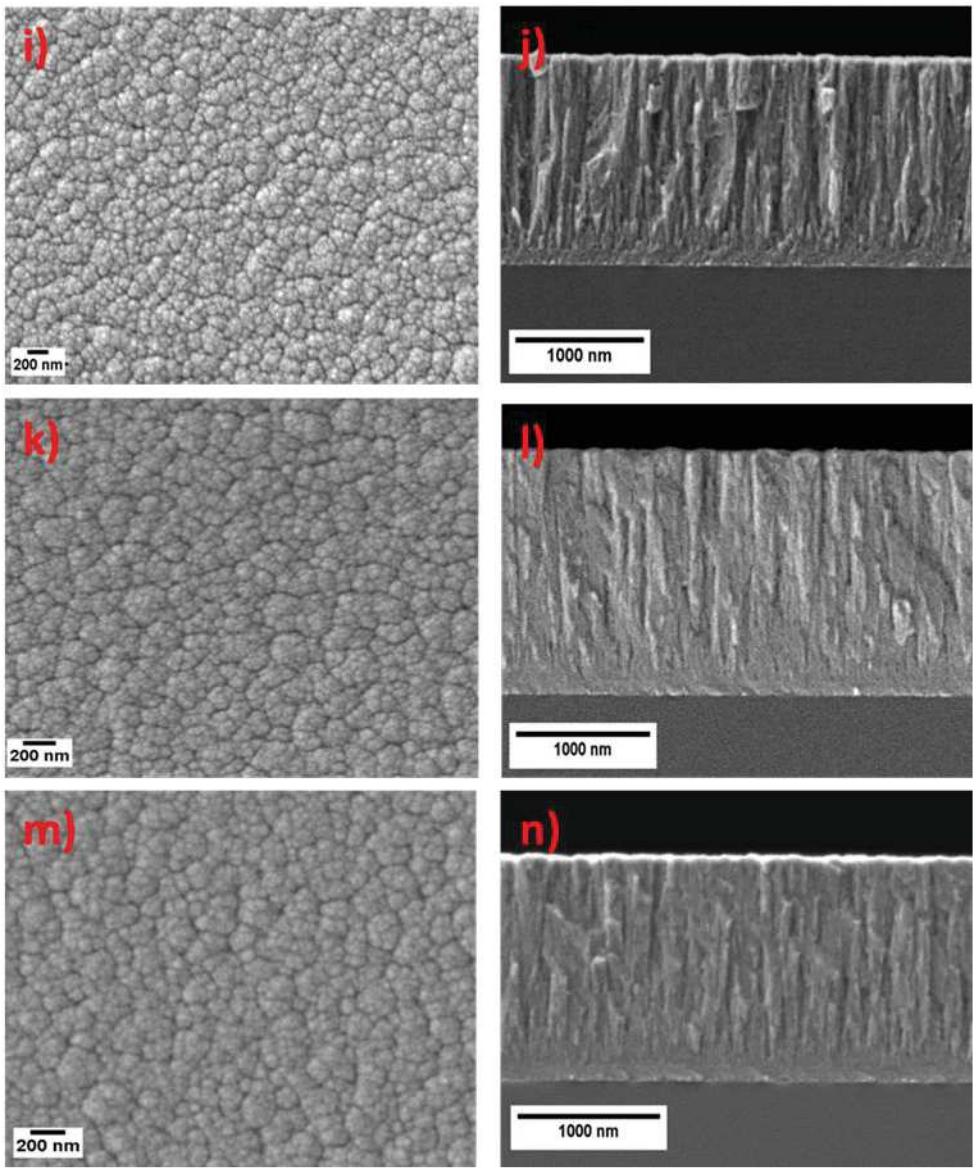

Figure 5-4: SEM micrographs of surface morphologies (Top-view) (a, c, e, g, i, k, m) and cross-section morphologies (b, d, f, h, j, l, n) of coatings deposited with increasing N content of 0 %, 18%, 24%, 28%, 30%, 35% and 37% N respectively.

The thickness of the coatings displayed trends similar to the compactness with the thickness decreasing, from the one of the MoS_2 coating (6.1 µm), with increasing the nitrogen content (as low as 1.2 µm). Despite more atoms being added as compared to the pure coating, the substantial thickness decreases are being attributed to the removal of porosity and increase of the density and compactness.

5.2.4. Structure

X-ray diffraction:

The structure of Mo-S-N coatings was analysed by grazing incidence XRD (GI-XRD) and is shown in figure 5-5. For the pure MoS_2 coating, the XRD reflections located at $2\theta = 14°$, 33°, 58°, and 60° indicated that the pattern was similar to typical sputtered TMDs (for MoS_2-ICDD 00-037-1492). The peak detected at ~14°, corresponding to the (002) planes, displayed very weak signal. The broad peak observed from 33°-50°, with an extended shoulder, is related to the (100) and (10L) planes. These observations are in accordance with the work of Weise et al. [160] who, for the first time, introduced the turbo-stratic stacking of the (10L) planes (L = 1,2,3,4,…). The low (002) / (100) peak intensity ratio is attributed to the deposition rate as it can make a considerable effect on the preferential orientation of the crystals in sputtered coatings. (002) planes have a high desorption rate if the deposition rate of the coatings is ~15 nm/min and above. With ~15 nm/min, the deposition rate of the second (002) layer becomes higher than the desorption rate of the first layer and, thus, (002) planar growth occurs. In this work, the deposition rate was much higher (~51 nm/min), which was optimum for the (100) planar growth as compared to the (002) [155,161].

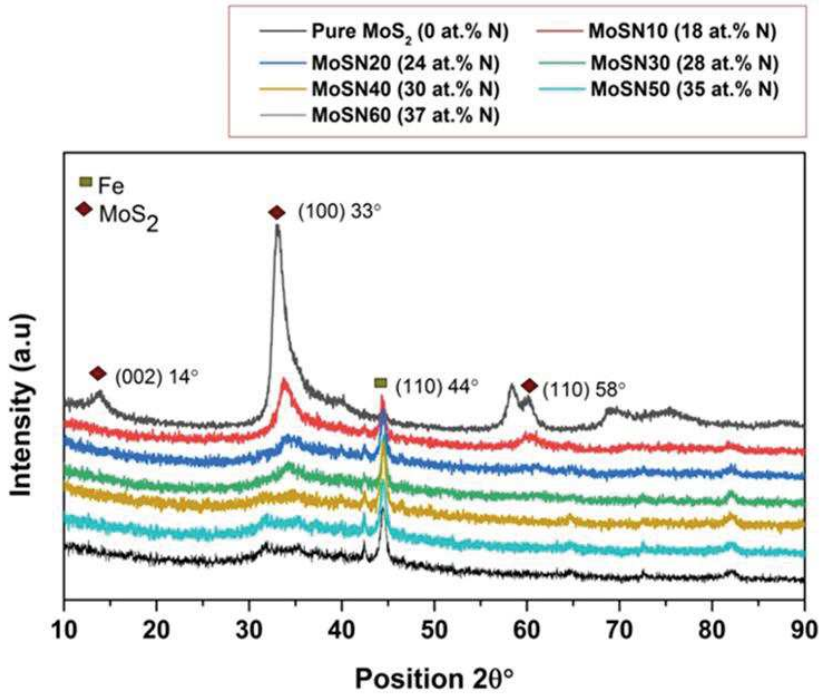

Figure 5-5: X-ray diffraction patterns of the coatings.

The incorporation of nitrogen atoms into the MoS_2 coatings, during deposition, led to significant changes in their structure. The Mo-S-N coating with the lowest nitrogen content of about 18 at. % showed some vestiges of the presence of (100) and (110) planes, but the (002) peaks totally disappeared. As the nitrogen incorporation was increased to 24 at. % and 28 at. %, the intensity of (100) peak was further reduced. It was previously reported that nitrogen could either get trapped in the basal planes of chalcogenides [162] or replace the chalcogen atom [105], causing short-range disorder in the atomic structure. Therefore, both mechanisms might be responsible for disrupting the organized growth and structure of MoS_2 crystals. Then, at 30 at. % of N and above, the coatings were completely XRDamorphous without showing any evidences of peaks. Further increments in nitrogen-alloying yielded similar amorphous structures, as shown by XRD spectra.

Overall, the results were in disagreement with the work of Zhang et al. [53] where the amorphousness was observed with 18 at. % of the nitrogen-alloying. This contradiction may be attributed to the difference in the deposition approach; in this work, the substrates face the MoS_2 target alternating with the additional plasma source. Therefore, when the substrates are in-front of the MoS_2 target, the nitrogen effect is somewhat lower and, hence MoS_2 crystallinity could be reached. When the nitrogen content (or flow) in the chamber increases, the freedom for MoS_2 to form crystals is hindered and, therefore, the coatings become completely amorphous. The tiny peak at 31° on Mo-S-N coating (35 at. % N) could correspond to the MoN structure underneath the coating in the interlayer zone, detected due to its lower thickness.

High resolution transmission electron microscopy (HR-TEM):

In order to observe the effects of nitrogen-alloying on the MoS_2 coatings, the FIB lamella prepared from three different zones of the selected coating (Mo-S-N40 with 30 at. % N) was imaged in cross-section via TEM. Figure 5-6 shows the HR-TEM micrographs. The amorphous nature of the coating is observed, especially towards the top of the coating, with very few traces of nanocrystalline lamellar MoS_2. Towards the substrate interface, a combination of amorphous regions with randomly oriented MoS_2 platelets was observed. The coating was dense (agreeing with SEM results in Figure 5-4) and showed a dendritic nanostructure throughout its thickness. The columnar features were confirmed to be S-rich and, hence, provided the conditions for the localised crystallisation of MoS_2 lamellae.

These few traces and small sizes were the reason that MoS_2 crystalline peaks were absent in the XRD analysis of this coating.

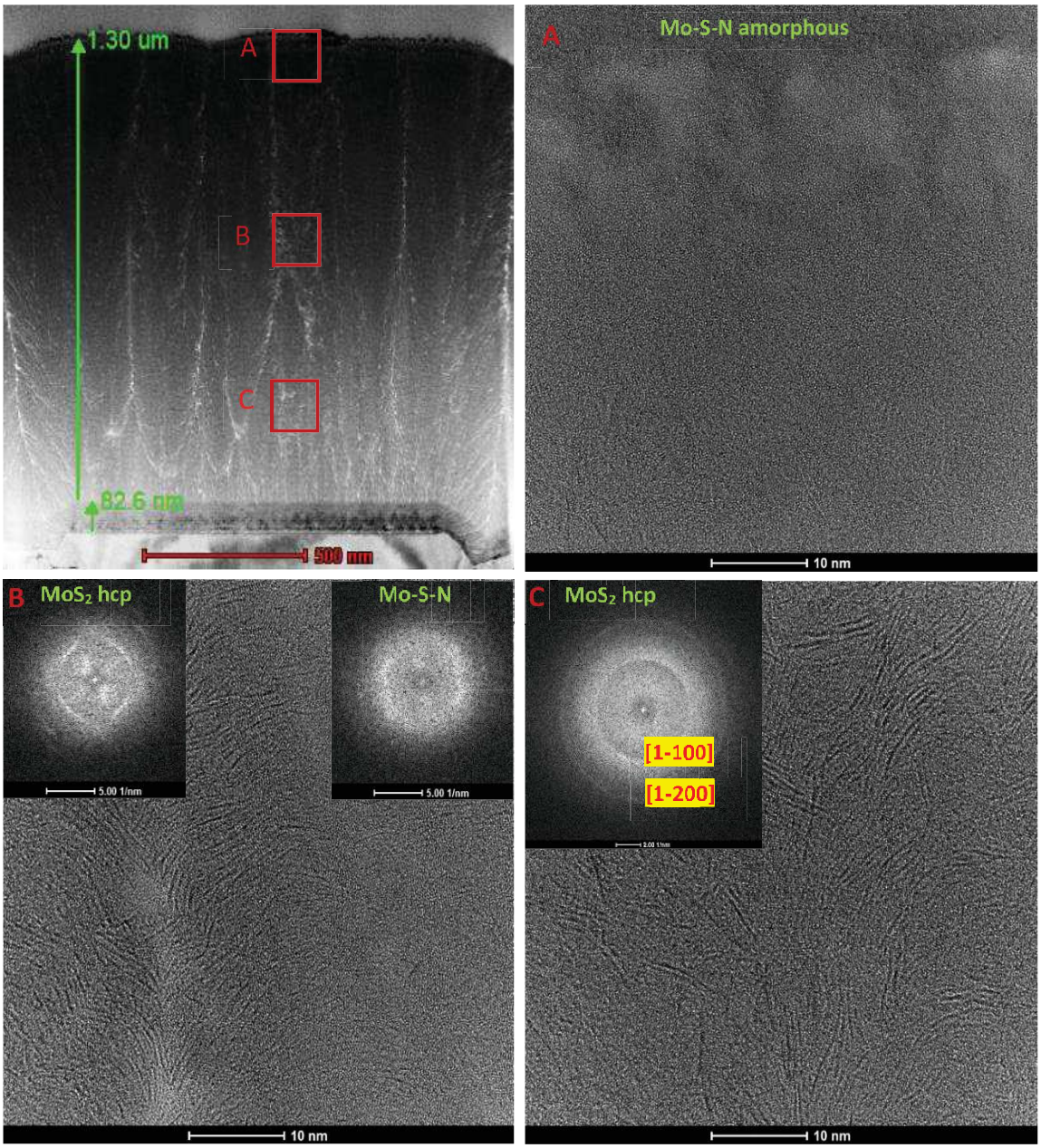

Figure 5-6: Microstructure of the as-deposited Mo-S-N40 (30 at. % N) coating; the corresponding FFT patterns are shown in insets.

5.2.5. Roughness

The surface roughness was also measured as a function of the addition of nitrogen using AFM (Figure 5-7). The incorporation of nitrogen would lead to the formation of

a nano-crystalline structure, preventing the formation of big crystals of MoS_2, avoiding voids and pores. SEM micrographs and X-ray diffraction results have shown that the incorporation of N was able to compact and amorphize the coatings. With amorphousness and compactness of the coatings, the roughness also decreased from 0 to 30 at. % N, and later increased with further nitrogen additions. These roughness increments could be related to the formation of some asperities on the coating surface.

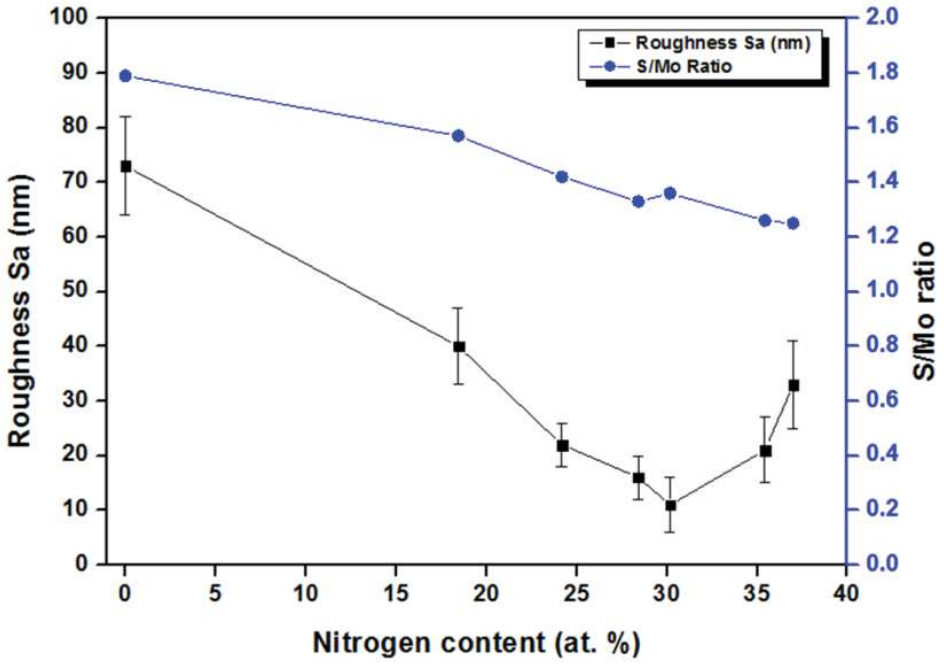

Figure 5-7: Variations in surface roughness and S/Mo ratio of the coatings with increasing nitrogen content.

5.2.6. Mechanical properties

Hardness and Young's modulus:

Figure 5-8 shows the hardness and effective Young's modulus of the deposited coatings and their variation with nitrogen content. The pure sputtered MoS_2 coating showed the lowest hardness values of 0.5 GPa, owing to its low packing density [163] and columnar morphology, in agreement with the SEM micrographs.

The hardness of the coatings increased to 1.5 GPa as soon as nitrogen was introduced in the chamber (Mo-S-N10, 18 at. % N). The hardness continued to increase with further additions of nitrogen. This increase is related to the improved compactness and density of

the coatings, which induce a higher resistance to dislocation movement and plastic deformation, as well as a higher load-bearing capacity [164]. The reduced crystallite size also plays a vital role in the improvement of the mechanical properties of the coatings [45,55]. No significant difference in the hardness was observed by increasing N from 30 to 37 at. % N, as the coating was already amorphous and highly compact for the 30 at. % N alloying. The effective Young's modulus followed similar trends as hardness. Overall, the hardness values increased from 0.5 GPa to 8.9 GPa, while the Young's modulus increased from 20 GPa to 149 GPa with increasing N-alloying from 0 to 37 at. % N.

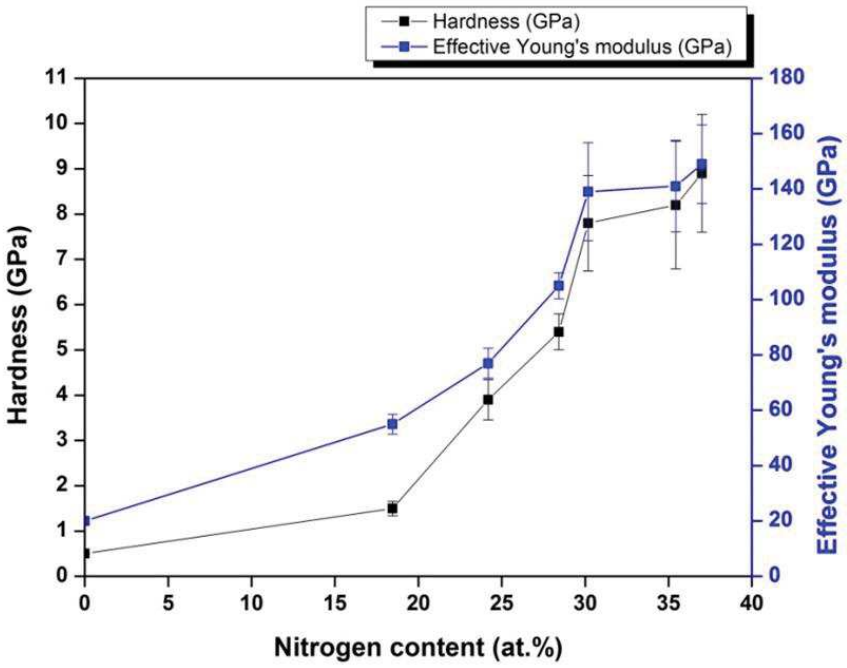

Figure 5-8: Hardness and effective Young's modulus of the coatings with increasing N content.

Scratch resistance:

Figure 5-9 shows the effect of nitrogen content on the initial load required for cohesive failure (L_{c1}). As soon as the nitrogen was introduced to the MoS_2 coatings, there was an improvement on the critical load for cohesive failure. At the start, the increase in nitrogen content increased the failure limit or lead to the late appearance of flakes in the scratch test, which was almost linear up to 24 at. % of nitrogen incorporation. At this stage, due to the presence of some crystallinity of MoS_2 within the coatings, flaking could occur at loads which increased with decreasing of either the S/Mo ratio or the crystallinity degree, as shown by X-ray diffraction. After this, a steep increase in the scratch resistance was

observed for Mo-S-N30 (28 at. % N). The surface appearance and the initial flaking for Mo-S-N40 (30 at. % N) coating can be observed in figure 4-2 d) which provided a 35.1 N cohesive critical load (L_{c1}). This sudden increase could be due to the enhanced amorphousness (or nanocomposite structure) of the coatings, which eliminates the presence of any lamellar crystals, thus avoiding the cohesive failures at low loads. The incorporation of nitrogen into the coatings has increased the mechanical strength through the induced amorphousness.

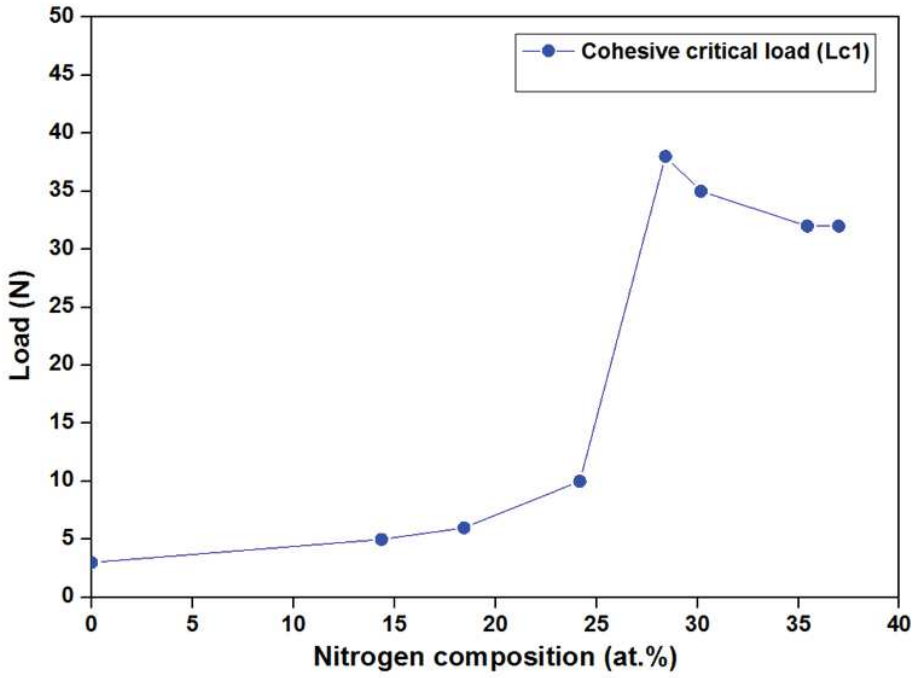

Figure 5-9: Scratch behaviour Lc_1 (cohesive critical load or cohesive failure limit) of pure MoS_2 and Mo-S-N coatings with respect to the nitrogen concentration.

5.3. Discussion

This chapter deals with the main characterisations of the Mo-S-N coatings, i.e. the analysis of their chemical composition, chemical bonding, structure, hardness and scratch resistance. These coatings were deposited after improving the adhesion using the gradient layer, as explained in chapter 4. The composition of the coatings bears a good correlation with the structure. In the case of the pure coating (MoS_2(N0)), the surface and cross-section images presented in figures 5-4 *a)* and *b*), revealed a porous morphology. This type of coating morphology showed a preferential orientation of the grains in the (100) direction in relation to the (002) as observed in figure 5-5 of the XRD diffractograms. The crystalline

anisotropy of the hexagonal MoS_2 contributes to the formation of fibrous-needle or platelet-like structures. It is well known that longer grains cause a shadowing effect, which in turn can create porosity during the rotation of the substrate. Due to the porous morphology and crystalline characteristics, the coatings provided very low load-bearing capacity and hardness (0.5 GPa).

For the Mo-S-N10 coating (18 at. % of N), a diminution of the size of the platelets was observed, figures 5-4 *c)* and *d)*. The incorporation of nitrogen provided a disorder in the atomic structure of Mo and S and triggered a grain refinement process. These observations are supported by the XRD analysis (figure 5-5). The intensity of the characteristic (100) peak for Mo-S-N10 coating decreases, which indicated a disruption in the nanostructure of the coating when compared to pure MoS_2 coating. This resulted in more compact coatings, thus, a steeply decreasing of the thickness with nitrogen-alloying. The decrease in the deposition rate was also due to the decrease of the sputtering yield of Mo and S in the reactive atmosphere. This cumulative effect led to a decrease in S/Mo ratio due to the incorporation of nitrogen into the coatings. Also, as soon as the secondary plasma source induced the nitrogen ions bombarding, N ions participated in the removal of the sulphur atoms. This further resulted either in the replacement of S by N or sub-plantation of N in the interstitial positions of MoS_2. The nitrogen-alloying thus induced amorphousness in the MoS_2 coatings.

Further increments of nitrogen to 28 at. % (30 sccm N_2 flow) resulted in the formation of amorphous and dense coatings, as well as, in a drastic reduction of the XRD peak intensity. Thus, figures 5-4 *g)* and *h)* show less porosity and a highly compact coating. Any further increase in the nitrogen content led to amorphous coatings (which are again in good agreement with the structure and surface morphology). It should also be mentioned that, although some sulphur atoms are replaced by nitrogen, a substantial amount of sulphur is still retained in the coatings. Therefore, the minimum S/Mo ratio was observed (1.25), which was still higher than all reports in the literature (see ref. [53,156]).

XPS studies carried out to understand the chemical bonding mechanism within the coating revealed quite interesting results. Even for 35 at. % of N (Mo-S-N50 coating) the Mo-S peak (228.3 eV) was dominant over Mo-N peak (229.0 eV). Furthermore, the S2s peak at 226.3 eV showed the presence of S-S bonds, whereas N-N bonds were detected at 397.5 eV. This reveals that a large amount of MoS_2 compound was formed even for highly

N-alloyed coating. The formation of such bonds is due to the deposition process, i.e. the use of alternating magnetron sputtering and secondary plasma source, which results in both $MoS(N)_2$ (reactive sputtering) and N bombardment (secondary plasma source). Thus, firstly, a process for the deposition of MoS_2 took place; afterwards, the ion bombardment promotes the re-sputtering of S and the incorporation of N. Thereby, some Mo-S bonds are replaced by Mo-N bonds during the exposure to the secondary plasma source. This effect also corroborates with the chemical composition, where the S/Mo ratio reached the lowest value, 1.26.

Even the smallest addition of N resulted in a significant increase in the hardness and elastic Young's modulus. The values continued to increase for higher N contents. This increase was the result of; (i) the densification of the coating structure and the increase in the compactness of the coatings; (ii) the amorphisation of the coatings and, (iii) the nanometric level of the MoS(N)/MoN(S) multilayer stacking caused by the hybrid deposition approach used in this work. The multilayer stacking promotes an increase in the hardness due to the interface strengthening effect (e.g., interface mixing and interface density). Similar observations were reported in the literature for other multilayer materials, e.g., for WS_2/MoS_2 [165] and TiN/VN [166] coatings. Despite the higher S/Mo ratio (compared to reported in literature), and a higher amount of the MoS_2 soft phase, the synergy of the factors mentioned above contributed to hardness values higher than those found in the literature [53,62,156,164].

Overall, the additional ion flux and bombardment from the secondary plasma source played a very crucial role in the deposition of Mo-S-N coatings. Firstly, it promoted the desorption of impurities, thereby the C (not shown) and O contents in the coating were found to be reduced compared to the coating without the use of additional plasma source as confirmed in table 5-2. Secondly, the incorporation of nitrogen and the ion bombardment promoted the atomic reorganization on the surface of the growing coating contributing to prevent voids and, hence, to improve the hardness by compaction. The nitrogen seems to be incorporated into the coating by two means: (i) due to the normal sputtering process in reactive mode in nitrogen-containing plasma and, (ii) by additional N ion bombardment by the secondary plasma source. Nitrogen either get entrapped between the basal planes [162] or can replace the chalcogen atom [105] causing disorder in the atomic placement. Based

on theoretical predictions and experiments, Komsa et al. [167] have shown that it was possible to dope MoS_2 by filling the vacancies created by the electron beam with impurity atoms. It was feasible to have a MoS_2 sheet with S vacancy filled in by an isolated atom of N. Later, Dolui et al. [168] described some possible alloying strategies for MoS_2 monolayers, using density functional theory, by a first substitutional alloying at both the Mo and S sites. They reported that the best strategy would be to grow S-poor coatings and, then, filling the vacancies with an appropriate atom, such as N. Due to the high formation energy of the vacancy, N substitution is energetically favoured since that energy is largely dependent on the growth conditions. Thus, based on the results achieved in the present study, by using a high ion bombardment through a secondary plasma source, a higher nitrogen alloying in the coatings can be achieved while maintaining a high S/Mo ratio. The coating, thus, has an amorphous structure consisting of a Mo-S-N compound with Mo bonded to S and N. Overall, it is safe to conclude that 30 at. % nitrogen content can provide a complete amorphous structure with moderate hardness. The structure of Mo-S-N coatings are nanocrystalline from 0-28 at. % N and changes to amorphous above 28 at. % N. Such nitrogen-alloyed coatings are expected to exhibit impressive tribological properties in vacuum and ambient air.

5.4. Conclusions

Mo-S-N coatings were deposited on Si (100) and M2 steel substrates using a semi-industrial DC magnetron sputtering apparatus with a single target of MoS_2 and a planetary rotating substrate holder. The chemical composition, chemical bonding, morphology, structure and mechanical properties were studied as a function of the N-content of Mo-S-N coatings. With heating and pumping prior to bias etching and deposition, it was possible to attain very low oxygen content (less than 1 at. %) in the coatings. The structure of the coatings changed with the incorporation of nitrogen. The coatings with less than 30 at. % N were nanocrystalline; for higher contents, coatings became XRD amorphous. The morphology was increasingly more compact with the incorporation of nitrogen. HR-TEM also confirmed the presence of amorphism in high N-content coatings. The S/Mo ratio also decreased and reached 1.25 for the highest N incorporation (37 at. % N), with a high hardness of 8.9 GPa. Though the S/Mo ratio decreased, the value was higher than that of reported in literature for the same amount of nitrogen-alloying. With the increase in N content, the scratch resistance of the coatings increased with the highest value of 38 N for

28 at. % N. It is observed that nitrogen was incorporated in an amorphous ternary compound, such as Mo-S-N, with Mo-N and Mo-S bonds. These coatings with enhanced adhesion, high S/Mo ratio, high compactness, high hardness, better scratch resistance and low contaminant contents have great potential in applications that demand superior tribological properties.

Chapter VI

6. TRIBOLOGICAL ANALYSIS

6.1. Introduction

After the optimization of the deposition and the fundamental characterization stages of the thesis, the detailed tribological investigation was carried out. Therefore, this chapter deals with the tribological analysis performed using a 'cylinder-on-flat' reciprocating tribometer. Initially, the vacuum tests were performed for the following pair arrangements: (i) steel cylinder versus coated flat, (ii) coated cylinder versus steel flat, (iii) coated cylinder versus coated flat. Furthermore, the testing load was varied in the configuration coated cylinder versus coated flat, and endurance tests of the coated cylinder versus steel flat were performed. Finally, one Mo-S-N coating, i.e., Mo-S-N40, was tribo-tested in ambient air atmosphere for different mating conditions. All the tests were carried out under an applied initial Hertzian contact stress in the range of 60 – 135 MPa. Often, in literature, the tribological testing of these materials is carried out at contact stresses in the range of 1 GPa. The amorphous MoS_x materials are in a metastable state. By providing them with a sufficient amount of energy, they transform in the contact from amorphous to lamellar structure which is necessary for the reduction of the friction. A minimum amount of energy is necessary for that transformation to occur. Hence, it is advantageous to reduce the contact stresses (from 1000 MPa) to the level that may be encountered in real service and verify that the energy dissipated by the friction to produce the lamellar structure remains adequate. In the following sections, only the results and discussions of the aforementioned tribological tests is presented. The details about the tribological testing is already presented in section 3.4.12. The work presented in this chapter is supported by the publication attached in annex B.

6.2. Results

6.2.1. Steel cylinder versus coated flat

The evolution of the COF and the specific wear rates of all Mo-S-N coatings sliding against the uncoated steel cylinder is shown in figure 6-1. All the coatings displayed almost

similar and highly stable steady-state friction curves. Significant differences were observed in the running-in period. All coatings displayed in this zone a bump in the initial part of the friction curves.

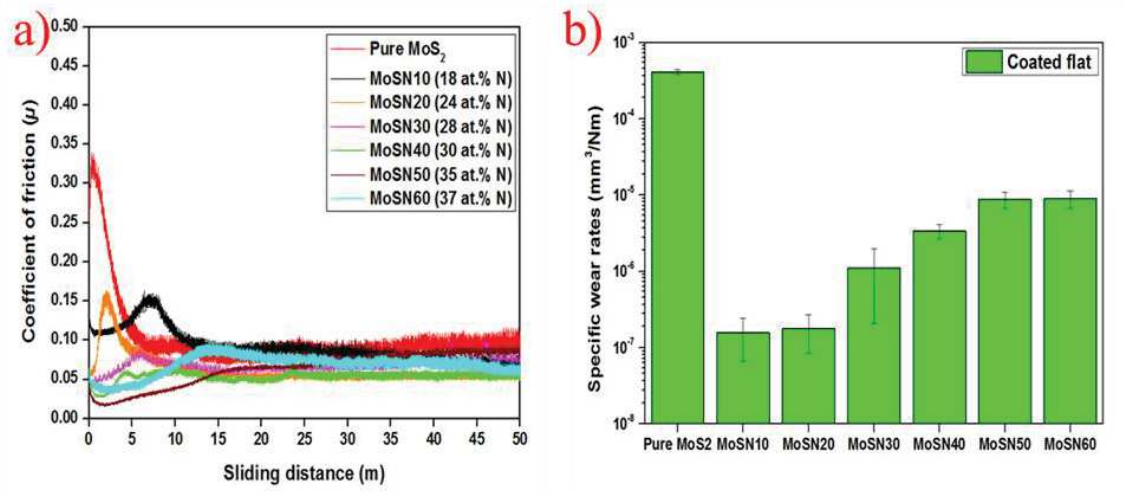

Figure 6-1: a) Tribological tests in vacuum for Mo-S-N coatings (on the flat) with 100Cr6 steel cylinder (counterbody) with respect to the sliding distance. b) The specific wear rates of the coated flats.

Two main trends characterize these bumps. On the one hand, the higher the roughness is, the higher is the height of the bumps, which suggests that mechanical interaction is occurring in this first part. On the other hand, the width of the bump increased with the hardness, which can be understood by the difficulty in wearing the material due to enhanced mechanical interactions. After the bump, a progressive decrease of COF takes place until the steady-state friction is reached. As seen in the literature, it is well established that TMDs display low COF due to the formation of easy to shear planes at the contact interface or contact surface [28]. Therefore, the running-in period should depend on the formation of this tribo-film. The pure MoS_2 coating displayed the minimum running-in period of ~5 m due to the high S/Mo ratio, which means more MoS_2 is available for the tribo-film formation. Then, globally, as N was introduced in the coatings, the running-in period increased as the MoS_2 availability to form the easy shear tribo-film, decreased. This is in good agreement with the decrease in the S/Mo ratio. Therefore, during the time the tribo-film was being formed (running-in period), a higher wear of the coating occurred at that region of the friction test. In addition to this, for the highest N contents, N-based compounds could be formed which might also be contributing to the increase in the wear during this stage. The formation of the tribo-film would mean reorientation of crystals and

nanocrystals in the direction of the sliding plane. For amorphous coatings, this would mean the transformation from the amorphous phase to the crystalline phase in the direction of the sliding plane.

Overall, the stable COF for all Mo-S-N coatings was in the range of 0.05-0.08. However, pure MoS_2 coating showed an increasing trend for COF, reaching a slightly higher value of ~0.10 at the end of the test. A possible explanation for this slow increase of the COF is based on the particular shape of the counter body, i.e., the flat and curved cylinder, as shown in figure 3-8 a) and b). Two points should be considered in this analysis: (i) despite the higher S/Mo ratio and consequent MoS_2 availability for the tribo-film formation, the very low hardness of the pure MoS_2 coating leads to a very high wear in the first few cycles compared to the other coatings; (ii) the low contact stresses being applied makes more difficult the tribo-film formation in the sliding contact. Due to these reasons, it is expected that for pure MoS_2 coating after, a few cycles, the cylinder plunges in relation to the original contact surface, thus increasing the length of the contact surface (see figure 3-8 b). Such a change, in addition to the much lower Young's modulus of this coating, contributes to a much higher contact area and smaller values of the contact stresses. This means that the higher the wear is, the lower the contact stresses will be. Suppose it is speculated that the contact stresses are close to the threshold value necessary for the tribo-film formation. In that case, an assumption which will be shown later can be true, i.e., the progressive decrease of the contact stresses can lead to a progressive deficiency in the formation of the tribo-film and the consequent increase of the COF. On the other hand, for the high N content coatings (30 at. % N and above), due to the increased hardness, the initial wear of the coating is much less, and thus the plunging-in is almost nil. This means that the contact area does not increase during the duration of the test, keeping the COF approximately constant in the assumed steady-state regime.

Figure 6-1 b) shows the specific wear rates for the coated parts (flats). The pure MoS_2 coating displayed the highest wear. The softness (low hardness), low compactness, and low load-bearing capabilities of this coating justifies the short running-in and fast tribo-film formation, as described above, as well as the much higher values of the wear in comparison with N-containing coatings. The increased compactness and hardness of the coatings with N additions decreased the wear rates compared to the pure coating. They remain hard until

they transform into MoS_2 on the contact surface. However, there is no improvement in wear resistance with increasing N content among the Mo-S-N coatings, despite their higher hardness. It should be noted that the wear-scar depths were usually very shallow (typically 40 – 100 nm for Mo-S-N coatings and 200 – 500 nm for pure MoS_2 coatings), indicating the starting of the wear process for the formers. As explained above, in this stage, the wear values are mainly dependent on the formation of the tribo-films. Until the effective action of the tribo-film, a high wear occurred, as high as longer the time needed for its formation. For very long tests and / or high depth wear craters, the hardness of the coatings would become more important, and an inverse trend for the specific wear rate would be expected, i.e., the higher the N content is, the higher the hardness and the wear resistance are.

6.2.2. Coated cylinder versus steel flat

In the previous case, the steel cylinder was sliding against the coated flat, bringing each zone of the coating subjected to a periodic short contact. In this section, the arrangement of the mating surfaces has been changed; the coated cylinder slides against the polished steel flat surface. In this situation, the coating is in continuous (uninterrupted) sliding contact with the counter body (steel flat surface), closer to the reality of many industrial applications where the coating remains in permanent contact with the sliding interface. Thus, in this configuration, the coating is placed on the sample for which the wear rate is the highest because of kinematic length consideration. Therefore, this sliding process is more demanding and severe for the coating than the steel cylinder versus coated flat condition.

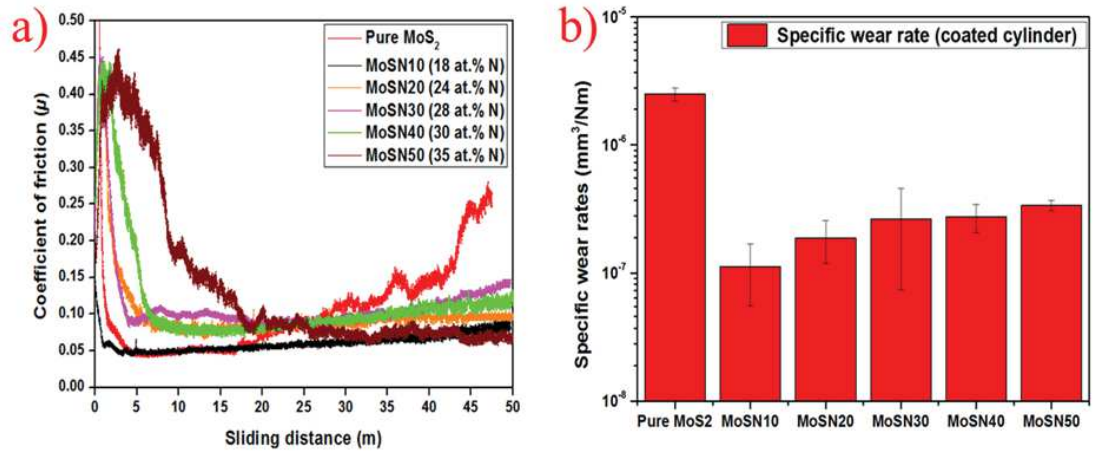

Figure 6-2: a) Friction coefficient evolution for coated steel cylinder against polished steel flat (Roughness of 1.4 nm) with respect to sliding distance in vacuum conditions. b) The specific wear rates of the coated cylinder for respective tests.

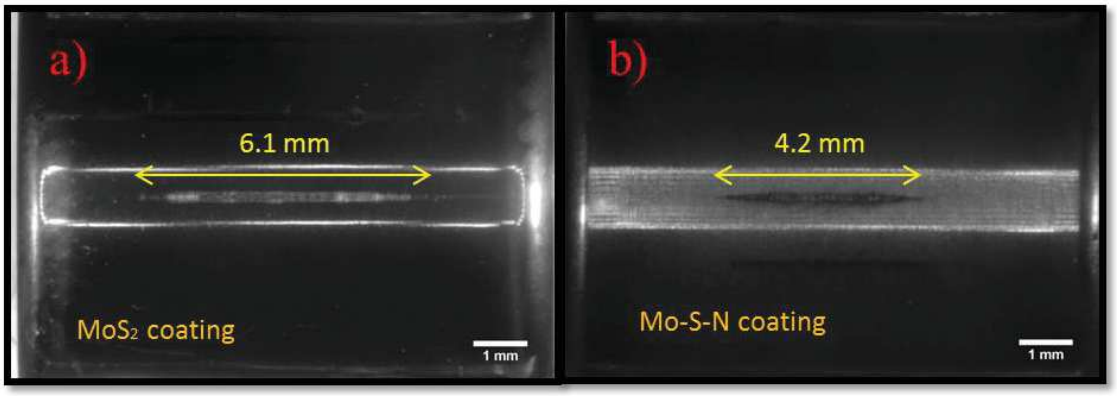

Figure 6-3: (same as Figure 3-8 c) and d)) a) Worn length of line contact on MoS_2 coated cylinder, b) Worn length of line contact on Mo-S-N coated cylinder after sliding against M2 steel flat.

The pure MoS_2 coating had a very short running-in period, shorter than in the previous case, which can be justified by the permanent contact of the coatings with the counterbody and an easier formation of the tribo-film (see figure 6-2 a)). The steady-state COF is maintained during 15 m sliding distance and, then, the COF increased strongly to 0.25; at this point, the test was stopped as if the contact with uncoated zones had occurred. Unexpectedly, the analysis of the wear track (see figure 6-3 a)) showed that no substrate could be detected. Moreover, the calculation of the depth of the worn coating, based on the width of the wear-scar and geometrical analysis, found a value close to 0.68 µm, very far from the thickness of the coating (6.1 µm). This trend confirms the explanation mentioned in section 6.2.1 for the slow increase of the COF but now in a catastrophic manner. As can be observed in figure 6-3 a), besides the flat part of the cylinder, it is clear that the contact

reached the curved part, enlarging the contact area and decreasing the Hertz contact stress. This had already occurred in the previous case; however, in this situation a further increase in the contact area takes place, decreasing the contact stress to values lower than the critical ones for the formation of the tribo-film. In fact, for the uncoated cylinder / coated flat situation the wear of the steel cylinder is almost nil, being the contact area in the linear part of the cylinder almost constant during the test. Because of the wear of the coating, only the plunging-in (prolonging the contact to the curved zone of the cylinder) has an influence on the contact area and the contact stress. Alternatively, in the case under analysis in this section, the cylinder is being worn out, and the contact area keeps increasing with the duration of the test (in addition to the extension to the curved zone). Subsequently, when a critical value of the contact area is reached, the corresponding contact stress is no longer sufficient to form the tribo-film: hence the friction rises.

For Mo-S-N coatings, the formation of the tribo-film is much faster than in the previous case (section 6.2.1). The coating with minimum N content displayed the lowest running-in period, and further additions of N increased this period. The coating with the highest nitrogen content (Mo-S-N50, 35 at. % N) displayed the longest running-in period. This increased running-in period can be attributed to the lower S/Mo ratio available for the tribo-film formation. Apart from the Mo-S-N50 (35 at. % N), in all the coatings the slow increasing trend of the COF can also be observed. As explained above, this progressive and slow increment in COF is related to the wear of the coatings (coated cylinder), which results in an increased contact area and, thus, decreased contact stresses. However, the much lower wear of these coatings (see figure 6-3 b)) does not promote significant changes in the contact stresses, keeping their values close to the necessary for the formation of the tribo-film. It is noted that almost no extension of the line contact to the curved zone is observed (see, e.g., figure 6-3 b)).

The specific wear rate of the pure MoS_2 coating was the highest, which decreased with the introduction of N in the coatings. The specific wear rate was minimum for the lowest N-alloying. Among the N-alloyed coatings, the specific wear rates increased with the N content. Therefore, the Mo-S-N50 (35 at. % N) coating displayed the highest wear rate. As explained earlier in this section, the line contact of the coated cylinder is always prevalent (in contact) with the steel surface. This creates a situation in which the material

is transformed easily and faster, to form the reoriented tribo-film in the case of the softer pure MoS_2 coating. Therefore, higher wear and low running-in period has been observed for this coating. The same phenomenon took place for all N-alloyed coatings, but the specific wear rate was lower (than pure MoS_2 coating) due to their increased compactness and hardness. Among Mo-S-N coatings, the reason behind the observed increase in the wear with increased N-alloying is the decrements in S/Mo ratios. As explained above, more wear of the coated cylinder was needed to provide sufficient MoS_2 for the tribo-film formation. This is in agreement with the delayed tribo-film formation under high N-alloying conditions.

6.2.3. Coated cylinder versus coated flat

The evolution of the friction curves in the steady-state region was very similar to the case of the steel cylinder versus coated flat presented in section 6.2.1 (compare figures 6-1 and 6-4). The main difference was the decrease in the duration of the running-in period and the lower initial intensity in the bump of the COF. The pure MoS_2 coating displayed the highest COF value at the end of the test, which results from the progressive difficulty in forming the tribo-film (as it was explained earlier in sections 6.2.1 and 6.2.2). As can be observed in figure 6-4 b), the wear in the cylinder is of the same order as in section 6.2.2, meaning that a decrease of the contact stresses is occurring, making it difficult for the formation of the tribo-film and leading to an increase of the COF during the test.

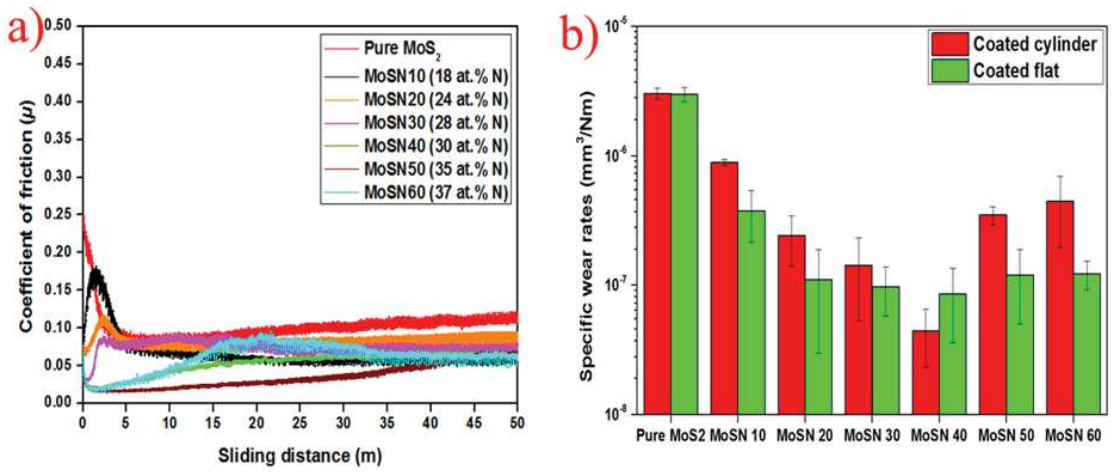

Figure 6-4: a) Evolution of the friction coefficient of all studied coatings with respect to sliding distance in a vacuum. The cylinder and flat are coated with the same deposition conditions. b) The specific wear rates for the coated cylinder and coated flat for all tests.

This trend was not as abrupt as shown in section 6.2.2 since the contact was now against a coated flat, making more MoS_2 lubricant available (in the contact) for the tribo-film formation. All the other coatings displayed almost similar and stable COF values in the last part of the tests. The intensity and position of the bumps in the COF curves are similar to those observed in section 6.2.1 and can be explained by combining the surface roughness and the set hardness / S/Mo ratio. For the relatively smoother coating surface (Mo-S-N40, 30 at. % N), almost no bump can be observed, suggesting that no mechanical interlocking is taking place in the running-in period. On the other hand, for the films where bumps are observed, the intensity of the bump typically increases with the roughness, as it would be expected. Concerning the extension of the bump, with direct consequences in the running-in period, as already mentioned, there is a close correlation between the mechanical strength and the extension of that period due to the increasing difficulty in overcoming the mechanical interlocking. Simultaneously, the hardness increase associated with a lower S/Mo ratio makes the formation of tribo-film harder, contributing to extending the running-in period. Overall, the COF for the last part of the test was in the range of 0.05-0.08 for Mo-S-N coatings.

The Mo-S-N coatings displayed low cylinder and flat wear compared to pure MoS_2 coatings due to the latter's low load-bearing capacity. Contrary to what was observed in the previous sections, both the coated flat and coated cylinder wear decreased with increasing nitrogen, up to 30 at. %. As already discussed above, this decrease should be expected due

to the increase in hardness, increase in compactness, and also due to a decrease in roughness of both coated parts. The trend is contrary to the other mating situations since both elements of the sliding pair are coated, making available immediately high amounts of material to form the tribo-film at very small wear volume, i.e., not needing a high quantity of wear debris and, thus, decreasing the initial wear volume. Therefore, from the very beginning, what is important for determining the wear rate is the mechanical strength of the sliding material. Again, it should be noted that the worn craters in the sliding elements are very shallow (only tens of nanometres), meaning that the wear process is in its very beginning. This is the reason why in the coatings with the highest hardness and the lowest S/Mo ratio, the initial process for forming the tribo-film is too long, consuming a high amount of material, and leading to an increase in the wear rate in comparison to the softer coatings with lower N contents (see figure 6-4 b)).

6.2.4. Variation of testing load

The effects of the variation of applied load on the evolution of the COF and the specific wear rate for coated cylinder versus coated flat are shown in figure 6-5, for one of the coatings showing the best tribological performance in section 6.2.3, i.e., Mo-S-N30 (28 at. % N). With 2 N applied load, the COF started from 0.12 and increased to 0.2 within ~12 m of sliding. The almost imperceptible bump observed for the 5 N tests was extremely enhanced for the 2 N. This coating has low roughness, which, as explained before, gives rise to very small mechanical interlocking in the beginning of the sliding test. However, for very low applied loads, the elastic deformation in the contact is much lower, allowing a higher interaction between roughness peaks in the two surfaces, thus leading to a higher COF.

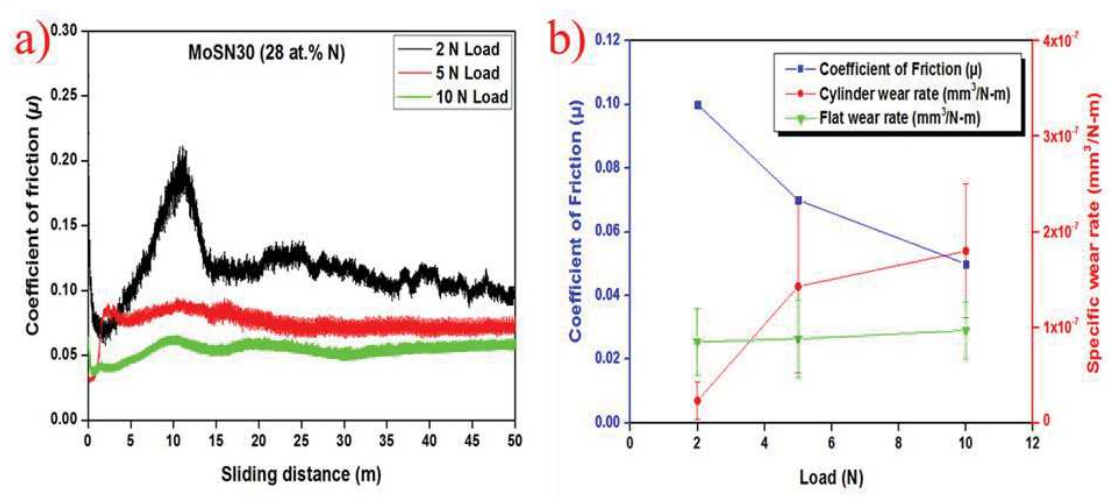

Figure 6-5: a) Evolution of the friction coefficient with varying load in a vacuum condition. The cylinder and flat are coated with Mo-S-N30 (28 at. % N). b) Coated cylinder and coated flat specific wear rates and COF with the applied normal loads.

As the applied load is lower, the destruction of the roughness peaks promoting the interlocking is more difficult, which explained the permanence of the bump until a higher number of cycles. Subsequently, the COF abruptly decreases due to the tribo-film formation. Then, a slowly decreasing trend for COF is observed, reaching, in the end, a COF of 0.1. With an increase in the applied load from 2 to 5 N, the running-in period is reduced. The steady-state value is a little lower than the one achieved with 2 N loads. For the highest applied load (10 N), the COF decreased further down to 0.05. Despite testing in low contact stress regimes, the results (i.e., decrease in COF with applied loads), are in accordance with the literature on the TMD based coatings [156,169]. This confirms that higher applied loads favour the reorientation of TMD planes parallel to the sliding surface, increasing the coverage of the contact zones with the tribo-film and decreasing the COF [156].

Although the specific wear rate in the coated flat is kept approximately constant for all applied loads, an increase in the specific wear rate of the cylinders (figure 6-5 b)) is observed with increasing load. As referred above, the tribo-film formation is more extensive when the load is increased (figure 6-5 a)), meaning that a higher amount of wear debris was required to promote this transformation. Therefore, the higher loads lead to higher wear in the coated cylinder (the wear in the coated flat is similar), and consequently, higher values of the specific wear rates are observed.

6.2.5. Endurance test in vacuum: coated cylinder versus steel flat

In the final stage of vacuum testing, the endurance of one of the Mo-S-N coating, i.e., Mo-S-N40 sliding under coated cylinder versus steel flat arrangement was analysed. This mating surface approach was selected because of the kinematic length consideration as this condition is more severe and near to actual industrial sliding mechanisms. The pure MoS_2 coating was also analysed for comparison purposes. The COF results for both coatings are shown in figure 6-6 a), while the figures 6-6 b) and c) show the cylinder wear for the pure MoS_2 and Mo-S-N coatings, respectively. It is clearly visible that the pure coating displayed a continuous increase of the COF. The test was stopped as the COF reached a value of ~0.28 while the Mo-S-N coating displayed low and stable COF (~0.05) till 300 m. After this, the COF started to increase steadily to a value of ~0.34, where the test was stopped manually. Due to the hardness of Mo-S-N coatings, the increase contact area was limited for a longer extent with the tribo-film facilitating the low friction up to about 250 m. Later, in the process of maintaining the tribo-film, more wear takes place. This results in an increase in the contact area and a decrease in the contact stresses.

Also, with respect to wear, the Mo-S-N40 coating performed far better than the pure MoS_2 and, was still not worn through the coated cylinder. The specific wear rate of Mo-S-N40 after 335 m of sliding was 2.77×10^{-7} $mm^3/N.m$, whereas, the pure MoS_2 showed 1.9×10^{-6} $mm^3/N.m$ wear rate with only 47 m of sliding. In short, this test shows the beneficial impact of N-alloying on the endurance of the nitrogen-alloyed MoS_2 coatings.

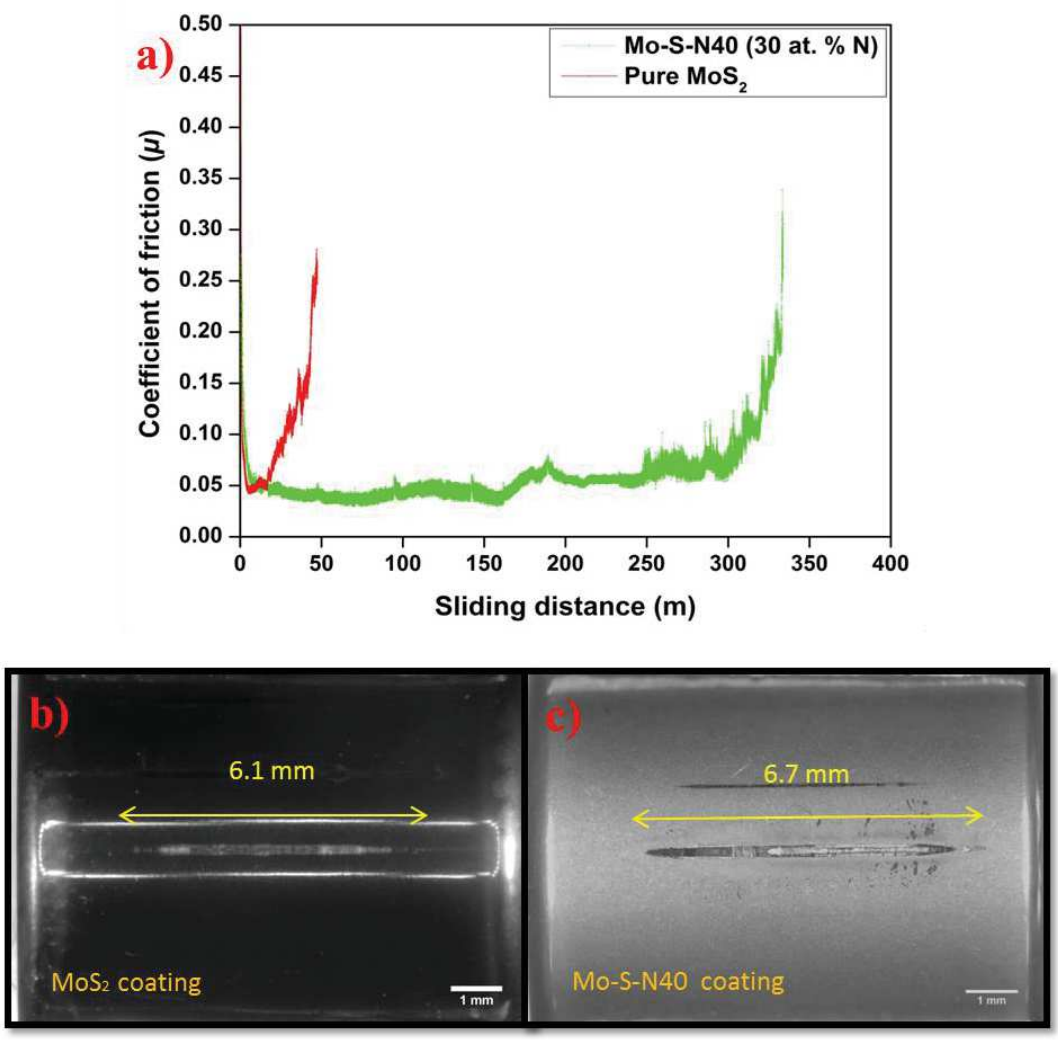

Figure 6-6: Endurance testing of Mo-S-N40 coatings in comparison to pure MoS_2 coatings. a) Evolution of friction coefficient of pure MoS_2 and Mo-S-N40 coating with respect to sliding distance tested in vacuum (10^{-4} Pa), b) Wear-scar of pure MoS_2 coated cylinder, c) Wear-scar of Mo-S-N40 coated cylinder that was tested for 365 m of sliding distance against steel flat.

6.2.6. Test in ambient air

One of the Mo-S-N coating was tested in an ambient air atmosphere as well. Again, the Mo-S-N40 (30 at. % N) was selected owing to its amorphous structure, least surface roughness, high hardness, low COF and least wear observed in vacuum testing. All the three mating surface tests were performed in this part of the thesis. The findings are shown in figure 6-7. It can be seen that the COF for all mating surfaces started from ~0.15 and increased progressively. All the friction curves adapted to their kinematic length considerations of cylinder-on-flat as observed in vacuum tests. The coated cylinder versus coated flat (in black), as well as the steel cylinder versus coated flat (in red), tests exhibit a

similar increase in the COF with the sliding distance but much less than the case of coated cylinder versus steel flat which showed a rapid increase. Overall, for all these conditions, the increase in COF can be explained by; i) low values of applied contact stresses which lead to an inability in a suitable tribo-film formation, ii) presence of surface oxides which prefers formation of non-lubricious MoO_3, iii) the curvature profile of the cylinder, in which the contact area increases on wearing and, consequently, decreases the contact stresses, and iv) low sliding speed of the reciprocating motion which is conducive to form new oxides on the flat surfaces in ambient air. Therefore, a layer of MoO_3 formed on the surface of the coated parts would drastically affect the rate of the formation and the uniformity of the MoS_2 tribo-films [105,170]. It can be said that, initially, there will be an increase in the friction until this oxidized surface layer is worn off or removed from the contact surface. Contrarily, despite the high COF, the coating did not wear through the coatings for any coated parts (coated flats or coated cylinders).

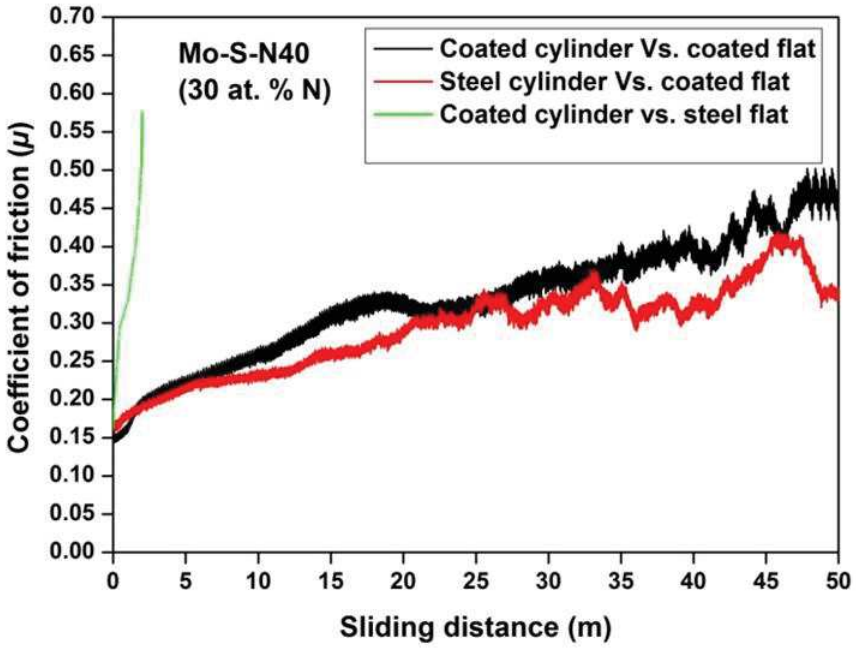

Figure 6-7: Ambient air test for one of the Mo-S-N coatings (i.e. Mo-S-N40 with 30 at. % N).

6.3. Discussion

This chapter mainly dealt with the study of vacuum tribological properties achieved after N-alloying of MoS_2 coatings. The pure coating was also discussed as a reference to differentiate the useful role of N-alloying. The literature lacks reports on the vacuum

tribological testing of Mo-S-N coatings, particularly for low contact stresses. Later, one of the coatings (i.e., Mo-S-N40 (30 at. % N)), was tested for its endurance in vacuum. The last stage was the ambient air sliding testing of the Mo-S-N40 coating. For solid lubricant coatings to be durable, high interfacial adhesion strength between the coatings and the substrates is one of the most important requirements for vacuum tribology and aerospace applications [171]. The importance of a hard underlayer was deemed essential for low friction in literature [172]. Dominguez et al. [173] reported that for the WSe_x system, a W-rich underlayer could provide good mechanical support to guarantee a low contact area. The Mo-S-N coatings utilized in this work showed a high adhesion (as described in chapter 4) and, hence, these coatings are very likely to offer improved tribological properties.

The detailed vacuum tribological studies were carried out under different conditions of applied loads and mating surfaces. For the first time, Mo-S-N coatings were tested with contact stresses complying with real industrial requirements. This choice of low contact stresses is in contrast to most of the literature, wherein solid lubricants were invariably tested under much higher applied contact stresses in the range 500-1500 MPa. Thus, the COF reported in the current study are much closer to the values during real applications, unlike those in literature [53,62,156,164]. Different mating conditions were tested since the initial state of mating materials can affect the COF values. It was found that the sliding with both surfaces coated (i.e., coated cylinder versus coated flat), provided a short running-in period and a stable COF when compared to the conditions where one surface is uncoated. In latter cases, a very high initial wear of the coated part is needed to form efficient tribo-films, which is drastically reduced if both elements of the sliding pair are participating in this process. After the formation of the tribo-film, an efficient sliding is achieved with low COF. Therefore, the coating versus coating provides a better wear resistance compared to steel versus coated surface by a faster tribo-film formation and durability. It should also be noted that the literature does not report any testing of the Mo-S-N or any other TMD system in the coating versus coating arrangement.

In high vacuum (10^{-4} Pa) conditions, due to the absence of oxygen, the formation and stability of the tribo-films are enhanced. It was observed that sufficient wear is necessary to provide a low tangential force. For Mo-S-N coatings, the possible bond formation in amorphous coatings (28 at. % N and above) would be a ternary disorder phase, with Mo bonded to S and N, arising from the distorting atomic placement in the

stoichiometric MoS_2 structure. Alternatively, nitrogen can also be present in the form of N_2 gas trapped within the lamellae, contributing to the amorphous structure. When sliding, the amorphous structure is transformed into MoS_2 crystalline tribo-films, which governs the low COF. The low COF achieved for Mo-S-N coatings sliding in vacuum agrees with this hypothesis, namely the MoS_2 tribo-films playing the dominant role in the low friction regime. A similar phenomenon was theoretically explained for W-S-N coatings by Isaeva et al. [58], where the WS_2 tribo-films governed the low friction. Muratore et al. [174] also showed such phenomenon earlier. The depth (thickness) of these tribo-films (transformed or deformed layers) depends on either the magnitude of the stresses in the contact region (directly proportional to the applied loads) or the properties of the coatings, such as the platelet size and packing density, the adhesion to the substrate, and the mechanical properties [163].

The results also showed the need for an initial wear as a source of lamellar MoS_2 for the tribo-films formation. In the Mo-S-N coatings, the higher the S/Mo ratio, the shorter is the period for the tribo-film formation. For instance, the softer coating (e.g., Mo-S-N10 (18 at. % N)) tends to wear less than the harder one (e.g., Mo-S-N50 (35 at. % N)). However, at the end of the test, the COF values of all the coatings were close to each other (see figures 6-1 and 6-2). Highly ordered intrinsic lamellar structure of MoS_2 phases in the top surface ensures low friction of the deposited coating, whereas the amorphous layers underneath provide the necessary hardness phase for supporting the applied stress; both phases play key roles in determining the wear-life of the deposited coatings. In the end, the MoS_2 tribo-films govern the friction and, hence, the end values of COF were similar.

Roughness also plays a critical role on the tribological behaviour of the coatings. In relation to the friction, due to the low applied stresses, mechanical interlocking occurs between the asperities of the surfaces (first part of the test). This effect leads to the presence of an initial bump in the friction curves, whose intensity and duration depend on the roughness level and the hardness of the coatings, respectively; the rougher the coating, the deeper the interlocking and the higher the intensity of the bump. With increasing N content up to 30 at. %, the roughness decreases, and the intensity of the bump vanishes. Subsequently, for higher N contents, the roughness increases, and the bump is again detected. The increase in the mechanical strength of the coatings makes the destruction of the mechanical interlocking more difficult, retarding its deleterious effects on the COF and

increasing the duration of the bump. After overcoming the mechanical interlocking, the progressive formation of the tribo-film justifies the observed decreasing trend of COF. Due to the specificity of the current tribological test, particularly the lateral profile of the counter cylinder, an increase of the COF with the number of cycles was observed in some cases. This trend can be explained by the progressive increase in the contact area when the parts are being worn out, which gives rise to a decrease in the contact stress and an increasing difficulty of adequately forming the tribo-film.

The wear of the sliding parts is decided by the hardness of the coatings as well as the availability of the potential lubricious material for forming the tribo-film. If the COF is similar in a specific type of sliding contact, it would be expected that the harder the material of the coating, the lower the wear rate. For this type of system such as Mo-S-N, the stable sliding is only achieved when a lubricious tribo-film based on MoS_2 is formed in the interface with the basal planes aligned in the sliding direction and parallel to the substrate. For the formation of this tribo-film, a running-in process must occur during which materials are being worn out. The amount of lubricious phase in the sliding contact will determine the number of cycles needed for establishing the tribo-film. The longer the running-in, the higher the amount of wear. In most cases, the initial volume of wear is small when compared to the total worn volume at the completion of the test. However, with this tribological test, the worn zones are very shallow at the end, meaning that the initial wear of the running-in process has an important influence on the final wear volume. The addition of N has two main influences in the coating; on the one hand, it increases the hardness and, on the other, it decreases the S/Mo ratio (and consequently the amount of the potential lubricious phase). These two trends have antagonic effects: the hardness improves the wear resistance, but the S/Mo increases the wear volume during the running-in process. Therefore, the evolution of the specific wear rate with the N content will depend on the compromise between these two effects. If the running-in period is too short (or if a high amount of lubricious phase exists, as in the case of mating “coated flat and coated cylinder”), for N contents lower than 30 at. %, the initial worn volume is not significant in relation to the total wear volume and, hence, the hardness is important: the wear rate decreases with the increase in the N content. It is important to remark that the running-in increases for the highest N contents (figure 6-4 a)), along with the wear rates. When a high amount of wear is necessary to form the tribo-film (e.g., in the mating “uncoated versus

coated") the initial wear volume is important, in relation to the total wear. The coatings with lower N contents exhibit lesser wear rates than those with higher N content despite their lower hardness, as shown in figures 6-1 b) and 6-2 b).

The effect of testing MoS_2 based coatings in ambient air has been extensively reported in the literature. Lince et al. [170] observed that the ambient air results in the significant oxidation of the lubricating layer of MoS_2, leading to the formation of non-lubricating MoO_3. In highly compact / less porous coatings, the amount of oxidation might be lower. However, the amount of oxidation would be enhanced at the surface of the coatings, where the tribological interactions in the lubricated devices occur, causing poor frictional properties, as compared with the vacuum sliding. Further details and reasons for the poor frictional properties of optimized Mo-S-N coatings in ambient air (compared to vacuum testing) are explained in the next chapter after an in-depth wear track analysis using HR-TEM studies.

6.4. Conclusions

This chapter has covered the first-ever low contact stresses vacuum tribological testing of Mo-S-N coatings deposited using a small semi-industrial DC magnetron sputtering chamber equipped with a single MoS_2 target and an additional secondary plasma source. The properties are analysed with respect to the N-alloying of MoS_2 coatings. The vacuum tribological tests were performed with different contact body configurations and applied loads. The loads were selected to provide an initial Hertzian contact stresses in the range of 60 – 135 MPa, complying with real industrial needs. Higher wear resistance was achieved for coating versus coating sliding, compared to the coating versus steel sliding. Though the mechanism behind low friction is similar in both cases (i.e., the formation of tribo-films from either the nano-crystalline or the amorphous structures), the achieved wear rates varied, depending on the sliding surfaces. If the running-in period is excluded, all coatings showed a COF in the range from 0.05-0.1 at the completion of the tests. Only in one case (pure MoS_2 film in the coated cylinder versus steel flat configuration), the test had to be stopped before the defined time due to a strong increase of the COF. This result was explained due to the inadequate formation of the lubricious tribo-film because of an unexpected decrease in the contact stresses. The COF was dependent on the instantaneous

contact stresses. As a general trend, the COF decreased with an increase in the contact stresses. Overall, a least specific wear rate of $8.6x10^{-8}$ $mm^3/N.m$ (coated flat) was observed for Mo-S-N40 (30 at. % N) in the coating versus coating interaction, and $1.5\ x10^{-7}$ $mm^3/N.m$ (coated flat) for Mo-S-N10 (18 at. % N) in the steel versus coating interaction. The endurance study in vacuum for Mo-S-N40 (30 at. % N) coating showed that the coatings were much more durable than the pure MoS_2 one. The reason for the increase in the COF is the increase in the contact area and the decrease in the contact stresses. In Mo-S-N40 (30 at. % N), the specific wear rate was lower due to the increased hardness, thus sustaining a longer test duration. The same coatings in ambient air exhibited an increased COF (0.3), due to the oxidation of the surface in ambient air resulting from the combined effects of moisture and oxygen. This work addresses some important issues when testing transition metal dichalcogenides-based coatings under low contact stress conditions. There is a threshold value for the contact stress for which no suitable tribo-film can be formed with the consequent increase in the COF. Finally, it is also proved that the consideration of coating versus coating mating surfaces is very essential for superior tribological performance.

Chapter VII

7. TRIBOLOGICAL BEHAVIOUR IN DIVERSE ENVIRONMENT

7.1. Introduction

Following the tribological testing in vacuum and ambient air environments, a detailed characterisation of the wear tracks (mainly the wear mechanism) after sliding is carried out. At this stage, only one coating, i.e., Mo-S-N40 having 30 at. % nitrogen was deposited for the analysis. This coating showed a COF of 0.05 in vacuum and 0.3 in ambient air when tested with low contact stresses against 100Cr6 steel counterbody. To investigate their performance in high contact stresses, further tests were performed. The tribological testing presented here is carried out using ball-on-disc (flat) tribometer. The testing was performed with high contact stresses (~800 MPa). Further details about the main characterisation and tribological testing can be seen in sections 3.4 and 3.4.13, respectively. Subsequent to the tribological testing, the wear tracks, after both testing conditions, were analysed in HR-TEM to investigate the underlying wear track behaviour involved in each case of the sliding environment. The results presented here give insight into the role of nitrogen and subsequent tribo-film formation in the vacuum and the effects of the surface oxides on the tribo-film formation in ambient air. The results are supported with publication in annex C.

7.2. Results

7.2.1. Main characterisation results of Mo-S-N40 coating

The Mo-S-N40 coating had nitrogen content of 30 at. %, S/Mo ratio of 1.36 and a thickness of 1.3 μm. The coating was compact and XRD amorphous. Due to the alternating substrate exposure to the MoS_2 target and the secondary plasma source (ion bombardment), a multilayer structure was formed. This type of deposition mechanism enabled the coating to incorporate a higher N content along with a high S/Mo ratio, unlike similar systems reported in the literature [53,156]. XPS analysis showed that for coatings with N content lower than 28 at. %, N1s peak at ~ 397.0 eV, corresponding to γ-Mo_2N [156], is enhanced

with increasing N content. Mo-N bonds, shown via peaks at 229.0 eV and 232.4 eV, also showed an increased intensity. However, for N contents equal or higher than 28 at. % (such as Mo-S-N40 with 30 at %. N), the global intensity of the N1s peak continues to grow, but the Mo-N bond intensity remained constant. Therefore, a suggestion was made that, initially, N replaced the S sites, distorting the lattice and reducing the crystallinity of the coatings, and, further addition of N, led to N_2 gas entrapment within the amorphous coating (28 at. % N and above).

7.2.2. Tribological analysis in vacuum and ambient air conditions

The COF evolution, resulting wear-track profiles, micrographs of the ball wear-scar and disc tracks after vacuum (10^{-2} Pa) and ambient air (24 °C and 20 – 30 % RH) tests are presented in figure 7-1. The frictional behaviour was dissimilar during sliding in a diverse atmosphere.

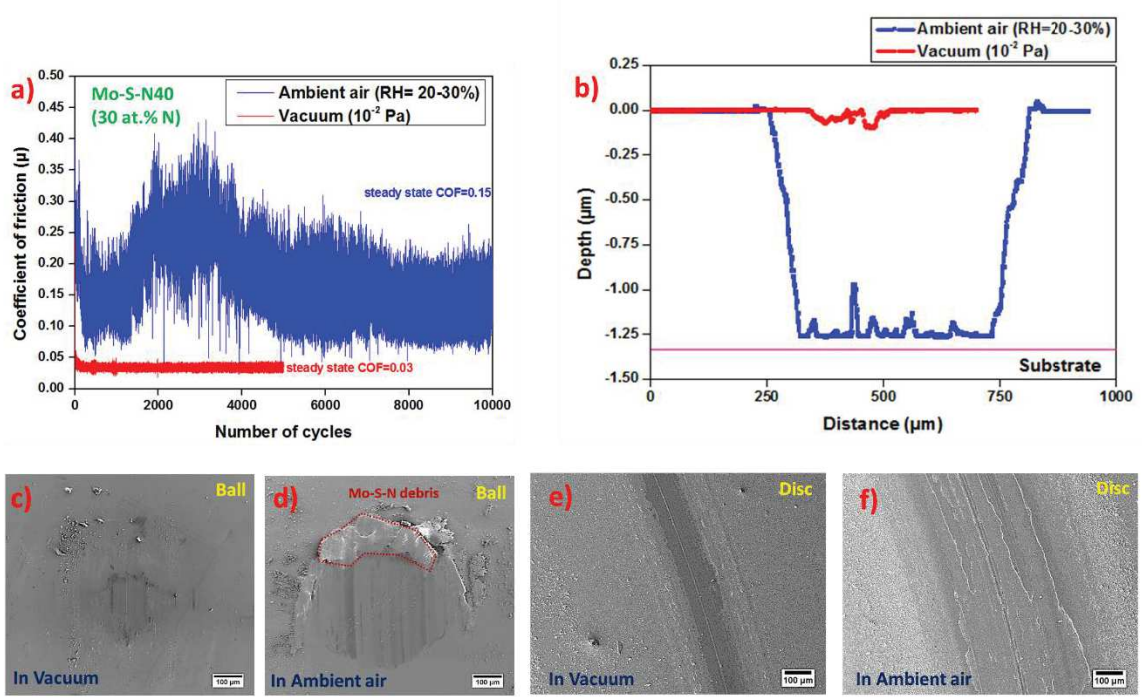

Figure 7-1: a) Evolution of COF for coated disc (flat) using 100Cr6 steel ball in ambient air and vacuum environments, (b) depth profile of wear-tracks, (c, d) wear-scar micrographs of steel balls and (e, f) worn region of the coated wear-tracks.

In vacuum, the COF stabilised after a brief running-in period at ~0.03. The maximum depth of the wear track was ~0.06 µm. The wear-scar images show negligible wear on the counterbody and a smooth wear-track with no evidences of large flakes or wear

debris. The resulting friction value implies that the MoS_2 tribo-film forms near the interface (figure 7-2 d). The MoS_2 (002) planes are formed due to the crystallisation / reorientation of basal planes parallel to the sliding surface and resulted in a low COF [175]. The specific wear rate determined from the profile was about $1.8x10^{-7}$ mm^3/N-m.

In ambient air, the COF reached a peak value of ~0.35 and, then, dropped to a steady-state friction value of ~0.15. The maximum wear depth was ~1.26 μm, a 20-fold increase compared to the vacuum test. The improved adhesion is attributed to the hard-gradient layer consisting of metallic bonds with low lubricious phase content, which prevented the delamination of the coatings from the steel. The bottom of the worn track in ambient air is flat and wide (figure 7-1 b), which corresponds to a significant wear on the steel ball (figure 7-1 d), caused by the absence of a protective tribo-film at the sliding interface. Large wear debris on the counterbody were identified as O-rich Mo-S-N material. In ambient air, the presence of H_2O and O_2 contributes significantly to the degradation of MoS_2, preventing the formation of a lubricious tribo-film from the amorphous coatings and forms surface oxides. Actually, during sliding, the weak interlamellar bonds break, increasing the potential of O to react with MoS_2. Furthermore, the formation of oxides (especially MoO_3), as clusters (particles), or asperities could have enhanced the wear of the coatings and steel ball, when present in the contact region (abrasion). The specific wear rate in ambient air was two orders of magnitude higher as compared to vacuum, i.e., $1.7x10^{-5}$ mm^3/N-m. However, it should be noted that the steady-state COF is significantly lower than what could be expected in steel versus metal contact, which could be attributed to the presence of either Mo-S-N zones (debris and residual coating in the wear-track (figure 7-3) or Mo-oxides. MoO_3 is known to provide relatively low friction [176].

7.2.3. HR-TEM analysis of wear tracks

In the post vacuum tribological testing, the entire wear track displayed zones covered by well-oriented planes parallel to the surface. These planes correspond to MoS_2 tribo-films. The cross-section of the wear-track corresponding to a particular area where the tribo-film delaminated cohesively, leaving a gap in relation to the as-deposited coating, is shown in figure 7-2 c). The separated / top part consists of large amounts of pure MoS_2, i.e., tribo-film in figure 7-2 d). These tribo-films are of long-range order (tens of nanometres) parallel to substrate. The crack is created by the exfoliation of the weakly

bound hexagonal structure of the MoS_2 tribo-film during sliding. In the top part of the coating, oriented planes are visible confirming their formation mechanism, i.e., transition from amorphous to lamellar structure at the sliding interface (figure 7-2 c). The amorphous coating underneath provides the required strength and hardness to support the solid lubricant interface.

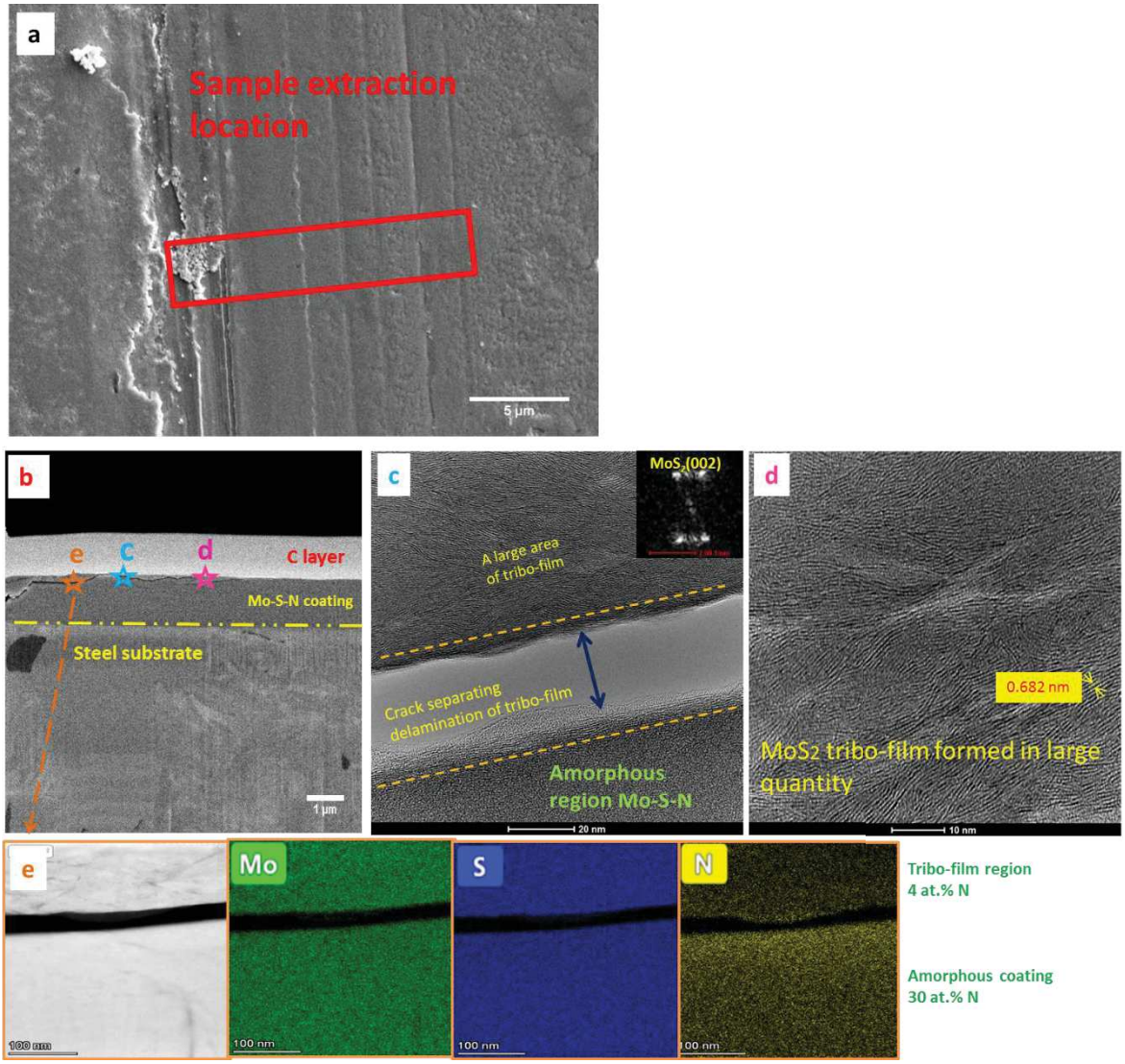

Figure 7-2: TEM analysis of wear track after tribo-testing in vacuum: a) Wear track with site of sample extraction. b) FIB cut cross-section of wear-track showing a flake lifted from the pristine coating. c) The crack caused by the delamination of the tribo-film. d) Large quantity of preferentially oriented MoS_2 tribo-film. e) STEM- EDX images showing the elemental distribution of Mo, S, and N at the interface.

The large quantity of tribo-film in the separated region spreads along the wear-track during tribo-testing leading to a short run-in time, low values of COF (see figure 7-1 a) and insignificant wear. The tribo-film provides the low shear strength needed for easy sliding.

Figure 7-2 e) shows the EDX elemental maps of the separated tribo-film regions, which are nitrogen deficient (approximately 4 at. % N) when compared to the measured 30 at. % of N in the amorphous coatings. The 4 at. % detected N could be attributed to nitrogen that had replaced some of the S sites. The remaining nitrogen (26 at. %) was released into the vacuum as a gas, and thus, did not appear in the quantification. So, our experimental work brings strong evidence to support the theoretical framework presented by Isaeva et al. [58]. Mo and S were found in similar concentrations in both regions; hence, in vacuum, the sliding motion causes wear down to a specified depth, which is transformed into the tribo-film. A fully formed tribo-film prevents further wear of the coating underneath. Negligible wear was observed on the surface of the counterbody, which is associated with sliding on a highly lubricious interface composed of pure MoS_2, as shown in figure 7-2 d). The high hardness and Young's modulus of the Mo-S-N coatings, with the lubricious interface, limit the deep penetration of the counterbody (sinking), thus maintaining a small contact area.

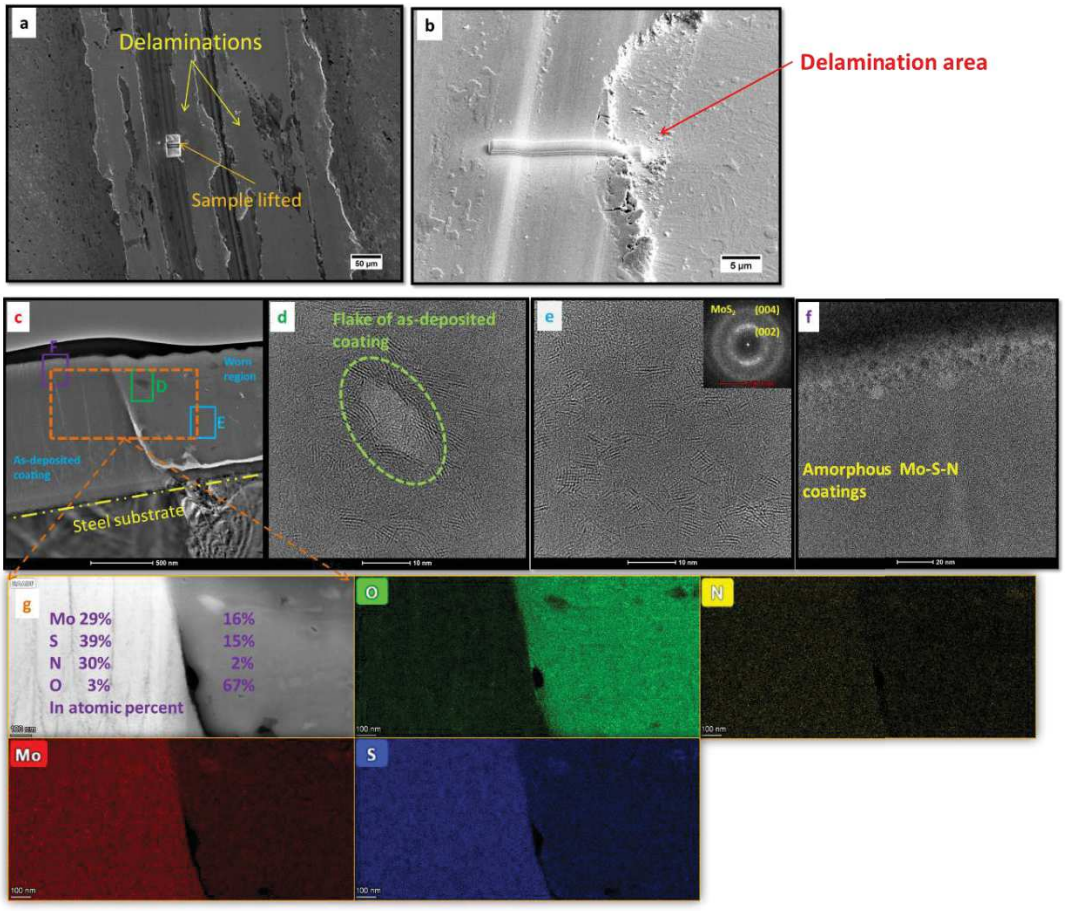

Figure 7-3: Cross-section of wear-track in ambient air test. (a, b) Specimen location. c) Low magnification cross-sectional image. d) Flake of as-deposited amorphous coating within the contact

worn volume. e) Disrupted lamellar MoS_2 layers in the worn volume. f) Region of pristine amorphous coatings outside the wear-track. g) STEM-EDX elemental mapping of wear-track and pristine coating.

Figure 7-3 shows: a region of large delamination on the wear-track, the location of the TEM lamella extracted, the cross-sectional micrographs and the elemental maps corresponding to the wear-track generated by tribo-testing in ambient air. The wear debris of the coating consists of randomly oriented nanometre-size traces of lamellar MoS_2 layers embedded in an O-rich brittle amorphous matrix (figure 7-3 e) and g)). A crack in the coating separates the as-deposited film and the wear debris (figure 7-3 c)). The local delamination of the coating and the significant wear debris are the result of the oxidation and the abrasive wear induced by the oxide particles. The top interface of the wear-track, (figure 7-3 f)) are devoid of tribo-films which could have induced low friction at the mechanical contact. The ball counterpart reached the adhesion improving layer (gradient layer) which was not worn through.

It is well known that in ambient air, the water vapour and the oxygen from the atmosphere accelerate the oxidation of MoS_2 [170]. This oxidation can affect the bulk of the material, creating internal blisters that act as weak points leading to cracking and high volumes of debris [177]. Additionally, when MoS_2 layers are exposed during sliding, the oxidation process is triggered yielding more debris and wear. This is evident in figure 7-3 d), in which the oxidised coating is mixed with nanoparticles of MoS_2. The STEM-EDX analysis confirms the severe oxidation of the worn debris. The S/Mo ratio is reduced from 1.34 to 0.93, along with a large concentration of oxygen (~ 67%).

Similar to the findings in the test performed in vacuum, a reduction of the nitrogen content at the sliding contact can be observed in ambient air conditions. The 22-fold increase in the O content implies that, with each cycle of friction test, the formed surface oxide would be trapped and dragged into the coatings forming a third body.

The main driving force for the significant increase in the wear observed in ambient air testing is the formation of surface oxides. Additionally, as Ramalho et al. [178] discussed, the linear relationship between the wear and the dissipated energy would be one of the reasons behind the increase in COF values and the poor tribological performance in air. The interaction with the atmospheric oxygen and humidity at the sliding interface prevents the coating from forming a continuous well-oriented tribo-film. Khare et al. [179] reported that the friction of MoS_2 in ambient air is a strong function of the amount of water

in the environment and the water diffused into the bulk. Probably due to the similar reasons, the present study has shown that the process of forming well-ordered tribo-film is absent. Instead, the amorphous coating was directly oxidised and / or remained amorphous, which leads to a high COF. In contrast, during the vacuum test, in the first few cycles, the surface oxides are removed along with the initial wear. With no oxygen or water vapour, the further worn coating transforms from amorphous into crystalline MoS_2 tribo-films oriented parallel to the substrate.

The nitrogen incorporated in the coating provides the required hardness through the amorphization during the deposition. This has been predicted to either form a ternary compound Mo-S-N (by replacing S sites) or distort the MoS_2 crystalline structure by diffusion into the layers. The chemical analysis performed on the as-deposited coating and the wear debris (shown in figure 7-3 g) suggests that N is released, does not bond to other elements to form nitrides, and cannot be found as part of wear debris on the coating nor the sliding counterpart. Therefore, the mechanical interaction is believed to cause the release of nitrogen most likely as an inert gas. These measurements support the theoretical hypothesis which claims that the gas is distorting the MoS_2 lamellar structure and only a small amount (~4 at. %) of the gas is found to be present at the sliding interface after testing. Hence it is believed this small amount of N replaces sulphur.

The thickness of the tribo-films formed by deformation depends on the applied pressure and the properties of the coatings such as the platelet size, packing density, the adhesion of the platelets to the substrate and the COF [163]. Tribo-testing in vacuum showed the local transformation of the amorphous coating into a crystalline lubricious interface, as well as the release of nitrogen in gaseous form. A sufficient thickness of the tribo-film prevents further wear, as observed in vacuum testing. These conditions are not met for sliding in ambient air, where oxidation occurred during the crystallisation process of MoS_2 forming an amorphous mixture which can contain MoO_3 and Mo-S-N particles. Oxides found at the sliding interface act as abrasive particles leading to severe wear and decreasing the contact stresses which is required for the crystallisation of pure MoS_2.

Even when testing in ambient air, a part of the coating always remained attached to the steel substrate despite the extensive delamination. This is the result of integrating the bonding multilayers, as described in chapter 4. This gradient layer provides improved adhesion of the coating to the steel due to the metal-metal quasi-epitaxial bonding. The

remaining part of the Mo-S-N coating and the formed oxides can explain the steady value of the COF at 0.15, value much lower than the one expected in a metal / metal contact.

7.3. Conclusions

Amorphous Mo-S-N coatings with 30 at. % N content were tribo-tested in vacuum (10^{-2} Pa) and ambient air in order to analyse the process of tribo-film formation and the role of N on the lubricating behaviour of Mo-S-N coatings. In the vacuum test, a steady-state friction is quickly reached with a COF value of 0.03. HR-TEM studies revealed that with insignificant wear, the transformation of the amorphous coatings, into a lamellar MoS_2 tribo-film and the release of nitrogen in N_2 form have occurred. The tribo-film formation would require the release of the trapped N_2 gas and the rearrangement of Mo and S atoms to form the hexagonal structure. The amorphous coating underneath the tribo-films provided the required hardness and the load-bearing capability. Testing in ambient air resulted in a long running-in period with a COF peak value of 0.35, which stabilised later at 0.15 but with a significant wear. HR-TEM studies revealed that the presence of surface oxides and moisture disturbed the continuous formation of the MoS_2 lamellae in ambient air. The reaction with oxygen led to the formation of MoO_3. There was no sufficient uninterrupted tribo-film formed at the sliding interface, which explains the high COF in ambient air.

Thus, it can be concluded that nitrogen is a favourable element for alloying / doping MoS_2 coatings. Nitrogen-alloying promotes the amorphisation of MoS_2, by distorting hexagonal structure, and making the coatings compact. On the other hand, during sliding, a large amount of N is released as N_2 gas, enabling the formation of MoS_2 tribo-films and providing an easy sliding. Even with increased wear in ambient air, the excellent adhesion of the coatings to steel revealed no delamination at the coating-substrate interface. These coatings are likely to be highly suitable as layered self-lubricating materials for vacuum applications.

Chapter VIII

8. CONCLUSIONS AND FUTURE WORKS

In this thesis, a systematic study was performed to improve the adhesion of TMD coatings (particularly MoS_2 and Mo-S-N). Then, the attention was focused on the less explored Mo-S-N coatings and their tribological performance. For the first part, a novel hybrid deposition procedure based on sputtering + ion bombardment was used to improve the adhesion of the coatings. Later, by varying the N content, the optimization of Mo-S-N coatings was performed in relation to the chemical composition, chemical bonding, morphology, structure and mechanical properties and their influence on the tribological behaviour. The tribological testing were performed for all the N-alloyed coatings using a cylinder-on-flat reciprocating tribometer with low applied contact stresses. One of the coatings was also tested in a ball-on-disc (flat) rotating tribometer to understand better the tribological behaviour in vacuum and ambient air environment.

In the first step, the scope was to deposit MoS_2 with high adhesion to a steel substrate. No additional metallic interlayer (e.g., Ti or Cr) was used to improve adhesion as usual for sputtering deposition processes; instead, the deposition from a single MoS_2 target along with an additional bombardment by a secondary plasma source was used. In a typical deposition run, firstly, the chamber was heated to achieve high purity with removal of the adsorbed moisture and water vapours. Subsequently, the bias etching of the substrate was performed utilizing the secondary plasma source in high biased conditions. The target was sputtered cleaned at low chamber pressure as well. Next, the deposition from the MoS_2 target started, also with a high substrate bias and a high ion flux from the plasma source. In this way, a sub-stoichiometric (very low S/Mo) layer was deposited, due to a strong re-sputtering of sulphur, providing a metallic bonding with the steel substrate. Then, the nitrogen was introduced to form nitrides with Mo and to prevent the lamellar formation when the sulphur will be increased later. The substrate bias was reduced to slowly increase the sulphur content in the growing coatings. Finally, the required N content coating was deposited by varying the nitrogen flow at low substrate bias conditions. The additional plasma source was maintained active along with the deposition of the coatings, for increasing the ion flux arriving to the growing films allowing near-surface modifications

by bombardment as, for example, on the chemical composition. The adopted deposition procedure allowed to achieve a high adhesion critical load on the steel substrate for Mo-S-N and pure MoS_2 coatings (> 80 N). The reason for such high adhesion was the interface mixing of Mo with steel. The MoN(S) and MoS(N) multi-layer also reinforced the adhesion of the layers on the top. This multilayer was due to the alternate deposition from the MoS_2 target followed by the higher N bombardment at the plasma source, as a consequence of the rotation of the substrate holder. This multilayer was observed by HR-TEM and confirmed by the complementary composition analysis of N and S carried out by ToF-SIMS. Thus, this adhesion improvement approach, excluding additional targets, not only simplifies the depositions in the industrial environment but also solves major industrial issues related to the integrity of the coating system.

The chemical composition, chemical bonding, morphology, structure and mechanical properties were studied as a function of the N-content of Mo-S-N coatings. With heating and pumping prior to the bias etching and deposition, very low oxygen content (less than 1 at. %) was achieved in the coatings. The structure of the coatings changed with the incorporation of nitrogen. The coatings with less than 30 at. % N were nanocrystalline; for higher contents, the coatings became XRD amorphous. The morphology was increasingly more compact with the incorporation of nitrogen. HR-TEM also confirmed the amorphism of high N-content coatings. The S/Mo ratio decreased and reached 1.25 for the highest N incorporation (37 at. % N), which presented a high hardness of 8.9 GPa. Though the S/Mo ratio decreased, the value was higher than that reported in literature for the same content of nitrogen-alloying. With increasing N content, the scratch resistance of the coatings improved, reaching the highest value of 38 N for 28 at. % N. Nitrogen was incorporated in the amorphous ternary compound, Mo-S-N, with Mo-N and Mo-S bonds. Thus, after this optimization process, Mo-S-N coatings were developed with enhanced adhesion, high S/Mo ratio, high compactness, high hardness, high scratch resistance and low contaminant content.

In a further step, the first-ever low contact stresses tribological testing of Mo-S-N coatings was performed in secondary vacuum and ambient air environment. The properties were analysed with respect to the N-alloying of the MoS_2 coatings. The vacuum tribological tests were performed with different contact body configurations and applied

loads. The loads were selected to provide an initial contact stresses in the range of 60 – 135 MPa, complying with real industrial needs. Higher wear resistance was achieved for the coating versus coating sliding pair, compared to the coating versus steel one. Though the mechanism behind low friction is similar in both cases (i.e., the formation of tribolayers from either the nano-crystalline or the amorphous structures), the achieved wear rates varied, depending on the sliding surfaces. If the running-in period is excluded, all coatings showed a COF in the range from 0.05–0.1 at the completion of the tests. Only in one case (pure MoS_2 film in the coated cylinder versus steel flat configuration), the test had to be stopped before the established time due to a strong increase of the COF. This result was explained by the inadequate formation of the lubricious tribolayer due to an unexpected decrease in the contact stresses. The COF was dependent on the instantaneous contact stresses. As a general trend, the COF decreased with an increase in the contact stresses. Overall, the least specific wear rate of 8.6×10^{-8} $mm^3/N.m$ (coated flat) was observed for Mo-S-N40 (30 at. % N) in the coating versus coating interaction, and 1.5×10^{-7} $mm^3/N.m$ (coated flat) for Mo-S-N10 (18 at. % N) in the steel versus coating interaction. The endurance study in vacuum for Mo-S-N40 (30 at. % N) coating showed that it lasts much longer than the pure MoS_2 one. The reason for the increase in the COF is the increase in the contact area and the decrease in the contact stresses. In Mo-S-N40 (30 at. % N), due to the increased hardness, the specific wear rate was lower, thus sustaining a longer test duration. The same coatings in ambient air exhibited an increase of the COF (0.3), due to the oxidation of the surface resulting from the combined effects of moisture and oxygen. This work addresses some important issues when testing transition metal dichalcogenides-based coatings under low contact stress conditions. There is a threshold value for the contact stress for which no suitable tribolayer can be formed with the consequent increase in the COF. Finally, it is also proved that the consideration of the coating versus coating mating surfaces is to be considered for superior tribological performance.

From the previous studies, the amorphous Mo-S-N40 coating with 30 at. % N showed higher COF in ambient air, although without any failure. Thus, a motivation was created to apply higher contact stresses to understand if the COF could be reduced. Subsequently, this coating was tested in vacuum (10^{-2} Pa) and ambient air using a ball-on-disc rotating tribometer, against a 100Cr6 steel ball, in order to analyse the process of the tribo-film formation and the role of N on the lubricating behaviour of Mo-S-N coatings. In

the vacuum test, a steady-state friction is quickly reached with a COF value of 0.03. HR-TEM studies revealed that, with insignificant wear, the transformation of the amorphous coatings into a lamellar MoS_2 tribo-film occurred as well as the release of nitrogen in N_2 form. The tribo-film formation would require the release of the trapped N_2 gas and the rearrangement of Mo and S atoms to form the hexagonal structure. The amorphous coating underneath the tribo-films provided the required hardness and the load-bearing capability. Testing in ambient air resulted in a long running-in period with a COF peak value of 0.35, which stabilised later at 0.15 but with a significant wear. In these conditions, HR-TEM studies revealed that the presence of surface oxides and moisture disturbed the continuous formation of the MoS_2 lamellae. The reaction with oxygen led to the formation of MoO_3. There was no sufficient uninterrupted tribo-film formed at the sliding interface, which explains the high COF in ambient air. Nevertheless, it should be remarked that the residues of the coating attached to the wear track are responsible for keeping the COF at much lower values than those expected in a metal / metal contact.

Thus, it can be concluded that nitrogen is a favourable element for alloying / doping MoS_2 coatings. Nitrogen-alloying promotes the amorphisation of MoS_2, by distorting the weak and porous hexagonal structure, and making the coatings compact. On the other hand, during sliding, a large amount of N is released as N_2, enabling the formation of MoS_2 tribo-films and providing an easy sliding. This study shows that through indirect measurements of the chemical composition of the as-deposited coating and wear debris, some nitrogen can be stored in gaseous form (N2) within the amorphous matrix and released from the contact during the sliding. Even with increased wear in ambient air, the excellent adhesion of the coatings to the steel revealed no delamination at the coating-substrate interface. These coatings are likely to be highly suitable as layered self-lubricating materials for vacuum applications.

Future works:

- Although the adhesion critical load of > 80 N is sufficient for most of the tribological applications, it will be worthy to improve it further. This can be done by increasing the thickness of layer 1 (chapter 4) or also by modifying the substrate holder rotation speed. This can increase or decrease each layer of the multilayer arrangement induced by the alternate deposition.
- Future studies also include the evolution of Mo-S-N coatings with the temperature. The effect of structural changes from amorphous Mo-S-N coatings at high temperature will also include the possible release of any trapped N_2 gas with the heat treatment. The study of the frictional behaviour of Mo-S-N coatings at room and high temperature before and after heat treatment should also be carried out.
- The tribological analysis in ambient air needs to be performed in more detail to find the limits for the tribolayer formation that could indicate ways to improve the frictional performance. Testing in dry N_2 atmosphere can complement the tribological performance in different atmospheres.
- It is worthy to in-depth investigate the role played by nitrogen during tribological analysis in diverse environments. With an in-situ sliding stage with a mass spectrometer, the amount of N_2 gas released from the coatings during testing in vacuum could be evaluated.
- The current developed coatings are already suitable for industrial use. Further deposition on 3D parts will be carried out at HEF group. Some parts to be coated are finger followers, piston pin, journal bearings, and shutter hinges in the vacuum system.
- The developed Mo-S-N coatings can also be compared with hydrogenated DLC (H: DLC) in terms of tribological performance in vacuum and ambient air.

BIBLIOGRAPHY

[1] Gwidon Stachowiak Andrew Batchelor, Engineering Tribology 4th Edition, 2013.

[2] M. Changizi, R. Weber, R. Kotecha, J. Palazzo, Are Wet-Induced Wrinkled Fingers Primate Rain Treads?, Brain. Behav. Evol. 77 (2011) 286–290. https://doi.org/10.1159/000328223.

[3] Y.N. Drozdov, N. V Lukashina, T.I. Nazarova, Using the achievements in tribology for teaching technical disciplines, J. Mach. Manuf. Reliab. 40 (2011) 97. https://doi.org/10.3103/S105261881102004X.

[4] B. Bhushan, Principles and applications of tribology, John Wiley & Sons, 1999.

[5] A. Erdemir, J. Fontaine, C. Donnet, An Overview of Superlubricity in Diamond-like Carbon Films BT - Tribology of Diamond-Like Carbon Films: Fundamentals and Applications, in: C. Donnet, A. Erdemir (Eds.), Springer US, Boston, MA, 2008: pp. 237–262. https://doi.org/10.1007/978-0-387-49891-1_8.

[6] H. Waghray, T.-S. Lee, B.J. Tatarchuk, A study of the tribological and electrical properties of sputtered and burnished transition metal dichalcogenide films, Surf. Coatings Technol. 76–77 (1995) 415–420. https://doi.org/https://doi.org/10.1016/0257-8972(95)02564-2.

[7] M.F. Cardinal, P.A. Castro, J. Baxi, H. Liang, F.J. Williams, Characterization and frictional behavior of nanostructured Ni–W–MoS2 composite coatings, Surf. Coatings Technol. 204 (2009) 85–90. https://doi.org/https://doi.org/10.1016/j.surfcoat.2009.06.037.

[8] A.R. Lansdown, Molybdenum Disulphide Lubrication, Elsevier, 1999. https://doi.org/10.1108/ilt.2000.01852aae.001.

[9] R.L. Fusaro, Space mechanisms needs for future NASA long duration space missions, in: AIAA/NASA/OAI Conf. Adv. SEI Technol. 1991, 1991. https://doi.org/10.2514/6.1991-3428.

[10] R.L. Fusaro, Preventing spacecraft failures due to tribological problems, NASA Tech. Memo. 210806. (2001) date accessed: 22nd December 2020.

https://doi.org/NASA/TM-2001-210806, NAS 1.15:210806, E-12713.

[11] E.W. Roberts, Thin solid lubricant films in space, Tribol. Int. 23 (1990) 95–104. https://doi.org/10.1016/0301-679X(90)90042-N.

[12] ESA/ESTEC/TOS-QM Materials and Processes Division; SME Initiative Course, Materials (Basel).

[13] I. Santos, G. Migliorero, High precision linear actuator development, in: 13th Eur. Sp. Mech. Tribol. Symp., 2009.

[14] C. Donnet, J. Fontaine, T. Le Mogne, M. Belin, C. Héau, J.P. Terrat, F. Vaux, G. Pont, Diamond-like carbon-based functionally gradient coatings for space tribology, Surf. Coatings Technol. 120–121 (1999) 548–554. https://doi.org/10.1016/S0257-8972(99)00432-6.

[15] ECSS-Q-ST-70-01C Space product assurance-cleanliness and contamination control, (2008) Date accessed: 22nd December 2020.

[16] J. Fontaine, Elaboration, caractérisation et tribologie de couches minces DLC (diamond-like carbon) pour la lubrification des mécanismes spatiaux, 2000. http://www.theses.fr/2000ECDL0017/document.

[17] JR Jones, Lubrication friction and wear- Space vehicle design criteria/structures, NASA/SP-8063. (1971).

[18] J.R. Lince, Effective Application of Solid Lubricants in Spacecraft Mechanisms, Lubr. . 8 (2020). https://doi.org/10.3390/lubricants8070074.

[19] J. Menzel, K.; Jung, H.J.; Schmidt, Development of an Actuator for Ambient to Cryo Application., in: 40th Aerosp. Mech. Symp. Cocoa Beach, FL, USA, pp. 389–400.

[20] M.R. Vazirisereshk, A. Martini, D.A. Strubbe, M.Z. Baykara, Solid lubrication with MoS2: A review, Lubricants. 7 (2019) 57. https://doi.org/https://doi.org/10.3390/lubricants7070057.

[21] E.W. Roberts, Space tribology: its role in spacecraft mechanisms, J. Phys. D. Appl. Phys. 45 (2012) 503001. https://doi.org/10.1088/0022-3727/45/50/503001.

[22] M.A. Sherbiney, J. Halling, Friction and wear of ion-plated soft metallic films,

Wear. 45 (1977) 211–220. https://doi.org/https://doi.org/10.1016/0043-1648(77)90075-8.

[23] A. Erdemir, C. Donnet, Tribology of diamond-like carbon films: recent progress and future prospects, J. Phys. D. Appl. Phys. 39 (2006) R311–R327. https://doi.org/10.1088/0022-3727/39/18/r01.

[24] A. Vanhulsel, F. Velasco, R. Jacobs, L. Eersels, D. Havermans, E.W. Roberts, I. Sherrington, M.J. Anderson, L. Gaillard, DLC solid lubricant coatings on ball bearings for space applications, Tribol. Int. 40 (2007) 1186–1194. https://doi.org/https://doi.org/10.1016/j.triboint.2006.12.005.

[25] M. Kalin, I. Velkavrh, J. Vižintin, L. Ožbolt, Review of boundary lubrication mechanisms of DLC coatings used in mechanical applications, Meccanica. 43 (2008) 623–637. https://doi.org/10.1007/s11012-008-9149-z.

[26] R.L.C. Miyoshi, K.; Murakawa, M.; Watanabe, S.; Takeuchi, S.; Wu, Tribological Characteristics and Applications of Superhard Coatings: CVD Diamond, DLC, and c-BN, in: Appl. Diam. Conf. Carbon Technol. Jt. Conf. Japan, 31 August–3 Sept. 1999, 1999: pp. 268–273.

[27] R.L. Fusaro, Effect of substrate surface finish on the lubrication and failure mechanisms of molybdenum disulfide films, ASLE Trans. 25 (1982) 141–156. https://doi.org/10.1080/05698198208983076.

[28] T. Polcar, A. Cavaleiro, Review on self-lubricant transition metal dichalcogenide nanocomposite coatings alloyed with carbon, Surf. Coat. Technol. 206 (2011) 686–695. https://doi.org/10.1016/j.surfcoat.2011.03.004.

[29] J. Moser, F. Lévy, Crystal reorientation and wear mechanisms in MoS2 lubricating thin films investigated by TEM, J. Mater. Res. 8 (1993) 206–213. https://doi.org/10.1017/s0884291400120539.

[30] K.J. Wahl, D.N. Dunn, I.L. Singer, Wear behavior of Pb–Mo–S solid lubricating coatings, Wear. 230 (1999) 175–183. https://doi.org/https://doi.org/10.1016/S0043-1648(99)00100-3.

[31] M.R. Hilton, G. Jayaram, L.D. Marks, Microstructure of cosputter-deposited

metal- and oxide-MoS $_2$ solid lubricant thin films, J. Mater. Res. 13 (1998) 1022–1032. https://doi.org/10.1557/JMR.1998.0143.

[32] N.M. Renevier, N. Lobiondo, V.C. Fox, D.G. Teer, J. Hampshire, Performance of MoS2/metal composite coatings used for dry machining and other industrial applications, Surf. Coatings Technol. 123 (2000) 84–91. https://doi.org/https://doi.org/10.1016/S0257-8972(99)00424-7.

[33] T.B. Stewart, P.D. Fleischauer, Chemistry of sputtered molybdenum disulfide films, Inorg. Chem. 21 (1982) 2426–2431. https://doi.org/10.1021/ic00136a060.

[34] J.R. Lince, M.R. Hilton, A.S. Bommannavar, Metal incorporation in sputter-deposited MoS2 films studied by extended x-ray absorption fine structure, J. Mater. Res. 10 (1995) 2091–2105. https://doi.org/DOI: 10.1557/JMR.1995.2091.

[35] G. Jayaram, L.D. Marks, M.R. Hilton, Nanostructure of Au-20% Pd layers in MoS2 multilayer solid lubricant films, Surf. Coatings Technol. 76–77 (1995) 393–399. https://doi.org/https://doi.org/10.1016/0257-8972(95)02520-0.

[36] J.R. Lince, M.R. Hilton, A.S. Bommannavar, EXAFS of sputter-deposited MoS2 films, Thin Solid Films. 264 (1995) 120–134. https://doi.org/https://doi.org/10.1016/0040-6090(95)06607-1.

[37] J.S. Zabinski, M.S. Donley, S.D. Walck, T.R. Schneider, N.T. Mcdevitt, The Effects of Dopants on the Chemistry and Tribology of Sputter-Deposited MoS2 Films, Tribol. Trans. 38 (1995) 894–904. https://doi.org/10.1080/10402009508983486.

[38] X. Ding, X.T. Zeng, X.Y. He, Z. Chen, Tribological properties of Cr- and Ti-doped MoS2 composite coatings under different humidity atmosphere, Surf. Coatings Technol. 205 (2010) 224–231. https://doi.org/https://doi.org/10.1016/j.surfcoat.2010.06.041.

[39] V. Rigato, G. Maggioni, A. Patelli, D. Boscarino, N.M. Renevier, D.G. Teer, Properties of sputter-deposited MoS2/metal composite coatings deposited by closed field unbalanced magnetron sputter ion plating, Surf. Coatings Technol. 131 (2000) 206–210. https://doi.org/https://doi.org/10.1016/S0257-8972(00)00797-0.

[40] J.J. Nainaparampil, A.R. Phani, J.E. Krzanowski, J.S. Zabinski, Pulsed laser-

ablated MoS2-Al films: friction and wear in humid conditions, Surf. Coatings Technol. 187 (2004) 326–335. https://doi.org/https://doi.org/10.1016/j.surfcoat.2004.02.043.

[41] D.G. Teer, J. Hampshire, V. Fox, V. Bellido-Gonzalez, The tribological properties of MoS2/metal composite coatings deposited by closed field magnetron sputtering, Surf. Coatings Technol. 94–95 (1997) 572–577. https://doi.org/https://doi.org/10.1016/S0257-8972(97)00498-2.

[42] B.C. Stupp, Synergistic effects of metals co-sputtered with MoS2, Thin Solid Films. 84 (1981) 257–266. https://doi.org/https://doi.org/10.1016/0040-6090(81)90023-7.

[43] J.R. Lince, H.I. Kim, P.M. Adams, D.J. Dickrell, M.T. Dugger, Nanostructural, electrical, and tribological properties of composite Au–MoS2 coatings, Thin Solid Films. 517 (2009) 5516–5522. https://doi.org/https://doi.org/10.1016/j.tsf.2009.03.210.

[44] T. Spalvins, Frictional and morphological properties of Au□MoS2 films sputtered from a compact target, Thin Solid Films. 118 (1984) 375–384. https://doi.org/https://doi.org/10.1016/0040-6090(84)90207-4.

[45] S. Mikhailov, A. Savan, E. Pflüger, L. Knoblauch, R. Hauert, M. Simmonds, H. Van Swygenhoven, Morphology and tribological properties of metal (oxide)–MoS2 nanostructured multilayer coatings, Surf. Coatings Technol. 105 (1998) 175–183. https://doi.org/https://doi.org/10.1016/S0257-8972(98)00483-6.

[46] T.W. Scharf, R.S. Goeke, P.G. Kotula, S. V Prasad, Synthesis of Au–MoS2 Nanocomposites: Thermal and Friction-Induced Changes to the Structure, ACS Appl. Mater. Interfaces. 5 (2013) 11762–11767. https://doi.org/10.1021/am4034476.

[47] A.A. Tedstone, D.J. Lewis, P. O'Brien, Synthesis, Properties, and Applications of Transition Metal-Doped Layered Transition Metal Dichalcogenides, Chem. Mater. 28 (2016) 1965–1974. https://doi.org/10.1021/acs.chemmater.6b00430.

[48] T. Polcar, A. Nossa, M. Evaristo, A. Cavaleiro, Nanocomposite coatings of

carbon-based and transition metal dichalcogenides phases: A review, Rev. Adv. Mater. Sci. 15 (2007) 118–126. http://www.ipme.ru/e-journals/...aleiro.pdf Date accessed: 22 December 2020.

[49] H. Cao, F. Wen, J.T.M. De Hosson, Y.T. Pei, Instant WS2 platelets reorientation of self-adaptive WS 2 / a-C tribocoating, Mater. Lett. 229 (2018) 64–67. https://doi.org/10.1016/j.matlet.2018.06.111.

[50] A. Cavaleiro, B. Trindade, M.T. Vieira, Deposition and characterization of fine-grained W–Ni–C/N ternary films, Surf. Coatings Technol. 116–119 (1999) 944–948. https://doi.org/https://doi.org/10.1016/S0257-8972(99)00276-5.

[51] A. Nossa, A. Cavaleiro, The influence of the addition of C and N on the wear behaviour of W-S-C/N coatings, Surf. Coatings Technol. 142–144 (2001) 984–991. https://doi.org/10.1016/S0257-8972(01)01249-X.

[52] H. Nyberg, J. Sundberg, E. Särhammar, F. Gustavsson, T. Kubart, T. Nyberg, U. Jansson, S. Jacobson, Extreme friction reductions during initial running-in of W–S–C–Ti low-friction coatings, Wear. 302 (2013) 987–997. https://doi.org/https://doi.org/10.1016/j.wear.2013.01.065.

[53] X. Zhang, L. Qiao, L. Chai, J. Xu, L. Shi, P. Wang, Structural, mechanical and tribological properties of Mo-S-N solid lubricant films, Surf. Coatings Technol. 296 (2016) 185–191. https://doi.org/10.1016/j.surfcoat.2016.04.040.

[54] M.T. Dugger, Atomic oxygen interaction with nickel multilayer and antimony oxide doped MoS2 films, Off. Sci. Tech. Inf. Tech. Reports. (1994) Date accessed: 22 December 2020.

[55] M.C. Simmonds, A. Savan, H. Van Swygenhoven, E. Pflüger, S. Mikhailov, Structural, morphological, chemical and tribological investigations of sputter deposited MoSx/metal multilayer coatings, Surf. Coatings Technol. 108–109 (1998) 340–344. https://doi.org/https://doi.org/10.1016/S0257-8972(98)00567-2.

[56] M. Evaristo, T. Polcar, A. Cavaleiro, Synthesis and properties of W–Se–C coatings deposited by PVD in reactive and non-reactive processes, Vacuum. 83 (2009) 1262–1265. https://doi.org/https://doi.org/10.1016/j.vacuum.2009.03.030.

[57] A. Nossa, A. Cavaleiro, Tribological Behaviour of N(C)-Alloyed W–S Films,

Tribol. Lett. 28 (2007) 59–70. https://doi.org/10.1007/s11249-007-9248-3.

[58] L. Isaeva, J. Sundberg, S. Mukherjee, C.J. Pelliccione, A. Lindblad, C.U. Segre, U. Jansson, D.D. Sarma, O. Eriksson, K. Kádas, Amorphous W-S-N thin films: The atomic structure behind ultra-low friction, Acta Mater. 82 (2015) 84–93. https://doi.org/10.1016/j.actamat.2014.08.043.

[59] J. Sundberg, H. Nyberg, E. Särhammar, T. Nyberg, S. Jacobson, U. Jansson, Influence of composition, structure and testing atmosphere on the tribological performance of W-S-N coatings, Surf. Coatings Technol. 258 (2014) 86–94. https://doi.org/10.1016/j.surfcoat.2014.09.061.

[60] F. Gustavsson, S. Jacobson, A. Cavaleiro, T. Polcar, Ultra-low friction W-S-N solid lubricant coating, Surf. Coatings Technol. 232 (2013) 541–548. https://doi.org/10.1016/j.surfcoat.2013.06.026.

[61] P. Mutafov, M. Evaristo, A. Cavaleiro, T. Polcar, Structure, mechanical and tribological properties of self-lubricant W-S-N coatings, Surf. Coatings Technol. 261 (2015) 7–14. https://doi.org/10.1016/j.surfcoat.2014.11.074.

[62] H. Ju, R. Wang, N. Ding, L. Yu, J. Xu, F. Ahmed, B. Zuo, Y. Geng, Improvement on the oxidation resistance and tribological properties of molybdenum disulfide film by doping nitrogen, Mater. Des. 186 (2020) 108300. https://doi.org/https://doi.org/10.1016/j.matdes.2019.108300.

[63] A. Nossa, A. Cavaleiro, Chemical and physical characterization of C(N)-doped W–S sputtered films, J. Mater. Res. 19 (2004) 2356–2365. https://doi.org/DOI: 10.1557/JMR.2004.0293.

[64] R. F. Bunshah, Handbook of deposition technologies for films and coatings: Science, Technology and Applications, Noyes publications, 1994.

[65] J.F. Shackelford, Y.-H. Han, S. Kim, S.-H. Kwon, CRC materials science and engineering handbook, CRC press, 2016.

[66] C. Donnet, A. Erdemir, J. Robertson, Tribology of diamond-like carbon films : fundamentals and applications, (2008) Xxvi, 664 p.

[67] L. Xia, G. Li, The frictional behavior of DLC films against bearing steel balls and

Si3N4 balls in different humid air and vacuum environments, Wear. 264 (2008) 1077–1084. https://doi.org/10.1016/j.wear.2007.08.010.

[68] J. Andersson, R.A. Erck, A. Erdemir, Friction of diamond-like carbon films in different atmospheres, Wear. 254 (2003) 1070–1075. https://doi.org/10.1016/S0043-1648(03)00336-3.

[69] T.W. Scharf, S. V Prasad, Solid lubricants: a review, J. Mater. Sci. 48 (2013) 511–531. https://doi.org/10.1007/s10853-012-7038-2.

[70] K. Holmberg, A. Matthews, H. Ronkainen, Coatings tribology—contact mechanisms and surface design, Tribol. Int. 31 (1998) 107–120. https://doi.org/https://doi.org/10.1016/S0301-679X(98)00013-9.

[71] K. Holmberg, H. Ronkainen, A. Matthews, Tribology of thin coatings, Ceram. Int. 26 (2000) 787–795. https://doi.org/https://doi.org/10.1016/S0272-8842(00)00015-8.

[72] F.P. Bowden, D. Tabor, The Friction and Lubrication of Solids, Oxford University Press, Oxford, 1986.

[73] K. William, Antifriction and antiabrasive metal, (1929).

[74] C. Donnet, J.M. Martin, T. Le Mogne, M. Belin, Super-low friction of MoS2 coatings in various environments, Tribol. Int. 29 (1996) 123–128. https://doi.org/https://doi.org/10.1016/0301-679X(95)00094-K.

[75] T. Spalvins, Structure of Sputtered Molybdenum Disulfide Films at Various Substrate Temperatures, A S L E Trans. 17 (1974) 1–7. https://doi.org/10.1080/05698197408981432.

[76] K. Holmberg, A. Matthews, Coatings tribology: properties, techniques and applications in surface engineering, Elsevier, Amsterdam, 1994.

[77] D. Luo, Selection of coatings for tribological applications, Ecole Centrale de Lyon, 2009. http://www.theses.fr/2009ECDL0017/document.

[78] W. Kern, K. K. Schuegraf, Handbook of thin film deposition processes and techniques: principles, methods, equipment and applications, Noyes Publications / William Andrew Publishing, Norwich, 2002.

[79] B. N. Chapman, J. C. Anderson, Science and technology of surface coating, Academic Press, 1974.

[80] P.. J. Kelly, R.. D. Arnell, Magnetron sputtering: a review of recent developments and applications, Vacuum. 56 (2000) 159–172. https://doi.org/10.1016/S0042-207X(99)00189-X.

[81] B. Bhushan, Introduction to tribology, Second Edi, John Wiley & Sons. Ltd, New York, 2013.

[82] K. Holmberg, A. Matthews, Coatings tribology: properties, mechanisms, techniques and applications in surface engineering, Elsevier, 2009.

[83] C. Donnet, A. Erdemir, Historical developments and new trends in tribological and solid lubricant coatings, Surf. Coat. Technol. 181 (2004) 76–84. https://doi.org/10.1016/j.surfcoat.2003.10.022.

[84] A.A. Voevodin, J.M. Schneider, C. Rebholz, A. Matthews, Multilayer composite ceramicmetal-DLC coatings for sliding wear applications, Tribol. Int. 29 (1996) 559–570. https://doi.org/10.1016/0301-679X(95)00121-J.

[85] J.S. Zabinski, M.S. Donley, V.J. Dyhouse, N.T. McDevitt, Chemical and tribological characterization of PbO- MoS2 films grown by pulsed laser deposition, Thin Solid Films. 214 (1992) 156–163. https://doi.org/https://doi.org/10.1016/0040-6090(92)90764-3.

[86] S.D. Walck, J.S. Zabinski, N.T. McDevitt, J.E. Bultman, Characterization of air-annealed, pulsed laser deposited ZnO-WS2 solid film lubricants by transmission electron microscopy, Thin Solid Films. 305 (1997) 130–143. https://doi.org/https://doi.org/10.1016/S0040-6090(97)00129-6.

[87] A.A. Voevodin, J.P. O'Neill, J.S. Zabinski, Nanocomposite tribological coatings for aerospace applications, Surf. Coatings Technol. 116–119 (1999) 36–45. https://doi.org/10.1016/S0257-8972(99)00228-5.

[88] A.A. Voevodin, J.S. Zabinski, Nanocomposite and nanostructured tribological materials for space applications, Compos. Sci. Technol. 65 (2005) 741–748. https://doi.org/10.1016/j.compscitech.2004.10.008.

[89] A.A. Voevodin, J.S. Zabinski, Supertough wear-resistant coatings with 'chameleon' surface adaptation, Thin Solid Films. 370 (2000) 223–231. https://doi.org/https://doi.org/10.1016/S0040-6090(00)00917-2.

[90] W.E. Jamison, S.L. Cosgrove, Friction Characteristics of Transition-Metal Disulfides and Diselenides, A S L E Trans. 14 (1971) 62–72. https://doi.org/10.1080/05698197108983228.

[91] Y. Zhao, Y. Zhang, Z. Yang, Y. Yan, K. Sun, Synthesis of MoS2and MoO2for their applications in H2generation and lithium ion batteries: a review, Sci. Technol. Adv. Mater. 14 (2013) 43501. https://doi.org/10.1088/1468-6996/14/4/043501.

[92] K. Ren, M.L. Sun, Y. Luo, S.K. Wang, J. Yu, W.C. Tang, First-principle study of electronic and optical properties of two-dimensional materials-based heterostructures based on transition metal dichalcogenides and boron phosphide, Appl. Surf. Sci. 476 (2019) 70–75. https://doi.org/10.1016/j.apsusc.2019.01.005.

[93] Z. Cui, K. Ren, Y. Zhao, X. Wang, H. Shu, J. Yu, W. Tang, M. Sun, Electronic and optical properties of van der Waals heterostructures of g-GaN and transition metal dichalcogenides, Appl. Surf. Sci. 492 (2019) 513–519. https://doi.org/10.1016/j.apsusc.2019.06.207.

[94] A. Nossa, A. Cavaleiro, Mechanical behaviour of W-S-N and W-S-C sputtered coatings deposited with a Ti interlayer, Surf. Coatings Technol. 163–164 (2003) 552–560. https://doi.org/10.1016/S0257-8972(02)00622-9.

[95] J.S. Zabinski, M.S. Donley, S. V Prasad, N.T. McDevitt, Synthesis and characterization of tungsten disulphide films grown by pulsed-laser deposition, J. Mater. Sci. 29 (1994) 4834–4839. https://doi.org/10.1007/BF00356530.

[96] G. Stachowiak, A.W. Batchelor, Engineering tribology, Butterworth-Heinemann, 2013.

[97] I.L. Singer, S. Fayeulle, P.D. Ehni, Wear behavior of triode-sputtered MoS 2 coatings in dry sliding contact with steel and ceramics, Wear. 195 (1996) 7–20. https://doi.org/https://doi.org/10.1016/0043-1648(95)06661-6.

[98] N.M. Renevier, N. Lobiondo, V.C. Fox, D.G. Teer, J. Hampshire, Performance of MoS2/metal composite coatings used for dry machining and other industrial

applications, Surf. Coatings Technol. 123 (2000) 84–91. https://doi.org/10.1016/S0257-8972(99)00424-7.

[99] W. Lauwerens, J. Wang, J. Navratil, E. Wieërs, J. D'haen, L.M. Stals, J.P. Celis, Y. Bruynseraede, Humidity resistant MoSx films prepared by pulsed magnetron sputtering, Surf. Coatings Technol. 131 (2000) 216–221. https://doi.org/https://doi.org/10.1016/S0257-8972(00)00796-9.

[100] I.L. Singer, R.N. Bolster, J. Wegand, S. Fayeulle, B.C. Stupp, Hertzian stress contribution to low friction behavior of thin MoS2 coatings, Appl. Phys. Lett. 57 (1990) 995–997. https://doi.org/10.1063/1.104276.

[101] E.W. Roberts, Institute of Mechanical Engineering Tribology-Friction,Lubrication and Wear, Fifty years On;, Inst. Mech. Eng. London, UK,. (1987) 503.

[102] J.L. Grosseau-Poussard, P. Moine, M. Brendle, Shear strength measurements of parallel MoSx thin films, Thin Solid Films. 307 (1997) 163–168. https://doi.org/https://doi.org/10.1016/S0040-6090(97)00205-8.

[103] J.R. Lince, Tribology of co-sputtered nanocomposite Au / MoS 2 solid lubricant films over a wide contact stress range, Tribol. Lett. 17 (2004) 419–428. https://doi.org/10.1023/B:TRIL.0000044490.03462.6e.

[104] C. Muratore, A.A. Voevodin, N.R. Glavin, Physical vapor deposition of 2D Van der Waals materials: a review, Thin Solid Films. 688 (2019) 137500. https://doi.org/https://doi.org/10.1016/j.tsf.2019.137500.

[105] P.D. Fleischauer, J.R. Lince, Comparison of oxidation and oxygen substitution in MoS2solid film lubricants, Tribol. Int. 32 (1999) 627–636. https://doi.org/10.1016/S0301-679X(99)00088-2.

[106] E. Serpini, Friction Mechanisms of MoS2 Surfaces with Different Crystallographic Order, (2017).

[107] G. Salomon, A.W.J. De Gee, J.H. Zaat, Mechano-chemical factors in MoS2-film lubrication, Wear. 7 (1964) 87–101. https://doi.org/10.1016/0043-1648(64)90081-X.

[108] C. Pritchard, J.W. Midgley, The Effect of Humidity on the Friction and Life of

Unbonded Molybdnum Disulphide Films, Wear. 13 (1968) 39–50. https://doi.org/https://doi.org/10.1016/0043-1648(69)90430-X.

[109] E.W. Roberts, Towards an Optimised Sputtered MoS2 Lubricant Film, 20th Aerosp. Symp. (1986) 103–119.

[110] E.W. Anderson, M.J.; Cropper, M.; Roberts, The Tribological Characteristics of Dicronite, Proc. Eur. Sp. Mech. Tribol. Symp. (ESMATS), Liverpool, UK. 19–21 Sept (2007).

[111] S. Gangopadhyay, R. Acharya, A.K. Chattopadhyay, S. Paul, Effect of substrate bias voltage on structural and mechanical properties of pulsed DC magnetron sputtered TiN–MoSx composite coatings, Vacuum. 84 (2010) 843–850. https://doi.org/https://doi.org/10.1016/j.vacuum.2009.11.010.

[112] A.C. A. Nossa, Optimisation of the deposition of a Ti interlayer to improve the adhesion of W-S films, Proc. Conf. Mater. 2001, 108 Encontro Da Soc. Port. Mater. 1st Int. Mater. Symp. Coimbra, Port. 9–11. (2001).

[113] P. Wang, L. Qiao, J. Xu, W. Li, W. Liu, Erosion Mechanism of MoS2-Based Films Exposed to Atomic Oxygen Environments, ACS Appl. Mater. Interfaces. 7 (2015) 12943–12950. https://doi.org/10.1021/acsami.5b02709.

[114] F. Bülbül, İ. Efeoğlu, Synergistic effect of bias and target currents for magnetron sputtered MoS2-Ti composite films, Mater. Test. 58 (2016) 471–474. https://doi.org/10.3139/120.110870.

[115] J. V. Pimentel, M. Danek, T. Polcar, A. Cavaleiro, Effect of rough surface patterning on the tribology of W-S-C-Cr self-lubricant coatings, Tribol. Int. 69 (2014) 77–83. https://doi.org/10.1016/j.triboint.2013.09.004.

[116] D. Lloyd, X. Liu, N. Boddeti, L. Cantley, R. Long, M.L. Dunn, J.S. Bunch, Adhesion, Stiffness, and Instability in Atomically Thin MoS2 Bubbles, Nano Lett. 17 (2017) 5329–5334. https://doi.org/10.1021/acs.nanolett.7b01735.

[117] V. Buck, A neglected parameter (water contamination) in sputtering of MoS2 films, Thin Solid Films. 139 (1986) 157–168. https://doi.org/https://doi.org/10.1016/0040-6090(86)90334-2.

[118] P.A. Bertrand, Orientation of rf-sputter-deposited MoS2 films, J. Mater. Res. 4

(1989) 180–184. https://doi.org/DOI: 10.1557/JMR.1989.0180.

[119] D.Y. Wang, C.L. Chang, Z.Y. Chen, W.Y. Ho, Microstructural and tribological characterization of MoS2-Ti composite solid lubricating films, Surf. Coatings Technol. 120–121 (1999) 629–635. https://doi.org/10.1016/S0257-8972(99)00431-4.

[120] A. Nossa, A. Cavaleiro, N.J.M. Carvalho, B.J. Kooi, J.T.M. De Hosson, On the microstructure of tungsten disulfide films alloyed with carbon and nitrogen, Thin Solid Films. 484 (2005) 389–395. https://doi.org/10.1016/j.tsf.2005.02.018.

[121] T. Polcar, M. Evaristo, A. Cavaleiro, Comparative study of the tribological behavior of self-lubricating W-S-C and Mo-Se-C sputtered coatings, Wear. 266 (2009) 388–392. https://doi.org/10.1016/j.wear.2008.04.011.

[122] M.C. Simmonds, A. Savan, E. Pflüger, H. Van Swygenhoven, Mechanical and tribological performance of MoS2 co-sputtered composites, Surf. Coatings Technol. 126 (2000) 15–24. https://doi.org/10.1016/S0257-8972(00)00521-1.

[123] H. Liu, X. Zhang, Improved tribological properties of sputtered MoS2 films through N+ implantation, Thin Solid Films. 240 (1994) 97–100. https://doi.org/https://doi.org/10.1016/0040-6090(94)90702-1.

[124] P. Gribi, Z.W. Sun, F. Levy, Effects of low-energy ion bombardment on RF sputtered MoS2-x films, J. Phys. D. Appl. Phys. 22 (1989) 238. https://doi.org/https://doi.org/10.1088/0022-3727/22/1/037.

[125] N.J. Mikkelsen, G. Sørensen, Low friction molybdenum surfaces produced by ion implantation of sulphur ions, Surf. Coatings Technol. 45 (1991) 9–14. https://doi.org/https://doi.org/10.1016/0257-8972(91)90200-G.

[126] Z. Daming, L. Jiajun, Z. Baoliang, L. Wenzhi, A study of the friction and wear performance of MoSx thin films produced by ion beam enhanced deposition and magnetron sputtering, Wear. 210 (1997) 45–49. https://doi.org/https://doi.org/10.1016/S0043-1648(97)00039-2.

[127] I. Efeoglu, Deposition and characterization of a multilayered-composite solid lubricant coating, Rev. Adv. Mater. Sci. 15 (2007) 87–94.

[128] M.R. Hilton, R. Bauer, S. V Didziulis, M.T. Dugger, J.M. Keem, J. Scholhamer, Structural and tribological studies of MoS2 solid lubricant films having tailored metal-multilayer nanostructures, Surf. Coatings Technol. 53 (1992) 13–23. https://doi.org/https://doi.org/10.1016/0257-8972(92)90099-V.

[129] X. Liu, G.J. Ma, G. Sun, Y.P. Duan, S.H. Liu, MoSx-Ta composite coatings on steel by d.c magnetron sputtering, Vacuum. 89 (2013) 203–208. https://doi.org/https://doi.org/10.1016/j.vacuum.2012.05.013.

[130] D. Jianxin, S. Wenlong, Z. Hui, Z. Jinlong, Performance of PVD MoS2/Zr-coated carbide in cutting processes, Int. J. Mach. Tools Manuf. 48 (2008) 1546–1552. https://doi.org/https://doi.org/10.1016/j.ijmachtools.2008.06.009.

[131] T. Bin Yaqub, T. Vuchkov, M. Evaristo, A. Cavaleiro, DCMS Mo-Se-C solid lubricant coatings – Synthesis, structural, mechanical and tribological property investigation, Surf. Coatings Technol. (2019) 124992. https://doi.org/10.1016/j.surfcoat.2019.124992.

[132] A.A. Voevodin, J.P. O'Neill, J.S. Zabinski, WC/DLC/WS2 nanocomposite coatings for aerospace tribology, Tribol. Lett. 6 (1999) 75–78. https://doi.org/10.1023/A:1019163707747.

[133] V.Y. Fominski, V.N. Nevolin, R.I. Romanov, I. Smurov, Ion-assisted deposition of MoSx films from laser-generated plume under pulsed electric field, J. Appl. Phys. 89 (2001) 1449–1457. https://doi.org/10.1063/1.1330558.

[134] X. Zhang, L. Qiao, L. Chai, J. Xu, L. Shi, P. Wang, Structural, mechanical and tribological properties of Mo-S-N solid lubricant films, Surf. Coatings Technol. 296 (2016) 185–191. https://doi.org/10.1016/j.surfcoat.2016.04.040.

[135] J. Noshiro, S. Watanabe, T. Sakurai, S. Miyake, Friction properties of co-sputtered sulfide/DLC solid lubricating films, Surf. Coatings Technol. 200 (2006) 5849–5854. https://doi.org/10.1016/j.surfcoat.2005.08.147.

[136] A. Nossa, A. Cavaleiro, Behaviour of nanocomposite coatings of W-S-N/C system under pin-on-disk testing, Mater. Sci. Forum. 455–456 (2004) 515–519. https://doi.org/10.4028/www.scientific.net/msf.455-456.515.

[137] J. Sundberg, H. Nyberg, E. Särhammar, F. Gustavsson, T. Kubart, T. Nyberg, S.

Jacobson, U. Jansson, Influence of Ti addition on the structure and properties of low-friction W-S-C coatings, Surf. Coatings Technol. 232 (2013) 340–348. https://doi.org/10.1016/j.surfcoat.2013.05.032.

[138] L. Isaeva, J. Sundberg, S. Mukherjee, C.J. Pelliccione, A. Lindblad, C.U. Segre, U. Jansson, D.D. Sarma, O. Eriksson, K. Kádas, Amorphous W-S-N thin films: The atomic structure behind ultra-low friction, Acta Mater. 82 (2015) 84–93. https://doi.org/10.1016/j.actamat.2014.08.043.

[139] Y. Wu, H. Li, L. Ji, L. Liu, Y. Ye, J. Chen, H. Zhou, Structure, Mechanical, and Tribological Properties of MoS2/a-C:H Composite Films, Tribol. Lett. 52 (2013) 371–380. https://doi.org/10.1007/s11249-013-0216-9.

[140] Z. Han, J. Tian, Q. Lai, X. Yu, G. Li, Effect of N2 partial pressure on the microstructure and mechanical properties of magnetron sputtered CrNx films, Surf. Coatings Technol. 162 (2003) 189–193. https://doi.org/https://doi.org/10.1016/S0257-8972(02)00667-9.

[141] Composition of M2 Tool Steel, (n.d.). http://www.astmsteel.com/product/m2-tool-steel-1-3343-hs-6-5-2c-skh51/ (accessed November 2, 2020).

[142] Composition of 100Cr6 Steel, (n.d.). https://www.astmsteel.com/product/52100-bearing-steel-aisi/ (accessed November 2, 2020).

[143] P.P.M. Beat Schmid, Christophe Heau, Process for the surface treatment of at least one piece using elementary electronic cyclotron resonance plasma sources, 2007. https://worldwide.espacenet.com/patent/search/family/039473320/publication/FR2922358B1?q=pn%3DFR2922358B1.

[144] E. Broitman, L. Hultman, Adhesion improvement of carbon-based coatings through a high ionization deposition technique, J. Phys. Conf. Ser. 370 (2012) 12009. https://doi.org/10.1088/1742-6596/370/1/012009.

[145] M. Birkholz, Thin film analysis by X-ray scattering, John Wiley & Sons, 2006.

[146] P. Chuchvalec, Hans-Jürgen Butt, Karlheinz Graf, Michael Kappl: Physics and Chemistry of Interfaces, Chem. List. 107 (2013) 562.

[147] W.C. Oliver, G.M. Pharr, An improved technique for determining hardness and

elastic modulus using load and displacement sensing indentation experiments, J. Mater. Res. (1992). https://doi.org/10.1557/JMR.1992.1564.

[148] D. Hatic, X. Cheng, T. Weibel, M. Rauhut, H. Hagen, Rockwell adhesion test-Approach to standard modernization, (2020).

[149] J.-P. Locquet, D. Neerinck, L. Stockman, Y. Bruynseraede, I.K. Schuller, Long-range order and lattice mismatch in metallic superlattices, Phys. Rev. B. 38 (1988) 3572–3575. https://doi.org/10.1103/PhysRevB.38.3572.

[150] P.H. Holloway, G.C. Nelson, Preferential sputtering of Ta2O5 by argon ions, J. Vac. Sci. Technol. 16 (1979) 793–796. https://doi.org/10.1116/1.570088.

[151] M. Moens, F.C. Adams, D.S. Simons, Dependence of interface widths on ion bombardment conditions in secondary ion mass spectrometric analysis of a nickel/chromium multilayer structure, Anal. Chem. 59 (1987) 1518–1529. https://doi.org/10.1021/ac00138a009.

[152] P.J. Burnett, D.S. Rickerby, The relationship between hardness and scratch adhession, Thin Solid Films. 154 (1987) 403–416. https://doi.org/https://doi.org/10.1016/0040-6090(87)90382-8.

[153] G. Eda, H. Yamaguchi, D. Voiry, T. Fujita, M. Chen, M. Chhowalla, Photoluminescence from chemically exfoliated MoS 2, Nano Lett. 11 (2011) 5111–5116. https://doi.org/10.1021/nl201874w.

[154] M. Donarelli, F. Bisti, F. Perrozzi, L. Ottaviano, Tunable sulfur desorption in exfoliated MoS2 by means of thermal annealing in ultra-high vacuum, Chem. Phys. Lett. 588 (2013) 198–202. https://doi.org/https://doi.org/10.1016/j.cplett.2013.10.034.

[155] T. Bin Yaqub, T. Vuchkov, P. Sanguino, T. Polcar, Comparative Study of DC and RF Sputtered MoSe 2 Coatings Containing Carbon - An Approach to Optimize Stoichiometry, Microstructure, Crystallinity and Hardness, (2020) 1–16. https://doi.org/10.3390/coatings10020133.

[156] T. Hudec, M. Mikula, L. Satrapinskyy, T. Roch, M. Truchlý, P. Švec, T. Huminiuc, T. Polcar, Structure, mechanical and tribological properties of Mo-S-N solid lubricant coatings, Appl. Surf. Sci. (2019).

https://doi.org/10.1016/j.apsusc.2019.03.294.

[157] I. Jauberteau, A. Bessaudou, R. Mayet, J. Cornette, L.J. Jauberteau, P. Carles, T. Merle-Méjean, Molybdenum Nitride Films: Crystal Structures, Synthesis, Mechanical, Electrical and Some Other Properties, Coatings . 5 (2015). https://doi.org/10.3390/coatings5040656.

[158] F. Niefind, J. Djamil, W. Bensch, B.R. Srinivasan, I. Sinev, W. Grünert, M. Deng, L. Kienle, A. Lotnyk, M.B. Mesch, J. Senker, L. Dura, T. Beweries, Room temperature synthesis of an amorphous MoS2 based composite stabilized by N-donor ligands and its light-driven photocatalytic hydrogen production, RSC Adv. 5 (2015) 67742–67751. https://doi.org/10.1039/C5RA14438H.

[159] T. Polcar, A. Cavaleiro, Self-adaptive low friction coatings based on transition metal dichalcogenides, Thin Solid Films. 519 (2011) 4037–4044. https://doi.org/10.1016/j.tsf.2011.01.180.

[160] G. Weise, N. Mattern, H. Hermann, A. Teresiak, I. Ba, W. Bru, Preparation, structure and properties of MoSx films, Thin Soli. 298 (1997) 98–106. https://doi.org/10.1016/S0040-6090(96)09165-1.

[161] C. Muratore, A.A. Voevodin, Control of molybdenum disulfide basal plane orientation during coating growth in pulsed magnetron sputtering discharges, Thin Solid Films. 517 (2009) 5605–5610. https://doi.org/10.1016/j.tsf.2009.01.190.

[162] K.D. Rasamani, F. Alimohammadi, Y. Sun, Interlayer-expanded MoS 2, Mater. Today. 20 (2017). https://doi.org/10.1016/j.mattod.2016.10.004.

[163] P.D. Fleischauer, M.R. Hilton, R. Bauer, Paper V (i) Effects of microstructure and adhesion on performance of sputter-deposited MoS2 solid lubricant coatings, Tribol. Ser. 17 (1990) 121–128. https://doi.org/10.1016/S0167-8922(08)70248-7.

[164] Y. Fu, T. He, W. Yang, J. Xu, B. Mu, X. Pang, P. Wang, Structure, Mechanical and Tribological Properties of MoSN/MoS2 Multilayer Films, Coatings. 9 (2019) 108. https://doi.org/10.3390/coatings9020108.

[165] S. Watanabe, J. Noshiro, S. Miyake, Friction properties of WS2/MoS2 multilayer films under vacuum environment, Surf. Coatings Technol. 188–189 (2004) 644–

648. https://doi.org/https://doi.org/10.1016/j.surfcoat.2004.07.029.

[166] U. Helmersson, S. Todorova, S.A. Barnett, J. -E. Sundgren, L.C. Markert, J.E. Greene, Growth of single-crystal TiN/VN strained-layer superlattices with extremely high mechanical hardness, J. Appl. Phys. 62 (1987) 481–484. https://doi.org/10.1063/1.339770.

[167] H.P. Komsa, J. Kotakoski, S. Kurasch, O. Lehtinen, U. Kaiser, A. V. Krasheninnikov, Two-dimensional transition metal dichalcogenides under electron irradiation: Defect production and doping, Phys. Rev. Lett. 109 (2012) 1–5. https://doi.org/10.1103/PhysRevLett.109.035503.

[168] K. Dolui, I. Rungger, C. Das Pemmaraju, S. Sanvito, Possible doping strategies for MoS2 monolayers: An ab initio study, Phys. Rev. B. 88 (2013) 75420. https://doi.org/10.1103/PhysRevB.88.075420.

[169] T. Polcar, M. Evaristo, A. Cavaleiro, Friction of self-lubricating W-S-C sputtered coatings sliding under increasing load, Plasma Process. Polym. 4 (2007) 541–546. https://doi.org/10.1002/ppap.200731402.

[170] J.R. Lince, S.H. Loewenthal, C.S. Clark, Tribological and chemical effects of long term humid air exposure on sputter-deposited nanocomposite MoS2 coatings, Wear. 432–433 (2019) 202935. https://doi.org/https://doi.org/10.1016/j.wear.2019.202935.

[171] K. Miyoshi, Considerations in vacuum tribology (adhesion, friction, wear, and solid lubrication in vacuum), Tribol. Int. 32 (1999) 605–616. https://doi.org/10.1016/S0301-679X(99)00093-6.

[172] D. V Shtansky, T.A. Lobova, V.Y. Fominski, S.A. Kulinich, I. V Lyasotsky, M.I. Petrzhik, E.A. Levashov, J.J. Moore, Structure and tribological properties of WSex, WSex/TiN, WSex/TiCN and WSex/TiSiN coatings, Surf. Coatings Technol. 183 (2004) 328–336. https://doi.org/https://doi.org/10.1016/j.surfcoat.2003.09.047.

[173] S. Dominguez-Meister, A. Justo, J.C. Sanchez-Lopez, Synthesis and tribological properties of WSex films prepared by magnetron sputtering, Mater. Chem. Phys. 142 (2013) 186–194. https://doi.org/10.1016/j.matchemphys.2013.07.004.

[174] C. Muratore, A.A. Voevodin, R. Goyena, A.. Fallis, I.D.M. Thomas, D.G. Teer, S. Domínguez-Meister, T.C. Rojas, M. Brizuela, J.C. Sánchez-López, Chameleon Coatings: Adaptive Surfaces to Reduce Friction and Wear in Extreme Environments, Annu. Rev. Mater. Res. 39 (2009) 297–324. https://doi.org/10.1146/annurev-matsci-082908-145259.

[175] T. Kubart, T. Polcar, L. Kopecký, R. Novák, D. Nováková, Temperature dependence of tribological properties of MoS2 and MoSe2 coatings, Surf. Coatings Technol. 193 (2005) 230–233. https://doi.org/10.1016/j.surfcoat.2004.08.146.

[176] E. A., B. BHUSHAN, Modern Tribology Handbook, CRC Press, 2001.

[177] B.C. Windom, W.G. Sawyer, D.W. Hahn, A Raman Spectroscopic Study of MoS2 and MoO3: Applications to Tribological Systems, Tribol. Lett. 42 (2011) 301–310. https://doi.org/10.1007/s11249-011-9774-x.

[178] A. Ramalho, J.C. Miranda, The relationship between wear and dissipated energy in sliding systems, Wear. 260 (2006) 361–367. https://doi.org/10.1016/j.wear.2005.02.121.

[179] H.S. Khare, D.L. Burris, Surface and subsurface contributions of oxidation and moisture to room temperature friction of molybdenum disulfide, Tribol. Lett. 53 (2014) 329–336. https://doi.org/10.1007/s11249-013-0273-0.

Annex A

Hebbar Kannur, K.; Yaqub, T. B.; Huminiuc, T.; Polcar, T.; Pupier, C.; Héau, C.; Cavaleiro, A. ***Synthesis and Structural Properties of Mo-S-N Sputtered Coatings*****.** ***Appl. Surf. Sci.*** **527 (2020) 146790. https://doi.org/10.1016/j.apsusc.2020.146790.**

Applied Surface Science 527 (2020) 146790

Contents lists available at ScienceDirect

Applied Surface Science

journal homepage: www.elsevier.com/locate/apsusc

Synthesis and structural properties of Mo-S-N sputtered coatings

Kaushik Hebbar Kannur[a,b,*], Talha Bin Yaqub[b], Teodor Huminiuc[c], Tomas Polcar[c], Christophe Pupier[a], Christophe Héau[a], Albano Cavaleiro[b]

[a] IREIS, HEF Group, ZI Sud – Avenue Benoît Fourneyron, CS 42077-42162 Andrézieux-Bouthéon, France
[b] SEG-CEMMPRE, Department of Mechanical Engineering, University of Coimbra, Rua Luís Reis Santos, 3030-788 Coimbra, Portugal
[c] nCATS, University of Southampton, University Road, Southampton SO17 1BJ, UK

ARTICLE INFO

Keywords:
Transition metal dichalcogenides
Solid lubricant coatings
DC magnetron sputtering
Mo-S-N coatings
Nitrogen-doped TMD coatings

ABSTRACT

Transition-metal-dichalcogenide coatings provide low friction because of characteristic low shear strength along the basal plane of the lamellar structure; however, the material can easily degrade through exfoliation and poor adhesion to the metallic substrates. In this work, an innovative approach was employed to improve the coating's adhesion. A secondary plasma source was used during deposition to generate an additional charged particle flux which was directed to the growing film independently of the magnetron cathode. Therefore, Mo-S-N solid lubricant films were deposited by DCMS from a single molybdenum disulphide (MoS_2) target in a reactive atmosphere. Nitrogen was introduced during the deposition with increasing partial pressures, resulting in a high N_2 content in the doped films (37 at. %). The variation in incident ion energy and flux of energetic species bombarding the growing film allows for the control of the S/Mo ratio through selective re-sputtering of sulphur from the film. The S/Mo ratio was progressively increased in the range of 1.2–1.8, resulting in a gradient from a metallic layer to the lubricious sulphide. Combining the ion bombardment with nitrogen incorporation, the cohesive critical load (Lc1) reached 38 N, 10 times more when compared to pure MoS_2 coating. Observation using HRTEM revealed an amorphous structure and strong bonding with the substrate.

1. Introduction

Transition metal dichalcogenides (TMDs): sulphides, selenides or tellurides of tungsten or molybdenum are well known for their lubricating properties [1]. Hexagonal MoS_2 and WS_2 are compounds with unique characteristics originating from an extreme degree of crystalline anisotropy and, due to this, the TMDs have gained considerable attention in the research community for a variety of mechanical, electronic and optical applications [2–5]. Despite the greater resistance to high temperature oxidation of WS_2 [6], MoS_2 has been more widely studied due to its lower cost and lubricating performance in a vacuum and dry atmosphere, Initially, MoS_2 coatings were deposited by burnishing [7], electrochemical process [8] and plasma vapour deposition [7–12] techniques. Following the development of magnetron sputtering techniques, further research efforts have been carried out to deposit these coatings with bespoke crystalline and chemical properties, which ultimately lead to improvements in the tribological performance [10]. However, sputtered MoS_2 films exhibit porous morphology which reduces their load-bearing capacity, oxidation resistance and adhesion to the substrates and adversely affect the mechanical and easy shear properties [13,14]. The possible solution to overcome these issues is the addition of a third element to the coatings, which can disrupt the crystal structure and the growth of weakly-bound pure chalcogenides to enhance the compactness and oxidation resistance. TMD have been doped with different metals such as Ti [15–21], Ag [22], Al [19], Co [22], Au [23–25], Cr [22], Fe [26], Ni [11,22,25,27], Pb [25,28], Pt [22], Ta [22,29], W [22], Zr [30]. Regardless of the beneficial results [20], the industrial implementation of metal doped MoS_2 coating is limited (e.g., MoST by Teer coatings [20]) due to either the rapid oxidation of tribofilms into metal oxides [31] or the detrimental effects of hard metal particles (e.g. Ti) abrasion of tribofilms [32]. Moreover, economics do not favour the use of metal doping: metal doping requires a minimum of two targets for the PVD systems (i.e. one for metal and one for TMDs), consequently, increasing costs for the processing and development.

Alternatively, Non-metal doping (e.g. N and C) has attracted both researchers and industry. Carbon introduction in TMDs was first reported by Voevodin et.al. [33]. To deposit TMD-C coatings using only one cathode, the carbon incorporation was achieved by reactive sputtering, with precursor gases such as CH_4 or C_2H_2. In such cases, hydrogen can react with the chalcogen not only changing the

* Corresponding author at: IREIS, HEF Group, ZI Sud – Avenue Benoît Fourneyron, CS 42077-42162 Andrézieux-Bouthéon, France.
E-mail address: khebbarkannur.ireis@hef.fr (K. Hebbar Kannur).

https://doi.org/10.1016/j.apsusc.2020.146790
Received 18 February 2020; Received in revised form 15 May 2020; Accepted 22 May 2020
Available online 28 May 2020

stoichiometry of MoS_2 but also acts as a contamination source [34].

Nitrogen doping, on the other hand, has been rarely explored but seems a promising strategy for changing the structure of the coatings. With the use of only one cathode (with the TMD target) allows reducing the production complexity and costs, providing the advantage of avoiding the contamination by other elements (no precursor gas) [35]. Moreover, when compared to carbon, a small amount of nitrogen can be sufficient to achieve a dense amorphous coating, further reducing the operating costs [36]. In order to grow mechanically stable coatings, it is important to prevent the easily sheared planes from forming or by reducing the crystallinity of the softer phase. This can easily be achieved by nitrogen doping [37]. Mutafov et al. [38] reported that magnetron sputtered amorphous W-S-N films exhibit a low coefficient of friction (COF) high load-bearing capacity and good wear resistance. The atomic level structure and bonding arrangements in amorphous W-S-N have been described by Isaeva et al. [36]. They also reported that, during sliding, nitrogen is released from the contact zone in a gaseous form (e.g. N_2, NO_2) without disturbing the formation of tribofilms. Zhang et al. [31] reported that the incorporation of a small amount of nitrogen into MoS_2 sputtered films produced a nanocomposite structure, increasing the hardness and reducing the wear. Similar works were also reported by Nossa et al. [39].

Until now, most of the studies on the TMD-N (in particular Mo-S-N) systems were performed for a stationary substrate holder placed in front of the target; the effect of rotating the substrate holder for industrial purpose is still unexplored. Also, as per literature, the desired amorphous phase was achieved at the cost of a high nitrogen doping and consequent sub-stoichiometry of the TMDs. Therefore, further studies are required to overcome chalcogen atom depletion with nitrogen additions. Another important shortcoming in TMD-N coatings is the lack of adhesion to the substrates, even after the use of metallic interlayers. All previous works report the use of Ti or Cr interlayers for adhesion improvement [40–42], with Ti being a more suitable option [20]. Nonetheless, Nossa et al. [43] showed that spalling occurred between the films and Ti interlayer during the scratch test, preventing the substrate exposure. Besides, TiN was also used as interlayer which resulted in an improved adhesion over Ti, due to a good interface bonding between TiN and Mo-S-N coatings [41]. However, the drawback is the associated cost increments due to the use of an additional Ti target sputtering.

This study is aimed to counter all these issues for TMD-N coatings by depositing those using DCMS. To our knowledge, this is the first time that DC magnetron sputtering has been used for depositing Mo-S-N coatings. Here, only one MoS_2 target was used to decrease the operating costs. An alternative to traditional metallic interlayers for enhancing the adhesion was the use of a novel N-doped metal-rich Mo-S-N layer, instead of Ti or Cr, avoiding the use of a second cathode. An additional plasma source was used to adjust the ion to neutral ratio during film growth, providing control over the coating morphology and S/Mo ratio. The achievement of a good coating integrity, as well as a high S/Mo ratio, is sought in order to make coatings capable of providing enhanced sliding performances. The deposition was followed by a detailed characterization of the coatings with respect to composition, morphology, structure and chemical bonding.

2. Experimental details

Mo-S-N films were deposited on polished Si (1 0 0) wafers and polished M2 steel (Ø25 mm × 6 mm, hardness of 62 HRC) substrates in a balanced DC magnetron sputtering configuration, using a custom-built TSD 400 semi-industrial plasma vapour deposition machine. The chamber was equipped with a single cathode and an additional independent plasma source, facing the substrate. The additional secondary plasma source serves the following function; (i) it creates a low argon pressure plasma which is used to etch the steel substrates, (ii) during the coating process, it is used to vary the ion to neutral ratio coming to the substrates, (iii) the plasma density or current density can be tuned at the substrate by adjusting the plasma source power. For the current process, the plasma source power was kept constant for all the deposition steps. Sintered molybdenum disulphide MoS_2 450 mm × 150 mm × 5 mm (99.5% purity) target was sputtered in N and Ar (99.99% purity) gas atmosphere. The substrates were placed over a planetary (double rotation) substrate holder rotating at a speed of 5 rpm. Prior to deposition, the chamber and substrates were heated to 150 °C for 5 h with consequent pumping to the base pressure of $\sim 10^{-4}$ Pa, to remove any moisture and adsorbed contaminants. The top view schematic diagram of the deposition chamber is shown in Fig. 1.

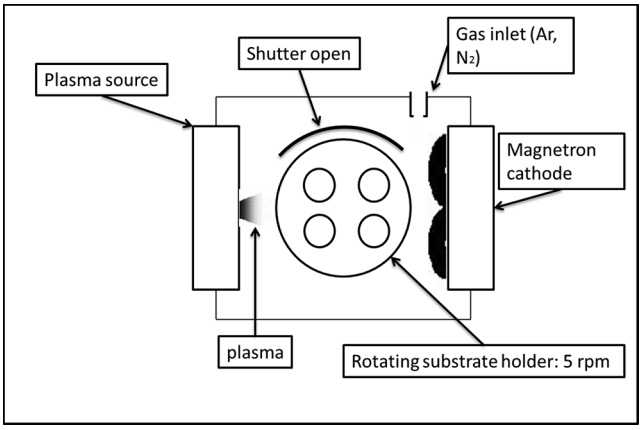

Fig. 1. Schematic setup of the TSD 400 PVD chamber (Top view).

Substrate etching was performed with Ar^+ ions bombardment by applying −150 V at 0.3 Pa using the additional plasma source, for 60 min, while the target was sputtered-cleaned for 7 min by applying 1000 W DC power. The first step in the coating recipe was the deposition of '*novel gradient layers*', which took 20 min. Here, the Mo rich layer was deposited by intense ion bombardment of the growing film with Ar^+ ions resulting in preferential resputtering of S atoms. This was done to obtain good metal-metal bonding with the steel substrate followed by the introduction of nitrogen in the presence of high ion energy and ion bombardment from the additional plasma source, to achieve nitrides containing sulphur. Then, progressively, the ion energy was decreased to incorporate more sulphur. After 20 min, the final coating was deposited in such a way that nitrogen would be already present within the coatings and plasma trying to prevent lamellar MoS_2 formation. During the deposition of Mo-S-N films, the Ar gas flow was kept constant at 70 sccm whereas the N_2 gas flow was varied between 0 and 60 sccm (Table 2) to achieve different N content in the coatings; the process pressure ranged from 0.45 to 0.70 Pa. The rotating substrates underwent alternating exposure to the cathode (target) and ion bombardment from the additional secondary plasma source. The coatings were deposited at 1000 W DC power applied to the target. A negative pulsed DC substrate bias of 50 V was applied during the deposition to enhance the compactness. The pulse conditions were set at 250 kHz of frequency, 950 ns of duration (76.25% duty cycle). The target to substrate distance was 100 mm. The total deposition time was 2 h in the N_2 reactive atmosphere. This deposition time was selected to yield a final coating thickness of 1.2–3 μm as shown in Fig. 2.

Coating's integrity or adhesion on the M2 steel substrates (Ø25 mm × 6 mm) was evaluated by scratch-testing (CSM Revetest). The specimens were scratched as the normal force was progressively increased from 5 to 80 N, using a Rockwell indenter (tip radius = 0.2 mm) at a scratch speed of 10 mm/min and a loading rate of 100 N/min. Three tests were done on each sample to confirm the critical load. Later, the critical adhesion loads were determined by analysing scratches by optical and scanning electron microscopies, based on the report of Camino et al. [44]. The chemical composition of the coatings was determined by wavelength dispersive spectroscopy, WDS (Oxford Instruments).

Spectroscopic studies of plasma-chemistry and element specific plasma imaging were performed to study the re-sputtering effect of sulphur from the substrate. A quartz window (transmittance cut-off ~180 nm) was arranged with a view parallel to the substrate surface and perpendicular to the substrate–plasma source (i.e. magnetron and secondary plasma source)

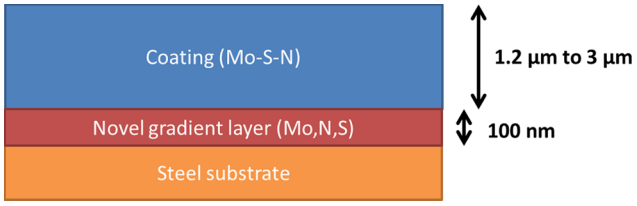

Fig. 2. Schematic representation of the layer structure and thickness.

axis, capturing light emitted from the plasma region between the plasma source and the substrate location. For spectral line recording, the fibre optic spectrometer (AVS-S2000) accepts light energy transmitted through single-strand optical fibre and disperses it via a fixed grating across the linear CCD array detector. The obtained spectral intensities versus wavelengths are processed using SpectraWIN BASIC 5.0 software. The monochromator provides ~0.1 nm resolution of spectral bands collected over a 300–1000 nm range. The peak intensity corresponding to the wavelength of 550 nm is considered for sulphur and 811 nm for argon which corresponds to the single ionized states of each element.

X-ray photoelectron spectroscopy (XPS) was used for chemical bonding analysis. The samples were analysed in a KratosAxis Ultra HAS equipment with monochromatic Al Kα X-beams (hν = 1486.6 eV). The power of the X-beam source was set to 90 W and a charge neutralizer was utilized during estimations. The survey spectra were gotten by setting the pass energy at 80 eV with a step of 1 eV and a dwell time of 200 ms. The high-resolution spectra of the regions of interest were acquired utilizing a pass energy of 40 eV with a step of 0.1 eV and a dwell time of 600 ms. Sputter etching was performed utilizing Ar + ion gun operated at 2.2 keV and current density of 2.2 μA/cm^2. The data collection and analysis were done at pressures lower than 10^{-6} Pa. The data was investigated utilizing the CasaXPS software. The baselines of the spectra were obtained utilizing the Shirley strategy and pinnacle fitting was finished utilizing Gaussian-Lorentzian functions. The surface morphologies, fractured cross-section morphologies and the thickness of the coatings were checked by field emission scanning electron microscopy-SEM (Zeiss Merlin). Grazing incidence (3°) X-ray diffraction (XRD) measurements were performed using an X-Pert Pro MPD diffractometer with Cu $K_{\alpha 1}$ (λ = 1.54 Å) radiation source.

The microstructural and high-resolution (HR) TEM imaging was performed using a probe corrected Jeol ARM 200F electron microscope operating in STEM mode at 200 kV acceleration voltage and an image corrected FEI Titan^3 operating in TEM mode at 300 kV acceleration voltage. The lamellae were prepared by focused ion beam (FIB) using a FEI Helios Nanolab electron microscope.

3. Results

3.1. Coating integrity

The innovative single target deposition coupled with additional secondary plasma source offered a remarkable improvement of adhesive strength and coating's integrity without the use of a third element metallic interlayer (such as Ti or Cr). The effect of coating architecture (novel gradient layer) on scratch resistance behaviour of pure MoS_2 coating and selected Mo-S-N coating has been shown in Table 1. The coatings deposited without the novel gradient layer had a substantially low adhesive failure limit while the introduction of the novel gradient layer in the coatings enhanced the adhesion failure resistance beyond the tested range. No evidence of delamination or penetration through the steel was observed. So, this enhancement is solely related to the strong adherence achieved by metal-metal bonding, induced by the deposition procedure.

The scratch test tracks were analysed in SEM and are shown in Fig. 3. It was again observed that the novel gradient layer improved the scratch resistance of the coating. Large flakes were observed as a result of cohesive cracking in the films deposited without the novel gradient layer. Similarly, nitrogen doping further enhanced the adhesion and scratch resistance. This improvement for nitrogen-doped coatings, as compared to the pure coatings, is attributed to the formation of dense structures that prevents delamination or exfoliation of lamella within the coatings, thus increased the load-bearing capacity.

Fig. 4 shows the effects of nitrogen content on the initial load required for cohesive failure (L_{c1}). As soon as the nitrogen was introduced to the MoS_2 coatings, there was improvement in the critical load for cohesive failure as said above. In general, the increase in nitrogen content increased the failure limit or late appearance of flakes in the scratch test. The increase was almost linearly until 24 at. % of nitrogen incorporation but, after this, a sudden increase in scratch resistance was observed. This sudden increase could be due to enhanced amorphousness (or nanocomposite structure) of the coatings, which eliminates the presence of any laminar crystals, thus avoiding cohesive failures. So, as expected, the nitrogen content and the novel gradient layers have played a major role in the enhancement of the cohesive failure resistance and provided a good adhesion of these coatings to the substrate without the need of any other metallic interlayer (or the use of a second target).

In order to investigate in depth the mechanisms behind this high stability and the scratch resistance of the deposited coatings, cross-sectional analysis was performed for one of the nitrogen-doped films deposited with the novel gradient layer.

Fig. 5 shows HR-TEM images at the substrate interface. A 10 nm thick Mo film followed by an ultrathin multilayer system with a periodicity of 5 nm was observed. The structural analysis showed that the first Mo layer forms the base for the growth of a nanocomposite MoN multilayer. The layer structure formation is caused by the planetary motion of the substrate holder and the alternative exposure to the magnetron cathode and the plasma source providing mainly argon and nitrogen ions, respectively.

Epitaxial stacking between Fe and Mo was observed along the substrate interface, as a result of a small lattice mismatch (7.3%) between the two unit cells, causing defect-free coherent crystal growth in large areas of the substrate. The first Mo layer becomes the seed for the formation of a laminar MoN composite. The hexagonal MoN provides increased hardness, shear strength and superior adhesion of the film. Nitrides are formed by selectively removing sulphur through surface resputtering by exposing the substrate to high ion energy (substrate bias) and nitrogen ion bombardment (secondary plasma source). As shown in Fig. 6, the growth direction of Mo followed by the MoN-rich composition gradient layer (S deficient) is dependent on the orientation of the neighbouring substrate grains; therefore, the novel gradient layer changes the crystalline direction depending on the substrate interface

Table 1
Table representing the cohesive failure limit and adhesive failure limit for pure MoS_2 and Mo-S-N coatings made with and without a novel gradient layer. The adhesive failure limit is beyond the tested load for coatings with novel gradient layer.

Sample	*Cohesive failure limit (Lc1)*	*Adhesive failure limit*
Pure MoS_2 coating without novel gradient layer	2.9 N	14.9 N
Pure MoS_2 coating with novel gradient layer	3.3 N	> 80 N
Mo-S-N coating without novel gradient layer	1.6 N	22.8 N
Mo-S-N coating with novel gradient layer	35.1 N	> 80 N

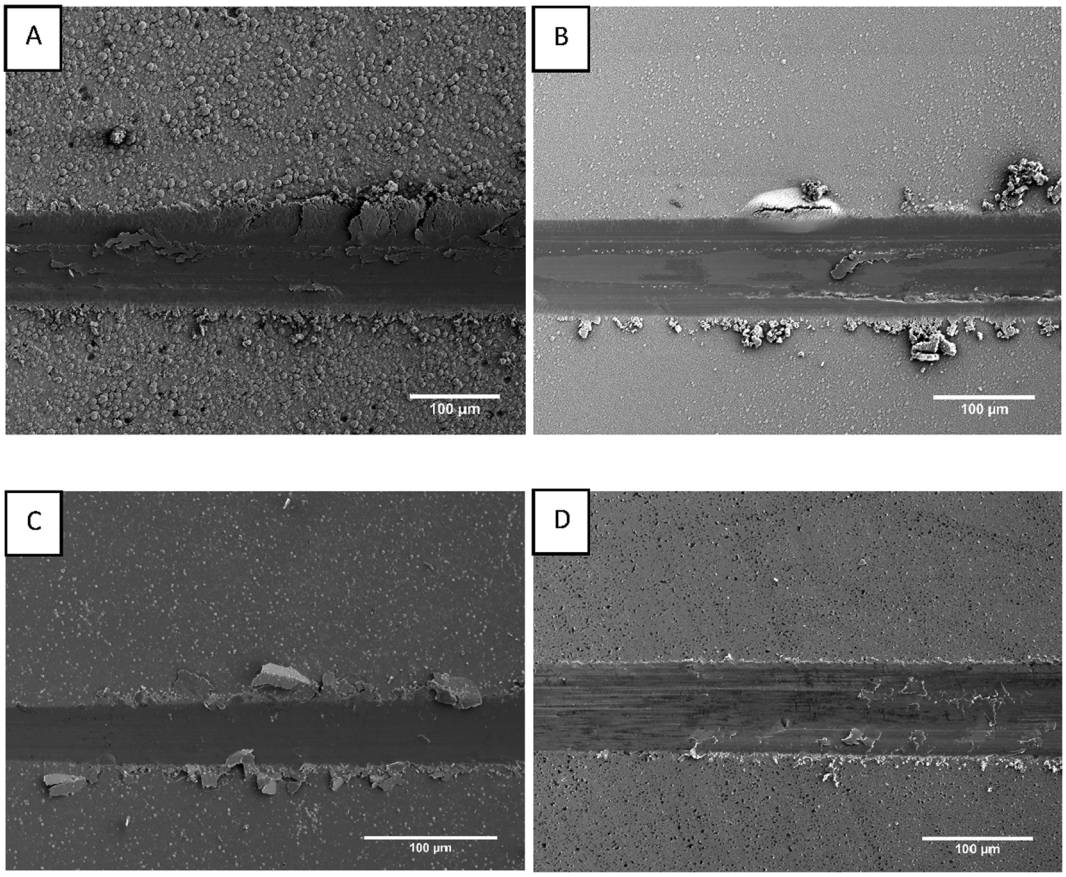

Fig. 3. SEM images of cohesive failures of materials with pure MoS_2 and Mo-S-N with and without novel gradient layer. (A) Pure MoS_2 coating **without** a novel gradient layer. (B) Pure MoS_2 coating **with** novel gradient layer. (C) Mo-S-N coating **without** novel gradient layer. (D) Mo-S-N coating **with** novel gradient layer.

orientation. In order for the Mo bonding layer to withstand the increased mechanical strain and allow for plastic deformation without brittle failure under increased loads, coherent interfaces are required. Fig. 6 show examples of such atomic arrangements which occur as a result of the matching crystal structures of Fe, Mo and MoN.

3.2. Chemical composition and deposition rate

The chemical composition of pure MoS_2 and all the Mo-S-N coatings with increasing nitrogen composition/content were analysed by wavelength dispersive spectroscopy (WDS) as shown in Table 2. It was observed that even for the pure MoS_2 coatings (0 at. % N), the S/Mo ratio was less than MoS_2 stoichiometric composition (S/Mo ~ 2).

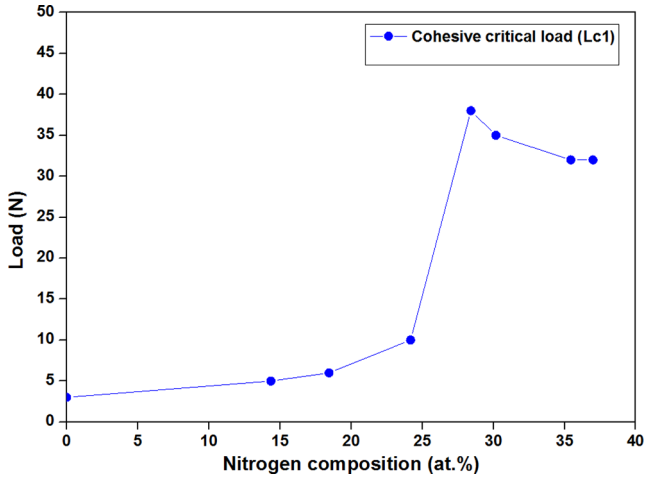

Fig. 4. Evolution of scratch behaviour Lc1 (cohesive critical load or cohesive failure limit) for pure MoS_2 and Mo-S-N films with respect to the nitrogen compositions.

Several physical mechanisms can be involved for sulphur depletion, like resputtering by fast reflected neutrals [43,45], resputtering by the ion bombardment [46] or even self-desorption of sulphur from the coating surface [47]. Fig. 7 represents some evidence of preferential resputtering of sulphur studied using optical spectroscopy, by collecting the light emissions of the plasma at secondary plasma source and target. From 0 V to 100 V, no significant increase in the ratio of intensities of sulphur to argon was observed in both cases (between target and substrate, and between secondary plasma source and substrate). This could indicate that the resputtering effect, due to the ion energy, is absent (0 V to 100 V). On the other hand, beyond 100 V, an increase in the emission intensities occurs, showing that the resputtering of S from the film becomes intense (as seen between secondary plasma source and substrate). Similar behaviour was also observed elsewhere [42]. So, such low or almost negligible resputtering at 50 V leads to the conclusion that the sub-stoichiometry of MoS_2(N0) can be better attributed to desorption of sulphur.

The substrate bias is known to increase the compactness of coatings through the re-deposition of atoms in less dense areas. The acceleration voltage also increases ad-atom mobility [21,48]. The measured S/Mo ratio for pure coating was 1.79 which is a higher value when compared to other reported results for pure MoS_2 films (S/Mo-1.6) [31,49]. This result is tentatively attributed to a highly degassed chamber due to a long heating and pumping prior to deposition. This procedure minimizes the presence of residual gases, like H_2O, which could react to sulphur atoms and, then, decreasing the S content of this element in the film. This was further evidenced by a comparative experiment

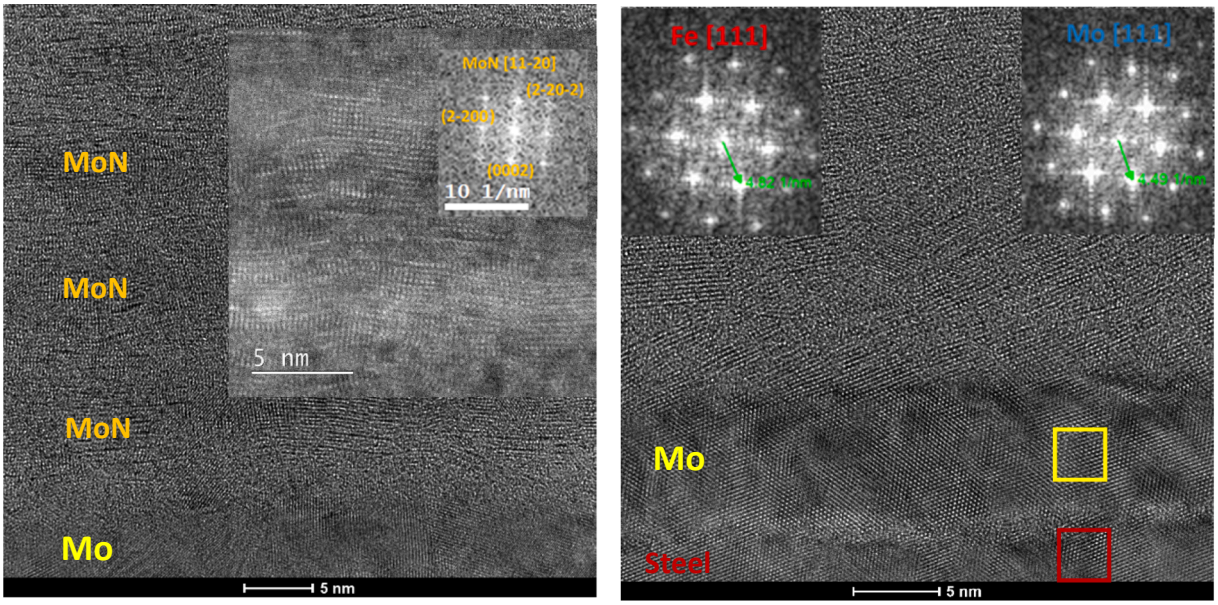

Fig. 5. (Left) Microstructure of novel gradient layers from an as-deposited coating cross-section. (Right) The first layer Mo over steel making metal-metal bonding with Fe; delivers improved adhesion. Preferential resputtering of sulphur had caused this layer to be sub-stoichiometry (S/Mo = approx. 0.3).

performed with just 1 h of degassing, for which an evident strong smell was detected (H_2S or SO_x) indicating the sulphur reacts with the residual gas. For the usual 5 h of heating prior to deposition, no smell was detected when the opening the chamber after the coating deposition, meaning that the chamber is almost free of contamination gases (mainly H_2O). On the other hand, the oxygen concentration in the N-doped and pure MoS_2 coatings was low at 0.5–1.5 at. % and up to 4 at. % respectively; a factor of ~2 lower as when compared to values reported in the literature [49].

The increase in the nitrogen flow rate during the deposition and the effect on the composition of the coating are shown in Table 2 and Fig. 8. The Mo content remained nearly unchanged whereas the sulphur content gradually decreased, suggesting that nitrogen is replacing sulphur in the Mo-S compound. Overall, the minimum value for S/Mo was 1.25 and the (S + N)/Mo ratio was in the range of 2.17–2.50. These values higher than 2 also shows that nitrogen molecules can be trapped between the lamellas of MoS_2 as it was reported by Isaeva et al. [36]. N can also be located at interstitial positions in the $MoS(N_2)$ compound which causes the formation of an amorphous structure.

To understand the influence of the ion bombardment, one of the coatings (Mo-S-N with 30 sccm flow) was deposited without the use of additional secondary plasma source (keeping the other parameters constant) and the results are shown in Table 3. The film without the use of additional secondary plasma source had only 18 at. % of nitrogen content and S/Mo ratio of 1.57 against the 28 at. % and 1.33, respectively, for MoSN30 (30 sccm nitrogen flow); the O content also was higher. This evolution is in agreement with the above described influence of the bombardment on the film growth promoting the resputtering of lighter elements from the growing film and its densification. The bombardment with nitrogen ions can facilitate their subplantation in the film and the replacement of the re-sputtered sulphur atoms.

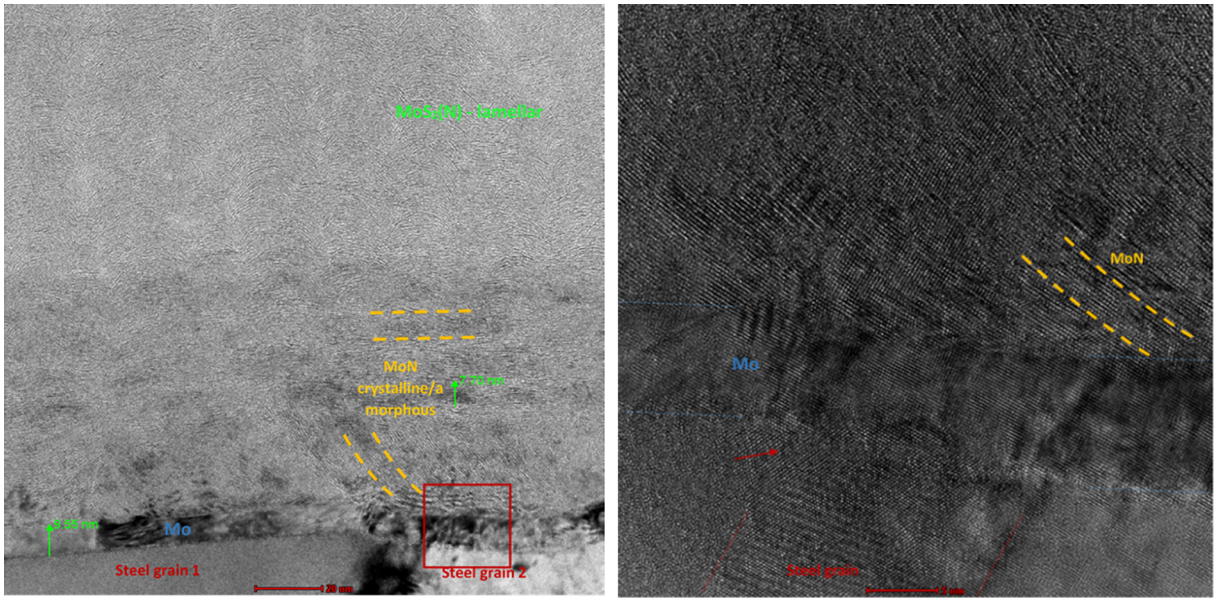

Fig. 6. (Left) Morphology of the Mo/MoN(S) novel gradient layer. (Right) Epitaxial deposition of Mo and MoN on steel substrate; strong substrate interface.

Table 2
The chemical composition of all Mo-S-N coatings. The number suffix of sample code indicates the nitrogen flow used for a particular test.

Sample	N_2 flow (sccm)	Mo (at. %)	S (at. %)	N (at. %)	S/Mo	Thickness (μm)	Deposition rate (nm/min)
MoS_2(N0)	0	35.4 ± 0.4	63.4 ± 0.5	0	1.79	6.1	51.3
MoSN10	10	30.8 ± 0.3	48.5 ± 0.3	18.4 ± 0.8	1.57	2.4	20.0
MoSN20	20	30.5 ± 0.4	43.2 ± 0.4	24.2 ± 0.7	1.42	2.2	18.5
MoSN30	30	30.2 ± 0.3	40.3 ± 0.3	28.4 ± 0.8	1.33	1.5	12.9
MoSN40	40	29.0 ± 0.4	39.4 ± 0.6	30.2 ± 0.5	1.36	1.3	11.5
MoSN50	50	27.9 ± 0.4	34.8 ± 0.4	35.4 ± 0.7	1.26	1.2	10.5
MoSN60	60	27.3 ± 0.4	34.1 ± 0.4	37.0 ± 0.8	1.25	1.2	10.0

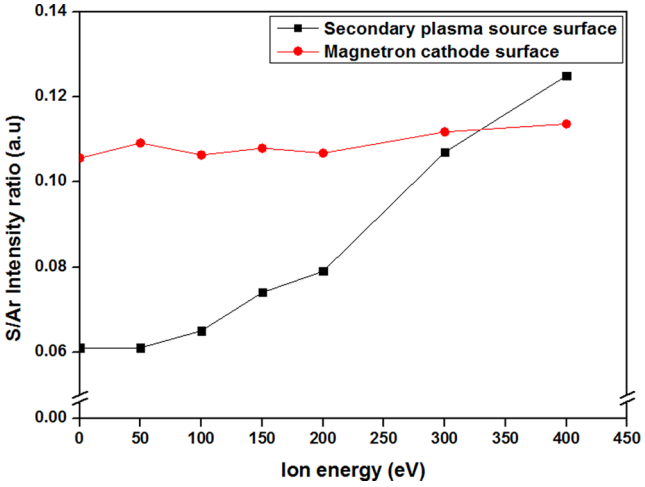

Fig. 7. Effect of resputtering of sulphur can be observed by optical emission of sulphur atom at 550 nm wavelength with respect to ion energy (eV) or substrate bias voltage. The intensity is normalised with Ar intensity for consistency. The tests were done with cathode power of 1000 W.

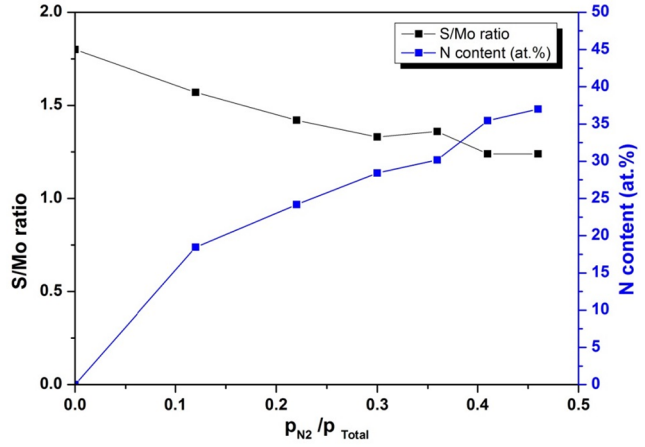

Fig. 8. Evolution of S/Mo ratio and N content in the films as a function of the partial pressure of nitrogen gas.

Table 2 shows that MoS_2(N0) coating has the highest deposition rate as compared to Mo-S-N coatings. The reported deposition rates correspond to the coatings without considering the growth of the novel gradient layer. Several factors can contribute to this trend as follows:

(i) With the introduction of nitrogen in the chamber, N_2 is mixed with Ar in the plasma, decreasing the sputtering efficiency, leading to a reduction of Mo and S sputtering yields [50].
(ii) Nitrogen is being ionized by the secondary plasma source, with the consequent increasing bombardment of the growing film. Therefore, the densification of film occurs. The bombardment and incorporation of N led to atomic arrangements and the removal of pores and voids, as it has been reported in the literature [49]. The compaction decreases the film thickness for the same amount of deposited material with the consequent decrease in the deposition rate.
(iii) The ion bombardment of the growing film induces the resputtering of the incoming species, decreasing the amount of deposited atoms and the deposition rate.

3.3. Chemical bonding

The ion bombardment of the growing film induces the resputtering of the incoming species, decreasing the amount of deposited atoms and the deposition rate. The character of the chemical bonding between the atoms forming Mo-S-N films was studied by XPS and the peak positions were identified using the NIST database [51]. The representative XPS Mo3d, S2p, N1s and $Mo3p_{3/2}$ core level spectra of N 0 at.% (0 sccm), N 18 at.% (10 sccm), N 28 at.% (30 sccm) and N 35 at.% (50 sccm) are shown in Fig. 9. The XPS spectra have been fitted by Gaussian-Lorentzian curves. The relative contents of the various valence states are estimated from the integral area under the Gaussian curves. The Mo3d spectrum is fitted to the doublet peaks at 229.0 eV and 232.4 eV [46], corresponding to MoN bonds with approx. 3.4 eV spin-orbit splitting; the 228.3 eV and 231.5 eV peaks with 3.2 eV spin-orbit splitting are corresponding to the chemical bonds between Mo and S typical for MoS_2, and the doublet peaks at 230.0 eV and 233.3 eV belongs to Mo-O with 3.3 eV splitting. It can be seen that the MoS2 contribution is still dominant in the Mo3d spectrum. The Mo-O bond is almost vanished indicating that there was no oxidation in the film bulk. The peak at 226.3 eV belongs to S2s. The S2p spectrum at 162.0 eV becomes slightly broader and lower intensity from 18 at. % (10 sccm) to 35 at. % (50 sccm) due to loss of S element in the film. The N1s spectrum partially overlaps with $Mo3p_{3/2}$ peaks, which is in good agreement with the reported in the literature [31,49]. With the increase of N content, the intensity of the N1s signal increases. The binding energy of N1s displays a main contribution at 397.5 eV, corresponding to N-Mo bonds. N1s XPS peaks are important to understand the Mo-S-N compound films because the N-Mo bond peaks increases with the incorporation of nitrogen into the coatings and similar results were also observed in other experiments [52,53]. From our measurements, we can conclude that,

Table 3
Chemical composition of Mo-S-N films with and without the use of secondary plasma source for Mo-S-N films with 30 sccm N_2 flow.

Sample	Mo (at. %)	S (at. %)	N (at. %)	O (at. %)	S/Mo	Deposition rate (nm/min)
With secondary plasma source	30.2 ± 0.3	40.3 ± 0.3	28.4 ± 0.8	1.1 ± 0.2	1.33	12.9
Without secondary plasma source	30.7 ± 0.3	48.4 ± 0.4	18.0 ± 0.4	2.9 ± 0.2	1.57	15.8

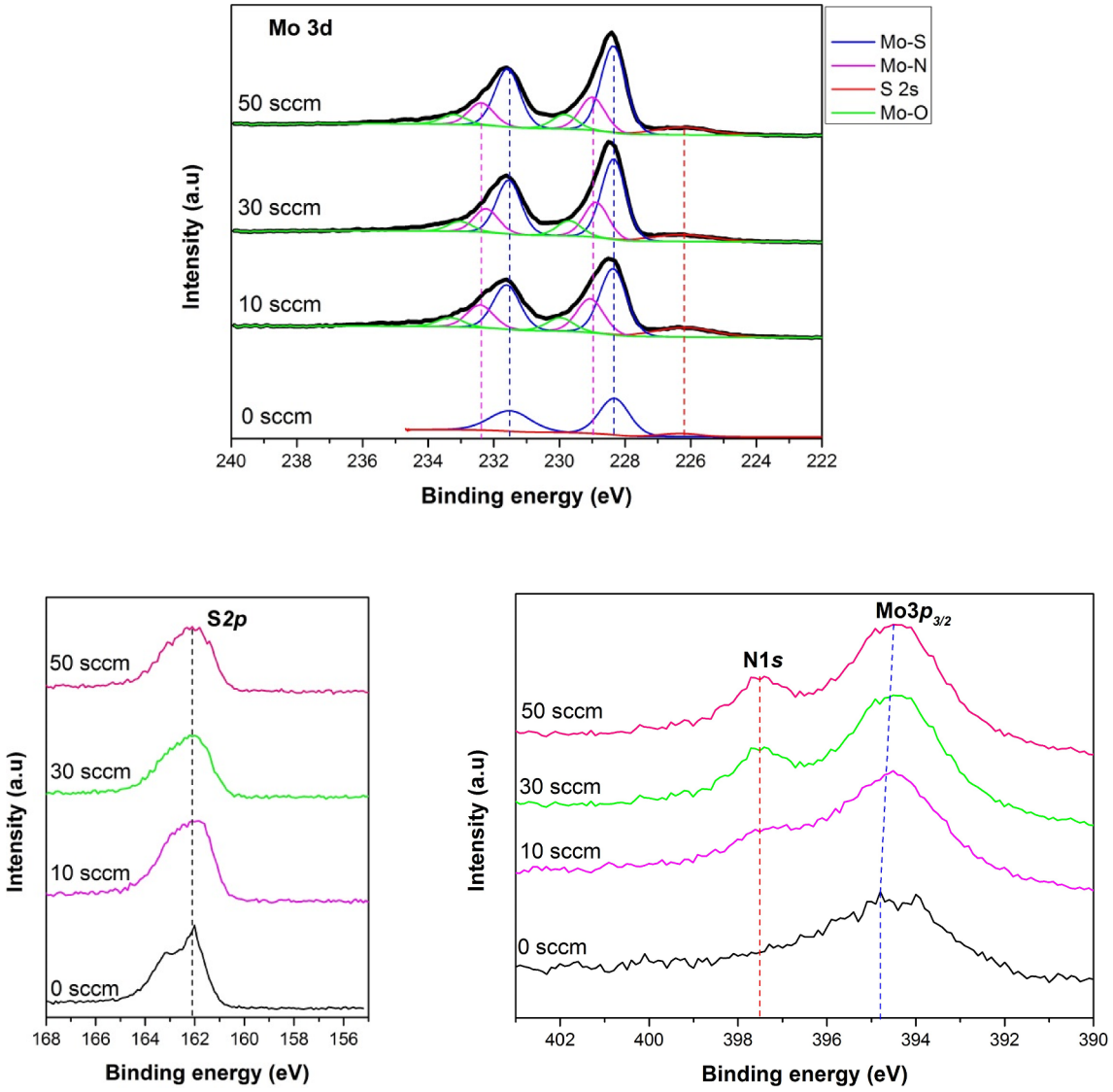

Fig. 9. XPS spectra from Mo3d, S2p and N1s-Mo3p $_{3/2}$ from the Mo-S-N films deposited at 18 at. % N (10 sccm), 28 at. % N (30 sccm) and 35 at. % N (50 sccm) respectively. 0 sccm refers to pure MoS_2 spectra.

with the increase of N content from 0 at. % (0 sccm) to 35 at. % (50 sccm), the relative amount of Mo-N seems to increase. Still, there is much more Mo-S present as evident from the intensity of S2s peaks at 226.3 eV and also the presence of Mo-S peaks. This is achieved through the periodic exposure to N-rich ion bombardment and MoS_2 target during the rotation of the substrate holder.

3.4. Fractured cross-section and surface morphology

Fig. 10 shows the fractured cross-section and surface morphologies of the deposited coatings. The sputtered pure MoS_2 coating displayed highly porous and low density cross-section morphology with a large contribution of dendritic growth throughout the coating (Fig. 10*a*). Surface morphology of this coating was in accordance with the cross-sectional results and the evidences of dendritic growth were clearly visible (Fig. 10*b*). For Mo-S-N coatings, even with the introduction of the lowest amount of nitrogen (18 at. %), the coatings started to become compact and displayed columnar morphology (Fig. 10*c*). The surface morphology micrograph for this coating also displayed less porous and sponge-like morphology (Fig. 10*d*). With further nitrogen incorporations, the compactness and density continued to increase, while the surface displayed cauliflower like morphology due to surface limited diffusion conditions [3,54]. A significant increase in the compactness was observed after 28 at. % N addition.

The thickness of the coatings displayed trends similar to compactness with the highest thickness of the MoS_2 coating (6.1 μm) decreasing with increasing the nitrogen content (as low as 1.2 μm). Despite more atoms being added as compared to the pure coating, the substantial thickness decreases are being attributed to the removal of porosity and increase of the density and compactness.

3.5. Crystal structure

The crystallographic structure of Mo-S-N coatings was analysed by grazing incidence XRD (GI-XRD) and it is shown in Fig. 11. For the pure MoS_2 coating, the XRD reflections located at 2θ = 14°, 33°, 58°, and 60° indicated that the pattern was similar to typical sputtered TMDs (for MoS_2- ICDD 00-037-1492). The peak detected at ~14°, corresponding to the (0 0 2) planes, displayed very weak signals. The broad peak observed from 33° to 45°, with an extended shoulder, is related to the (1 0 0) and (10*L*) planes. These observations were in accordance with the work of Weise et al. [55] who for the first time introduced the turbostratic stacking of the (10L) planes (L = 1,2,3,4,…).

The low (0 0 2)/(1 0 0) peak intensity ratio is attributed to the

deposition rate as it can make a considerable effect on the orientation of the crystals in sputtered coatings. (0 0 2) planes have a high desorption rate if the deposition rate of the coatings is 15 nm/min and above. With ~15 nm/min, the deposition rate of second (0 0 2) layer becomes higher than the desorption rate of the first layer and thus (0 0 2) planar growth occurs. Here, the deposition rate was much higher (~51 nm/min) which was optimum for the (1 0 0) planar growth as compared to the (0 0 2) [48,56].

Incorporation of nitrogen atoms into the MoS_2 coatings, during deposition, led to significant changes in their crystal structure. Mo-S-N films with the lowest nitrogen content of about 18 at. % showed some vestiges of the presence of (1 0 0) and (1 1 0) planes but the (0 0 2) peaks totally disappeared behaving similar to pure coatings. As the nitrogen incorporation was increased to 24 at. % and 28 at. % the intensity of (1 0 0) peak was further reduced. It has been previously reported that nitrogen can either get trapped in the basal planes of

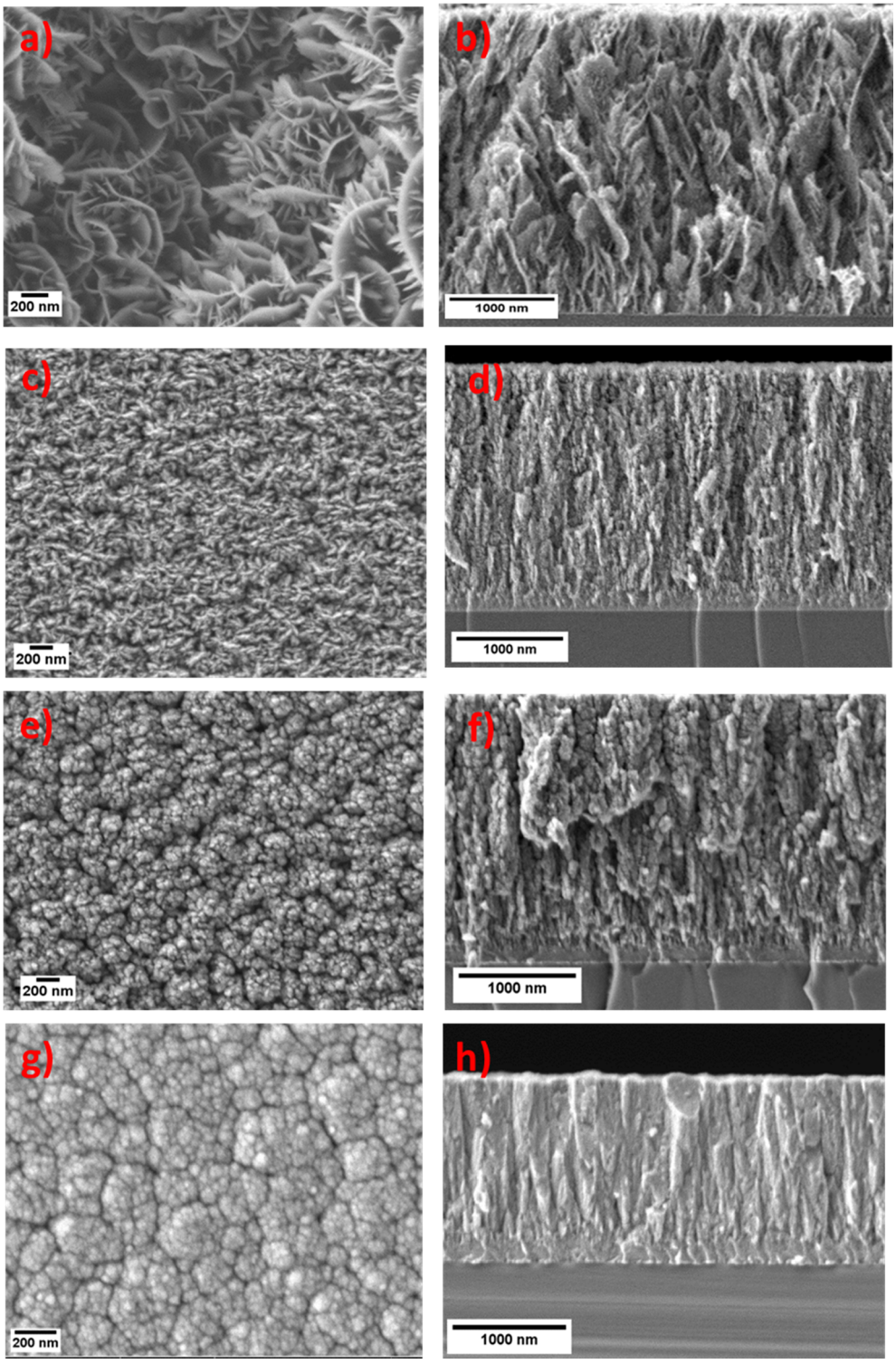

Fig. 10. SEM micrographs of surface (a, c, e, g, i, k, m) and cross-section morphologies (b, d, f, h, j, l, n) of films deposited with increasing N content of 0%, 18%, 24%, 28%, 30%, 35% and 37% N respectively.

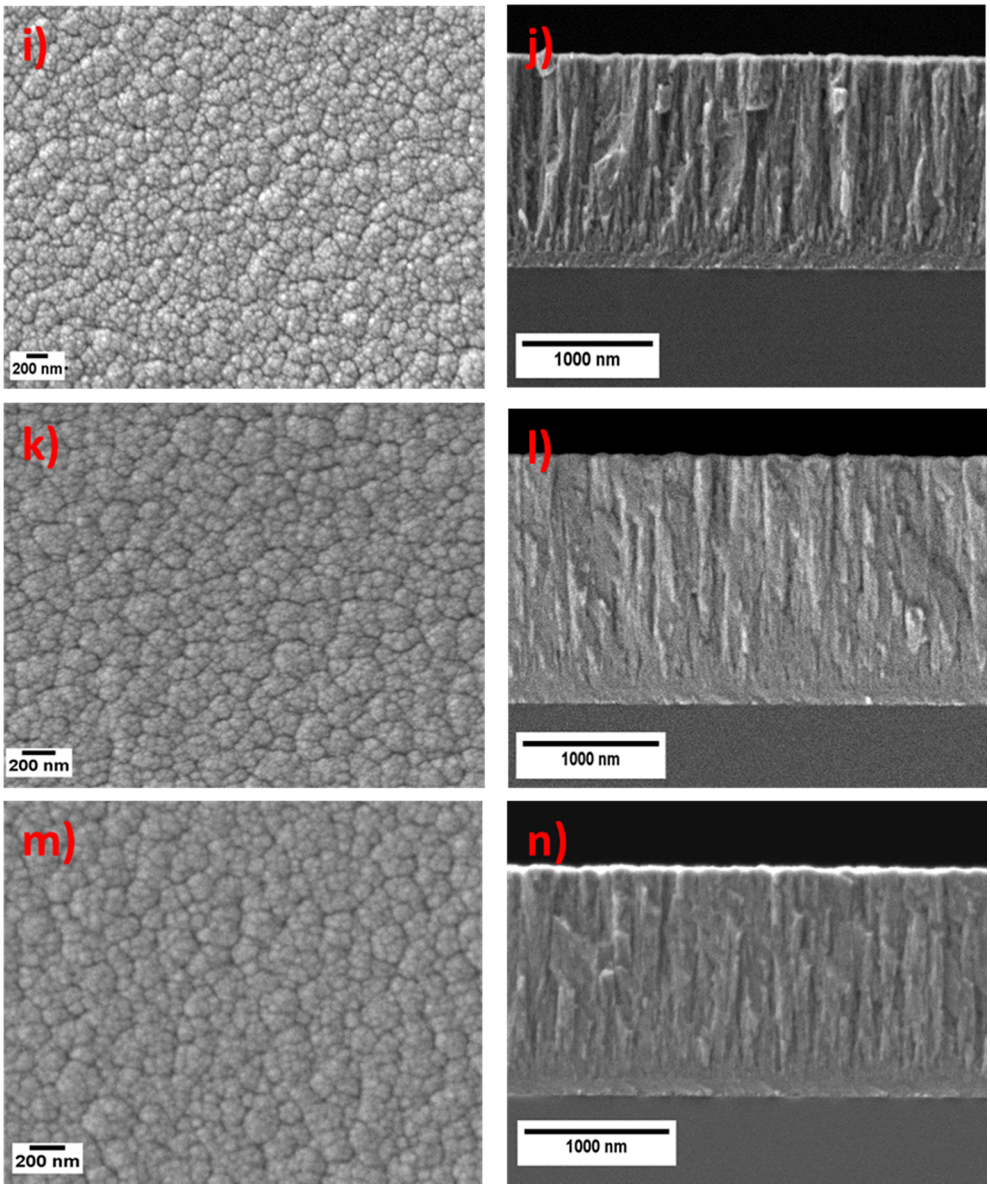

Fig. 10. (*continued*)

chalcogenides [57] or can replace the chalcogen atom [58] causing short-range disorder in the atomic structure. So, either of the mechanisms might be responsible for disrupting the organized growth and structure of MoS_2 crystals. Then at 30 at. % of N and above, the coatings were completely XRD amorphous and without any evidences of the crystalline MoS_2 peaks. Further increments in nitrogen doping yielded similar amorphous structures as shown by XRD spectra.

Overall, the results obtained were in disagreement with the work of Zhang et al. [31] where the amorphousness was observed with 18 at. % of the nitrogen doping. This difference is attributed to the deposition approach as in our case; the substrates face the MoS_2 target alternating with the additional plasma source. This means that when the substrates are in-front of the MoS_2 target, the nitrogen effect is a bit lower and thus the MoS_2 crystallinity was observed. As the nitrogen content (or flow) in the chamber increases, the freedom for MoS_2 to form crystals is hindered and, therefore, the coatings become completely amorphous. The tiny peak at 31° on Mo-S-N coating (35 at. % N) could correspond to the MoN structure, underneath the coating in the interlayer zone as mentioned above, detected due to the lower thickness of the film.

3.6. Nanostructure

In order to observe the effects of nitrogen doping on the MoS_2 coatings, the lamella prepared from three different zones of the selected coating (with 30 at. % N) was imaged in cross-section via TEM. Fig. 12 shows the obtained HR-TEM micrographs. We observed an amorphous nature of the coating, especially towards the top of the film with very few traces of the nanocrystalline lamellar MoS_2. Towards the substrate interface, a combination of amorphous regions and regions with randomly oriented MoS_2 platelets was observed. The coating was dense (agreeing with SEM results) and showed a dendritic nanostructure throughout the thickness of the film. The columnar features were shown to be S-rich and hence provided the conditions for the localised crystallisation of MoS_2 lamellae. These few traces and small sizes were the reason that MoS_2 crystalline peaks were absent in XRD analysis of this coating.

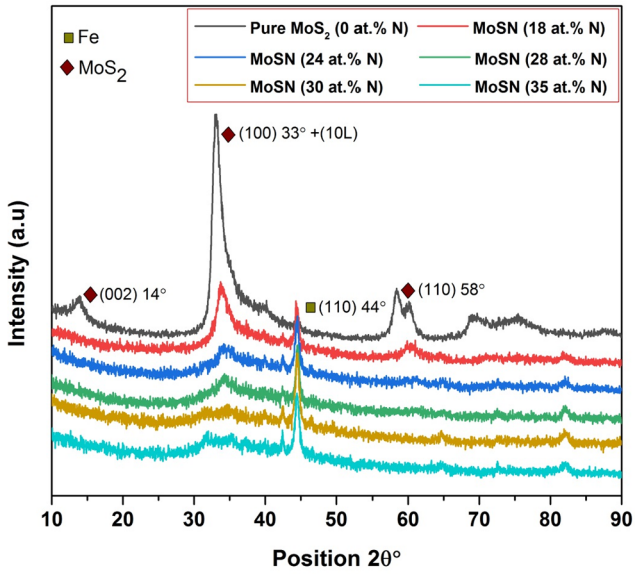

Fig. 11. X-ray diffraction patterns of the coatings.

4. Discussions

Mo-S-N coatings were deposited by single-target DC magnetron sputtering with pulsed DC substrate bias in a planetary rotating semi-industrial machine with an additional secondary plasma source. The importance of secondary plasma source was well established for the deposition of Mo-S-N coatings to develop a novel deposition condition meant for obtaining distinctive properties. The additional secondary plasma source serves the following functions; (i) it creates low argon pressure plasma which is used to etch the steel. During this etching process, the oxides on the surface are removed from the ion bombardment resulting in the contaminant-free surface promoting a better adhesion of the coatings. (ii) During the coating process, it is used to vary the ion to neutral ratio of the species arriving to the substrates. (iii) The plasma density or current density can be tuned at the substrate by adjusting the plasma source power. With the help of this source, the nitrogen content in the coating was also enhanced for any particular flow of nitrogen gas into the chamber. Another important step was to obtain a highly degassed chamber prior to deposition. Heating at 150 °C for 5 h along with pumping made the chamber free of H_2O on either the substrates or over the chamber walls. The oxygen content measured in the coatings was very low compared to what other researchers found in their coatings (50% lesser). This semi-industrial PVD machine has a large capacity of keeping many samples at a time which will rotate inside the chamber passing alternately in front of the target and the

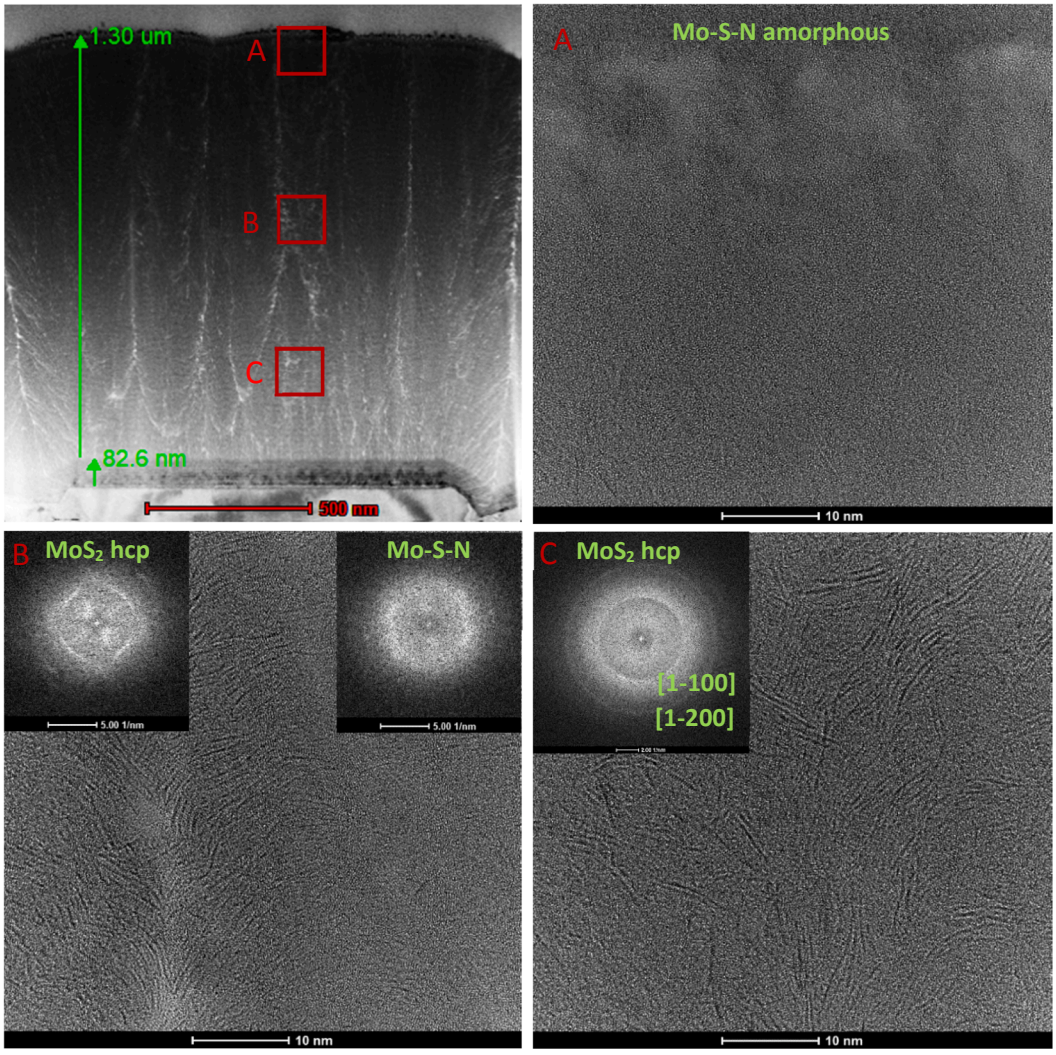

Fig. 12. Microstructure of the as-deposited Mo-S-N (30 at. % N) film with the corresponding FFT patterns are shown in insets.

additional independent secondary plasma source. This allows the deposition process to achieve homogeneity over many samples/substrates kept in a single batch.

In this study, along with the doping of nitrogen with MoS_2, an attempt was made to improve the coating adhesion to steel substrates which is one of the drawbacks for such coatings in industries. Moreover, an innovative strategy is being applied to improve the adhesion without the use of any third element metallic interlayer (e.g. Ti or Cr).

The deposition process started (after heating with pumping and etching) with making a metal-metal bonding with steel using the only target of MoS_2. A thin Mo rich layer was created with high ion energy and high ion bombardment resulting in preferential re-sputtering of sulphur from the growing film leaving just a Mo- rich layer. Later, nitrogen was introduced which created a MoN (S deficient) layer. Due to the alternating between target and secondary plasma source, a multilayer feature made of varying nitrogen contents existed, as observed in Fig. 5. The ion bombardment also contributed to further incorporation of nitrogen in the coatings. Following this, the ion energy was reduced in order to keep sulphur in the coatings in the presence of nitrogen in the plasma. This was made to distort the formation of crystalline MoS_2 thus, preventing exfoliation/delamination within coatings. The coatings were deposited at -50 V substrate bias for 2 h after 20 min of the novel gradient layer.

The coating integrity was tested using the scratch test which validates the strategy employed to improve the adhesion. For the case of coating with novel gradient layers, the adhesion failure limit was beyond the tested range (> 80 N). Even the Mo-S-N coating without the novel gradient layer showed some increase in the adhesion failure limit compared to the pure MoS_2 coatings. Alloying with nitrogen and using the novel gradient layer, the cohesive failure limit had a 10 fold increase compared to pure MoS_2 coatings (Table 1). Cohesive failures were identified by the initial flaking of the surface. The improvement was attributed to the prevention of any exfoliation due to the amorphousness of the Mo-S-N coatings.

The composition of the coatings had a good correlation with the structure. For the case of MoS_2(N0) coating, the surface and cross-section images presented in Fig. 10(*a* and *b*), revealed a porous morphology. This type of coating morphology showed preferential orientation of grains in (1 0 0) direction than (0 0 2) as seen in Fig. 11 of XRD spectra. The crystalline anisotropy of hexagonal MoS_2 contributes to the formation of fibrous-needle or platelet-like structures. It is very well known that longer grains cause shadowing effect which in-turn can create porosity during the rotation of the substrate.

For the MoSN10 coating (18 at. % of N), a diminution of the size of platelets is observed in Fig. 10(*c* and *d*). The incorporation of nitrogen provided disorder in the atomic structure of Mo and S and triggered a grain refinement process. The observations are supported by the XRD analysis presented in Fig. 11. The intensity of the characteristic (1 0 0) peak for MoSN10 coating decreases, which indicated a disruption in the nanostructure of the coating when compared to pure MoS_2 coating. The presence of nanostructure, gave rise to more compact coatings, thus steeply decreasing the thickness with nitrogen doping. The decrease in the deposition rate is also due to the decrease of the sputtering yield of Mo and S in the reactive atmosphere. This overall leads to a decrease in S/Mo ratio due to the incorporation of nitrogen into coatings. As the nitrogen ions are bombarding induced by the secondary plasma source, they participate in the removal of sulphur atoms and their replacement or get sub-planted in interstitial positions in the MoS_2 structure. Nitrogen alloying thus induces amorphousness in the MoS_2 coatings.

Further addition of nitrogen to 28 at. % (30 sccm N_2 flow), results in the formation of amorphous and dense coating as well as in the drastic reduction of the XRD peak intensity. Fig. 10(*g* and *h*) also show less porosity and highly compact coating. All further increase in nitrogen content has led to amorphous coatings which are in good agreement with the structure and surface morphology. Thus, nitrogen alloyed coatings showed a reduced thickness compared to pure MoS_2 coating. Though some sulphur atom could have been replaced by nitrogen, a substantial amount of sulphur was still retained within the coating even for 37 at. % of N (MoSN60 coating). In this case, the minimum S/Mo ratio was observed (1.25).

To understand the chemical bonding mechanism within the coating, XPS revealed quite interesting results. Even for 35 at. % of N (MoSN50 coating) the Mo-S peak (228.3 eV) was dominant over Mo-N peak (229.0 eV). Also, the S2s peak at 226.3 eV showed the presence of S–S bonds whereas N–N bonds were detected at 397.5 eV. This reveals that a good amount of MoS_2 compound was formed even for highly doped films. The formation of such bonds could be due to the deposition process, to the use of alternating magnetron sputtering and secondary plasma source which incorporates N/Mo/S and N (in small quantity), respectively. Thus, a process of deposition of MoS_2 takes place, after bombardment some S is re-sputtered and N is incorporated. Thereby, only some Mo-S bonds are replaced with Mo-N bonds at secondary plasma source. This also corroborates with the chemical composition where S/Mo ratio was 1.26.

The ion bombardment from plasma source also promotes desorption of impurities, thereby the C (not shown) and O contents in the coating is found to be reduced in comparison to the coating without the use of plasma source as seen in Table 3. The additional plasma source plays a very crucial role in desorption of impurities, the incorporation of nitrogen by bombardment and the reorganises the surface of the coating to prevent voids. Therefore, the nitrogen is incorporated into the coating by two means: (i) due to the normal sputtering process in reactive mode in nitrogen-containing plasma and, (ii) by additional N ion bombardment by the secondary plasma source. Nitrogen can either get entrapped between the basal planes [57] or can replace the chalcogen atom [58] causing disorder in the atomic placement. Komsa et al. [59] showed, based on theoretical predictions and experiments, that it was possible to dope MoS_2 by filling the vacancies created by the electron beam with impurity atoms. It was feasible to have a MoS_2 sheet with S vacancy filled in by an isolated atom of N. Later, Dolui et al. [60] described some possible doping strategies for MoS_2 monolayers, using density functional theory, by a first substitutional doping at both the Mo and S sites. They reported that the best strategy would be to grow S-poor films and, then, filling the vacancies with an appropriate atom, such as N. Due to the high formation energy of the vacancy, N substitution is energetically favoured since that energy is largely dependent on the growth conditions. Based on this work, the highest nitrogen content films is achieved by using high ion bombardment with the secondary plasma source, high S/Mo ratio, should have a structure consisting of a Mo-S-N compound with Mo bonded to S and N. Such a compound would be amorphous in nature.

Finally, it is safe to say that at least 30% nitrogen content can provide a complete amorphous structure. Thus, in our case, the structure of Mo-S-N coatings are crystalline or nanocrystalline from 0 to 28 at. % N and changes to amorphous above 28 at.% N. Such nitrogen-doped coatings have a high potential for projecting impressive tribological properties in vacuum and humid air.

5. Conclusions

In this study, Mo-S-N coatings were deposited using a semi-industrial DC magnetron sputtering apparatus with a single target of MoS_2 and planetary rotating substrate holder on Si (1 0 0) and M2 steel substrates. The chemical composition, morphology, structure and chemical bonding were studied as a function of the N-content of Mo-S-N coatings. An innovative novel gradient layer was synthesised to improve the adhesion of the coatings with the steel substrates having metal-metal bonding (strong bonding). Then, adhesion failure limit beyond the tested range of 80 N was achieved with a single MoS_2 target and without the need to use any metallic interlayers (e.g. Ti or Cr). This simplifies the depositions in the industrial environment solving a major industrial issue. The initial Lc1 representing the initial cohesive

cracking/flaking of the coatings was 38 N for the 28 at. % nitrogen content coating. With heating and pumping prior to etching and deposition, it was possible to attain very low oxygen content in coatings, less than 1 at. %. The structure of the coatings changed with the incorporation of nitrogen. The coatings with less than 30 at. % N was nanocrystalline; for higher contents coatings became XRD amorphous. The morphology was increasingly more compact with the incorporation of nitrogen. HRTEM also confirmed the presence of amorphism in high N-content coatings. The S/Mo ratio was also improved and maintained to 1.25 for the highest N incorporation (37 at. % N). The ideal atomic arrangement based on the above results would be that nitrogen was incorporated in a ternary compound, such as Mo-S-N, with Mo–N and Mo–S bonds. These coatings with enhanced adhesion, high S/Mo ratio, very high compactness and low contaminant contents have great potential to show high hardness and other interesting mechanical and tribological properties.

CRediT authorship contribution statement

Kaushik Hebbar Kannur: Writing - original draft, Methodology, Investigation, Formal analysis. **Talha Bin Yaqub:** Investigation. **Teodor Huminiuc:** Investigation. **Tomas Polcar:** Project administration, Funding acquisition, Resources. **Christophe Pupier:** Project administration, Resources. **Christophe Heau:** Writing - review & editing, Supervision, Resources. **Albano Cavaleiro:** Writing - review & editing, Supervision, Resources.

Declaration of Competing Interest

The authors declare that they have no known competing financial interests or personal relationships that could have appeared to influence the work reported in this paper.

Acknowledgements

This project has received funding from the European Union Horizon 2020 research and innovation programme under grant agreement No. 721642: SOLUTION.

The electron microscopy imaging was performed with the support of the South of England Analytical Electron Microscope (EP/K040375/1), within the David Cockayne Centre for Electron Microscopy, Department of Materials, University of Oxford. Alongside financial support provided by the Henry Royce Institute (EP/R010145/1) and CEITEC Nano Research Infrastructure (ID LM2015041, MEYS CR, 2016–2019), CEITEC Brno University of Technology.

The authors would also like to thank funding from CEMMPRE – UID/EMS/00285/2019 [co-financed via FEDER and FCT (COMPETE)].

References

[1] W.E. Jamison, S.L. Cosgrove, Friction characteristics of transition-metal disulfides and diselenides, A S L E Trans. 14 (1971) 62–72, https://doi.org/10.1080/05698197108983228.

[2] Y. Zhao, Y. Zhang, Z. Yang, Y. Yan, K. Sun, Synthesis of MoS2and MoO2for their applications in H2 generation and lithium ion batteries: a review, Sci. Technol. Adv. Mater. 14 (2013) 43501, https://doi.org/10.1088/1468-6996/14/4/043501.

[3] T. Polcar, A. Cavaleiro, Review on self-lubricant transition metal dichalcogenide nanocomposite coatings alloyed with carbon, Surf. Coat. Technol. 206 (2011) 686–695, https://doi.org/10.1016/j.surfcoat.2011.03.004.

[4] K. Ren, M.L. Sun, Y. Luo, S.K. Wang, J. Yu, W.C. Tang, First-principle study of electronic and optical properties of two-dimensional materials-based heterostructures based on transition metal dichalcogenides and boron phosphide, Appl. Surf. Sci. 476 (2019) 70–75, https://doi.org/10.1016/j.apsusc.2019.01.005.

[5] Z. Cui, K. Ren, Y. Zhao, X. Wang, H. Shu, J. Yu, W. Tang, M. Sun, Electronic and optical properties of van der Waals heterostructures of g-GaN and transition metal dichalcogenides, Appl. Surf. Sci. 492 (2019) 513–519, https://doi.org/10.1016/j.apsusc.2019.06.207.

[6] J.S. Zabinski, M.S. Donley, S.V. Prasad, N.T. McDevitt, Synthesis and characterization of tungsten disulphide films grown by pulsed-laser deposition, J. Mater. Sci. 29 (1994) 4834–4839, https://doi.org/10.1007/BF00356530.

[7] H. Waghray, T.-S. Lee, B.J. Tatarchuk, A study of the tribological and electrical properties of sputtered and burnished transition metal dichalcogenide films, Surf. Coatings Technol. 76–77 (1995) 415–420, https://doi.org/10.1016/0257-8972(95)02564-2.

[8] M.F. Cardinal, P.A. Castro, J. Baxi, H. Liang, F.J. Williams, Characterization and frictional behavior of nanostructured Ni–W–MoS2 composite coatings, Surf. Coatings Technol. 204 (2009) 85–90, https://doi.org/10.1016/j.surfcoat.2009.06.037.

[9] G. Stachowiak, A.W. Batchelor, Engineering Tribology, Butterworth-Heinemann, 2013.

[10] A.R. Lansdown, Molybdenum Disulphide Lubrication, Elsevier, 1999, , https://doi.org/10.1108/ilt.2000.01852aae.001.

[11] J. Moser, F. Lévy, Crystal reorientation and wear mechanisms in MoS2 lubricating thin films investigated by TEM, J. Mater. Res. 8 (1993) 206–213, https://doi.org/10.1017/s0884291400120539.

[12] I.L. Singer, S. Fayeulle, P.D. Ehni, Wear behavior of triode-sputtered MoS 2 coatings in dry sliding contact with steel and ceramics, Wear. 195 (1996) 7–20, https://doi.org/10.1016/0043-1648(95)06661-6.

[13] N.M. Renevier, N. Lobiondo, V.C. Fox, D.G. Teer, J. Hampshire, Performance of MoS2/metal composite coatings used for dry machining and other industrial applications, Surf. Coatings Technol. 123 (2000) 84–91, https://doi.org/10.1016/S0257-8972(99)00424-7.

[14] W. Lauwerens, J. Wang, J. Navratil, E. Wieërs, J. D'haen, L.M. Stals, J.P. Celis, Y. Bruynseraede, Humidity resistant MoSx films prepared by pulsed magnetron sputtering, Surf. Coatings Technol. 131 (2000) 216–221.

[15] P. Wang, L. Qiao, J. Xu, W. Li, W. Liu, Erosion mechanism of MoS2-based films exposed to atomic oxygen environments, ACS Appl. Mater. Interfaces. 7 (2015) 12943–12950, https://doi.org/10.1021/acsami.5b02709.

[16] X. Ding, X.T. Zeng, X.Y. He, Z. Chen, Tribological properties of Cr- and Ti-doped MoS2 composite coatings under different humidity atmosphere, Surf. Coatings Technol. 205 (2010) 224–231, https://doi.org/10.1016/j.surfcoat.2010.06.041.

[17] V. Rigato, G. Maggioni, A. Patelli, D. Boscarino, N.M. Renevier, D.G. Teer, Properties of sputter-deposited MoS2/metal composite coatings deposited by closed field unbalanced magnetron sputter ion plating, Surf. Coatings Technol. 131 (2000) 206–210, https://doi.org/10.1016/S0257-8972(00)00797-0.

[18] F. Bülbül, İ. Efeoğlu, Synergistic effect of bias and target currents for magnetron sputtered MoS2-Ti composite films, Mater. Test. 58 (2016) 471–474, https://doi.org/10.3139/120.110870.

[19] J.J. Nainaparampil, A.R. Phani, J.E. Krzanowski, J.S. Zabinski, Pulsed laser-ablated MoS2-Al films: friction and wear in humid conditions, Surf. Coatings Technol. 187 (2004) 326–335, https://doi.org/10.1016/j.surfcoat.2004.02.043.

[20] D.G. Teer, J. Hampshire, V. Fox, V. Bellido-Gonzalez, The tribological properties of MoS2/metal composite coatings deposited by closed field magnetron sputtering, Surf. Coatings Technol. 94–95 (1997) 572–577, https://doi.org/10.1016/S0257-8972(97)00498-2.

[21] S. Gangopadhyay, R. Acharya, A.K. Chattopadhyay, S. Paul, Effect of substrate bias voltage on structural and mechanical properties of pulsed DC magnetron sputtered TiN–MoSx composite coatings, Vacuum 84 (2010) 843–850, https://doi.org/10.1016/j.vacuum.2009.11.010.

[22] B.C. Stupp, Synergistic effects of metals co-sputtered with MoS2, Thin Solid Films 84 (1981) 257–266, https://doi.org/10.1016/0040-6090(81)90023-7.

[23] J.R. Lince, H.I. Kim, P.M. Adams, D.J. Dickrell, M.T. Dugger, Nanostructural, electrical, and tribological properties of composite Au–MoS2 coatings, Thin Solid Films 517 (2009) 5516–5522, https://doi.org/10.1016/j.tsf.2009.03.210.

[24] T. Spalvins, Frictional and morphological properties of Au MoS2 films sputtered from a compact target, Thin Solid Films. 118 (1984) 375–384, https://doi.org/10.1016/0040-6090(84)90207-4.

[25] S. Mikhailov, A. Savan, E. Pflüger, L. Knoblauch, R. Hauert, M. Simmonds, H. Van Swygenhoven, Morphology and tribological properties of metal (oxide)–MoS2 nanostructured multilayer coatings, Surf. Coatings Technol. 105 (1998) 175–183, https://doi.org/10.1016/S0257-8972(98)00483-6.

[26] J.S. Zabinski, M.S. Donley, S.D. Walck, T.R. Schneider, N.T. Mcdevitt, The effects of dopants on the chemistry and tribology of sputter-deposited MoS2 films, Tribol. Trans. 38 (1995) 894–904, https://doi.org/10.1080/10402009508983486.

[27] M.R. Hilton, R. Bauer, S.V. Didziulis, M.T. Dugger, J.M. Keem, J. Scholhamer, Structural and tribological studies of MoS2 solid lubricant films having tailored metal-multilayer nanostructures, Surf. Coatings Technol. 53 (1992) 13–23, https://doi.org/10.1016/0257-8972(92)90099-V.

[28] K.J. Wahl, D.N. Dunn, I.L. Singer, Wear behavior of Pb–Mo–S solid lubricating coatings, Wear 230 (1999) 175–183, https://doi.org/10.1016/S0043-1648(99)00100-3.

[29] X. Liu, G.J. Ma, G. Sun, Y.P. Duan, S.H. Liu, MoSx-Ta composite coatings on steel by d.c magnetron sputtering, Vacuum 89 (2013) 203–208.

[30] D. Jianxin, S. Wenlong, Z. Hui, Z. Jinlong, Performance of PVD MoS2/Zr-coated carbide in cutting processes, Int. J. Mach. Tools Manuf. 48 (2008) 1546–1552, https://doi.org/10.1016/j.ijmachtools.2008.06.009.

[31] X. Zhang, L. Qiao, L. Chai, J. Xu, L. Shi, P. Wang, Structural, mechanical and tribological properties of Mo-S-N solid lubricant films, Surf. Coatings Technol. 296 (2016) 185–191, https://doi.org/10.1016/j.surfcoat.2016.04.040.

[32] H. Nyberg, J. Sundberg, E. Särhammar, F. Gustavsson, T. Kubart, T. Nyberg, U. Jansson, S. Jacobson, Extreme friction reductions during initial running-in of W-S–C–Ti low-friction coatings, Wear 302 (2013) 987–997, https://doi.org/10.1016/j.wear.2013.01.065.

[33] A.A. Voevodin, J.P. O'Neill, J.S. Zabinski, WC/DLC/WS2 nanocomposite coatings for aerospace tribology, Tribol. Lett. 6 (1999) 75–78, https://doi.org/10.1023/A:1019163707747.

[34] M. Evaristo, T. Polcar, A. Cavaleiro, Synthesis and properties of W-Se–C coatings deposited by PVD in reactive and non-reactive processes, Vacuum. 83 (2009) 1262–1265, https://doi.org/10.1016/j.vacuum.2009.03.030.
[35] A. Nossa, A. Cavaleiro, Tribological behaviour of N(C)-alloyed W-S films, Tribol. Lett. 28 (2007) 59–70, https://doi.org/10.1007/s11249-007-9248-3.
[36] L. Isaeva, J. Sundberg, S. Mukherjee, C.J. Pelliccione, A. Lindblad, C.U. Segre, U. Jansson, D.D. Sarma, O. Eriksson, K. Kádas, Amorphous W-S-N thin films: the atomic structure behind ultra-low friction, Acta Mater. 82 (2015) 84–93, https://doi.org/10.1016/j.actamat.2014.08.043.
[37] J. Sundberg, H. Nyberg, E. Särhammar, T. Nyberg, S. Jacobson, U. Jansson, Influence of composition, structure and testing atmosphere on the tribological performance of W-S-N coatings, Surf. Coatings Technol. 258 (2014) 86–94, https://doi.org/10.1016/j.surfcoat.2014.09.061.
[38] P. Mutafov, M. Evaristo, A. Cavaleiro, T. Polcar, Structure, mechanical and tribological properties of self-lubricant W-S-N coatings, Surf. Coatings Technol. 261 (2015) 7–14, https://doi.org/10.1016/j.surfcoat.2014.11.074.
[39] A. Nossa, A. Cavaleiro, Chemical and physical characterization of C(N)-doped W–S sputtered films, J. Mater. Res. 19 (2004) 2356–2365. https://doi.org/DOI: 10.1557/JMR.2004.0293.
[40] A. Nossa, A. Cavaleiro, The influence of the addition of C and N on the wear behaviour of W-S-C/N coatings, Surf. Coatings Technol. 142–144 (2001) 984–991, https://doi.org/10.1016/S0257-8972(01)01249-X.
[41] Z. Daming, L. Jiajun, Z. Baoliang, L. Wenzhi, A study of the friction and wear performance of MoSx thin films produced by ion beam enhanced deposition and magnetron sputtering, Wear. 210 (1997) 45–49, https://doi.org/10.1016/S0043-1648(97)00039-2.
[42] V.Y. Fominski, V.N. Nevolin, R.I. Romanov, I. Smurov, Ion-assisted deposition of MoSx films from laser-generated plume under pulsed electric field, J. Appl. Phys. 89 (2001) 1449–1457, https://doi.org/10.1063/1.1330558.
[43] A. Nossa, A. Cavaleiro, Mechanical behaviour of W-S-N and W-S-C sputtered coatings deposited with a Ti interlayer, Surf. Coatings Technol. 163–164 (2003) 552–560, https://doi.org/10.1016/S0257-8972(02)00622-9.
[44] et al. D. Camino, D. Teer, J. Von Stebut, M. Gee, N. Jennett, J. Banks, Scratch adhesion testing of coated surfaces-Challenges and new directions, Adhes. Meas. Film. \& Coatings. 2.2 (2001).
[45] A. Nossa, A. Cavaleiro, N.J.M. Carvalho, B.J. Kooi, J.T.M. De Hosson, On the microstructure of tungsten disulfide films alloyed with carbon and nitrogen, Thin Solid Films 484 (2005) 389–395, https://doi.org/10.1016/j.tsf.2005.02.018.
[46] G. Eda, H. Yamaguchi, D. Voiry, T. Fujita, M. Chen, M. Chhowalla, Photoluminescence from chemically exfoliated MoS 2, Nano Lett. 11 (2011) 5111–5116, https://doi.org/10.1021/nl201874w.
[47] M. Donarelli, F. Bisti, F. Perrozzi, L. Ottaviano, Tunable sulfur desorption in exfoliated MoS2 by means of thermal annealing in ultra-high vacuum, Chem. Phys. Lett. 588 (2013) 198–202, https://doi.org/10.1016/j.cplett.2013.10.034.
[48] T. Bin Yaqub, T. Vuchkov, P. Sanguino, T. Polcar, Comparative Study of DC and RF Sputtered MoSe 2 Coatings Containing Carbon - An Approach to Optimize Stoichiometry , Microstructure , Crystallinity and Hardness, (2020) 1–16. DOI:10.3390/coatings10020133.
[49] T. Hudec, M. Mikula, L. Satrapinskyy, T. Roch, M. Truchlý, P. Švec, T. Huminiuc, T. Polcar, Structure, mechanical and tribological properties ofMo-S-N solid lubricant coatings, Appl. Surf. Sci. (2019), https://doi.org/10.1016/j.apsusc.2019.03.294.
[50] Z. Han, J. Tian, Q. Lai, X. Yu, G. Li, Effect of N2 partial pressure on the microstructure and mechanical properties of magnetron sputtered CrNx films, Surf. Coatings Technol. 162 (2003) 189–193, https://doi.org/10.1016/S0257-8972(02)00667-9.
[51] NIST X-ray Photoelectron Spectroscopy Database Version 4.1, Natl. Inst. Stand. Technol. Gaithersbg. (2012). http://srdata.nist.gov/xps/.
[52] I. Jauberteau, A. Bessaudou, R. Mayet, J. Cornette, L.J. Jauberteau, P. Carles, T. Merle-Méjean, Molybdenum nitride films: crystal structures, synthesis, mechanical, electrical and some other properties, Coatings 5 (2015), https://doi.org/10.3390/coatings5040656.
[53] F. Niefind, J. Djamil, W. Bensch, B.R. Srinivasan, I. Sinev, W. Grünert, M. Deng, L. Kienle, A. Lotnyk, M.B. Mesch, J. Senker, L. Dura, T. Beweries, Room temperature synthesis of an amorphous MoS2 based composite stabilized by N-donor ligands and its light-driven photocatalytic hydrogen production, RSC Adv. 5 (2015) 67742–67751, https://doi.org/10.1039/C5RA14438H.
[54] T. Polcar, A. Cavaleiro, Self-adaptive low friction coatings based on transition metal dichalcogenides, Thin Solid Films 519 (2011) 4037–4044, https://doi.org/10.1016/j.tsf.2011.01.180.
[55] G. Weise, N. Mattern, H. Hermann, A. Teresiak, I. Ba, W. Bru, Preparation, structure and properties of MoSx films, Thin Soli. 298 (1997) 98–106, https://doi.org/10.1016/S0040-6090(96)09165-1.
[56] C. Muratore, A.A. Voevodin, Control of molybdenum disul fi de basal plane orientation during coating growth in pulsed magnetron sputtering discharges, Thin Solid Films 517 (2009) 5605–5610, https://doi.org/10.1016/j.tsf.2009.01.190.
[57] K.D. Rasamani, F. Alimohammadi, Y. Sun, Interlayer-expanded MoS 2, Mater. Today 20 (2017), https://doi.org/10.1016/j.mattod.2016.10.004.
[58] P.D. Fleischauer, J.R. Lince, Comparison of oxidation and oxygen substitution in MoS2solid film lubricants, Tribol. Int. 32 (1999) 627–636, https://doi.org/10.1016/S0301-679X(99)00088-2.
[59] H.P. Komsa, J. Kotakoski, S. Kurasch, O. Lehtinen, U. Kaiser, A.V. Krasheninnikov, Two-dimensional transition metal dichalcogenides under electron irradiation: defect production and doping, Phys. Rev. Lett. 109 (2012) 1–5, https://doi.org/10.1103/PhysRevLett.109.035503.
[60] K. Dolui, I. Rungger, C. Das Pemmaraju, S. Sanvito, Possible doping strategies for MoS2 monolayers: An ab initio study, Phys. Rev. B. 88 (2013) 75420. DOI:10.1103/PhysRevB.88.075420.

Annex B

Hebbar Kannur, K.; Yaqub, T. B; Pupier, C.; Héau, C.; Cavaleiro, A. ***Mechanical Properties and Vacuum Tribological Performance of Mo-S-N Sputtered Coatings*****.** ***ACS Appl. Mater. Interfaces*** **12 (2020) 43299–43310.**
https://doi.org/10.1021/acsami.0c12655.

.

ACS APPLIED MATERIALS & INTERFACES

www.acsami.org

Research Article

Mechanical Properties and Vacuum Tribological Performance of Mo−S−N Sputtered Coatings

Kaushik Hebbar Kannur,* Talha Bin Yaqub, Christophe Pupier, Christophe Héau, and Albano Cavaleiro

Cite This: *ACS Appl. Mater. Interfaces* 2020, 12, 43299−43310

Read Online

ACCESS | Metrics & More | Article Recommendations | Supporting Information

ABSTRACT: MoS_2 is the most widely used dry lubricant for low friction applications in vacuum environments. However, due to its lamellar nature it exfoliates during sliding, leading to high wear, high coefficient of friction (COF), and low stability. Here, we report the mechanical properties and the vacuum (10^{-4} Pa) tribological performance of nitrogen-alloyed transition-metal-dichalcogenide (TMD-N) coatings. The coatings were deposited using a hybrid deposition method, that is, reactive direct current (DC) sputtering of MoS_2 target assisted by an additional plasma source. The tribological tests were performed at relatively low contact stresses to replicate real industrial needs. The interaction between different mating surfaces (coating versus steel, coating versus coating) has been reported. Additionally, the effects of loads on the sliding properties were also studied for coating versus coating interactions. A maximum hardness of 8.9 GPa was measured for the 37 atom % N-alloyed coating. In all mating conditions, the pure MoS_2 coating had COF in the range of 0.1−0.25 and the least specific wear rates were found to be 3.0×10^{-6} $mm^3/N{\cdot}m$ for flat and 2.5×10^{-6} $mm^3/N{\cdot}m$ for cylinder. As compared to MoS_2 coating, the COF and specific wear rates decreased with N additions. The COF was in the range of 0.05−0.1 for Mo−S−N coatings, while coating versus coating displayed the lowest specific wear rates (8.6×10^{-8} $mm^3/N{\cdot}m$ for flat and 4.4×10^{-8} $mm^3/N{\cdot}m$ for cylinder). Finally, the increase in load resulted in a decrease of COF, but an increase in the wear rate was observed. The detailed mechanism behind the behavior of the COF for the different mating conditions was presented and discussed. This work brings some important issues when testing transition metal dichalcogenide-based coatings under low contact stress conditions more appropriate for simulating real service applications.

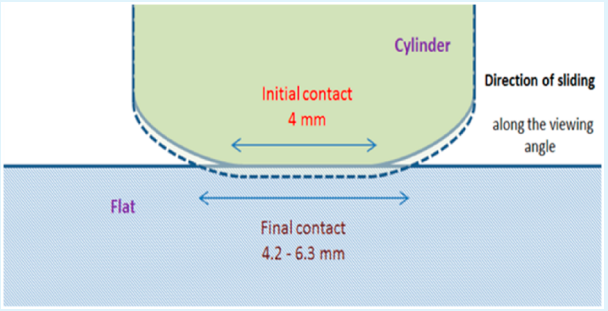

KEYWORDS: *transition metal dichalcogenides, solid lubrication, Mo−S−N coatings, cylinder-on-flat tribology, low contact stresses*

1. INTRODUCTION

Many critical devices in vacuum technology, like spacecraft, involve relative motion of contacting surfaces. Hence, the tribological stability of the components is a crucial concern in the efficiency and stability of these devices.[1,2] In this regard, these applications demand low friction (COF in range of 0.1) and low wear (specific wear rates below 10^{-6} mm^3/Nm) in order to achieve low power consumption, extreme reliability, high stability, and highly precise sliding processes.[3] Space mechanisms are required to operate in vacuum conditions but also during their assembly stage, testing phase, and storage time under ambient atmosphere.[4] Continuous research has been going on for the development of a system capable of providing better tribological properties in a vacuum. One possible solution is the use of solid lubricant coatings. The use of solid lubricant coatings became a subject of high interest whenever conventional liquid lubrication is prohibited, such as in extreme operating conditions or the necessity of a clean environment.[5] With the introduction of the plasma vapor deposition (PVD) process for the deposition of self-lubricant coatings, the research on solid lubricants has gained increasing attention.

Nanocomposite solid lubricant coatings based on TMDs are potential candidates for low friction and wear applications in dry and vacuum environments. The research on TMDs for aerospace applications started in the early 1960s[6] and is now a subject of research for the past few decades. This considerable attention is attributed to their excellent sliding properties and potential for the replacement of liquid lubricants and other low friction coatings.[7] Pure TMDs display remarkably low friction values of 0.1 to 0.001 in dry and ultrahigh vacuum conditions.[8−11] Their low friction behavior is attributed to the crystal structure, which plays a vital role in the sliding process. Strong covalent bonding exists between the metal and chalcogen atoms, while weak van der Waals bonding prevails between adjacent layers, allowing the easy shear of the planes.[7] Despite

Received: July 13, 2020
Accepted: August 25, 2020
Published: August 25, 2020

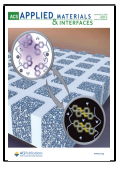

ideal conditions from the friction perspective, the low packing density (or porosity) and the presence of dangling bonds in sputtered TMDs not only decrease their load-bearing capability but also make them vulnerable to oxidation, moisture, and other environmental attacks. Additionally, pure TMDs fail to provide long-term durability and consistent tribological performances due to the exfoliation of the lamellar layers. These drawbacks, coupled with a low adhesion to substrates, result in the high wear of the TMD coatings. Ultimately, the coatings become unsuitable for efficient mechano-tribological applications.

To overcome these issues, TMDs have been alloyed with different metals[12−21] and nonmetals (e.g., C and N).[7,22−29] Metal doping has shown beneficial results[15] but drawbacks, such as (i) the detrimental effects of hard metal particles (e.g., Ti), (ii) abrasion of tribo-films,[30] (iii) rapid oxidation of tribo-films into metal oxides,[31] (iv) delamination of the TMD/metal multilayer interfaces due to thermal cycling in space environments,[32] and (v) high COF and wear with the increase in metal layer thickness,[33] have limited its use. Additionally, the reactive sputtering of metals (in gaseous form) is not possible, and the use of two sputtering targets further adds complexity in the repeatability of the process, due to the need for synchronization between the two cathodes. In the case of nonmetals, carbon alloying has attracted both industry and researchers due to its impressive properties but again reactive sputtering is an issue. The carbon incorporation in reactive sputtering was tried by using precursor gases such as CH_4 or C_2H_2. In such cases, hydrogen can react with the chalcogen, not only changing the stoichiometry of MoS_2 but also becoming a contamination source.[34]

Nitrogen doping has been less explored but seems a more suitable option to improve the properties of TMDs. Pure nitrogen can be used for reactive sputtering, avoiding the contamination (by other elements) along with low operational costs.[35] Furthermore, when compared to carbon, a small amount of nitrogen can be sufficient to achieve a dense amorphous coating, further reducing the operating costs.[36] Moreover, the improvement in the hardness can be greater than with C doping for similar C and N contents. In order to grow mechanically stable coatings, it is crucial either to prevent the easily sheared planes that are formed parallel to the sliding direction or to reduce the crystallinity of the soft TMD phase; this can easily be achieved by nitrogen doping.[37] On the other hand, despite disturbing the crystalline structure of MoS_2 in the coating, N does not affect the crystalline tribo-film formation to provide the required low friction.[30,38] Mutafov et al.[39] reported that magnetron sputtered amorphous W−S−N films exhibited a low COF, high load-bearing capacity, and good wear resistance. Isaeva et al.[36] with a theoretical approach reported that during the sliding of W−S−N coatings nitrogen was released from the contact region in the gaseous form (e.g., N_2, NO_2) without disturbing the formation of the tribo-films. Ju et al.[40] recently reported that Mo−S−N coatings showed higher oxidation resistance due to the formation of Mo—N bonds. Zhang et al.[31] reported that the incorporation of a small amount of nitrogen into MoS_2 sputtered films produced a nanocomposite structure, increasing the hardness and reducing the wear. High hardness was observed for a high N content coating (28 atom % N) but the COF and the specific wear rate also rose. On the other hand, low N content coatings (10 and 17 atom % N) had lower COF and specific wear rates. With the increase in N content, the increasing values of the wear rate and COF were attributed to the reduced S/Mo ratio (∼0.7) which hindered the formation of the well-ordered tribo-film at the contact area leading to the failure of coating. Similar works were also reported by Nossa et al.[41]

In our previous work,[29] Mo−S−N coatings were deposited using a novel hybrid deposition approach to improve the composition, compactness, structure, and adhesion. It was observed that the use of the secondary plasma source allowed the N ion bombardment of the growing film. Therefore, an enhanced N content, along with a higher S/Mo ratio in comparison to the literature, could be achieved.[26,31] As per literature, a higher S/Mo ratio in the deposited coatings can have a positive influence on the formation of well-ordered MoS_2 tribolayers during sliding.[42] Moreover, Grosseau-Poussard et al.[43] pointed out that it is possible to form the hexagonal structure of MoS_2 only if the x-value of MoS_x coating or its composites, is greater than 1.1. The structural studies revealed that coatings with 0−28 atom % N content were crystalline or nanocrystalline, while further N additions resulted in the prevalence of an amorphous phase. Likewise, N content of 28 atom % and above led to a very high compactness without any vestiges of porosity. Moreover, it was reported that the deposition approach resulted in an enhanced adhesion. The critical adhesion loads were higher than 80 N, a highly desirable characteristic that was not commonly reported in any other previous studies. It is expected that these properties will contribute to the excellent mechanical and tribological behavior of the deposited films.[29]

Therefore, this study is a continuation of the previous work focusing on the exploration of the mechano-tribological properties for real industrial requirements. It is well-known that the contact stresses in many tribological applications are relatively low, that is, in the range of 10−150 MPa, for example, in journal bearings.[44] Most of the tribological studies for alloyed TMDs until now dealt with contact stresses in the high range (500−1500 MPa)[26,28,31,38,39] with almost negligible focus on low contact stresses. Considering the results reported in ref 45, the study of these Mo−S−N coatings can also be an interesting domain to be explored at low contact stresses. Additionally, most of the Mo−S−N coatings were only studied in dry N_2 and humid air conditions. The vacuum tribology of this system has not been reported except for the work of Fu et al.[46] and Zhang et al.[31] Again, in these works, tests were conducted at much higher applied contact stresses (∼1500 MPa and ∼950 MPa), which is not a realistic approach for applications such as those existing in space industries/components.

Thus, this current work deals with vacuum tribology of optimized Mo−S−N coatings in low contact stress regime, so that the results can considerably be more practical and reliable for industrial implementation, especially for space applications. It is believed that the achieved results presented in this study will have a high impact from an industrial perspective.

2. EXPERIMENTAL DETAILS

The pure and N-alloyed MoS_2 coatings were deposited in a custom-built TSD 400 semi-industrial unit. The chamber was equipped with a single cathode and an additional secondary plasma source (to ionize gas mixture). A MoS_2 target (450 mm × 150 mm, 99.5% purity) was DC magnetron sputtered in N_2 and Ar (99.99% purity) gas atmosphere. The MoS_2 target and the plasma source powers were kept constant for all the depositions, while the N_2 flow was varied for compositional changes in the coatings. Polished M2 steel (Ø 25 mm, hardness = 62 HRC) and 100Cr6 steel cylinder, SKF cylindrical roller RC-10 × 10C (Ø 10 mm, 10 mm length, hardness = 61 HRC) were used as substrates (Figure 1A). The substrates were placed over a planetary (double

https://dx.doi.org/10.1021/acsami.0c12655
ACS Appl. Mater. Interfaces 2020, 12, 43299−43310

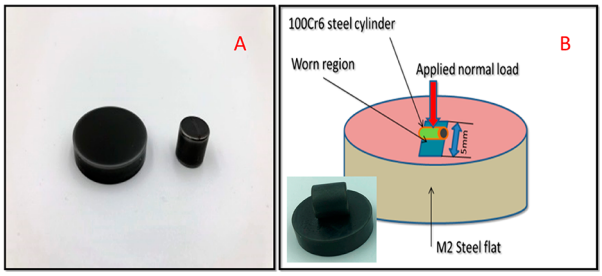

Figure 1. (A) Image of the coated flat and coated cylinder postdeposition used in tribo-testings. (B) Pictorial representation of the linear reciprocating cylinder on a flat tribometer.

rotation) substrate holder, which was rotating at a speed of 5 rpm, to achieve a uniform coating. Prior to depositions, the chamber and substrates were heated to 150 °C for 5 h (a process known as bake-out) along with pumping to the base pressure of ~10^{-4} Pa. This was done to enhance the adsorbed gas removal. The schematic diagram of the deposition chamber, secondary plasma source, deposition parameters detail, and the main characterization results (composition, morphology, microstructure, crystal structure, and adhesion) of the coatings can be found in ref 29.

The roughness measurements were performed using a contact mode atomic force microscope, manufactured by Nanosurf AG (Liestal, Switzerland). To eliminate the external noise, the AFM was placed on an active vibration isolation table (TS-150, S.I.S, Herzogenrath, Germany). The scans were performed at a rate of 0.1 line/s with the final image to be 20 μm × 20 μm in size. The average roughness parameter (Sa) was considered as the roughness of the coatings. The tests were performed immediately after the deposition to prevent oxidation damages.

Nanoindentation (Micro Materials Nano Test Platform) hardness measurements were performed using Berkovich diamond indenter under 3 mN load. A total of 32 indentations were performed at two different locations.

Linear reciprocating sliding tests were carried out in vacuum (at 10^{-4} Pa) using a cylinder-on-flat tribometer (see Figure 1B). The tribometer system is designed for the cylinder to self-align on the flat surface. The used cylinders made of 100Cr6 steel are manufactured for roller bearings. Their geometry is very reproducible but is not exactly a cylinder. It can be considered as a cylinder over the 4 mm center on the middle of the length. There is a small bulge/curvature along 3 mm at the end of the length of the cylinder, which impacts the initial contact stresses (see profile in Figure 2A). This results in an initial effective line contact length of ~4 mm. The effective length can increase during testing because of wear, depending on the sliding parameters and mating surfaces (see Figure 2B). Figure 2C,D shows the increase in the initial contact length after testing for a coated cylinder versus an uncoated M2 steel flat. A stroke length of 5 mm and a linear speed of 2 mm/s were selected for all of the tests. All of the tests were carried out at 5 N applied load, which resulted in a maximum initial Hertzian contact stress of ~95 MPa (typical of a journal bearing). Usually, the tribology tests of these materials are carried out at contact stresses in the range of 1000 MPa. Amorphous MoSx materials are in a metastable state. By providing them with a sufficient amount of energy, they transform in the contact from amorphous to lamellar structure necessary for friction reduction. One can expect that a minimum energy is necessary for that transformation to occur. Hence, it is interesting to reduce the contact stresses to the one that may be encountered in service to verify that the energy dissipated by friction to produce lamellar structure remains to be enough. The tests were carried out for 5000 cycles (50 m distance) with each cycle comprising both to-and-fro motion. All the coatings slide sufficiently to achieve a steady-state regime. Three different conditions of mating surfaces were tested during tribological analysis: (1) uncoated 100Cr6 steel cylinder versus coated flat, (2) coated cylinder versus uncoated M2 steel flat, and (3) coated cylinder versus coated flat. In the last case, the coatings of the cylinder and flat were the same for each test. The sample displaying the best frictional properties in case 3 was further tested at 2 N (contact stress = ~60 MPa) and 10 N (contact stress = ~135 MPa). The tangential load was measured by a high precision sensor (FUTEK) connected with the data recorder (SEFRAM). After the tests, the cylinder wear-width and length of line contact was measured in an optical microscope to determine the wear volume and the specific wear rate. For confirmation, the wear volume was also calculated using MarSurf CM mobile 3D optical profilometer (MARS) and MountainMaps software (DigitalSurf). For the case of flats, the depth profile of the wear-scar was taken using 3D optical profilometry (BRUKER), and the specific wear rate of the coating was calculated as the worn material volume per sliding distance and normal load. All of the tests were performed thrice to ensure repeatability.

3. RESULTS

3.1. Main Characteristics of the Deposited Coatings. The relation between nitrogen content, S/Mo ratio, and the coating roughness is depicted in Figure 3. The addition of nitrogen not only decreased the S/Mo ratio but also reduced the crystallinity and increased the compactness of the coatings. This decrease of S/Mo is related to the differences in the sputtering yield of Mo and S from the growing film, induced by the higher N ion bombardment. The S/Mo ratio was 1.36 for Mo−S−N40 (30 atom % N) and 1.25 for Mo−S−N60 (37 atom % N). Despite the substoichiometric values achieved for S/Mo ratios, the resulting chemical composition is closer to the desired values when compared to similar coatings presented in the literature (S/Mo ~ 0.8 for 30 atom % N).[26,31] This is expected to have a positive impact on the tribological properties of this system. The coatings became highly compact and X-ray diffraction amorphous for the higher N contents. The XRD measurements revealed that from 0 to 28 atom % N content, the coatings were crystalline or nanocrystalline. Further addition of nitrogen, for example, Mo−S−N40 (30 atom % N), caused the coatings to become XRD-amorphous (see ref 29 and Supporting Information). With amorphousness and compactness of the coatings, the roughness also decreased from 0 to 30 atom % N and later increased with further nitrogen additions. These roughness increments could be related to the formation of some asperities on the coating surface. Further details about the main characterization results of these coatings can be found in ref 29.

3.2. Mechanical Properties. Figure 4 shows the hardness and effective Young's modulus of the deposited coatings and their variation with nitrogen content. The pure sputtered MoS_2 coating showed the lowest hardness values of 0.5 GPa because of its low packing density[47] and columnar morphology, in agreement with the previous study.[29] The hardness of the films increased to 1.5 GPa (Mo−S−N10, 18 atom % N) as soon as nitrogen was introduced in the chamber. The hardness continued to increase with further additions of nitrogen. This increase is related to the improved compactness and density of the coatings,[29] which induces high resistance to plastic deformation, dislocation movement, and high load-bearing capacity.

The reduced crystallite size also plays a vital role in the improvement of the mechanical properties of the coating.[19,29,33] No significant difference in hardness was observed by increasing N from 30 to 37 atom % N, as the coating was already amorphous and highly compact at 30 atom % N alloying. The effective Young's modulus followed similar trends as hardness. Overall, the hardness values increased from 0.5 to 8.9 GPa, while the Young's modulus increased from 20 to 149 GPa with increasing N-alloying from 0 to 37 atom % N.

3.3. Tribological Properties. *3.3.1. Steel Cylinder versus Coated Flat.* In this configuration, the coating is on the flat

https://dx.doi.org/10.1021/acsami.0c12655
ACS Appl. Mater. Interfaces 2020, 12, 43299−43310

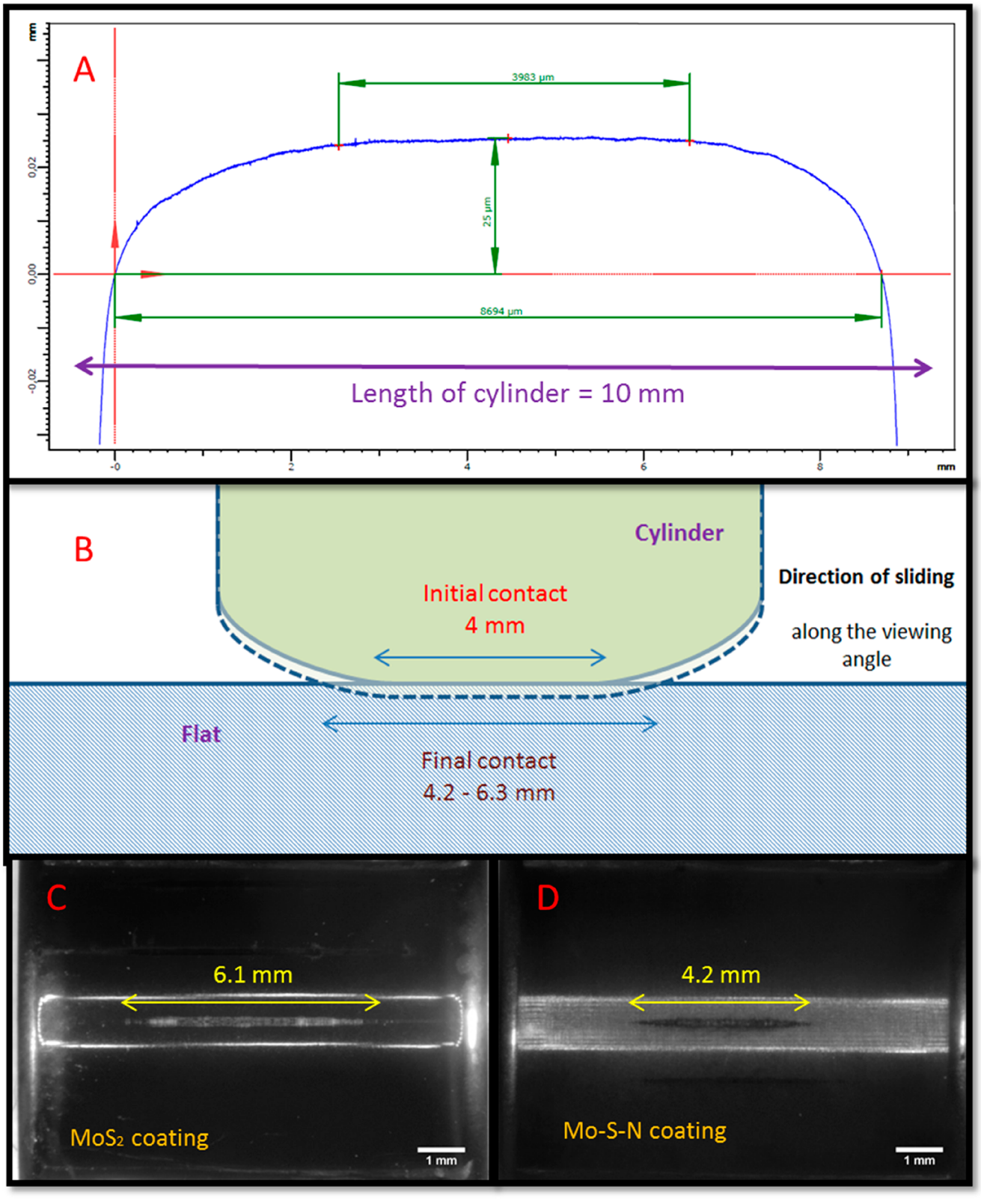

Figure 2. (A) The profile along the length of the steel cylinder shows the bulge/curvature with ~4 mm of flat. (B) The schematic view of an increase in the length of line contact with the evolution of wear. (C) The worn length of line contact on MoS_2 coated cylinder. (D) The worn length of line contact on Mo−S−N coated cylinder after sliding against the M2 steel flat.

sample behaving with the lowest wear rate on the point of view of the kinematic length. The evolution of the COF and the specific wear rate of all Mo−S−N coatings sliding against the uncoated steel cylinder under 5 N applied load are shown in Figure 5. All of the coatings displayed almost similar and highly stable steady-state friction curves. Significant differences were observed in the running-in period. All coatings displayed in this zone a bump in the initial part of the friction curves. Two main

https://dx.doi.org/10.1021/acsami.0c12655
ACS Appl. Mater. Interfaces 2020, 12, 43299−43310

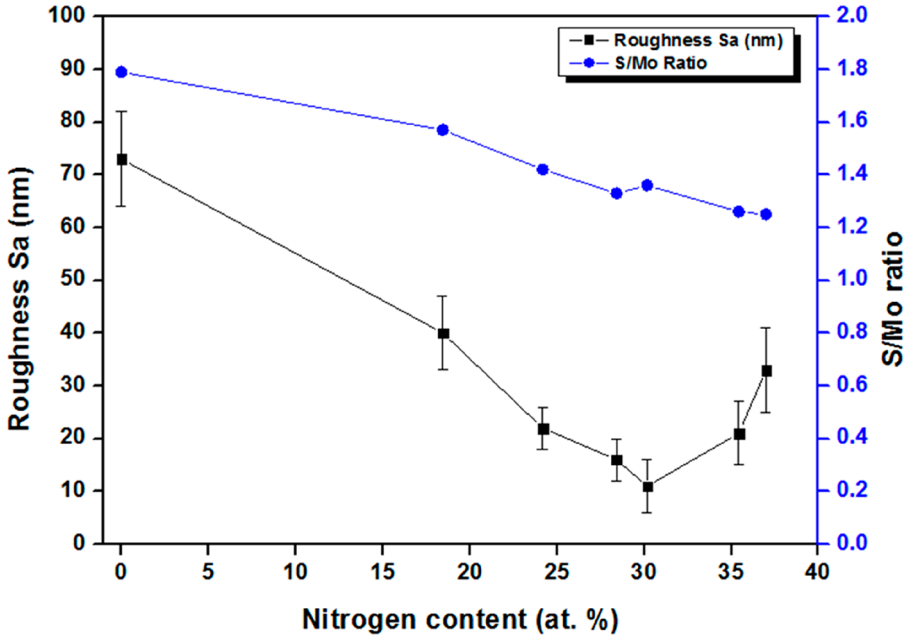

Figure 3. Variations in surface roughness and S/Mo ratio of the coatings with increasing nitrogen content.

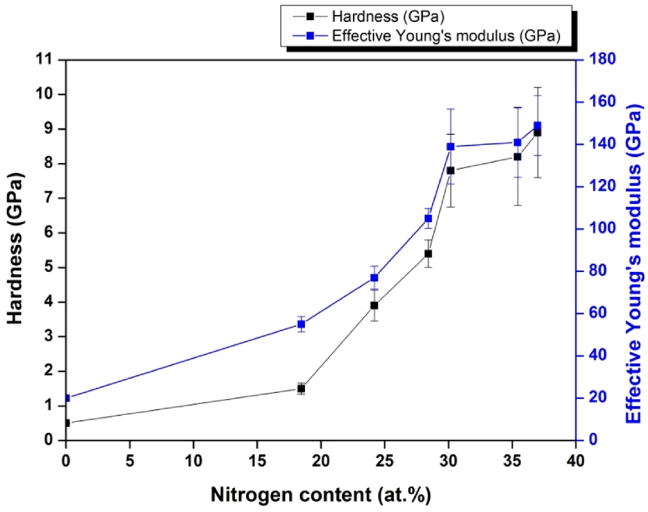

Figure 4. Hardness and effective Young's modulus of the coatings with increasing N content.

trends characterize these bumps. On the one hand, the higher the roughness is, and the higher the height of the bumps is, which suggests that mechanical interaction is occurring in this first part. On the other hand, the width of the bump increased with the hardness, which can be understood by the difficulty in wearing the material due to enhanced mechanical interactions. After the bump, a progressive decrease of COF takes place until the friction steady-state is reached. It is well established in the literature that TMDs display low COF due to the formation of easy to shear planes at the contact interface or contact surface.[7] Therefore, the running-in period should depend on the formation of this tribolayer. The pure MoS_2 coating displayed the minimum running-in period of ~5 m due to the high S/Mo ratio, which means more MoS_2 is available for the tribolayer formation. Then globally, as N was introduced in the coatings, the running-in period increased as the MoS_2 availability to form the easy shear tribolayer decreased. This is in good agreement with the decrease in the S/Mo ratio. Therefore, during the time the tribolayer was being formed (running-in period), a higher wear of the coating occurred at that region of the friction test. In addition to this, for the highest N contents N-based compounds could be expected which might also be contributing to the increase in the wear during this stage. The formation of tribolayer would mean reorientation of crystals and nanocrystals in the direction of the sliding plane, and for amorphous coatings this would mean the transformation from the amorphous phase to crystalline phase in the direction of the sliding plane.

Overall, the stable COF for all Mo−S−N coatings was in the range of 0.05−0.08. However, the pure MoS_2 coating showed an increasing trend for COF, reaching a slightly higher value of ~0.10 at the end of the test. A possible explanation for this slow increase of the COF is based on the particular shape of the counter body, that is, the flat and curved cylinder as shown in Figure 2A,B. Two points should be considered in this analysis: (i) despite the higher S/Mo ratio and consequent MoS_2 availability for the tribolayer formation, the very low hardness of the pure MoS_2 coating leads to a very high wear in the first few cycles compared to the other coatings; (ii) the low contact stresses being applied makes more difficult the tribolayer formation in the sliding contact. Because of these reasons, after a few cycles it is expected that for pure MoS_2 coating the cylinder plunges in relation to the original contact surface, thus increasing the length of the contact surface (see Figure 2B). Such a change, in addition to the much lower Young's modulus of this coating, contributes to a much higher contact area and smaller values of the contact stresses. This means that the higher the wear is, the lower the contact stresses will be. If it is speculated that the contact stresses are close to the threshold value necessary for the tribolayer formation, an assumption which will be shown later can be true, that is, the progressive decrease of the contact stresses can lead to a progressive deficiency in the formation of the tribolayer and the consequent increase of the COF. On the other hand, for the high N content coatings (30 atom % N and above), due to the increased hardness the initial wear of the coating is much less and thus the plunging-in is almost nil. This means that the contact area does not increase during the

https://dx.doi.org/10.1021/acsami.0c12655
ACS Appl. Mater. Interfaces 2020, 12, 43299−43310

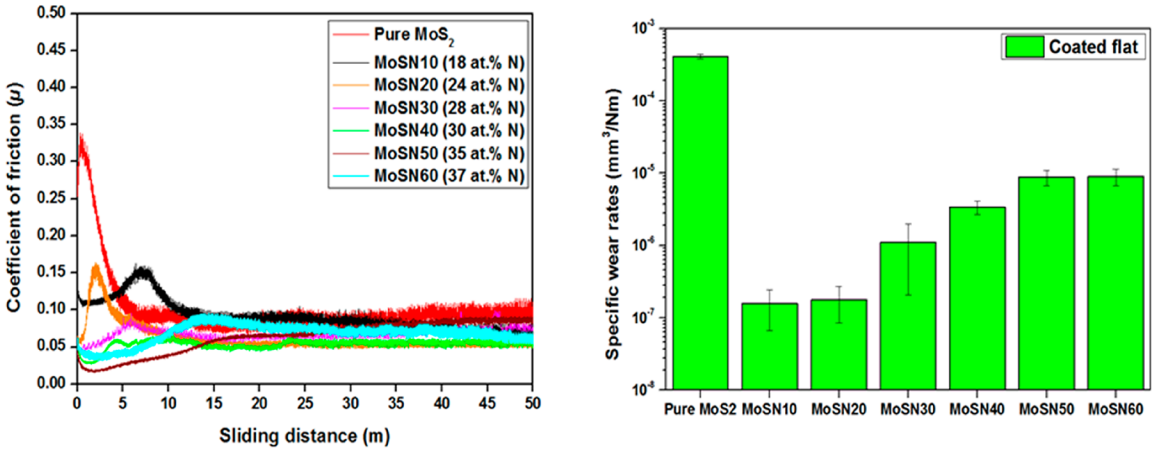

Figure 5. (Left) Tribological tests in vacuum for Mo−S−N coatings (on the flat) with 100Cr6 steel cylinder (counterbody) with respect to the sliding distance. (Right) The specific wear rates of the coated flats.

duration of the test, keeping the COF approximately constant in the assumed steady-state regime.

Figure 5 (right) shows the specific wear rates for the coated parts (flats). The pure MoS_2 coating displayed the highest wear. The softness (low hardness), low compactness, and low load-bearing capabilities of this coating justifies the short running-in and fast tribolayer formation, as described above, as well as the much higher values of the wear in comparison with N-containing films. The increased compactness and hardness of the coatings with N additions decreased the wear rates, as compared to the pure coating. They remain hard until they transform into MoS_2 on the contact surface. However, among the Mo−S−N coatings, there is not an improved wear resistance with increasing N content, despite their higher hardness. It should be noted that the wear-scar depths were usually very shallow (typically 40−100 nm for Mo−S−N coatings and 200−500 nm for pure MoS_2 coatings), indicating the starting of the wear process for the formers. As it was explained above, in this stage the values of the wear are mainly dependent on the formation of the tribolayers. Until the effective action of the tribolayer, a high wear occurred, as high as the longer time needed for its formation. For very long tests and/or high depth wear craters, the hardness of the coatings would become more important, and an inverse trend for the specific wear rate would be expected, that is, the higher the N content is, the higher the hardness and the wear resistance are.

3.3.2. Coated Cylinder versus Steel Flat. In the previous case, the steel cylinder was sliding against the coated flat, being each zone of the coating subjected to a periodic contact. In this section, the arrangement of the mating surfaces has been changed; the coated cylinder slides against the polished steel flat surface. In this situation, the coating is in continuous (uninterrupted) sliding contact with the counter body (steel flat surface), closer to the reality of many industrial applications where the coating remains in permanent contact with the sliding interface. Thus, in this configuration the coating is placed on the sample for which the wear rate is the highest because of kinematic length consideration. Therefore, this sliding process is more demanding and severe for the coating than the steel cylinder versus coated flat condition.

The pure MoS_2 coating had a very short running-in period, shorter than in the previous case, which can be justified by the permanent contact of coatings with counterbody and an easier formation of the tribolayer (see Figure 6 (left)). The steady-state COF is kept during the 15 m sliding distance and then the COF increased strongly to 0.25; at this point, the test was stopped as if the contact with uncoated zones had occurred. Unexpectedly, the analysis of the wear track (see Figure 2C) showed that no substrate could be detected. Moreover, the calculation of the depth of the worn coating, based on the width of the wear-scar and geometrical analysis, found a value close to 0.68 μm, very far from the thickness of the coating (6.1 μm). This trend confirms the explanation mentioned in Section 3.3.1 for the slow increase of the COF but now in a catastrophic manner. As can be observed in Figure 2C, besides the flat part of the cylinder it is clear that the contact reached the curved part, enlarging the contact area and decreasing the Hertz contact stress. This had already occurred in the previous case; however, in this situation a further increase in the contact area takes place, decreasing the contact stress to values lower than the critical ones for the formation of the tribolayer. In fact, for the uncoated cylinder/coated flat situation the wear of the steel cylinder is almost nil, being the contact area in the linear part of the cylinder is almost constant during the test. Because of the wear of the coating, only the plunging-in, prolonging the contact to the curved zone of the cylinder, has an influence on the contact area and the contact stress. Alternatively, in the case under analysis in this section the cylinder is being worn out, and the contact area is increasing with the duration of the test besides the extension to the curved zone. Then, when a critical value of the contact area is reached the corresponding contact stress is not sufficient anymore to form the tribolayer, and the friction rises.

For Mo−S−N coatings, the formation of the tribolayer is much faster than in the previous case (Section 3.3.1). The coating with minimum N content displayed the lowest running-in period, and further additions of N increased this period. The coating with the highest nitrogen content (Mo−S−N50, 35 atom % N) displayed the longest running-in period. This increased running-in period can be attributed to the lower S/Mo ratio availability for tribolayer formation. With the exception of the Mo−S−N50 (35 atom % N), in all the coatings the slow increasing trend of the COF can also be observed. As explained above, this progressive and slow increment in COF is related to the wear of the coatings (coated cylinder), which results in an increased contact area and thus decreased contact stresses. However, the much lower wear of these coatings (see Figure 2D) does not promote significant changes in the contact stresses, keeping their values close for the formation of the

https://dx.doi.org/10.1021/acsami.0c12655
ACS Appl. Mater. Interfaces 2020, 12, 43299−43310

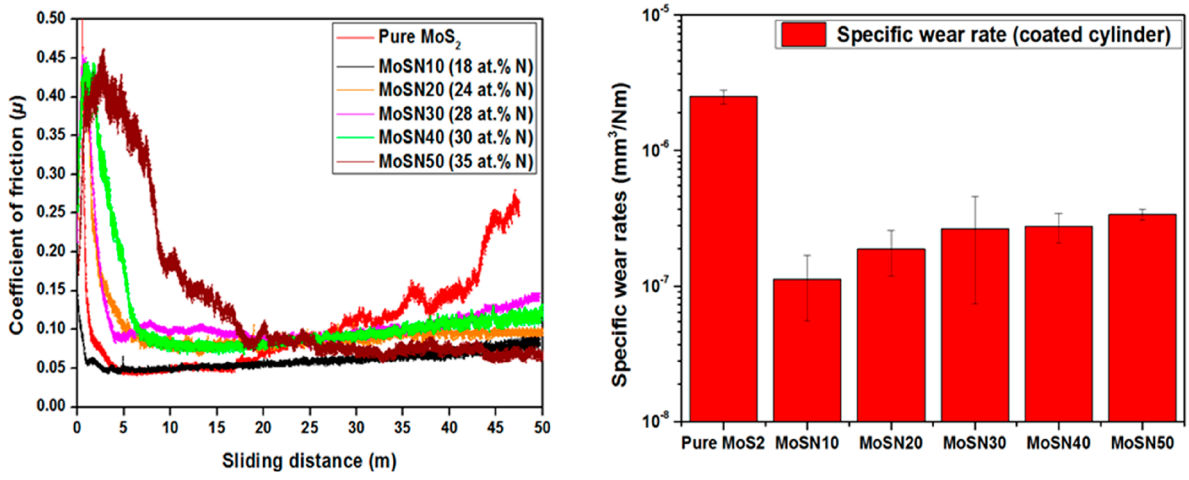

Figure 6. (Left) Friction coefficient evolution for the coated steel cylinder against the polished steel flat (roughness of 1.4 nm) with respect to sliding distance in vacuum conditions. (Right) The specific wear rates of the coated cylinder for respective tests.

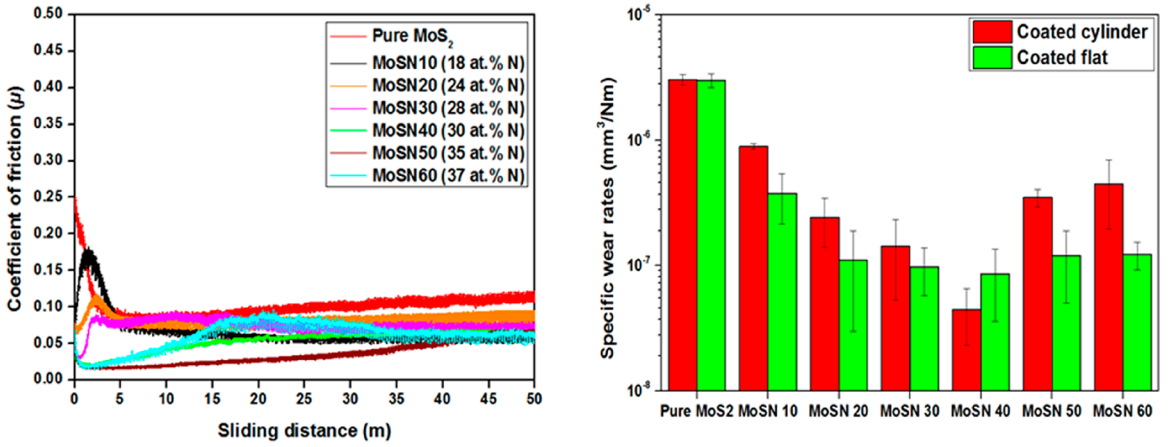

Figure 7. (Left) Evolution of the friction coefficient of all studied coatings with respect to sliding distance in a vacuum. The cylinder and flat are coated with the same deposition conditions. (Right) The specific wear rates for the coated cylinder and coated flat for all tests.

tribolayer. It is noted that almost no extension of the line contact to the curved zone is observed (see, e.g., Figure 2D).

The specific wear rate of the pure MoS_2 coating was the highest, which decreased with the introduction of N in the coatings (see Figure 6 (right)). The specific wear rate was minimum for the lowest N-alloying. Among the N-alloyed coatings, the specific wear rates increased with the N content. Therefore, the Mo−S−N50 (35 atom % N) coating displayed the highest wear rate. As explained earlier in this section, the line contact of the coated cylinder is always in contact with the steel surface. This creates a situation in which the material is easier and faster transformed to form the reoriented tribolayer in the case of the softer pure MoS_2 coating. Therefore, higher wear and low running-in period has been observed for this coating. The same phenomenon took place for all N-alloyed coatings, but the specific wear rate was lower (than pure MoS_2 coating) due to their increased hardness. Among Mo−S−N coatings, the reason behind the observed increase in the wear with increased N-alloying is the decrements in S/Mo ratios. As explained above, more wear of the coated cylinder was needed to provide sufficient MoS_2 for the tribolayer formation. This is in agreement with the delayed tribolayer formation under high N-alloying conditions.

3.3.3. Coated Cylinder versus Coated Flat. The evolution of the friction curves in the steady-state region was very similar to the case of the steel cylinder versus coated flat presented in Section 3.3.1 (compare Figures 5 and 7). The main difference was the decrease in the duration of the running-in period and the lower initial intensity in the bump of the COF. The pure MoS_2 coating displayed the highest COF value at the end of the test, which results from the progressive difficulty in forming the tribolayer, as it was explained in Sections 3.3.1 and 3.3.2. As can be observed in Figure 7 (right), the wear in the cylinder is of the same order as in Section 3.3.2, meaning that a decrease of the contact stresses is occurring, making it difficult for the formation of the tribolayer and leading to an increase of the COF during the test. This trend was not as abrupt as in Section 3.3.2 since the contact was now against a coated flat, which makes more MoS_2 lubricant available (in the contact) for the tribolayer formation. All of the other coatings displayed almost similar and stable COF values in the last part of the tests. The intensity and position of the bumps in the COF curves are similar to those observed in Section 3.3.1 and can be explained by the combination of the surface roughness and the set hardness/S/Mo ratio. For the relatively smoother film (Mo−S−N40, 30 atom %N), almost no bump can be observed, suggesting that no mechanical interlocking is taking place in the running-in period. On the

https://dx.doi.org/10.1021/acsami.0c12655
ACS Appl. Mater. Interfaces 2020, 12, 43299−43310

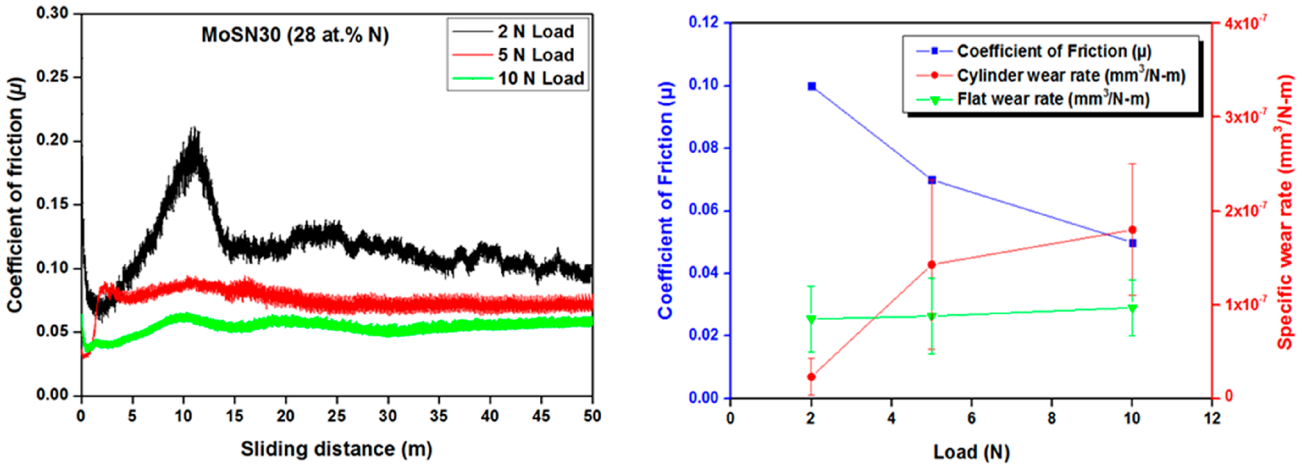

Figure 8. (Left) Evolution of the friction coefficient with varying load in a vacuum condition. The cylinder and flat are coated with Mo−S−N30 (28 atom % N). (Right) Coated cylinder and coated flat specific wear rates and COF with the applied normal loads.

other hand, for the films where bumps are observed the intensity of the bump is typically increasing with the roughness, as it would be expected. Concerning the extension of the bump, with direct consequences in the running-in period, as already mentioned, there is a close correlation between the mechanical strength and the extension of that period due to the increasing difficulty in overcoming the mechanical interlocking. Simultaneously, the hardness increase associated with a lower S/Mo ratio makes the formation of tribolayer harder, contributing to extending the running-in period. Overall, the COF was for the last part of the test in the range of 0.05−0.08 for Mo−S−N coatings.

The Mo−S−N coatings displayed low cylinder and flat wear as compared to pure MoS_2 coatings due to the low load-bearing capacity of the latter. Inversely to what was observed in the previous sections, both the coated flat and coated cylinder wear decreased with increasing nitrogen up to 30 atom %. As already discussed above, this decrease should be expected due to the increase in hardness, increase in compactness, and also due to a decrease in roughness of both coated parts. The trend is contrary to the other mating situations since both elements of the sliding pair are coated, making available immediately high amounts of material to form the tribolayer at very small wear volume, that is, not needing a high quantity of wear debris and thus, decreasing the initial wear volume. Therefore, from the very beginning what is important for determining the wear rate is the mechanical strength of the sliding material. Again, it should be noted that the worn craters in the sliding elements are very shallow (tens of nanometers), meaning that the wear process is in its very beginning. This is the reason why in the coatings with the highest hardness and the lowest S/Mo ratio, the initial process for forming the tribolayer is too long, consuming a high amount of material, and leading to an increase in the wear rate in comparison to the softer coatings with lower N contents (see Figure 7 (right)).

3.3.4. Variation of Testing Load. The effects of the variation of applied load on the evolution of the COF and the specific wear rate for coated cylinder versus coated flat are shown in Figure 8 for one of the coatings showing the best tribological performance in Section 3.3.3, that is, Mo−S−N30 (28 atom % N). With 2 N applied load, the COF started from 0.12 and increased to 0.2 within ∼12 m of sliding. The almost imperceptible bump observed for the 5 N tests was extremely enhanced for the 2 N. This coating has low roughness, which, as explained before, gives rise to very small mechanical interlocking in the beginning of the sliding test. However, for very low applied loads the elastic deformation in the contact is much lower, allowing a higher interaction between roughness peaks in the two surfaces and then leading to a higher COF. As the applied load is lower, the destruction of the roughness peaks promoting the interlocking is more difficult, which explained the permanence of the bump until a higher number of cycles. After this, the COF abruptly decreases, due to the tribolayer formation. Then, a slowly decreasing trend for COF is observed, reaching in the end a COF of 0.1. With an increase in the applied load from 2 to 5 N, the running-in period is reduced. The steady-state value is a little lower than the one achieved with 2 N loads. For the highest applied load (10 N), the COF decreased further down to 0.05. Despite testing in low contact stress regimes, the achieved results (i.e., decrease in COF with applied loads) is in accordance with the literature, that is, higher applied loads favor the reorientation of TMD planes parallel to the sliding surface, increasing the coverage of the contact zones with the tribolayer and decreasing the COF.[26]

Although the specific wear rate in the coated flat is kept approximately constant for all applied loads, an increase in the specific wear rate of the cylinders (Figure 8 (right)) is observed with increasing load. As referred above, the tribolayer formation is more extensive when the load is increased (Figure 8 (left)), meaning that a higher amount of wear debris was required to promote this transformation. Therefore, the higher loads led to higher wear in the coated cylinder (the wear in the coated flat is similar) and consequently higher values in the specific wear rates.

4. DISCUSSION

This work mainly dealt with the improvements of mechanical and vacuum tribological properties achieved by N-alloying of MoS_2 coatings. The pure coating was also discussed as a reference to differentiate the useful role of N-alloying. The literature lacks reports on the vacuum tribological testing of Mo−S−N coatings, particularly for low contact stresses. The testing was carried out at different mating material combinations. For solid lubricant coatings to be durable, high interfacial adhesion strength between the coatings and the substrates is one of the most important requirements for vacuum tribology and

https://dx.doi.org/10.1021/acsami.0c12655
ACS Appl. Mater. Interfaces 2020, 12, 43299−43310

aerospace applications.[48] The importance of a hard underlayer was deemed essential for extreme low friction in literature.[49] Dominguez et al.[50] reported that for the WSe_x system having a W-rich underlayer provided good mechanical support to guarantee a low contact area. The Mo−S−N coatings utilized in this work were previously reported to show high adhesion,[29] which is expected to lead to better mechanical and tribological properties.

Even the smallest addition of N resulted in a significant increase in the hardness and elastic Young's modulus. The values continued to increase for higher N contents. This increase is the result of (i) densification of the film structure and increase in the compactness of the coatings; (ii) amorphization of the coatings with the incorporation of N, and (iii) the nanometric level of the MoS(N)/MoN(S) multilayer stacking caused by the hybrid deposition approach used in this work.[29] The multilayer stacking promotes an increase in the hardness due to an increase in the shear modulus. This ultimately increases the energy required for the dislocation propagation at the interfaces between nanometric layers. Similar observations were reported in the literature for other multilayer materials, for example, for WS_2/MoS_2[51] and TiN/VN[52] coatings. Despite the higher S/Mo ratio and then a higher amount of the MoS_2 soft phase, the synergy of the factors mentioned above allows us to provide hardness values higher than those found in the literature.[26,31,40,46]

The detailed vacuum tribological studies were carried out under different conditions of applied loads and mating surfaces. For the first time, Mo−S−N coatings were tested with contact stresses complying with real industrial requirements. This choice of low contact stresses is in contrast to most of the literature, where solid lubricants are tested under much higher applied contact stresses in the range 500−1500 MPa. Thus, the COF reported in the current study would simulate the values during real applications, unlike those in literature.[26,31,40,46] Different mating conditions were tested as the initial state of mating materials can affect the COF values. It was found that the sliding of coatings with itself (i.e., coated cylinder versus coated flat) provided a short running-in period and a stable COF if compared to the condition where one surface is uncoated. In latter cases, a very high initial high wear of the coated part is needed to form efficient tribolayers, which are drastically reduced if both elements of the sliding pair are participating in this process. After the formation of the tribolayer, an efficient sliding is achieved with low COF. Therefore, coating versus coating can give better wear resistance by faster tribolayer formation and durability compared to steel versus coating. It must also be noted that the literature does not report any testing of the Mo−S−N system in the coating versus coating setup.

In vacuum (10^{-4} Pa) conditions, due to the absence of oxygen the formation and stability of the tribolayers are enhanced. It was observed that sufficient wear is necessary to provide low tangential force. For Mo−S−N coatings, the possible bond formation in amorphous coatings (28 atom % N and above) would be a ternary disorder phase with Mo bonded to S and N, arising from the distorting atomic placement in stoichiometric MoS_2 structure. Alternatively, nitrogen can also be present in the form of N_2 gas trapped within the lamellae, contributing to the amorphous structure. When sliding, the amorphous structure is transformed into MoS_2 crystalline tribolayers, which governs the low COF. The low COF achieved for Mo−S−N coatings sliding in a vacuum is in agreement with this hypothesis with the MoS_2 tribolayers playing the dominant role in the low friction regime in a vacuum. A similar phenomenon was theoretically explained for W−S−N coatings by Isaeva et al.,[36] where WS_2 tribo-films were governing the low friction. Muratore et al.[53] also had shown such phenomenon earlier. The depth (thickness) of these tribo-films (transformed or deformed layers) depends on the magnitude of the stresses in the contact region (directly proportional to applied loads) and on properties of the coatings, such as the platelet size and packing density, the adhesion of the coating to the substrate, and the mechanical properties.[47]

The results also showed the need for an initial wear as a source of lamellar MoS_2 for the tribolayers formation. Therefore, for Mo−S−N coatings the higher the S/Mo ratio is, the shorter the period for the tribolayer formation is, that is, the softer coating (e.g., Mo−S−N10 18 atom % N) tends to wear less than the harder one (e.g., Mo−S−N50 35 atom % N). However, COF values of all were close to each other at the end of the test (Figures 5 and 6). Highly ordered intrinsic lamellar structures of MoS_2 phases in the top surface ensure the low friction of the deposited film, whereas the amorphous layers underneath provide the necessary hardness phase for supporting the applied stress; both phases play key roles in determining the wear-life of the deposited film. In the end, the MoS_2 tribolayers were governing the friction and so the end values of COF were similar.

Roughness also played an essential role on the tribological behavior of the coatings. In relation to the friction, due to the low applied stresses mechanical interlocking is occurring between the asperities of the surfaces in the first part of the test. This effect led to the presence of an initial bump in the friction curves whose intensity and duration depend on the roughness level and hardness of the coatings, respectively. The rougher the coating is, the deeper the interlocking is, and the higher the intensity of the bump is. With increasing N content up to 30 atom %, the roughness decreases and the intensity of the bump vanishes for this value. Then, for higher N contents the roughness increases and the bump is again detected. The increase in the mechanical strength of the coatings makes the destruction of the mechanical interlocking more difficult, retarding its deleterious effects on the COF and increasing the duration of the bump. After overcoming the mechanical interlocking, the progressive formation of the tribolayer justifies the observed decreasing trend of COF. Because of the specificity of the current tribological test in particular and the lateral profile of the counterbody (cylinder) in some cases, an increase of the COF with the number of cycles was observed. This trend can be explained by the progressive increase in the contact area when the parts are being worn out, which gives rise to a decrease in the contact stress and an increasing difficulty of adequately forming the tribolayer.

The wear of the sliding parts was dependent on the compromise between the hardness of the coatings and the availability of potential lubricious material for forming the tribolayer. If the COF is similar in a specific type of sliding contact, it would be expected that the harder the material of the coating is, the lower the wear rate is. For this type of system, such as Mo−S−N, the stable sliding is only achieved when a lubricious tribolayer based on MoS_2 is formed in the interface with basal planes aligned in the sliding direction and parallel to the substrate. For the formation of this tribolayer, a running-in process has to occur during which materials are being worn out. The amount of lubricious phase in the sliding contact will determine the number of cycles needed for establishing the tribolayer. The longer the running-in is, the higher the amount of wear is. In most cases, the initial volume of wear is small when compared to the total worn volume in the final test. However,

https://dx.doi.org/10.1021/acsami.0c12655
ACS Appl. Mater. Interfaces 2020, 12, 43299−43310

with this tribological test the worn zones are in the end very shallow, meaning that the initial wear of the running-in process is an important part of the final wear volume. The addition of N has two main influences in the coating; on the one hand it increases the hardness, and on the other hand it decreases the S/Mo ratio (and then the amount of the potential lubricious phase). These two trends have antagonic effects: the hardness improves the wear resistance, but the S/Mo increases the wear volume during the running-in process. Therefore, the evolution of the specific wear rate with the N content will depend on the compromise between those two effects. If the running-in period is too short (high amount of lubricious phase as in the case of mating "coated flat and coated cylinder") for all N contents, that is, lower than 30 atom %, the initial worn volume is not significant in relation to the total wear volume, and then the hardness is important: the wear rate decreases with the increase in the N content. It is important to remark that for the highest N contents the running-in increases (Figure 7 (left)), and the wear coefficient increases again. When a high amount of wear is necessary to form the tribolayer (e.g., in the mating "uncoated versus coated"), the initial wear volume is important in relation to the total wear, showing the coatings with lower N contents, tested in these situations, having lower wear rate than those with higher N content (and higher hardness), as shown in Figures 5 and 6 (right).

5. CONCLUSIONS

This paper describes the mechanical properties and the first-ever low contact stress vacuum tribological testing of Mo−S−N coatings deposited using a semi-industrial DC magnetron sputtering chamber equipped with a single MoS_2 target and an additional secondary plasma source. The properties are analyzed with respect to the N-alloying of MoS_2 coatings. With incorporation of 37 atom % of N, a maximum hardness of 8.9 GPa was attained. The vacuum tribological tests were performed with different contact body configurations and applied loads. The loads were selected to provide initial contact stresses in the range of 60−135 MPa, complying with real industrial needs. For coating versus coating sliding, better wear resistance was achieved compared to the coating versus steel sliding. Though the mechanism behind low friction is similar, that is, the formation of tribolayers from either the nanocrystalline or the amorphous structures, the achieved wear rates varied, depending on the sliding surfaces. If the running-in period is excluded, all coatings shown in the final test a COF in the range from 0.05 to 0.1. Only in one case (pure MoS_2 film in the coated cylinder/uncoated flat configuration), the test was stopped before the defined time due to a strong increase of the COF. This result was explained by an insufficient formation of the lubricious tribolayer due to an unexpected decrease in the contact stresses. The COF was dependent on the instantaneous contact stresses and as a general trend, it decreased with an increase in contact stresses. Overall, a least specific wear rate of 8.6×10^{-8} $mm^3/N{\cdot}m$ (coated flat) was observed for Mo−S−N40 (30 atom % N) in coating versus coating interaction, and 1.5×10^{-7} $mm^3/N{\cdot}m$ (coated flat) for Mo−S−N10 (18 atom % N) for steel versus coating interaction. This work brings some important issues when testing transition metal dichalcogenides-based coatings under low contact stress conditions. There is a threshold value for the contact stress for which no suitable tribolayer can be formed with the consequent increase in the COF. In the final, for better tribological performance the use of coating versus coating mating surfaces is recommended.

ASSOCIATED CONTENT

Supporting Information

The Supporting Information is available free of charge at https://pubs.acs.org/doi/10.1021/acsami.0c12655.

X-ray diffractogram of all of the coatings (PDF)

AUTHOR INFORMATION

Corresponding Author

Kaushik Hebbar Kannur − *IREIS, HEF Group, 42162 Andrézieux-Bouthéon, France; Department of Mechanical Engineering, CEMMPRE, University of Coimbra, 3030-788 Coimbra, Portugal;* orcid.org/0000-0003-4976-8961; Phone: +33 7 67 87 97 25; Email: khebbarkannur.ireis@hef.fr

Authors

Talha Bin Yaqub − *Department of Mechanical Engineering, CEMMPRE, University of Coimbra, 3030-788 Coimbra, Portugal; IPN - LED & MAT - Instituto Pedro Nunes, Laboratory of Tests, Wear and Materials, 3030-199 Coimbra, Portugal*

Christophe Pupier − *IREIS, HEF Group, 42162 Andrézieux-Bouthéon, France*

Christophe Héau − *IREIS, HEF Group, 42162 Andrézieux-Bouthéon, France*

Albano Cavaleiro − *Department of Mechanical Engineering, CEMMPRE, University of Coimbra, 3030-788 Coimbra, Portugal;* orcid.org/0000-0001-8251-5099

Complete contact information is available at: https://pubs.acs.org/10.1021/acsami.0c12655

Notes

The authors declare no competing financial interest.

ACKNOWLEDGMENTS

This project has received funding from the European Union Horizon 2020 research and innovation programme under Grant Agreement 721642: SOLUTION. The authors would also like to thank funding from CEMMPRE − UID/EMS/00285/2019 [cofinanced via FEDER and FCT (COMPETE)].

REFERENCES

(1) Fusaro, R. L. Space Mechanisms Needs for Future NASA Long Duration Space Missions. In *AIAA/NASA/OAI Conference on Advanced SEI Technologies, 1991*; 1991. DOI: 10.2514/6.1991-3428.

(2) Fusaro, R. L. Preventing Spacecraft Failures Due to Tribological Problems. *NASA Tech. Memo. 210806* 2001, No. April. https://doi.org/NASA/TM-2001-210806 (accessed 25th May 2020), NAS 1.15:210806, E-12713.

(3) Roberts, E. W. Thin Solid Lubricant Films in Space. *Tribol. Int.* **1990**, *23* (2), 95−104.

(4) Donnet, C.; Fontaine, J.; Le Mogne, T.; Belin, M.; Héau, C.; Terrat, J. P.; Vaux, F.; Pont, G. Diamond-like Carbon-Based Functionally Gradient Coatings for Space Tribology. *Surf. Coat. Technol.* **1999**, *120−121*, 548−554.

(5) Zhang, X.; Luster, B.; Church, A.; Muratore, C.; Voevodin, A. A.; Kohli, P.; Aouadi, S.; Talapatra, S. Carbon Nanotube-MoS2 Composites as Solid Lubricants. *ACS Appl. Mater. Interfaces* **2009**, *1* (3), 735−739.

(6) Fusaro, R. L. Effect of Substrate Surface Finish on the Lubrication and Failure Mechanisms of Molybdenum Disulfide Films. *ASLE Trans.* **1982**, *25* (2), 141−156.

(7) Polcar, T.; Cavaleiro, A. Review on Self-Lubricant Transition Metal Dichalcogenide Nanocomposite Coatings Alloyed with Carbon. *Surf. Coat. Technol.* **2011**, *206* (4), 686−695.

(8) Moser, J.; Lévy, F. Crystal Reorientation and Wear Mechanisms in MoS2 Lubricating Thin Films Investigated by TEM. *J. Mater. Res.* **1993**, *8* (1), 206−213.
(9) Wahl, K. J.; Dunn, D. N.; Singer, I. L. Wear Behavior of Pb−Mo−S Solid Lubricating Coatings. *Wear* **1999**, *230* (2), 175−183.
(10) Hilton, M. R.; Jayaram, G.; Marks, L. D. Microstructure of Cosputter-Deposited Metal- and Oxide-MoS $_2$ Solid Lubricant Thin Films. *J. Mater. Res.* **1998**, *13* (4), 1022−1032.
(11) Renevier, N. M.; Lobiondo, N.; Fox, V. C.; Teer, D. G.; Hampshire, J. Performance of MoS2/Metal Composite Coatings Used for Dry Machining and Other Industrial Applications. *Surf. Coat. Technol.* **2000**, *123* (1), 84−91.
(12) Ding, X.; Zeng, X. T.; He, X. Y.; Chen, Z. Tribological Properties of Cr- and Ti-Doped MoS2 Composite Coatings under Different Humidity Atmosphere. *Surf. Coat. Technol.* **2010**, *205* (1), 224−231.
(13) Rigato, V.; Maggioni, G.; Patelli, A.; Boscarino, D.; Renevier, N. M.; Teer, D. G. Properties of Sputter-Deposited MoS2/Metal Composite Coatings Deposited by Closed Field Unbalanced Magnetron Sputter Ion Plating. *Surf. Coat. Technol.* **2000**, *131* (1), 206−210.
(14) Nainaparampil, J. J.; Phani, A. R.; Krzanowski, J. E.; Zabinski, J. S. Pulsed Laser-Ablated MoS2-Al Films: Friction and Wear in Humid Conditions. *Surf. Coat. Technol.* **2004**, *187* (2), 326−335.
(15) Teer, D. G.; Hampshire, J.; Fox, V.; Bellido-Gonzalez, V. The Tribological Properties of MoS2/Metal Composite Coatings Deposited by Closed Field Magnetron Sputtering. *Surf. Coat. Technol.* **1997**, *94*−*95*, 572−577.
(16) Stupp, B. C. Synergistic Effects of Metals Co-Sputtered with MoS2. *Thin Solid Films* **1981**, *84* (3), 257−266.
(17) Lince, J. R.; Kim, H. I.; Adams, P. M.; Dickrell, D. J.; Dugger, M. T. Nanostructural, Electrical, and Tribological Properties of Composite Au−MoS2 Coatings. *Thin Solid Films* **2009**, *517* (18), 5516−5522.
(18) Spalvins, T. Frictional and Morphological Properties of Au—MoS2 Films Sputtered from a Compact Target. *Thin Solid Films* **1984**, *118* (3), 375−384.
(19) Mikhailov, S.; Savan, A.; Pflüger, E.; Knoblauch, L.; Hauert, R.; Simmonds, M.; Van Swygenhoven, H. Morphology and Tribological Properties of Metal (Oxide)−MoS2 Nanostructured Multilayer Coatings. *Surf. Coat. Technol.* **1998**, *105* (1), 175−183.
(20) Scharf, T. W.; Goeke, R. S.; Kotula, P. G.; Prasad, S. V. Synthesis of Au−MoS2 Nanocomposites: Thermal and Friction-Induced Changes to the Structure. *ACS Appl. Mater. Interfaces* **2013**, *5* (22), 11762−11767.
(21) Tedstone, A. A.; Lewis, D. J.; O'Brien, P. Synthesis, Properties, and Applications of Transition Metal-Doped Layered Transition Metal Dichalcogenides. *Chem. Mater.* **2016**, *28* (7), 1965−1974.
(22) Polcar, T.; Nossa, A.; Evaristo, M.; Cavaleiro, A. Nanocomposite Coatings of Carbon-Based and Transition Metal Dichalcogenides Phases: A Review. *Rev. Adv. Mater. Sci.* **2007**, *15* (2), 118−126.
(23) Cao, H.; Wen, F.; De Hosson, J. T. M.; Pei, Y. T. Instant WS2 Platelets Reorientation of Self-Adaptive WS 2/a-C Tribocoating. *Mater. Lett.* **2018**, *229*, 64−67.
(24) Yaqub, T. B.; Vuchkov, T.; Sanguino, P.; Polcar, T.; Cavaleiro, A. Comparative Study of DC and RF Sputtered MoSe2 Coatings Containing Carbon—An Approach to Optimize Stoichiometry, Microstructure, Crystallinity and Hardness. *Coatings* **2020**, *10* (2), 133.
(25) Yaqub, T. B.; Vuchkov, T.; Evaristo, M.; Cavaleiro, A. DCMS Mo-Se-C Solid Lubricant Coatings − Synthesis, Structural, Mechanical and Tribological Property Investigation. *Surf. Coat. Technol.* **2019**, *378*, 124992.
(26) Hudec, T.; Mikula, M.; Satrapinskyy, L.; Roch, T.; Truchlý, M.; Švec, P.; Huminiuc, T.; Polcar, T. Structure, Mechanical and Tribological Properties OfMo-S-N Solid Lubricant Coatings. *Appl. Surf. Sci.* **2019**, *486*, 1.
(27) Cavaleiro, A.; Trindade, B.; Vieira, M. T. Deposition and Characterization of Fine-Grained W−Ni−C/N Ternary Films. *Surf. Coat. Technol.* **1999**, *116*−*119*, 944−948.
(28) Nossa, A.; Cavaleiro, A. The Influence of the Addition of C and N on the Wear Behaviour of W-S-C/N Coatings. *Surf. Coat. Technol.* **2001**, *142*−*144*, 984−991.
(29) Hebbar Kannur, K.; Yaqub, T. B.; Huminiuc, T.; Polcar, T.; Pupier, C.; Heau, C.; Cavaleiro, A. Synthesis and Structural Properties of Mo-S-N Sputtered Coatings. *Appl. Surf. Sci.* **2020**, *527*, 146790.
(30) Nyberg, H.; Sundberg, J.; Särhammar, E.; Gustaversusson, F.; Kubart, T.; Nyberg, T.; Jansson, U.; Jacobson, S. Extreme Friction Reductions during Initial Running-in of W−S−C−Ti Low-Friction Coatings. *Wear* **2013**, *302* (1), 987−997.
(31) Zhang, X.; Qiao, L.; Chai, L.; Xu, J.; Shi, L.; Wang, P. Structural, Mechanical and Tribological Properties of Mo-S-N Solid Lubricant Films. *Surf. Coat. Technol.* **2016**, *296*, 185−191.
(32) Dugger, M. T. Atomic Oxygen Interaction with Nickel Multilayer and Antimony Oxide Doped MoS{sub 2} Films (Conference) _ OSTI. *Office of Scientific & Technical Information Technical Reports*; Sandia National Laboratories: Albuquerque, NM (United States), 1994.
(33) Simmonds, M. C.; Savan, A.; Van Swygenhoven, H.; Pflüger, E.; Mikhailov, S. Structural, Morphological, Chemical and Tribological Investigations of Sputter Deposited MoSx/Metal Multilayer Coatings. *Surf. Coat. Technol.* **1998**, *108*−*109*, 340−344.
(34) Evaristo, M.; Polcar, T.; Cavaleiro, A. Synthesis and Properties of W−Se−C Coatings Deposited by PVD in Reactive and Non-Reactive Processes. *Vacuum* **2009**, *83* (10), 1262−1265.
(35) Nossa, A.; Cavaleiro, A. Tribological Behaviour of N(C)-Alloyed W−S Films. *Tribol. Lett.* **2007**, *28* (1), 59−70.
(36) Isaeva, L.; Sundberg, J.; Mukherjee, S.; Pelliccione, C. J.; Lindblad, A.; Segre, C. U.; Jansson, U.; Sarma, D. D.; Eriksson, O.; Kádas, K. Amorphous W-S-N Thin Films: The Atomic Structure behind Ultra-Low Friction. *Acta Mater.* **2015**, *82*, 84−93.
(37) Sundberg, J.; Nyberg, H.; Särhammar, E.; Nyberg, T.; Jacobson, S.; Jansson, U. Influence of Composition, Structure and Testing Atmosphere on the Tribological Performance of W-S-N Coatings. *Surf. Coat. Technol.* **2014**, *258*, 86−94.
(38) Gustaversusson, F.; Jacobson, S.; Cavaleiro, A.; Polcar, T. Ultra-Low Friction W-S-N Solid Lubricant Coating. *Surf. Coat. Technol.* **2013**, *232*, 541−548.
(39) Mutafov, P.; Evaristo, M.; Cavaleiro, A.; Polcar, T. Structure, Mechanical and Tribological Properties of Self-Lubricant W-S-N Coatings. *Surf. Coat. Technol.* **2015**, *261*, 7−14.
(40) Ju, H.; Wang, R.; Ding, N.; Yu, L.; Xu, J.; Ahmed, F.; Zuo, B.; Geng, Y. Improvement on the Oxidation Resistance and Tribological Properties of Molybdenum Disulfide Film by Doping Nitrogen. *Mater. Des.* **2020**, *186*, 108300.
(41) Nossa, A.; Cavaleiro, A. Chemical and Physical Characterization of C(N)-Doped W−S Sputtered Films. *J. Mater. Res.* **2004**, *19* (8), 2356−2365.
(42) Bülbül, F.; Efeoğlu, İ; Arslan, E. The Effect of Bias Voltage and Working Pressure on S/Mo Ratio at MoS2−Ti Composite Films. *Appl. Surf. Sci.* **2007**, *253* (9), 4415−4419.
(43) Grosseau-Poussard, J. L.; Moine, P.; Villain, J. P. Microstructural and Tribological Characterization of MoSx Coatings Produced by High-Energy Ion-Beam-Assisted Deposition. *Thin Solid Films* **1993**, *224* (1), 52−57.
(44) Hiraoka, N. Wear Life Mechanism of Journal Bearings with Bonded MoS2 Film Lubricants in Air and Vacuum. *Wear* **2001**, *249* (10−11), 1014−1020.
(45) Yaqub, T. B.; Hebbar Kannur, K.; Vuchkov, T.; Pupier, C.; Heau, C.; Cavaleiro, A. Molybdenum Diselenide Coatings as Universal Dry Lubricants for Terrestrial and Aerospace Applications. *Mater. Lett.* **2020**, *275*, 128035.
(46) Fu, Y.; He, T.; Yang, W.; Xu, J.; Mu, B.; Pang, X.; Wang, P. Structure, Mechanical and Tribological Properties of MoSN/MoS2Multilayer Films. *Coatings* **2019**, *9* (2), 108.
(47) Fleischauer, P. D.; Hilton, M. R.; Bauer, R. Paper V (i) Effects of Microstructure and Adhesion on Performance of Sputter-Deposited MoS2 Solid Lubricant Coatings. *Tribol. Ser.* **1990**, *17* (C), 121−128.
(48) Miyoshi, K. Considerations in Vacuum Tribology (Adhesion, Friction, Wear, and Solid Lubrication in Vacuum). *Tribol. Int.* **1999**, *32* (11), 605−616.
(49) Shtansky, D. V.; Lobova, T. A.; Fominski, V. Y.; Kulinich, S. A.; Lyasotsky, I. V.; Petrzhik, M. I.; Levashov, E. A.; Moore, J. J. Structure

https://dx.doi.org/10.1021/acsami.0c12655
ACS Appl. Mater. Interfaces 2020, 12, 43299−43310

and Tribological Properties of WSex, WSex/TiN, WSex/TiCN and WSex/TiSiN Coatings. *Surf. Coat. Technol.* **2004**, *183* (2), 328−336.
(50) Dominguez-Meister, S.; Justo, A.; Sanchez-Lopez, J. C. Synthesis and Tribological Properties of WSex Films Prepared by Magnetron Sputtering. *Mater. Chem. Phys.* **2013**, *142* (1), 186−194.
(51) Watanabe, S.; Noshiro, J.; Miyake, S. Friction Properties of WS2/MoS2Multilayer Films under Vacuum Environment. *Surf. Coat. Technol.* **2004**, *188*−*189*, 644−648.
(52) Helmersson, U.; Todorova, S.; Barnett, S. A.; Sundgren, J.-E.; Markert, L. C.; Greene, J. E. Growth of Single-crystal TiN/VN Strained-layer Superlattices with Extremely High Mechanical Hardness. *J. Appl. Phys.* **1987**, *62* (2), 481−484.
(53) Muratore, C.; Voevodin, A. A.; Goyena, R.; Fallis, A.; Thomas, I. D. M.; Teer, D. G.; Domínguez-Meister, S.; Rojas, T. C.; Brizuela, M.; Sánchez-López, J. C. Chameleon Coatings: Adaptive Surfaces to Reduce Friction and Wear in Extreme Environments. *Annu. Rev. Mater. Res.* **2009**, *39* (1), 297−324.

https://dx.doi.org/10.1021/acsami.0c12655
ACS Appl. Mater. Interfaces 2020, 12, 43299−43310

Annex C

Hebbar Kannur, K; Huminiuc, T.; Yaqub, T. B.; Polcar, T.; Pupier, C.; Héau, C.; Cavaleiro, A. An insight on the MoS_2 tribo-film formation to determine the friction performance of Mo-S-N sputtered coatings, *Surf. and Coat. Technol.* 408 (2021) 126791. https://doi.org/https://doi.org/10.1016/j.surfcoat.2020.126791.

Surface & Coatings Technology 408 (2021) 126791

Contents lists available at ScienceDirect

Surface & Coatings Technology

journal homepage: www.elsevier.com/locate/surfcoat

An insight on the MoS_2 tribo-film formation to determine the friction performance of Mo-S-N sputtered coatings

Kaushik Hebbar Kannur [a,b,*], Teodor Huminiuc [d], Talha Bin Yaqub [b,c], Tomas Polcar [d], Christophe Pupier [a], Christophe Héau [a], Albano Cavaleiro [b]

[a] IREIS, HEF Group, ZI Sud - Avenue Benoît Fourneyron, CS 42077 – 42162 Andrézieux-Bouthéon, France
[b] University of Coimbra, Department of Mechanical Engineering, CEMMPRE, Rua Luís Reis Santos, 3030-788 Coimbra, Portugal
[c] IPN - LED & MAT - Instituto Pedro Nunes, Laboratory of Tests, Wear and Materials, Rua Pedro Nunes, 3030-199 Coimbra, Portugal
[d] nCATS, University of Southampton, University Road, Southampton SO17 1BJ, United Kingdom

ARTICLE INFO

Keywords:
Transition metal dichalcogenides
Solid lubricant coatings
Direct current magnetron sputtering
Mo-S-N coatings
Nitrogen-alloying mechanism
Molybdenum disulfide

ABSTRACT

Amorphous Mo-S-N coatings are known to provide excellent tribological properties in diverse environments due to easy sliding under the influence of MoS_2 tribo-films. However, the role of nitrogen incorporation, the formation mechanism of MoS_2 tribo-film at the sliding interface and the changes in the friction behaviour under different environments are not fully understood. In this study, an amorphous coating with 30 at. % N was deposited in a semi-industrial reactive direct current magnetron sputtering (DCMS) system, using a single MoS_2 target in combination with a secondary plasma source. The coating was predicted to have either a Mo-S-N phase with N filling some of the S sites or a $MoS_2(N_2)$ structure where the gas molecules prevent the formation of a crystalline lamellar structure. Tribological studies performed in vacuum and ambient air resulted in steady-state COF values of 0.03 and 0.15, respectively. High-resolution transmission electron microscopy (HRTEM) analysis performed on the wear-tracks revealed that the low coefficient of friction (COF) in vacuum was attributed to the formation of a thick and continuous lamellar tribo-film with a low amount of nitrogen. Contrarily, in ambient air, the surface oxidation disturbed the formation of a continuous MoS_2 tribo-film from the amorphous coatings, leading to an increase in the COF and wear rate. This study shows through indirect measurements of the chemical composition of the as-deposited coating and wear debris that nitrogen is stored in gaseous form (N_2) within the amorphous matrix and is released from the contact during sliding.

1. Introduction

Transition Metal Dichalcogenides (TMD), such as MoS_2, are classified as self-lubricating solids for effective energy-saving and providing long service life for a multitude of mechanical components used in aerospace, thermonuclear and other industries [1]. MoS_2 has a lamellar structure that facilitates the formation of highly lubricious tribo-films, especially in vacuum or dry conditions [2]. However, MoS_2 coatings react easily with atmospheric oxygen and moisture, thus degrading their sliding capabilities in complex environments [3]. Additionally, low hardness and load-bearing capacity have limited their application due to high probabilities of premature mechanical failures. Previous studies have shown that alloying TMDs with some metals (Ti, Al, and Ni) and non-metals (C and N) could improve the low load-bearing capacity, provide the required hardness and enhance the oxidation resistance [4–9].

Nitrogen doping was generally less explored but seems to be a more suitable option for improving the tribological properties of TMDs. Pure nitrogen can be used for reactive sputtering, avoiding contamination by other elements and providing low operational costs [10]. Mo-S-N coatings have been deposited in a variety of ways including RF magnetron sputtering [11–13] and, plasma-assisted sputtering techniques such as in HITUS [14]. Only recently, via single-target DC magnetron sputtering with an additional independent plasma source, a cost-effective method was introduced as an industrial friendly approach [8,15]. Furthermore, when compared to carbon, a small amount of nitrogen can be sufficient to achieve a dense amorphous coating with a significant increase in the hardness [16]. In order to grow mechanically stable coatings, it is crucial to prevent the easily sheared planes of pure MoS_2 from forming in a large scale [17]. Despite disturbing the atomic structure of MoS_2 in the

* Corresponding author at: IREIS, HEF Group, ZI Sud - Avenue Benoît Fourneyron, CS 42077 – 42162 Andrézieux-Bouthéon, France.
E-mail address: khebbarkannur.ireis@hef.fr (K. Hebbar Kannur).

https://doi.org/10.1016/j.surfcoat.2020.126791
Received 9 October 2020; Received in revised form 3 December 2020; Accepted 20 December 2020
Available online 2 January 2021

coating, N does not impede the formation of crystalline tribo-film providing low friction [7,18]. The tribo-layer is identified as pure MoS_2 [19,20]. The original Mo-S-N coatings are known to be mostly XRD amorphous as per the observation of the previous studies [8,13]. Mutafov et al. [21] reported a low COF, high load-bearing capacity, and good wear resistance for magnetron sputtered amorphous W-S-N films. The crystal structure and the bonding arrangements in amorphous W-S-N were modelled by Isaeva et al. [16]. Through this theoretical study, it was reported that during sliding nitrogen is released from the contact region in a gaseous form (e.g., N_2, NO_2) without altering the formation of tribo-films.

The low friction mechanism of Mo-S-N coatings, under vacuum and ambient air conditions as well as the role of N in the contact zone, is still not described in the literature. To overcome this scarcity of literature, in the current study, Mo-S-N coatings were tribo-tested in vacuum and ambient air. Later, the wear-tracks were thoroughly observed in HRTEM. The specimens from the wear-tracks were prepared using a focused ion beam (FIB). The micro and nano-structural features of the worn regions were analysed to highlight the mechanism of the tribo-film formation in both sliding environments. More importantly, a better understanding of the role of nitrogen in facilitating low friction in Mo-S-N coatings was studied.

2. Experimental details

A rectangular MoS_2 target (450 mm × 150 mm, 99.5% purity) was DC sputtered in N_2 and Ar (99.99% purity) gas atmosphere using a custom-built TSD 400 semi-industrial chamber to deposit N-doped MoS_2 coatings. The chamber was equipped with a single cathode (MoS_2) and a secondary plasma source (for ion bombardment). The target and plasma source power were kept constant throughout the deposition with a 40 sccm nitrogen feed resulting in a partial pressure of N_2 gas p_{N2}/p_{total} of 0.36 (Mo-S-N40 [8]). Polished M2 steel discs (Ø 25 mm, 62 HRC hardness) were used as substrates and placed over a planetary (double rotation) holder revolving at 5 rpm to achieve a uniform coating. Prior to deposition, the chamber and substrates were heated to 150 °C for 5 h and pumped to a base pressure of ~10^{-4} Pa, to remove any moisture and adsorbed contaminants. Before final coatings deposition, a gradient layer was deposited to improve the adhesion to the steel substrate. This gradient layer is composed of three parts starting from steel: (i) a quasi-epitaxial metal-metal interface between Mo and the steel achieved by the strong re-sputtering of sulphur from the coating by utilizing an intense and high ion energy (substrate bias) bombardment; (ii) introduction of nitrogen into the deposition chamber with similar ion bombardment conditions contributing to the formation of a MoN-based laminar structure; (iii) progressive reduction of the substrate bias to allow the incorporation of the sulphur in the coating. A schematic diagram of the deposition chamber, the secondary plasma source, the detailed characterisation of the gradient layer and the coatings are presented in ref. [8].

The sliding tests were performed in a custom-built rotating ball-on-disc tribometer using a 100Cr6 steel ball (Ø 10 mm) as counter body. The testing was performed in vacuum (10^{-2} Pa) for 5000 cycles and ambient air (24 °C and 20–30% relative humidity) for 10,000 cycles under an applied load of 5 N (initial Hertzian contact stresses ~ 800 MPa) and a sliding speed of 50 mm/s.

The HRTEM imaging was performed using an image corrected FEI Titan^3 operating at 300 kV acceleration voltage. The samples for HRTEM were prepared by focused ion beam (FIB) using an FEI Helios Nanolab electron microscope.

3. Results and discussion

3.1. Main characteristics of deposited coating

The MoSN40 coating had of 30 at. % nitrogen, S/Mo ratio of 1.36 and a thickness of 1.3 μm. The film was compact and XRD amorphous. The detailed characterisation details can be found in ref. [8]. Due to the alternate substrate exposure to the MoS_2 target and the secondary plasma source (ion bombardment), a multi-layer structure was formed. This type of deposition mechanism enabled the film to incorporate a higher N content along with a high S/Mo ratio, unlike similar experiments reported in the literature [13,14]. It was observed in our previous works [8], by XPS analysis that for coatings with N content lower than 28 at. %, the presence of N1s spectrum fitted to 397.0 eV peak, corresponding to γ-Mo_2N [14], is enhanced with increasing N content. Mo-N bonds, shown via peaks at 229.0 eV and 232.4 eV, also showed an increased intensity. However, for N contents equal or higher than 28 at. % (such as Mo-S-N40 with 30 at. % N), the global intensity of the N1s peak continues to grow but the Mo-N bond intensity remained constant. It is, therefore, believed that N replaces S sites initially, distorting the lattice and reducing the crystallinity of the coatings, and, further additions of N, led to the formation of amorphous coatings (28 at. % N and above) along with N_2 gas entrapment within the amorphous matrix of the coatings.

3.2. Tribological properties

The COF evolution, resulting wear-track profiles, micrographs of ball wear-scar and disc tracks after vacuum and ambient air tests are presented in Fig. 1. Different frictional behaviour was observed for each atmosphere.

In vacuum, the COF stabilised after a brief running-in period at ~0.03. The maximum depth of wear was ~0.06 μm. The wear-scar images show negligible wear on the counterbody and a smooth wear-track with no evidences of large flakes or wear debris. The resulting friction value implies that the MoS_2 tribo-film forms at the interface (Fig. 2C). The MoS_2 (002) planes formed due to the crystallisation/reorientation of basal planes parallel to the sliding surface and resulted in a low COF [22]. The specific wear rate determined from the profile was about 1.8×10^{-7} mm^3/N-m.

In ambient air, the COF reached a peak value of ~0.35 and then dropped to a friction steady-state value of ~0.15. The maximum wear depth was ~1.26 μm, a 20-fold increase when compared to the test in vacuum. The improved adhesion is attributed to the hard-gradient layer consisting of metallic bonds with low lubricious phase content, which prevented the delamination of the coatings from the steel. The bottom of the worn track in ambient air is flat and wide (Fig. 1B), which corresponds to a significant wear on the steel ball (Fig. 1D), caused by the absence of a protective tribo-film at the sliding interface. Large wear debris on the counterbody was identified as O-rich Mo-S-N material (SEM-EDX analysis data presented as supporting information). In ambient air, the presence of H_2O and O_2 contributes significantly to the degradation of MoS_2, prevents the formation of a lubricious tribo-film from the amorphous coatings and forms surface oxides. Actually, during sliding, the weak interlamellar bonds break, increasing the potential of O to react with MoS_2. Furthermore, the formation of oxides (especially MoO_3), as clusters or asperities could enhance the wear of the coatings when present in the contact region (abrasion). The specific wear rate was two orders of magnitude higher: 1.7×10^{-5} mm^3/N-m in ambient air. However, it should be noted that the steady-state COF is much lower than what could be expected in a steel/metal contact, which could be attributed to the presence of either Mo-S-N zones (debris and residual film in the wear-track (Fig. 3) or Mo-oxides. MoO_3 is known to provide relatively low friction [23].

In post vacuum tribological testing, the entire wear track displayed zones covered by well-oriented planes parallel to the surface. These planes correspond to MoS_2 tribo-films. The cross-section of the wear-track corresponding to a particular area where the tribo-film delaminated cohesively, leaving a gap in relation to the as-deposited coating is shown in Fig. 2B. The separated/top part consists of large amounts of pure MoS_2 i.e., the tribo-film (Fig. 2C). The crack is created by the

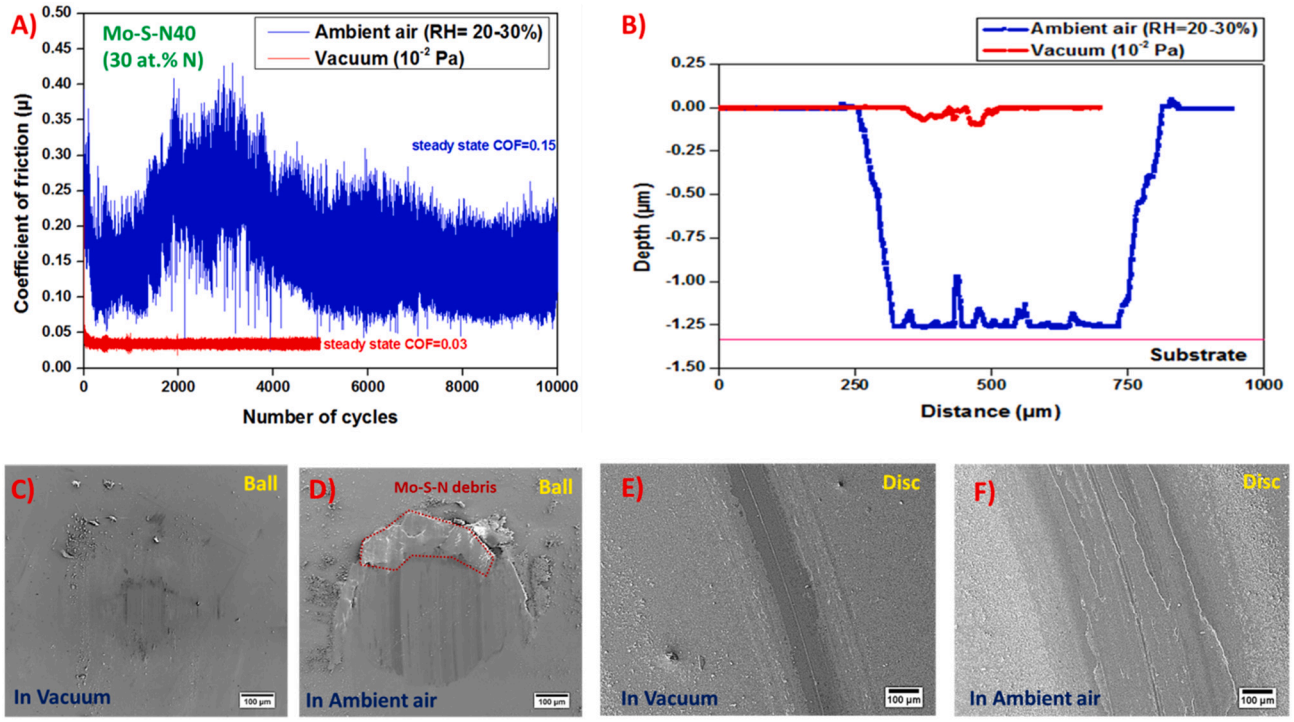

Fig. 1. A) Evolution of COF in ambient air and vacuum environments. (B) Depth profile of wear-tracks. (C, D) wear-scar images of steel balls and (E, F) worn region of coated wear-tracks.

exfoliation of the weakly bound hexagonal structure of the MoS_2 tribo-film during sliding. In the top part of the coating, oriented planes are visible confirming their formation mechanism at the sliding interface (Fig. 2B). The amorphous coating underneath provides the required strength and hardness to support the solid lubricant interface. The large quantity of tribo-film in the separated region spreads along the wear-track during tribo-testing leading to a short run-in time, low values of COF (see Fig. 1A) and insignificant wear. The tribo-film provides the low shear strength needed for easy sliding. Fig. 2D shows the EDX elemental maps of the separated tribo-film regions which are nitrogen deficient (approx. 4 at.% N) when compared to the measured 30 at. % of N in the amorphous coatings. The 4 at. % detected N can be attributed to N that had replaced some of the S sites. The remaining nitrogen was released into the vacuum as a gas. So, our experimental work brings strong evidence to support the theoretical framework presented by Isaeva et al. [16]. Mo and S were found in similar concentrations in both regions; hence, in vacuum, the sliding motion causes wear down to a specified depth, which is transformed into the tribo-film. A fully formed tribo-film prevents further wear of the coating underneath. Negligible wear was observed on the surface of the counterbody and this is associated with sliding on a highly lubricious interface composed of lamellar pure MoS_2 as shown in Fig. 2C. The high hardness and Young's modulus of the Mo-S-N coatings, with the lubricious interface, limit the deep penetration of the counterbody (sinking), thus maintaining a small contact area.

Fig. 3 shows a region of large delamination on the wear-track, the location of the TEM lamella extracted, the cross-sectional micrographs and the elemental maps corresponding to the wear-track generated by tribo-testing in ambient air. The wear debris of the coating consists of randomly oriented nanometre-size traces of lamellar MoS_2 layers embedded in an O rich brittle amorphous matrix (Fig. 3E and G). A crack in the coating separates the as-deposited film and the wear debris (Fig. 3C). The local delamination of the coating and the significant wear debris are the result of the oxidation and the abrasive wear induced by the oxide particles. The top interface of the wear-track, (Fig. 3F), does not consist of tribo-films which could induce low friction at the mechanical contact. The ball counterpart reached the adhesion layer which was not worn through.

In ambient air, the water vapour and the oxygen in the atmosphere accelerate the oxidation of MoS_2. The oxidation can affect the bulk of the material, creating internal blisters that act as weak points leading to cracking and high volumes of debris [24]. Additionally, when MoS_2 layers are exposed during sliding, the oxidation process is triggered yielding more debris and wear. This is evident in Fig. 3D, in which the oxidised coating is mixed with nanoparticles of MoS_2. The STEM-EDX analysis confirms the severe oxidation of the worn debris. The S/Mo ratio is reduced from 1.34 to 0.93 along with a large concentration of oxygen (67%).

Similar to the test performed in vacuum, a reduction of the nitrogen content at the sliding contact can be observed in ambient air conditions. The 22-fold increase in the O content implies that with each cycle of friction test, the formed surface oxide would be trapped and dragged into the coatings forming a third body.

The main driving force for the significant increase in the wear observed in ambient air testing is the formation of surface oxides. Additionally, Ramalho et al. [25] discussed the linear relationship between the wear and the dissipated energy which would be one of the reasons behind the increase in COF values and the poor tribological performance in the air. The interaction with the atmospheric oxygen and humidity at the sliding interface prevents the coating from forming a continuous well-oriented tribo-film. Khare et al. [26] reported that the friction of MoS_2 in ambient air is a strong function of the amount of water in the environment and the diffused water into the bulk. This study shows that the process of forming well-ordered tribo-film is absent. Instead, the amorphous coating was directly oxidised and/or remained amorphous, which lead to a high COF. In contrast, during the vacuum test, in the first few cycles, the surface oxides are removed along with the initial wear. With no oxygen or water vapour, the further worn coating transforms from amorphous into crystalline MoS_2 tribo-films oriented parallel to the substrate.

The nitrogen incorporated in the coating provides the required hardness through the amorphization during the deposition and was predicted to either form a ternary compound Mo-S-N (by replacing S

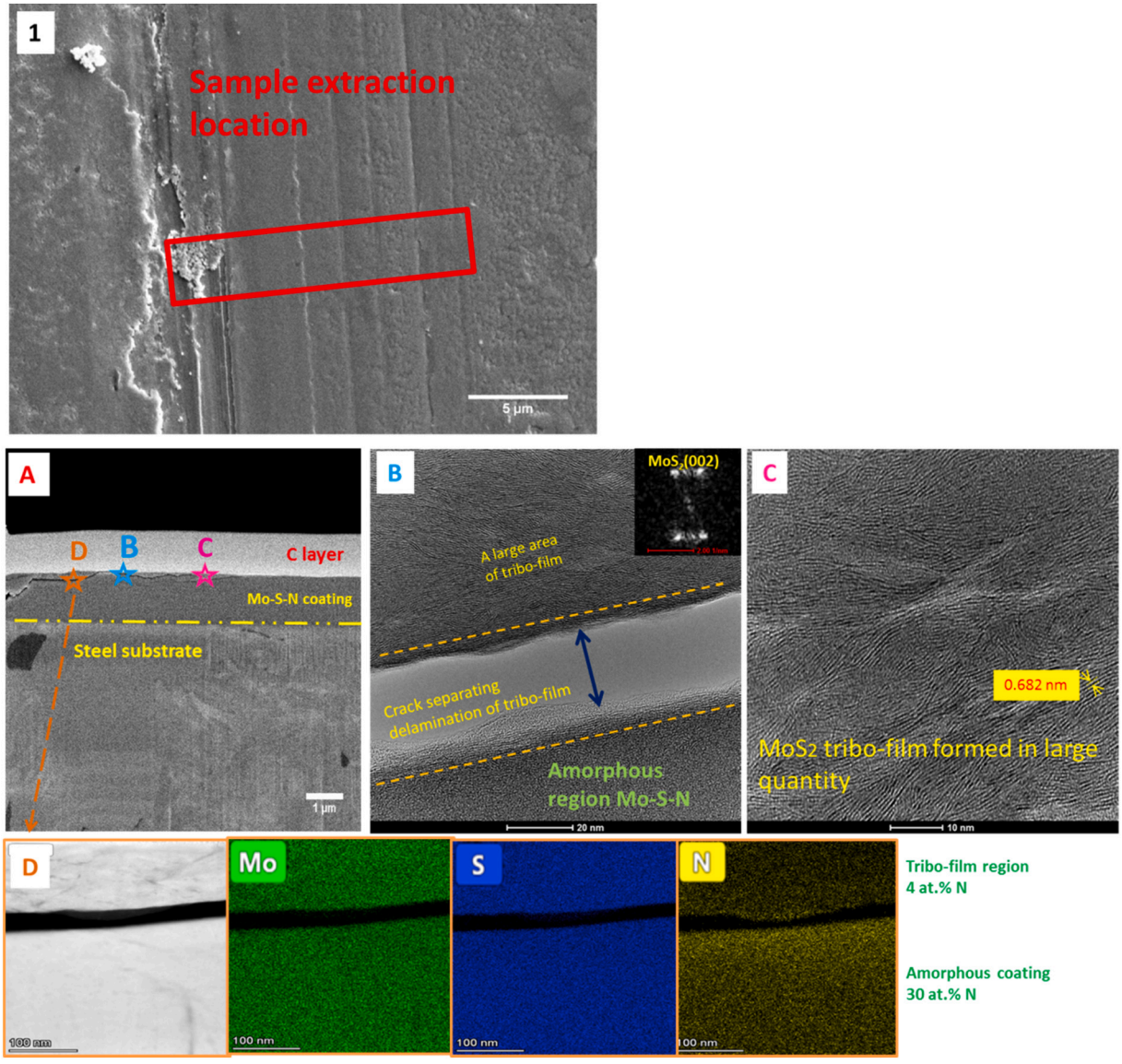

Fig. 2. TEM analysis of wear track after tribo-testing in vacuum: 1) Wear track with site of sample extraction. A) FIB cut cross-section of wear-track showing a flake lifted from the pristine coating. B) The crack caused by the delamination of the tribo-film. C) Large quantity of preferentially oriented MoS_2 tribo-film. D) STEM- EDX images showing the elemental distribution of Mo, S, and N at the interface.

sites) or distort the MoS_2 crystalline structure by diffusion into the layers. The chemical analysis performed on the as-deposited coating and the wear debris (shown in Figs. 3G and S1) suggests that N is released, does not bond to other elements to form nitrides and cannot be found as part of wear debris on the film nor the sliding counterpart. The mechanical interaction is therefore believed to cause the release of nitrogen most likely as an inert gas. These measurements support the theoretical hypothesis which claims that the gas is distorting the MoS_2 lamellar structure and only a small amount (~4 at. %) of the gas is found to be present at the sliding interface after testing. Hence it is believed this small amount of N replaces sulphur.

The thickness of the tribo-films formed by deformation depends on the applied pressure and the properties of the films, such as the platelet size and packing density, the adhesion of the base of the platelets to the substrate and the COF [27].

Tribo-testing in vacuum showed the local transformation of the amorphous coating into a crystalline lubricious interface as well as the release of nitrogen in gaseous form. A sufficient thickness of tribo-film prevents more wear as observed in vacuum testing. These conditions are not met for sliding in ambient air, where oxidation occurred during the crystallisation process of MoS_2 forming an amorphous mixture which can contain MoO_3 and Mo-S-N particles. Oxides found at the sliding interface act as abrasive particles leading to severe wear and decreasing the contact stress which is required for the crystallisation of pure MoS_2.

Even when testing in ambient air, despite the extensive delamination, a part of the coating always remained attached to the steel substrate. This is the result of integrating the novel bonding multilayer, as described in our previous work [8]. This gradient layer provides improved adhesion of the coating to the steel due to the metal-metal quasi-epitaxial bonding.

4. Conclusions

Amorphous Mo-S-N coatings with 30 at. % N content were tribo-tested in vacuum (10^{-2} Pa) and ambient air in order to differentiate the process of tribo-film formation and the role of N on the lubricating behaviour of Mo-S-N coatings. In the vacuum tests, a steady-state is quickly reached with a COF value of 0.03. TEM studies revealed that with insignificant wear, the transformation of the amorphous coatings,

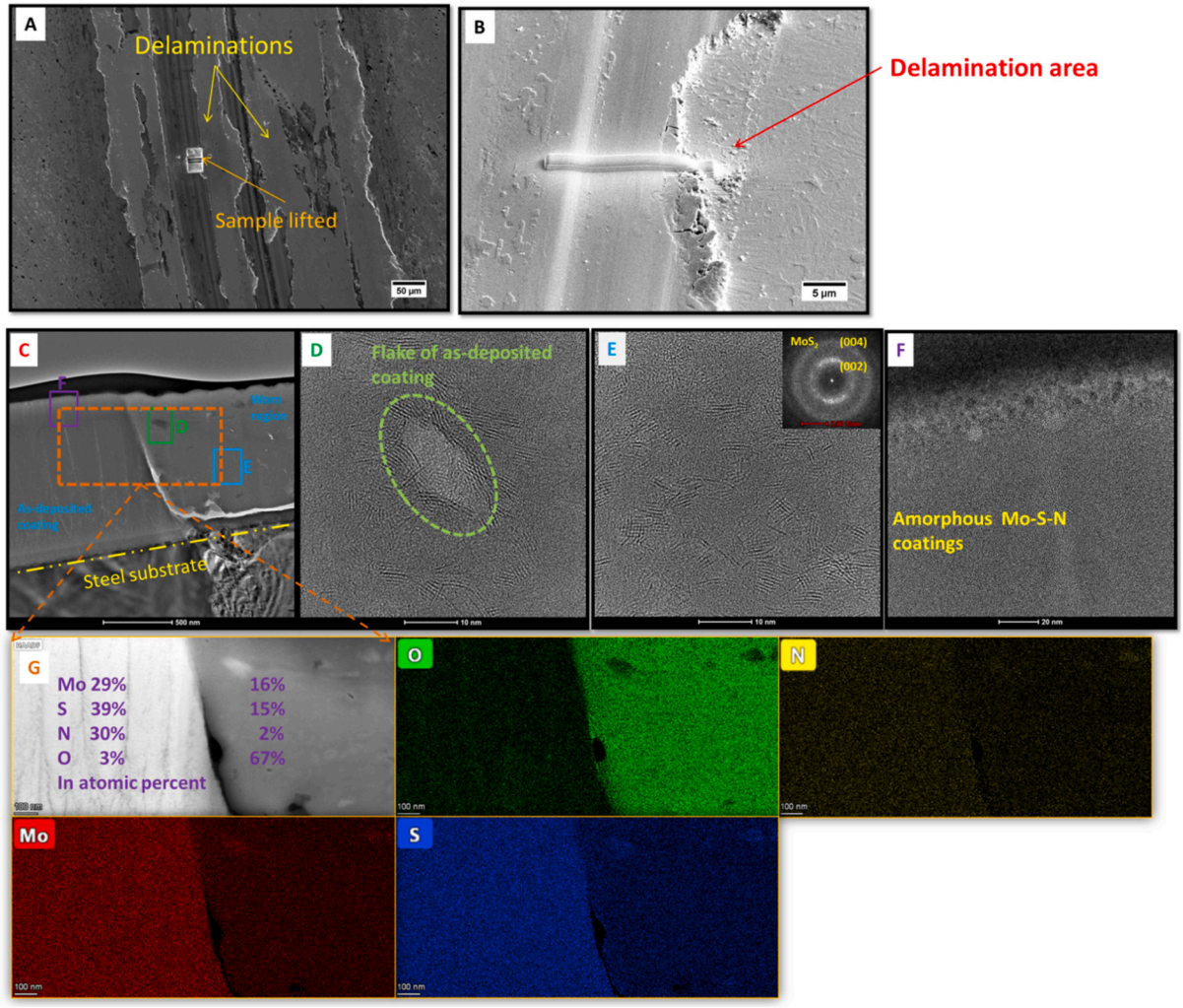

Fig. 3. Cross-section of wear-track in ambient air test. A, B) Specimen location. C) Low magnification cross-sectional image. D) Flake of as-deposited amorphous coating within the contact worn volume. E) Disrupted lamellar MoS_2 layers in the worn volume. F) Region of as-deposited amorphous coatings outside the wear-track. G) STEM-EDX elemental mapping of wear-track and as-deposited coating.

into a lamellar MoS_2 tribo-film and the release of nitrogen in N_2 form have occurred. The tribo-film formation would require the release of the trapped N_2 gas and the rearrangement of Mo and S atoms to form the hexagonal structure. The amorphous coating underneath the tribo-films provided the required hardness and the load-bearing capability. Testing in ambient air resulted in a long running-in period with a COF peak value of 0.35 which stabilised later at 0.15 but with a significant wear. TEM studies revealed that the presence of surface oxides and moisture disturbed the continuous formation of the MoS_2 lamellae in ambient air. The reaction with oxygen led to the formation of MoO_3. There was no sufficient uninterrupted tribo-film formed at the sliding interface, which explains the high COF in ambient air.

Thus, it can be said that nitrogen is a favourable element for doping/alloying MoS_2 coatings. Nitrogen-alloying promotes the amorphisation of MoS_2, by distorting the weak and porous hexagonal structure, and making the coatings compact. On the other hand, during sliding, a large amount of N is released as N_2 gas, enabling the formation of MoS_2 tribo-films and providing an easy sliding. Even with increased wear in ambient air, the excellent adhesion of the coatings to steel guaranteed no delamination at the coating-substrate interface. These coatings are likely to be used as layered self-lubricating materials for vacuum applications.

CRediT authorship contribution statement

Kaushik Hebbar Kannur: Writing – original draft, Methodology, Investigation, Formal analysis. **Teodor Huminiuc:** Writing – review & editing, Investigation. **Talha Bin Yaqub:** Investigation. **Tomas Polcar:** Project administration, Funding acquisition, Resources. **Christophe Pupier:** Project administration, Resources. **Christophe Héau:** Writing – review & editing, Supervision, Resources. **Albano Cavaleiro:** Writing – review & editing, Supervision, Resources.

Declaration of competing interest

The authors declare that they have no known competing financial interests or personal relationships that could have appeared to influence the work reported in this paper.

Acknowledgements

This project has received funding from the European Union Horizon 2020 research and innovation programme under grant agreement No. 721642: SOLUTION. The electron microscopy imaging was performed with the support of CEITEC Nano Research Infrastructure (ID LM2015041, MEYS CR, 2016–2019), CEITEC Brno University of Technology. The authors would also like to thank funding from CEMMPRE –

UID/EMS/00285/2019 [co-financed via FEDER and FCT (COMPETE)].

Appendix A. Supplementary data

Supplementary data to this article can be found online at https://doi.org/10.1016/j.surfcoat.2020.126791.

References

[1] S.M. Aouadi, B. Luster, P. Kohli, C. Muratore, A.A. Voevodin, Progress in the development of adaptive nitride-based coatings for high temperature tribological applications, Surf. Coat. Technol. 204 (2009) 962–968, https://doi.org/10.1016/j.surfcoat.2009.04.010.

[2] N.M.U. Renevier, J. Hamphire, V.C. Fox, J. Witts, T. Allen, D.G. Teer, Advantages of Using Self-lubricating, Hard, Wear-resistant MoS 2 -based Coatings, 2001, pp. 67–77.

[3] H. Singh, K.C. Mutyala, R.D. Evans, G.L. Doll, An investigation of material and tribological properties of Sb2O3/au-doped MoS2 solid lubricant films under sliding and rolling contact in different environments, Surf. Coatings Technol. 284 (2015) 281–289, https://doi.org/10.1016/j.surfcoat.2015.05.049.

[4] X. Ding, X.T. Zeng, X.Y. He, Z. Chen, Tribological properties of Cr- and Ti-doped MoS2 composite coatings under different humidity atmosphere, Surf. Coatings Technol. 205 (2010) 224–231, https://doi.org/10.1016/j.surfcoat.2010.06.041.

[5] T. Spalvins, Frictional and morphological properties of au MoS2 films sputtered from a compact target, Thin Solid Films 118 (1984) 375–384, https://doi.org/10.1016/0040-6090(84)90207-4.

[6] A. Nossa, A. Cavaleiro, The influence of the addition of C and N on the wear behaviour of W-S-C/N coatings, Surf. Coatings Technol. 142–144 (2001) 984–991, https://doi.org/10.1016/S0257-8972(01)01249-X.

[7] F. Gustavsson, S. Jacobson, A. Cavaleiro, T. Polcar, Ultra-low friction W-S-N solid lubricant coating, Surf. Coatings Technol. 232 (2013) 541–548, https://doi.org/10.1016/j.surfcoat.2013.06.026.

[8] K. Hebbar Kannur, T. Bin Yaqub, T. Huminiuc, T. Polcar, C. Pupier, C. Heau, A. Cavaleiro, Synthesis and structural properties of Mo-S-N sputtered coatings, Appl. Surf. Sci. (2020) 146790, https://doi.org/10.1016/j.apsusc.2020.146790.

[9] T. Bin Yaqub, K. Hebbar Kannur, T. Vuchkov, C. Pupier, C. Heau, A. Cavaleiro, Molybdenum diselenide coatings as universal dry lubricants for terrestrial and aerospace applications, Mater. Lett. (2020) 128035, https://doi.org/10.1016/j.matlet.2020.128035.

[10] A. Nossa, A. Cavaleiro, Tribological behaviour of N(C)-alloyed W–S films, Tribol. Lett. 28 (2007) 59–70, https://doi.org/10.1007/s11249-007-9248-3.

[11] Y. Fu, T. He, W. Yang, J. Xu, B. Mu, X. Pang, P. Wang, Structure, mechanical and Tribological properties of MoSN/MoS2 multilayer films, Coatings. 9 (2019) 108, https://doi.org/10.3390/coatings9020108.

[12] H. Ju, R. Wang, N. Ding, L. Yu, J. Xu, F. Ahmed, B. Zuo, Y. Geng, Improvement on the oxidation resistance and tribological properties of molybdenum disulfide film by doping nitrogen, Mater. Des. 186 (2020), 108300, https://doi.org/10.1016/j.matdes.2019.108300.

[13] X. Zhang, L. Qiao, L. Chai, J. Xu, L. Shi, P. Wang, Structural, mechanical and tribological properties of Mo-S-N solid lubricant films, Surf. Coatings Technol. 296 (2016) 185–191, https://doi.org/10.1016/j.surfcoat.2016.04.040.

[14] T. Hudec, M. Mikula, L. Satrapinskyy, T. Roch, M. Truchlý, P. Švec Jr., T. Huminiuc, T. Polcar, Structure, mechanical and tribological properties of Mo-S-N solid lubricant coatings, Appl. Surf. Sci. 486 (2019) 1–14, https://doi.org/10.1016/j.apsusc.2019.03.294.

[15] K. Hebbar Kannur, T. Bin Yaqub, C. Pupier, C. Héau, A. Cavaleiro, Mechanical properties and vacuum tribological performance of Mo-S-N sputtered coatings, ACS Appl. Mater. Interfaces 12 (2020) 43299–43310, https://doi.org/10.1021/acsami.0c12655.

[16] L. Isaeva, J. Sundberg, S. Mukherjee, C.J. Pelliccione, A. Lindblad, C.U. Segre, U. Jansson, D.D. Sarma, O. Eriksson, K. Kádas, Amorphous W-S-N thin films: the atomic structure behind ultra-low friction, Acta Mater. 82 (2015) 84–93, https://doi.org/10.1016/j.actamat.2014.08.043.

[17] J. Sundberg, H. Nyberg, E. Särhammar, T. Nyberg, S. Jacobson, U. Jansson, Influence of composition, structure and testing atmosphere on the tribological performance of W-S-N coatings, Surf. Coatings Technol. 258 (2014) 86–94, https://doi.org/10.1016/j.surfcoat.2014.09.061.

[18] H. Nyberg, J. Sundberg, E. Särhammar, F. Gustavsson, T. Kubart, T. Nyberg, U. Jansson, S. Jacobson, Extreme friction reductions during initial running-in of W–S–C–Ti low-friction coatings, Wear. 302 (2013) 987–997, https://doi.org/10.1016/j.wear.2013.01.065.

[19] J.M. Martin, C. Donnet, T. Le Mogne, T. Epicier, Superlubricity of molybdenum disulphide, Phys. Rev. B 48 (1993) 10583–10586, https://doi.org/10.1103/PhysRevB.48.10583.

[20] T. Polcar, A. Cavaleiro, Review on self-lubricant transition metal dichalcogenide nanocomposite coatings alloyed with carbon, Surf. Coat. Technol. 206 (2011) 686–695, https://doi.org/10.1016/j.surfcoat.2011.03.004.

[21] P. Mutafov, M. Evaristo, A. Cavaleiro, T. Polcar, Structure, mechanical and tribological properties of self-lubricant W-S-N coatings, Surf. Coatings Technol. 261 (2015) 7–14, https://doi.org/10.1016/j.surfcoat.2014.11.074.

[22] T. Kubart, T. Polcar, L. Kopecký, R. Novák, D. Nováková, Temperature dependence of tribological properties of MoS2 and MoSe2 coatings, Surf. Coatings Technol. 193 (2005) 230–233, https://doi.org/10.1016/j.surfcoat.2004.08.146.

[23] E. A., B, BHUSHAN, CRC Press, Modern Tribology Handbook, 2001.

[24] B.C. Windom, W.G. Sawyer, D.W. Hahn, A Raman spectroscopic study of MoS2 and MoO3: applications to Tribological systems, Tribol. Lett. 42 (2011) 301–310, https://doi.org/10.1007/s11249-011-9774-x.

[25] A. Ramalho, J.C. Miranda, The relationship between wear and dissipated energy in sliding systems, Wear. 260 (2006) 361–367, https://doi.org/10.1016/j.wear.2005.02.121.

[26] H.S. Khare, D.L. Burris, Surface and subsurface contributions of oxidation and moisture to room temperature friction of molybdenum disulfide, Tribol. Lett. 53 (2014) 329–336, https://doi.org/10.1007/s11249-013-0273-0.

[27] P.D. Fleischauer, M.R. Hilton, R. Bauer, V. Paper, (i) Effects of microstructure and adhesion on performance of sputter-deposited MoS2 solid lubricant coatings, Tribol. Ser. 17 (1990) 121–128, https://doi.org/10.1016/S0167-8922(08)70248-7.